

**NUMERICAL MODELLING
AND DESIGN OPTIMISATION OF
STIRLING ENGINES FOR POWER
PRODUCTION**

KWANCHAI KRAITONG

PhD

2012

**NUMERICAL MODELLING
AND DESIGN OPTIMISATION OF
STIRLING ENGINES FOR POWER
PRODUCTION**

KWANCHAI KRAITONG

A thesis submitted in partial fulfilment
of the requirements of the
University of Northumbria at Newcastle
for the degree of
Doctor of Philosophy

Research undertaken in the
School of Computing, Engineering
and Information Sciences

June 2012

Abstract

This research is in the area of Thermal Energy Conversion, more specifically, in the conversion of solar thermal energy. This form of renewable energy can be utilised for production of power by using thermo-mechanical conversion systems – Stirling engines.

The advantage of such the systems is in their capability to work on low and high temperature differences which is created by the concentrated solar radiation. To design and build efficient, high performance engines in a feasible period of time it is necessary to develop advanced mathematical models based on thermodynamic analysis which accurately describe heat and mass transfer processes taking place inside machines.

The aim of this work was to develop such models, evaluate their accuracy by calibrating them against published and available experimental data and against more advanced three-dimensional Computational Fluid Dynamics models. The refined mathematical models then were coupled to Genetic Algorithm optimisation codes to find a rational set of engine's design parameters which would ensure the high performance of machines.

The validation of the developed Stirling engine models demonstrated that there was a good agreement between numerical results and published experimental data. The new set of design parameters of the engine obtained from the optimisation procedure provides further enhancement of the engine performance. The mathematical

Abstract

modelling and design approaches developed in this study with the use of optimization procedures can be successfully applied in practice for creation of more efficient and advanced Stirling engines for power production.

List of Contents

<i>Abstract</i>	<i>I</i>
<i>List of Contents</i>	<i>III</i>
<i>List of Figures</i>	<i>VII</i>
<i>List of Tables</i>	<i>XII</i>
<i>Acknowledgement</i>	<i>XIII</i>
<i>Declaration</i>	<i>XIV</i>
<i>Nomenclature</i>	<i>XV</i>
<i>Chapter 1 Introduction</i>	<i>1</i>
1.1 The objectives of research.....	4
1.2 Research methodology	4
1.3 The thesis structure.....	6
1.4 Original contribution to knowledge	8
<i>Chapter 2 Literature review</i>	<i>9</i>
2.1 Stirling engine modelling.....	9
2.1.1 Empirical modelling.....	9
2.1.2 Thermodynamic modelling	11

List of Contents

2.1.2.1 The first-order models	12
2.1.2.2 The second-order models.....	12
2.1.2.3 The third-order models	18
2.1.2.4 Multi-dimensional modelling	20
2.2 Optimisation of the design of Stirling engines.....	22
2.3 Optimisation based on the Genetic algorithm method.....	28
2.4 Designs of Stirling engine prototypes	29
2.5 Conclusions	37

Chapter 3 General principles of the second-order mathematical modelling of the LTD and conventional Stirling engines

39

3.1 The second-order mathematical modelling of the LTD Stirling engine	39
3.1.1 Physical model	39
3.1.2 The second-order mathematical model	42
3.1.3 Numerical simulation procedure	59
3.2 The second-order mathematical modelling of the conventional Stirling engines	61
3.2.1 Physical model	61
3.2.2 The second-order mathematical model	64
3.2.3 Numerical simulation procedure	77

List of Contents

<i>Chapter 4 General principles of three- dimensional CFD modelling</i>	80
4.1 Three-dimensional CFD modelling background.....	80
4.2 Numerical simulation procedure	86
 <i>Chapter 5 General principles of the Genetic Algorithm method</i>	88
5.1 Introduction to the Genetic algorithms	88
5.2 Genetic algorithm procedure for finding the optimal design parameters of Stirling engines.....	90
5.2.1 Definition of the objective function and variables.....	90
5.2.1.1 Definition of the objective function and variables for finding the optimal design of a LTD Stirling engine	91
5.2.1.2 Definition of the objective function and variables for the optimal design of a conventional Stirling engine....	93
5.2.2 Generation of the initial population	95
5.2.3 Evaluation	95
5.2.4 Selection process.....	96
5.2.5 Mating process	96
5.2.6 Mutation process	96
5.2.7 Convergence check	97

List of Contents

Chapter 6 Mathematical modelling and optimisation of the design of a LTD

<i>Stirling engine</i>	99
6.1 Results obtained using the second-order mathematical model	100
6.1.1 Analysis of the working process	100
6.1.2 Validation of the second-order mathematical model of a LTD Stirling engine	106
6.2 Results obtained using 3D CFD modelling.....	110
6.2.1 Analysis of the CFD modelling results	112
6.2.2 Validation of CFD modelling	123
6.3 Optimization of the design parameters of the LTD Stirling engine	124

Chapter 7 Mathematical modelling and optimisation of the design of conventional

<i>Stirling engines</i>	132
7.1 Results obtained from the new developed second-order mathematical model	132
7.1.1 Analysis of the working process	133
7.1.2 Validation of the new developed second-order mathematical model of conventional Stirling engines	141
7.2 Optimization of the design parameters of the conventional Stirling engine	149

List of Contents

<i>Chapter 8 Conclusions and recommendations for future work</i>	155
8.1 Conclusions	155
8.1.1 Conclusions from research work on the development of the optimal design of the LTD Stirling engine	155
8.1.2 Conclusions from research work on the development of the optimal design of conventional Stirling engines	157
8.2 Recommendations for future work.....	159
<i>References</i>	161
<i>Appendix A: MATLAB Codes for the second-order mathematical modelling and optimisation of LTD Stirling engines</i>	172
<i>Appendix B: Publications</i>	192
Publication 1	193
Publication 2.....	201

List of Figures

Figure 1.1 A schematic of a Stirling engine with separate “hot” and “cold” cylinders, a heater, a cooler and a regenerator and an example of a variation of the gas pressures (P) and volumes (V) in the “hot” and “cold” cylinders of the engine and pressure-volume (P-V) diagrams in the thermodynamic cycle.	2
Figure 2.1 A LTD Stirling engine with scotch-yoke linkage [68].....	30
Figure 2.2 Schematic diagrams of two gamma-type Stirling engines [69].....	32
Figure 2.3 A LTD solar Stirling engine without a regenerator [72]	33
Figure 2.4 A schematic diagram of the gamma-type Stirling engine [73].....	33
Figure 2.5 A schematic diagram of the beta-type Stirling engine [74].....	34
Figure 2.6 A schematic diagram of the manufactured Stirling engine with two displacer pistons [75]	34
Figure 2.7 A beta-type Stirling engine [78]	35
Figure 2.8 A multi-phase free piston Stirling engine [79]	35
Figure 2.9 Details of a prototype of a Stirling engine [80]	36
Figure 2.10 Cut-away view of the 5 kW demonstrational Stirling engine convertor [81].....	36

List of Figures

Figure 3.1 The schematic diagram of a gamma-type kinematical LTD Stirling engine	40
Figure 3.2 The schematic diagram of the twin-power piston LTD.....	41
Stirling engine from Kongtragool and Wongwises [70]	41
Figure 3.3 The calculation scheme of the LTD Stirling engine	42
Figure 3.4 The diagram of the power transmission mechanism of a reciprocating engine.....	53
Figure 3.5 The flowchart of the second-order mathematical modelling of the LTD Stirling engine.....	60
Figure 3.6 The cross-section of the small conventional gamma Stirling engine [14]	62
Figure 3.7 The calculation scheme of the conventional Stirling engines	64
Figure 3.8 The flowchart of the second-order modelling of the conventional Stirling engines	79
Figure 5.1 A diagram of the continuous GA for the determination of the optimal design parameters of the LTD and conventional Stirling engines	91
Figure 6.1 The variation of the volumes in the engine	103
Figure 6.2 The variation of the pressures in the engine	103
Figure 6.3 The variation of the pressure drop in the engine	104
Figure 6.4 The variation of the temperatures in the engine	104

List of Figures

Figure 6.5 The variation of the heat rates in the engine.....	107
Figure 6.6 P-V diagrams	107
Figure 6.7 The predicted brake power with respect to the engine speed	108
Figure 6.8 The predicted overall efficiency of the engine with respect to the engine speed	108
Figure 6.9 A simplified geometry and computational mesh of the LTD Stirling engine.....	111
Figure 6.10 The velocity distribution of the gas inside the engine at the instance of cycle when the crankshaft angle is 90°	113
Figure 6.11 The velocity distribution of the gas inside the engine at the instance of cycle when the crankshaft angle is 180°	113
Figure 6.12 The velocity distribution of the gas inside the engine at the instance of cycle when the crankshaft angle is 270°	114
Figure 6.13 The velocity distribution of the gas inside the engine at the instance of cycle when the crankshaft angle is 360°	114
Figure 6.14 The temperature distribution of the gas inside the engine at the instance of cycle when the crankshaft angle is 90°	117
Figure 6.15 The temperature distribution of the gas inside the engine at the instance of cycle when the crankshaft angle is 180°	117

List of Figures

Figure 6.16	The temperature distribution of the gas inside the engine at the instance of cycle when the crankshaft angle is 270°	118
Figure 6.17	The temperature distribution of the gas inside the engine at the instance of cycle when the crankshaft angle is 360°	118
Figure 6.18	The average gas temperatures in each space of the engine over its cycle	119
Figure 6.19	The pressure distribution of the gas inside the engine at the instance of the cycle when the crankshaft angle is 90°	120
Figure 6.20	The pressure distribution of the gas inside the engine at the instance of the cycle when the crankshaft angle is 180°	120
Figure 6.21	The pressure distribution of the gas inside the engine at the instance of the cycle when the crankshaft angle is 270°	121
Figure 6.22	The pressure distribution of the gas inside the engine at the instance of the cycle when the crankshaft angle is 360°	121
Figure 6.23	The average pressures in each space of the engine over its operating cycle	122
Figure 6.24	P-V diagrams of the engine obtained using the 3D CFD modelling ...	122
Figure 6.25	The best value of the brake power for each generation	125
Figure 6.26	The brake power as a function of the power piston stroke	128

List of Figures

Figure 6.27 The brake power as a function of the power piston diameter.....	128
Figure 6.28 The brake power as a function of the displacer stroke	129
Figure 6.29 The brake power as a function of the displacer thickness	129
Figure 6.30 P-V diagrams of the first optimal design using the 3D CFD modelling	131
Figure 6.31 P-V diagrams of the second optimal design using the 3D CFD modelling	131
Figure 7.1 The variation of the volumes in the engine	134
Figure 7.2 The variation of the gas pressures in the engine.....	134
Figure 7.3 The variation of the pressure drops in the engine.....	135
Figure 7.4 The variation of the gas temperatures in the engine	135
Figure 7.5 The variation of the heat transfer rates in the engine.....	139
Figure 7.6 The variation of the heat loss rates in the engine.....	139
Figure 7.7 P-V diagrams for the conventional Stirling engine	140
Figure 7.8 Comparison of the gas temperatures.....	143
Figure 7.9 Comparison of the gas pressures in the compression space	143
Figure 7.10 Comparison of the total pressure drops	144

List of Figures

Figure 7.11 Comparison of the pressure drops in the heater	144
Figure 7.12 Comparison of the pressure drops in the regenerator	145
Figure 7.13 Comparison of the pressure drops in the cooler	145
Figure 7.14 The best indicated power of each generation against the number of generations	150
Figure 7.15 The indicated power against the diameter of the heater tube	152
Figure 7.16 The indicated power against the length of the heater tube	152
Figure 7.17 The indicated power against the diameter of the cooler tube	153
Figure 7.18 The indicated power against the length of the cooler tube	153
Figure 7.19 The indicated power against the diameter of the regenerator chamber	154
Figure 7.20 The indicated power against the length of the regenerator chamber	154

List of Tables

Table 3.1 The physical dimensions of the LTD Stirling engine for the numerical analysis from Kongtragool and Wongwisets [70].	41
Table 3.2 The physical dimensions of the small conventional gamma Stirling engine [14].	63
Table 6.1 Comparison of the theoretical and experimental results on the LTD Stirling engine's power production	124
Table 6.2 The first set of the optimal engine design parameters obtained using the optimization procedure	126
Table 6.3 The second set of the optimal engine design parameters obtained using the optimisation procedure	127
Table 7.1 Comparison of theoretical and experimental results on the engine's power production	140
Table 7.2 The indicated power obtained by using the various correlations in the new developed second-order mathematical model	148
Table 7.3 The engine design parameters obtained from the GA optimization	150

Acknowledgement

I wish to express my sincere appreciation to my supervisor, Professor Khamid Mahkamov, for his help and encouragement throughout this study.

Authors also would like to thank Professor Somchai Wongwises and Assistant Professor Bancha Kongtragool for providing data on their twin power piston LTD Stirling engine.

This PhD study is supported by the Ministry of Science and Technology of Royal Thai Government.

I would like to thank all my friends at Northumbria University and Durham University for their support and friendship.

Finally, I wish to specially thank my family for their constant support and care.

Declaration

Declaration

I declare that the work contained in this thesis has not been submitted for any other award and that it is all my own work. I also confirm that this work fully acknowledges opinions, ideas and contributions from the work of others.

Name: Kwanchai Kraitong

Signature:

Date: June 2012

Nomenclature

Symbols

A	=	area (m ²)
C_p	=	specific heat at constant pressure (J/ kgK)
C_v	=	specific heat at constant volume (J/ kgK)
D	=	diameter (m)
F_{load}	=	external load acting to the piston (N)
F_{ox}	=	axial force to crank shaft of axis x in the piston connection (N)
F_{oy}	=	axial force to crank shaft of axis y in the piston connection (N)
F_r	=	friction force due to ring package in the piston part (N)
H	=	thickness (m)
I	=	inertia (kgm ²)
L	=	ratio of the length OC to the length OA
N_{pop}	=	number of chromosome
NTU	=	number of heat transfer unit
Nu	=	Nusselt number
\bar{Nu}	=	mean Nusselt number
P	=	power (W)
P_k	=	production of turbulence
Pr	=	Prandtl number
Q	=	heat rate (W)
Q_i	=	solar irradiation (W/ m ²)

Nomenclature

$Q(t)$	=	piston load along the cylinder axis (N)
R	=	gas constant value
Re	=	Reynolds number
\bar{Re}	=	mean Reynolds number
S	=	side force (N)
T	=	temperature (K)
U	=	velocity (m/s)
V	=	volume (m ³)
W	=	work (J)
X_{rate}	=	the selection rate
X_{mu}	=	the mutation rate
Z	=	stroke (m)
d_h	=	hydraulic diameter (m)
e_{eff}	=	effectiveness of the regenerator
f	=	frequency (Hz)
f_c	=	friction factor
f_r	=	Reynolds friction coefficient
g	=	gravitational acceleration (m/s ²)
Δgap	=	gap length between the displacer and the cylinder (m)
h	=	convection heat transfer coefficient (W/ m ² K)
iga	=	number of generation
j	=	ratio of the length AR to the length AB
k	=	thermal conductivity (W/mK)
l	=	length (m)

Nomenclature

$maxvalue$	=	maximum fitness value in the value map
m	=	mass (kg)
\dot{m}	=	mass flow rate (kg/s)
p	=	pressure (Pa)
p_{inst}	=	instantaneous cylinder pressure (bar)
Δp	=	pressure drop (Pa)
r	=	radius (m)
t	=	time (sec)
$value$	=	fitness value
x	=	displacement of the piston (m)
x_0	=	stroke displacement of the piston (m)
y	=	displacement of the displacer (m)
y_0	=	stroke displacement of the displacer (m)

Subscripts

A	=	free convection heat transfer coefficient to air free stream
B	=	rolling bearing
C	=	cooler space
D	=	displacer
H	=	heater space
P	=	power piston
S	=	swept volume
T	=	total
b	=	brake

Nomenclature

c	=	compression space
$c1$	=	compression space in the displacer chamber
$c2$	=	compression space in the power piston cylinder
$crank$	=	crankshaft
$cyclic$	=	cycle
d	=	dead volume
e	=	expansion space
$free$	=	free flow area
g	=	working gas
h	=	heat transfer area
i	=	indicated
l	=	cross sectional area
$loss,disip$	=	heat loss due to the flow friction in the generator
$loss,lir$	=	heat loss due to heat transfer due to the heat conduction
$loss,shl$	=	shuttle heat loss due to heat transfer from the heater space to cooler space
m	=	matrix in the regenerator
pi	=	piston
r	=	regenerator space
rod	=	connection rod
0	=	ambient

Nomenclature

Greek Symbols

α	=	absorptivity
β	=	crank angle displacement in Figure 3.4
ε	=	emissivity
ϕ	=	connecting rod angle
φ	=	phase angle
μ	=	dynamic viscosity (Pa.s)
μ_k	=	coefficient of friction
θ	=	piston crank angle
ρ	=	density (kg/m ³)
σ	=	Stefan-Boltzman constant = $5.667 \times 10^{-8} \text{ W/m}^2\text{K}^4$
τ	=	time period (sec)
ω	=	angular velocity (rad/s)

Chapter 1

Introduction

The energy crisis is one of the main problems faced by the world's population. Solar energy which is clean and free energy has been focused upon as an alternative energy for the reduction of the fossil fuel consumption rate for electricity production. A solar Stirling engine is a type of the energy conversion machine which is able to operate on solar energy. In general, Stirling engines can make a use of any type of external heat source which provide temperature difference of various magnitude in the thermodynamic cycle. The principle of operation of Stirling engines is based on closed regenerative thermodynamic cycle in which process of expansion of the working fluid (usually helium, hydrogen or air) takes place at elevated pressure level due to heat input through a special heat exchanger – a heater. Process of the compression takes place at lower pressure levels due to heat rejection from the working fluid in another special heat exchanger, called a cooler. To split the expansion and compression processes in space in order to maintain the heater and cooler at constant high and low temperatures, respectively the internal gas circuit of the engine is divided into separate expansion and compression spaces (cylinders) which usually have their own pistons. These pistons provide displacement (flow) and correct distribution of the working fluid between expansion and compression spaces

Chapter 1

which is necessary to maintain high level of pressure during expansion process and lower pressure levels during compression process. Additionally, in order to avoid direct contact between the heater and cooler and corresponding heat losses, a third special heat exchanger is fitted between which is called regenerator. Figure 1.1 shows a schematic of a two cylinder Stirling engine with typical volume, pressure variations and PV diagrams in the thermodynamic cycle.

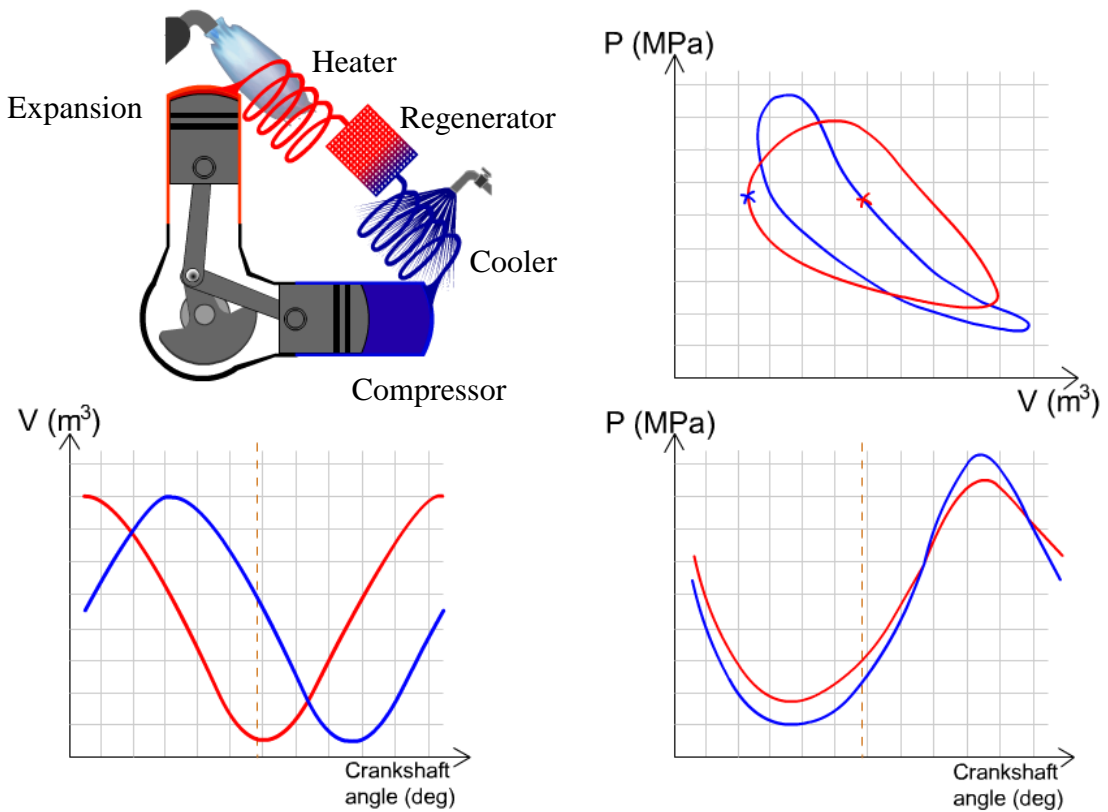


Figure 1.1 A schematic of a Stirling engine with separate “hot” and “cold” cylinders, a heater, a cooler and a regenerator and an example of a variation of the gas pressures (P) and volumes (V) in the “hot” and “cold” cylinders of the engine and pressure-volume (P-V) diagrams in the thermodynamic cycle.

Chapter 1

Low temperature difference (LTD) Stirling engine and conventional Stirling engines with application of medium temperature difference (MTD) and high temperature difference (HTD) have started to attract a considerable attention for conversion of the solar energy into the electrical power in developing countries. LTD, MTD and HTD engines have temperature of heaters at the range 80-150, 150-400 and 400-800 °C, respectively. The LTD Stirling engine, though having a relatively low efficiency, can be manufactured using uncomplicated technologies and equipment at comparatively low cost. Kongtragool and Wongwises [1] proposed a design of a double-acting gamma configuration kinematical LTD Stirling engine which is suitable for using solar energy as a heat source. Conventional MTD Stirling engines are very similar in design to the conventional HTD Stirling engines, and both these types of engines are an object of growing interest for solar energy applications.

The solar irradiance has enough potential to produce the hot fluid with temperatures up to 165 °C using solar evacuated collectors [2] and up to 400 °C using a concentrating mirror system (usually parabolic troughs) [3]. The produced hot fluid then can be used to operate LTD and MTD Stirling engines for electricity generation. It is, however, necessary to consider together all thermal, fluid and mechanical design aspects of operation of a power system in order to achieve the good performance of Stirling engines [4].

Thus, in this research, the advanced methods for determination of optimal design parameters of a gamma-type LTD Stirling engine and conventional Stirling engines have been developed. The efficient and accurate mathematical models taking into account various losses during engine's operation have been developed and then

Chapter 1

coupled to an optimisation code. Additionally, three dimensional (3D) CFD simulations have been performed for more accurate analysis of heat and mass transfer processes in Stirling engines.

1.1 The objectives of research

The objective of these research investigations are as follows:

1. To develop advanced accurate second-order mathematical models of a gamma-type kinematical LTD Stirling engine and of conventional Stirling engines.
2. To numerically analyse the performance of engines by using the developed mathematical models.
3. To analyse the performance of engines by using Computational Fluid Dynamic (CFD) modelling and use these results for validation of the developed second-order mathematical models of Stirling engines.
4. To develop a procedure for optimisation of the design of Stirling engines.

1.2 Research methodology

The work was split into several stages which can be described as follows:

1. The second-order mathematical model of the LTD Stirling engine was developed which takes into account thermal, hydraulic and mechanical losses during the operation of the engine.

Chapter 1

2. Numerical analysis of the working process and losses in the LTD Stirling engine was performed using the developed second-order mathematical model.

3. The obtained theoretical results were compared to the experimental information published in open literature and the model was refined.

4. Numerical analysis of the working process of the LTD Stirling engine was performed using the 3D CFD modelling. The theoretical results from these CFD simulations also were used to calibrate the developed second-order mathematical model of the LTD Stirling engine.

5. The developed second-order mathematical model was coupled to a Genetic Algorithm (GA) optimization code and optimal rational design parameters of the LTD Stirling engine were determined.

6. The LTD Stirling engine with the optimal engine design parameters was analysed using 3D CFD modelling in order to check the accuracy of predictions from the previous stage of investigations.

7. The advanced second-order mathematical model of a conventional Stirling engine was developed which takes into account hydraulic and heat losses.

8. Numerical analysis of the working process and losses in the conventional Stirling engine was performed using the developed second-order mathematical model.

Chapter 1

9. The obtained theoretical results were compared to the available experimental results and improvements were introduced into the developed mathematical model.

10. The refined second-order mathematical model was coupled to a GA optimization code to determine the rational design parameters of the conventional Stirling engine.

1.3 The thesis structure

The structure of the thesis reflects the sequence of investigation stages described above and the thesis is split into the following eight chapters:

Chapter 1 Introduction: The chapter briefly describes the aims of this research and the structure of thesis and highlights the contribution to knowledge in the field.

Chapter 2 Literature review: Previous studies related to the development of LTD and conventional Stirling engines were reviewed. The chapter briefly describes published results on designing, experimental testing, numerical simulations using thermodynamic and CFD models and on determination of optimal design of Stirling engine using different optimisation methods.

Chapter 3 General principles of the second-order mathematical modelling of the LTD and conventional Stirling engines: General principles of the advanced second-order thermodynamic mathematical model of the LTD and conventional Stirling engines are presented in this section. Physical models of engines which are

Chapter 1

under investigation are also described. Mathematical models are described in details with all equations used and numerical procedures followed in simulations.

Chapter 4 General principles of three-dimensional CFD modelling: General principles of three-dimensional CFD modelling are presented in this section with a detailed description of the numerical simulation procedures.

Chapter 5 General principles of the Genetic Algorithm method: This chapter describes principles of the continuous Genetic Algorithm (GA) procedure used for determination of optimal design parameters of Stirling engines.

Chapter 6 Mathematical modelling and optimisation of the design of a LTD Stirling engine: This chapter presents results of the analysis of the working process of the LTD Stirling engine using the developed second-order mathematical model and a 3D CFD modelling technique. Theoretical results were compared to published experimental results for the model validation purpose. The chapter describes results on the determination of the optimal engine design using GA optimisation code coupled to the second-order mathematical model. In the last section of the chapter 3D CFD simulations were run on the engine with the optimal design parameters to ensure the accuracy of the optimisation results.

Chapter 7 Mathematical modelling and optimisation of the design of conventional Stirling engines: Results of the analysis of the working process of the conventional Stirling engine using the developed second-order mathematical model are described and discussed in this section. The obtained theoretical results were compared to available experimental results for the model validation. The optimal

Chapter 1

design parameters of the conventional Stirling engine were obtained using the GA optimisation code.

Chapter 8 Conclusions and recommendations for future work: Conclusions from investigations carried out in this work are made and recommendations for the future work are proposed.

1.4 Original contribution to knowledge

The improved second-order mathematical models of the working process of LTD and conventional Stirling engines were developed in this study. The optimisation procedure for determination of rational design parameters of Stirling engines was developed using coupling of the developed mathematical models and the GA optimization code.

Chapter 2

Literature review

In this chapter, a brief review of various studies on the development of LTD Stirling engines and conventional Stirling engines for the MTD and HTD application related to designing of Stirling engine prototypes, mathematical modelling and optimisation is presented. The section presents Stirling engine mathematical modelling, describing empirical, thermodynamic and multi-dimensional CFD modelling studies, which were carried out previously and also works on the optimisation of Stirling engines using Genetic Algorithm methods.

However, the outline of principles of working of a Stirling engine is provided for more clear understanding. Stirling

2.1 Stirling engine modelling

Models used for calculation of the working process and performance of Stirling engines can be classified as of empirical, analytical and numerical types.

2.1.1 Empirical modelling

A number of studies were performed to develop the empirical correlations for the estimation of the engine power output and the engine efficiency.

Chapter 2

West [5] proposed to use a dimensionless parameter called Beale number to predict the engine power (named after Prof. William Beale).

The Beale number is defined in terms of a Stirling engine's operating parameters:

$$B_n = \frac{W_o}{p_{mean} V_{S-P} f} \quad (2.1)$$

where B_n is the Beale number; W_o is the power output of the engine (W); p_{mean} is the mean average gas pressure (bar); V_{S-P} is swept volume of the power piston (cm^3); f is the engine cycle frequency (Hz).

The Beale number with value of 0.015 was suggested to use for a wide range of Stirling engines with different configurations. To take into account the effect of the temperature range in the working cycle, West proposed to introduce into the Beale number the empirical factor F of 0.035 to more accurately calculate the engine's power output. Senft in [6] recommended that for LTD Stirling engines the greater value of the factor F is required to improve the accuracy of predictions.

To find an appropriate correlation for calculating the power output of the LTD Stirling engine of the gamma configuration, Kongtragool and Wongwises in [7] investigated the experimental performance of the engine. They came to the conclusion that the Beale's formula was not valid for conditions in which there were the high temperature ratio. However, they recommended that the original Beale formula and the mean pressure based power output formula with a certain magnitude of the factor F would make it possible to accurately predict the engine's power output.

Chapter 2

Other example of development of an empirical correlation for prediction power out of Stirling engines include works of Prieto et al. [8] and Prieto et al. [9]. They analysed a wide range of experimental results and applied methods of the dynamic similarity and quasi-static simulations for various LTD and HTD Stirling engines. To improve the accuracy of predictions of the indicated power of Stirling engines, Prieto and Stefanovski [10] used dimensionless analysis to characterise the gas leakage and mechanical power losses. The dimensionless mechanical power losses were determined using the empirical data. Several Stirling engines were modelled using this dimensionless analysis. In [11] Prieto et al. found that such the correlation based on dimensionless analysis of the engine's working process and different losses in the cycle provided more accurate prediction of the performance of three LTD Stirling engines compared to that obtained using the modified Kolin's model.

2.1.2 Thermodynamic modelling

Numerous mathematical models based on thermodynamic theory have been developed for studying different designs of Stirling engines and their cycles. These models were classified in [12], [13] and [14] by splitting them in a big number of groups using various criteria. In these investigations, however, the models are categorised into one-dimensional and multi-dimensional model. In turn, one-dimensional model of Stirling engines is subdivided into three subgroups called the first, the second and third-order models.

Chapter 2

2.1.2.1 The first-order models

The first-order models are based on algebraic equations of mass and energy conservation equations applied to describe the working process of Stirling engines and such approach allows us to obtain analytical equations to estimate power output and efficiency of machines.

Schmidt model described in [15] was the first in the series of the first-order models and this model made it possible to derive analytical equation [16] to describe pressure variations in the cycle assuming that an engine's space could be presented as three main spaces, namely the compression space, the expansion space and the dead volume. It was assumed that processes in each of these spaces take place at a corresponding constant temperature levels.

Toda et al. [17] presented a model which takes into account the effectiveness of the drive mechanism in the Schmidt theory to analyse the engine performance of the LTD Stirling engine of a gamma configuration. The results of experiments on a 10 kW LTD Stirling engine demonstrated that the mechanical effectiveness of the engine has a strong influence on the shaft power of engine.

2.1.2.2 The second-order models

The second-order models are superior to the first-order thermodynamic models. Such the models may generally be based on Schmidt analysis. Usually, an engine's internal gas volume is separated into several spaces. For each space a set of ordinary differential equations of the mass and energy conservation are used to describe heat and mass transfer processes. Various heat and the pressure losses occurring in real

Chapter 2

engines are taken into account in the model for a more accurate prediction of the engine's performance.

Martini [12] presented such the isothermal model based on Schmidt theory and taking into account heat losses and pressure losses. The temperatures of hot and cold gases were obtained by taking into account temperature drops in the heater and cooler. Numerical predictions for the GPU-3 Stirling engine had the 20 % error compared to experimental results.

The first second-order model using an adiabatic analysis was developed by Finkelstein in 1960 and described in [15]. The model defined as adiabatic compression and expansion spaces whilst all heat exchangers were treated as perfect heat exchangers with isothermal processes. Urieli and Berchowitz [18] described the further development of the adiabatic model by Finkelstein. The model was implemented as a computer code and corresponding differential equations were solved using the fourth-order Runge-Kutta method. Additionally, to improve numerical predictions, Urieli and Berchowitz [18] developed a so-called Simple analysis which in fact was the adiabatic model with incorporated non-ideal heat exchangers. Isothermal processes were still assumed in all heat exchangers but the heater's and cooler's gas temperatures were then recalculated applying the heat transfer equations.

There have been some Stirling engine models developed based on the Simple analysis approach. Abbas et al. [19] developed method based on the Simple model taking into account a presence of a non-ideal regenerator. The regenerator space was divided into two parts in this work and the model also included calculation of

Chapter 2

various losses such as the shuttle loss, regenerator loss, regenerator wall heat conduction and pumping loss. The work loss due to a pressure drop was subtracted from the indicated work. Another model using the Simple analysis was developed by Strauss and Dobson [20] in which the pumping work loss and regenerator heat loss described in Urieli [21] were evaluated. The original method to include into calculations the regenerator wall heat conduction was described in this paper. Heat losses and the pumping work loss were included into the value of the rejected heat in the cooler. This caused the reduction of the pressure inside the engine and of the power output. When compared to experimental data, the model demonstrated a good accuracy in predicting performance of the General Motor GPU-3 Stirling engine.

In addition to the Simple analysis method, the quasi steady flow model of Stirling engines was published by Urieli and Berchowitz in [18]. The concept of non-ideal heat exchanger was realised and introduced into the calculation procedure. The heat exchanger wall temperature was defined as a constant during operation of the machine. The model required the use of heat transfer correlations. The fourth-order Runge-Kutta technique was used to solve a set of ordinary differential equations. The pressure drop in heat exchangers was determined and it rectified pressure values in the expansion and compression spaces. Urieli and Berchowitz [18] validated the model with experimental data for the General Motor GPU-3 Stirling engine and reported an improved accuracy of predictions compared to the Simple analysis method.

Several mathematical models for Stirling engines were developed based on the quasi steady flow approach. Thus such models were developed for analysis of the SOLO

Chapter 2

161 Stirling engine with the alpha configuration to be used in the Eurodish 10 kW_e dish/Stirling system by Granodos et al. [22] and Nepveu et al. [23]. Granodos et al. [22] developed their model which is combined with calculations of the cavity type receiver in MATLAB. In this study the engine's volume was split into 19 control volumes with ten control volumes being allocated to the regenerator. The developed quasi steady flow model took into account the pressure drop in the channels of heat exchangers. The model developed by Nepveu et al. [23] considered 32 control volumes in the engine's gas circuit with the regenerator being split into 8 control volumes. As in the previous case, the model described in [23] also coupled to calculations of the heat receiver. This model's validation was carried out using experimental results obtained by Reinalter et al. [24] on the Eurodish 10 kW_e dish/Stirling unit installed at the CNRS-PROME laboratory, France. Parlak et al. [25] analysed the performance of a gamma-type Stirling engine using the developed model based on the quasi steady flow approach. The procedure for determination of the pressure in each working space using the values of the calculated pressure drop was main feature of the model. For calculations of medium temperature difference engines, Tlili et al. [26] developed the second-order adiabatic mathematical model based on the quasi steady flow approach described by Urieli and Berchowitz [18]. They called this the Dynamic model and in the modelling procedure took into account various thermal losses and pressure drops in each component of a MTD Stirling engine. The losses included the energy dissipation due to the pressure drop in all heat exchanges, internal and external conduction losses in the regenerator and shuttle losses caused by reciprocating motion of a displacer. The gas spring hysteresis losses in the compression and expansion spaces were taken into account to

Chapter 2

improve predictions of the engine performance by Timoumi et al. [27]. In this paper authors also used for calibration experimental data obtained from the General Motor GPU-3 Stirling engine and reported that there was a good correlation between the numerical and experimental results.

Schulz and Schwendig [28] described a mathematical model for simulation of Stirling engines. The pressure drop and heat transfer in the oscillating flow of gas through the heat exchanger were considered at turbulent flow conditions. The ordinary differential equations for each control volume of a Stirling engine were presented and the real gas state equation was used in the model. The absolute value of Nusselt number for laminar and turbulent flow conditions were calculated in the modelling process. It was found that there was a good agreement when theoretical results were compared to experimental data for a Vuilleumier engine.

Mahkamov and Ingham [29] analysed the working process and influence of mechanical losses in a 1-kW solar Stirling engine of an alpha configuration. The second-order mathematical model which considered the hydraulic losses and heat transfer in all control volumes. For the determination of the mechanical losses, cycle variations in the frictional force between the sealing ring and the cylinder (single and double sealing rings), in the sealing of the shaft, the frictional torque in all rolling bearings and the aerodynamic resistance of a flywheel were calculated. As a result of simulations, the predicted indicated power of 3190 W and the brake power of 1585 W were obtained. It was shown that total mechanical losses in the Stirling engine were approximately 50 % of the indicated power.

Chapter 2

Ataer and Karabulut in [30] presented a mathematical model for analysis of a V-type Stirling-cycle refrigerator which does not take into account the pressure drop in the cycle. The machine was split into fourteen control volumes and the mass and energy conservation equations were written for each volume. The constant heat transfer coefficient was used to calculate heat transfer in the cooler and heater. The model was implemented as a FORTRAN computer program. Karabulut et al. [31] further developed the model by adding a set of kinematic equations to analyse a Stirling engine with a concentric piston and displacer. However, the constant heat transfer coefficient was still used when considering heat transfer on heater and cooler surfaces.

Anderson et al. [32] developed a Stirling engine model with 13 control volumes with ordinary differential energy and mass conservation equations written for each volume. The model was realized as the MusSIM code [32] to solve these equations. The model validation was carried out using a 9 kW Stirling engine and there was an acceptable agreement in numerical predictions.

Several mathematical models of LTD Stirling engines were developed which took into account differences in their design compared to conventional Stirling engines. Martaj et al. [33] carried out thermodynamic study of a LTD Stirling engine using the steady state energy, entropy and exergy analysis. The engine was divided into three isothermal cells, namely the heating, cooling and regenerator cells and these were analysed using energy, mass, entropy and exergy balance equations. It was found that the thermal and exergy efficiencies for the whole machine were inversely proportional to the regenerator's dead volume. They found that there was an

Chapter 2

acceptable agreement between calculated and experimental work outputs for the engine operating with a rotational speed of 199 rpm. Robson et al. [34] developed a mathematical model of a LTD Ringbom Stirling engine which describes parameters of the gas in expansion and compression spaces and in a regenerator. The model takes into account a power piston that is connected to the flywheel with a displacer being a free piston. The mass and energy conservation differential equations for gas in each space were applied. Kinematical and kinetic equations of the transmission mechanism were used to describe the characteristics of piston motions and to determine the engine's power output. The pressure variation description obtained using the developed mathematical model was in a good correlation with experimental results obtained on the LTD Stirling engine designed by Senft. However, it was concluded that in this model a very small time step is necessary during integration of equations to obtain convergence in the simulation of the unsteady behaviour of the engine.

2.1.2.3 The third-order models

The third-order model is more complex compared to the second-order one and needs much more intensive numerical calculations. In the third-order model mass, volume and momentum equations are written for several control volumes of the gas circuit of the engine in the form of partial differential equations.

Examples of such models are reviewed by Dyson et al. [35] and Anderson [36]. GLIMPS is the simulation code developed by Gedeon in 1986 and based on a third-order model. The 2D finite difference grid in terms of time and space was used to solve the mass, energy and momentum partial differential equations. The governing

Chapter 2

equations were applied for both the working gas and the structure of engine. In 1994 Gedeon developed a new program called Sage which is based on the methods used in GLIMPS code but benefited from a friendly graphical user interface. Tew et al. [37] reported that the simulation of Stirling engines using Sage code was performed in a NASA's project.

H-FAST that is Stirling engine analysis code using the harmonic analysis method was presented by Huang cited in [35]. The mass, energy and momentum equations were formed in simplify assumption. Furthermore, the result was deducted with several losses to obtain the correct result.

Anderson in [36] described in details the PROSA software (version 3.0) developed by Thomas. Anderson et al. in [38] presented a one-dimensional modelling approach for a Stirling engine which takes into account the compressibility in the unsteady gas flow. The losses due to the finite temperature heat transfer, the flow friction were described using the empirical correlations. Such the modelling approach implemented as MusSIM software and was illustrated on the SM5 Stirling engine. When compared with experimental data, simulation results were in a good agreement with experimental data. It was pointed out that using correct empirical correlations for calculating the heat transfer and friction in the regenerator and heat transfer in the displacer clearance is very important for the accurate prediction of the efficiency and power output. Furthermore, the optimisation study with the use of the shooting method was performed in this work.

Chapter 2

2.1.2.4 Multi-dimensional modelling

In addition to using various one-dimensional models for analysis of a working process of Stirling engines, there have been some investigations performed on application of two-dimensional (2D) and three-dimensional (3D) modelling in order to better predict the working performance of each component of Stirling engines.

Mahkamov and Ingham [39] demonstrated the application of 2D CFD modelling for analysis of the working process of a V-type solar Stirling engine. An axisymmetric CFD model with the standard $k-\varepsilon$ turbulence model for compressible flow was chosen to numerically simulate the operational cycle. Preliminary to that, the second-order mathematical model which includes heat and hydraulic losses was used and its results were compared with the results of the CFD model. The better accuracy in the prediction of the engine performance with the CFD model was reported.

Ibrahim et al. [40] reported on the development of a 2D CFD model for analysing the components of Stirling engines. The so-called CAST model was used to solve the governing equations with the $k-\varepsilon$ turbulence model. The predicted gas hysteresis loss from CAST was compared to results obtained from simulations using the commercial CFD software, namely CFD-ACE+. The acceptable agreement between numerical results was found but these significantly differed from experimental results obtained on the test rig.

Further to analysing the working process with application of the 2D CFD modelling, the 3D CFD modelling has been used for the design improvement of a Stirling engine. Thus, Mahkamov and Djumanov [41] analysed the whole Stirling engine

Chapter 2

operation using 3D CFD modelling with commercial software, namely ANSYS. The modelling deployed the $k-\varepsilon$ turbulence model for numerical investigations of the working process inside a gamma-type Stirling engine. Obtained numerical data included temperature, pressure and the velocity contours in the Stirling engine and the indicated power of the Stirling engine was calculated using obtained pressure-volume diagrams in the expansion and compression spaces. Tan et al. [42] presented, using as a tool the 3D CFD (ANSYS) modelling, working process details of a small beta-type kinematical Stirling engine coupled to a parabolic dish concentrator. Two improved design configurations were suggested to increase the indicated power of the engine. Moreover, Mahkamov [43] carried out 3D CFD modelling for the design improvement of a biomass engine. In this paper the working process of a gamma-type Stirling engine run on biomass (heat source) was first investigated by using the developed second-order mathematical model and then the 3D CFD model was applied for calculations. It was demonstrated that the accuracy of the second-order and CFD models was 30 and 12-18 %, respectively, when compared to experimental data. The commercial CFD software, ANSYS, was used for simulating the gas flow and heat transfer in each component of the Stirling engine and the standard $k-\varepsilon$ turbulence model for compressible flow was deployed in modelling the cycle. The design improvements were proposed which included a new regenerator with the increased porosity and the change of engine's configuration to the alpha-type. A similar work was performed by Mahkamov and Eid [44] for a Stirling engine heated by synthetic oil. The investigation of the heat transfer phenomena from synthetic oil to the heater of a V-type Stirling engine was performed. The engine was designed for

Chapter 2

application as a part of a medium temperature solar power plant. The 3D CFD simulations using ANSYS were run to design the heater of the engine.

Dyson et al. [45] reported the computational simulations using 3D CFD modelling based on ANSYS for a part of opposed Stirling convertors. The temperature contours in the cooler, heater and regenerator were presented and also pressure variations in the expansion and compression spaces were determined. The numerical results obtained using the 3D CFD model were compared to results obtained with the use of the one dimensional model software, namely Sage.

Some of the above described mathematical models of Stirling engines were used as tools for optimisation of design of Stirling engines. Such investigations are presented in the next section.

2.2 Optimisation of the design of Stirling engines

This section reviews a number of papers related to the optimisation of Stirling engines using various mathematical models and optimisation methods.

Blank and Wu [46] presented results of investigations of an extra-terrestrial Stirling engine operating with solar heat source using the irreversible thermodynamic cycle analysis. The optimum power and the efficiency at the optimum power condition were calculated using the finite time approach.

Erbay and Yavuz [47] also analysed the performance of the Stirling heat engine at the maximum power conditions. The power and the efficiency were determined by using the model of the thermodynamic cycle of a Stirling engine with a realistic

Chapter 2

regenerative heat exchanger. The maximum power density technique was used for analysing the engine performance.

Costea et al. [48] optimised the operating temperature for a solar Stirling engine using the mathematical model based on the Stirling thermodynamic cycle. This model took into account fluid friction and mechanical losses in the engine using empirical correlations. Results were obtained by solving a system of nonlinear equations using the method of Lagrangian undetermined multipliers.

Hsu et al. [49] investigated the performance of a free piston Stirling engine operated using the heat from an incinerator. In order to determine the optimal design of an engine, the efficiency and optimal power output at variable heat source and heat sink temperatures were investigated by using a cycle-averaged heat transfer coefficient model. It was found that the efficiency and optimal power output were proportional to the heat source temperature. Additionally, Hsieh et al. [50] studied the feasibility of the power production using the waste heat of an incinerator and a free piston Stirling engine. The performance of a Stirling engine was predicted by using the heat transfer model with irreversible heat transfer processes and the optimisation of the work output was investigated using the Lagrange multipliers method. The maximum power was used as an objective function in the optimisation procedure.

Martaj et al. [51] presented the energy, entropy and exergy analyses of the hot-end and cold-end heat exchangers and the regenerator of a Stirling engine. The mathematical model of the Stirling engine with the finite dimension thermodynamics processes was used in this paper. The engine was analysed using the entropy and exergy balance equations under the steady state condition. In order to optimise the

Chapter 2

performance of the Stirling engine, this research defined the criteria parameters in terms of the maximum power, the maximum thermal efficiency, the minimum entropy generation and the maximum exergy efficiency. A MATLAB computer program was used to run optimisation calculations.

Boer presented in [52] the one dimensional model for analysing the regenerator of Stirling engines. The model was analytically derived from a simplified model and included viscous and thermal losses. The optimisation performed provided the optimal condition for the regenerator conductance and the piston phase angle for the maximum power output

Yaqi et al. [53] investigated the optimisation of the solar HTD Dish-Stirling engine. The finite heat transfer and heat losses were considered in the model. The optimisation performed in terms of the heat absorber temperature, the concentrating ratio of the system, the effectiveness of the regenerator and the heat leak coefficients resulted in the maximum efficiency of the Dish-Stirling power unit.

Optimisation of Stirling engines based on deploying the Schmidt model is of a particular interest in this subject field. Senft [54] developed the model for optimisation using the principle of the forced work integrated to the classical Schmidt theory. The optimisation calculations provided the values of the optimal swept volume ratio and phase angle to achieve the maximum brake work. The geometry of a gamma-type Stirling engine was optimised and discussed in this work. Schmidt model was also used by Cullen et al. [55] to obtain preliminary results of modelling an Otto/Stirling cycle hybrid engine. The simulations with respect to the engine speed using the Schmidt model were compared to the simulation results

Chapter 2

obtained using the direct method. The mathematical model based on the Schmidt model was described by Formosa and Despesse in [56]. The regenerator efficiency, the heat exchanger effectiveness and a number of heat loss sources were taken into account in this model. Comparison of the calculated power output with published results from other models for the GPU-3 Stirling engine [27] was carried out to validate the developed model. From optimisation calculations, the effect on the brake power output of the fluid mass, the frequency and the cooler efficiency were determined. However, the author suggested that the proposed model could be used only for the preliminary designing of the engines.

For better accuracy, higher order models of Stirling engines should be used for analysis and optimisation. Altman [57] presented a commercial program for analysing the working process of Stirling engines and obtaining the optimal design parameters. Thus, a numerical analysis program named SNAPpro was first presented in 1999/2000 for designing the various types of Stirling engine. The isothermal second-order model described by Martini [12] was the design tool for simulating the working process. This program written as an Excel program calculated the performance of the Stirling engines and also presented graphs such as P-V diagrams and heat losses. Moreover, it was coupled to Genetic algorithm code and could optimise up to 20 engine design parameters.

Orunov et al. [58] presented the design of the tri-generation power unit on the basis of an alpha Stirling-Stirling cycle for generating electricity and heat/cold production. The first-order model of a Stirling cycle with taking into account hydraulic losses was used at the first stage of the design process. At the second stage, the second-

Chapter 2

order model taking into hydraulic losses in the all heat exchangers was used for analysing the working gas process. In the optimisation procedure, the dimensionless work parameter and dimensionless length of the heater, cooler and regenerator were used as the optimisation criteria.

Timoumi et al. [27] described the optimisation procedure for the engine parameters of the GPU-3 Stirling engine. The developed quasi steady flow model called Dynamic model was used for the parametric analysis. The effects of the thermal conductivity and heat capacity of materials, the porosity of the regenerator, the temperature of the gas flowing into the regenerator, the regenerator volume, the mass of the working fluid and also the expansion volume on the engine performance were investigated.

Zarinchang and Yarmahmoudi in [59] demonstrated the optimisation of a 20 kW Stirling engine. The optimisation was performed by using so-called OPTIMUM code based on the second-order Stirling engine model. The main heat exchangers such as the heater, cooler and regenerator were redesigned by using the sensitivity analysis. Then the results were recalculated by using the third-order program called STRENG for better predicting the engine performance.

Some studies, though being on the research of conventional Stirling engines, are related to the optimisation of designs of LTD Stirling engines. Some of such papers are reviewed.

Rochelle [60] proposed the mathematical model based on the finite dimension thermodynamics processes and used for simulation and optimisation of a LTD

Chapter 2

Stirling engine with a gamma configuration. The model uses several operating parameters in the dimensionless form. The ratio between the displacer swept volume and the working volume was optimised so to achieve the maximum efficiency and the maximum work output in the LTD Stirling engine without and with a perfect regenerator. The results of the optimisation provided optimal dimensionless values for both above cases.

Abdullah et al. in [61] analysed the design of the engine by using the first and third order mathematical models for a double-acting LTD Stirling engine operating at the temperature difference of 50 °C with a heat source being a thermosyphon solar water heater producing the hot water with the temperature of 70 °C. The preliminary design parameters were obtained using the Schmidt analysis and then the third-order model based on Martini's model [61] was deployed to provide the optimal design parameters. It was demonstrated that there were considerable heat and frictional losses inside all heat exchangers of the Stirling engine. The parametric study of the diameter of the cooler and heater tubes were performed.

From review of published paper carried out in this section, it is obvious that the optimisation methods used for designing engines required the mathematical models providing the closed form solution and furthermore the parametric analysis was commonly used for obtaining the optimal engine parameter. Only few published papers describe application of Genetic algorithm method for the optimisation of Stirling engines.

Chapter 2

2.3 Optimisation based on the Genetic algorithm method

The Genetic algorithm (GA) method, though is very limitedly applied to Stirling engines, has been widely employed in various engineering fields. This section presents a brief review of some studies with application of the GA for the design optimisation of engine and also of the thermal equipment. The detailed description of general principles of Genetic Algorithm optimisation method is provided in Chapter 5.

Four turbofan engine parameters such as the Mach number, compression pressure ratio, fan pressure ratio and bypass ratio were optimised using GA by Homaifar et al. in [62]. It was demonstrated that the GA procedure could provide the best values of the thrust per mass flow rate and the overall efficiency. Kesgin [63] demonstrated the application of GA for the optimisation of the design of a natural gas engine. The GA was coupled to the developed model for predicting NO_x emission and efficiency and these parameters were considered as the objective functions for optimisation.

The GA method was also applied for the optimisation of a heat exchanger which is an important component of a heat engine or thermal system. Tayal et al. in [64] developed a computer program for determination of the optimal design of heat exchangers. The HTRI program called ST-5 was used for calculating the heat transfer area in the GA procedure. The minimum overall costs were obtained using different GA strategies. The GA and simulated annealing (SA) methods were compared and discussed in this work. Mohagheghi and Shayegan in [65] used the GA as an optimisation code for obtaining the thermodynamic optimal design of heat exchangers in a heat recovery steam generator (HRSG) of the combined cycle

Chapter 2

gas turbine (CCGT). The GA was the suitable optimisation approach for HRSG because of the non-linear characteristics of the system. The results of the optimisation were demonstrated for different types of HRSG. Ponce-Ortega et al. [66] determined the optimal design of shell-and-tube heat exchangers by using the GA method. The Bell-Delaware method was used for designing heat exchangers. The GA was applied due to the high degree of nonlinearity in the Bell-Delaware method. The parameters such as the number of tube passages, standard internal and external tube diameters, tube layout and pitch, number of sealing strips, inlet and outlet baffle spacing and the shell-side and tube-side pressure drops were found so to optimise the cost of the heat exchanger. A comprehensive review of studies with the use of the GA optimisation applied to heat transfer problems can be found in a review paper published by Gosselin et al. [67].

2.4 Designs of Stirling engine prototypes

A review of some prototypes of LTD and conventional Stirling engines for power production developed using Stirling engine modelling in the designing procedure is presented in this section.

Hongprapas et al. [68] described a LTD Stirling engine with a flat-plate solar collector, see Figure 2.1, operating with the hot water temperature of 100 °C used as a heat source. A gamma-configuration LTD Stirling engine was designed by using the Beale number approach. It was indicated by Kongtragool and Wongwisets in [7] that the mean pressure power formula with appropriate F factor could be used for the design of LTD Stirling engines. Figure 2.2 presents diagrams of two gamma-type LTD Stirling engines with two and four power pistons, respectively, manufactured

Chapter 2

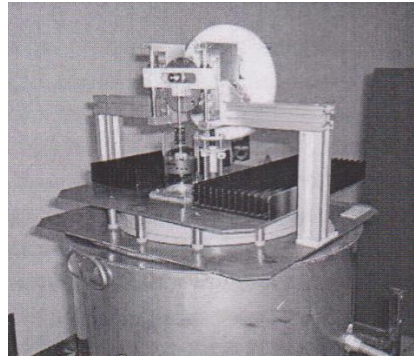


Figure 2.1 A LTD Stirling engine with scotch-yoke linkage [68]

by Kongtragool and Wongwises [69]. These prototypes were tested in the laboratory using a gas burner. Kongtragool and Wongwises [70] and Kongtragool and Wongwises [71] also described tests of the above engines using a solar simulator as a heat source.

Tavakolpour et al. [72] carried out research on the development of the design of a prototype of a gamma-type two-cylinder solar-powered LTD Stirling engine without a regenerator and with a flat-plate solar collector as a heat source as shown in Figure 2.3. The Schmidt method was used to model the LTD Stirling engine operating at the temperature difference of 80 °C.

Cinar and Karabulut [73] designed and built a gamma Stirling engine using air and helium as a working fluid as presented in Figure 2.4. A Stirling engine with the beta configuration shown in Figure 2.5 was manufactured by Cinar et al. and described in [74]. Batmaz and Ustun [75] used the Stirling engine model described by Karabulut et al. in [31] for design and manufacturing a V-type Stirling engine with double heaters and with helium as the working fluid as shown in Figure 2.6. A prototype of

Chapter 2

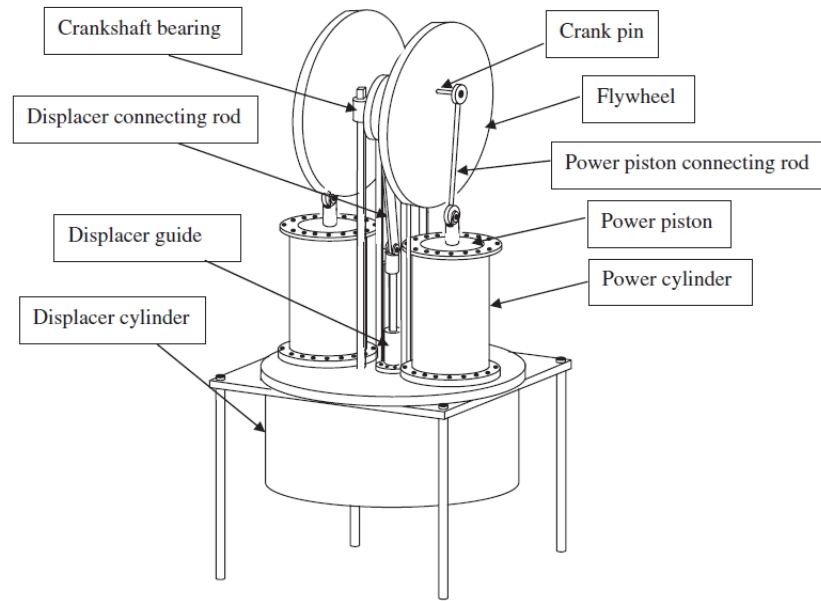
a beta-type Stirling engine with a displacer drive mechanism in the form of a lever was designed and manufactured by Karabulut et al. [76] with mathematical modelling taking into account the gas leakage loss. The design improvement, namely the increasing the heat transfer area in the displacer cylinder, was performed by Karabulut et al. in [77]. The developed beta-type Stirling engine with air as the working fluid was tested with a heat source with a temperature of 200 °C. Helium was used as the working fluid for operating the developed beta-type Stirling engine by Karabulut et al. [78]. The developed beta-type Stirling engine manufactured by Karabulut and co-workers is presented in Figure 2.7.

Minassians [79] applied the second-order model with heat, hydraulic loss and gas hysteresis losses for designing a LTD Stirling engine with a low cost. A multi-phase free piston Stirling engine shown in Figure 2.8 was designed and fabricated as result of these investigations.

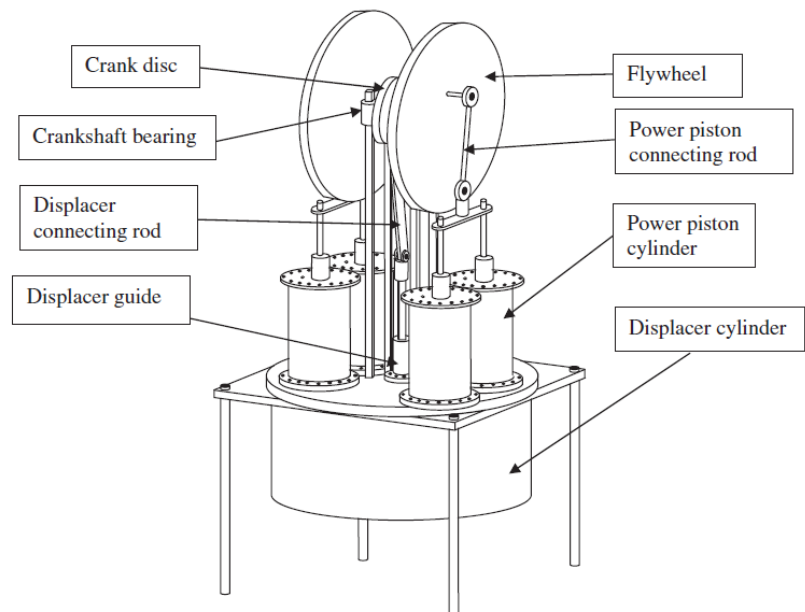
Sripakagorn and Srikam in [80] designed a prototype of a beta-type MTD Stirling engine, see Figure 2.9. It was designed with the use of an empirical formula and the simple method described by Urieli and Berchowitz in [18].

Design of a 5 kW free piston Stirling engine for the space application shown in Figure 2.10 was presented by Brandhorst and Chapman [81]. The design was considerably effected by the requirement for a lunar fission power source and the H-FAST code and 3D CFD modelling technique were used to derive design parameters. The predicted engine performance was compared with the result obtained using the Sage code. As a result, piston stokes of 22 mm and 24 mm were obtained for this 5 and 6 kW Stirling engine convertors, respectively.

Chapter 2



a) A schematic diagram of the two power piston Stirling engine



b) A schematic diagram of the four power piston Stirling engine

Figure 2.2 Schematic diagrams of two gamma-type Stirling engines [69]

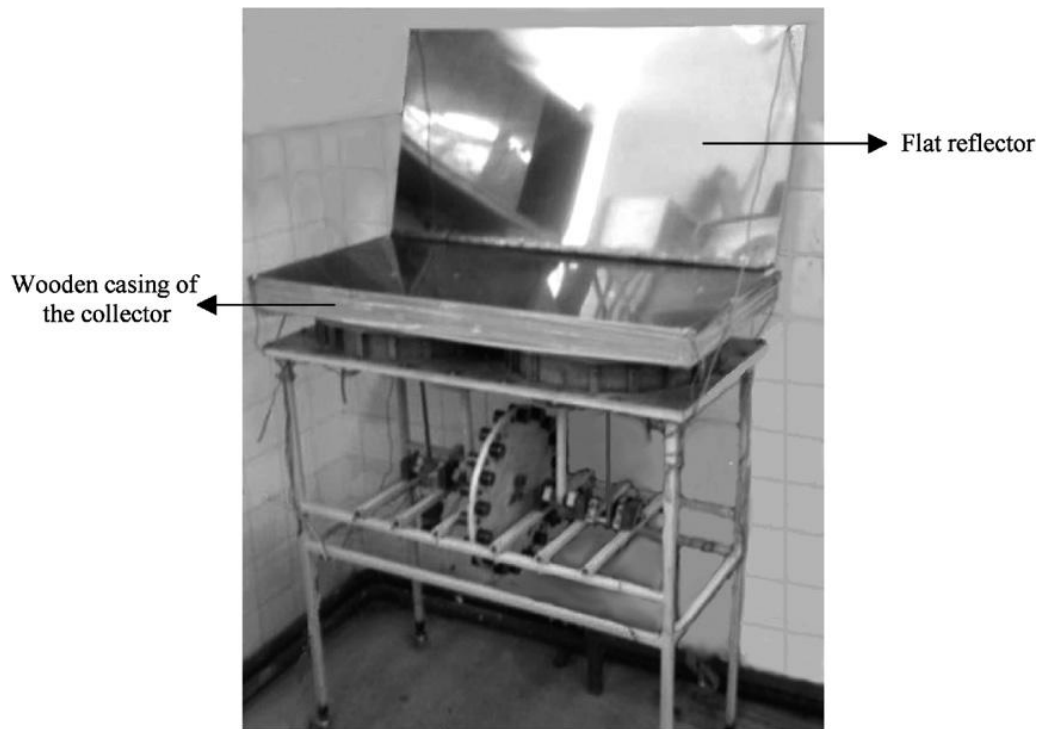


Figure 2.3 A LTD solar Stirling engine without a regenerator [72]

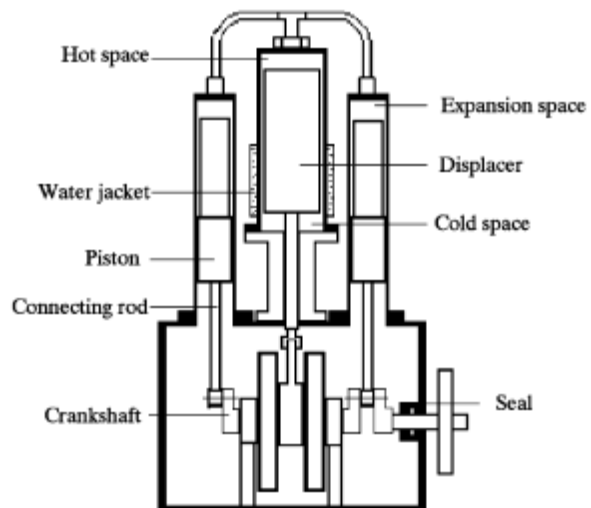


Figure 2.4 A schematic diagram of the gamma-type Stirling engine [73]

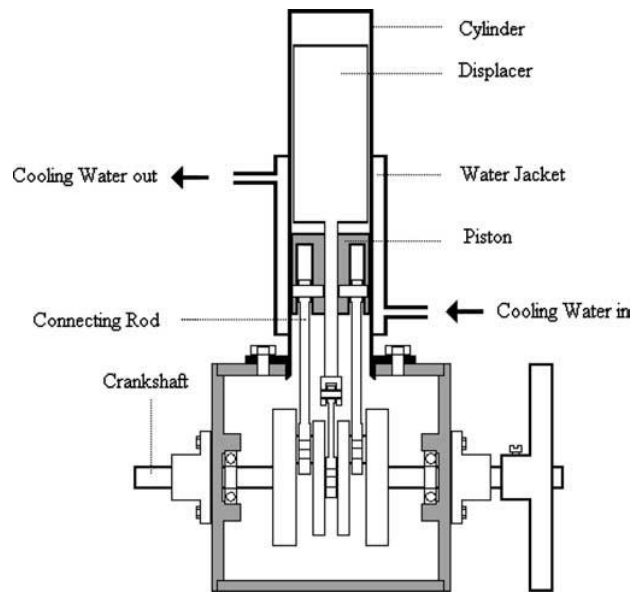


Figure 2.5 A schematic diagram of the beta-type Stirling engine [74]

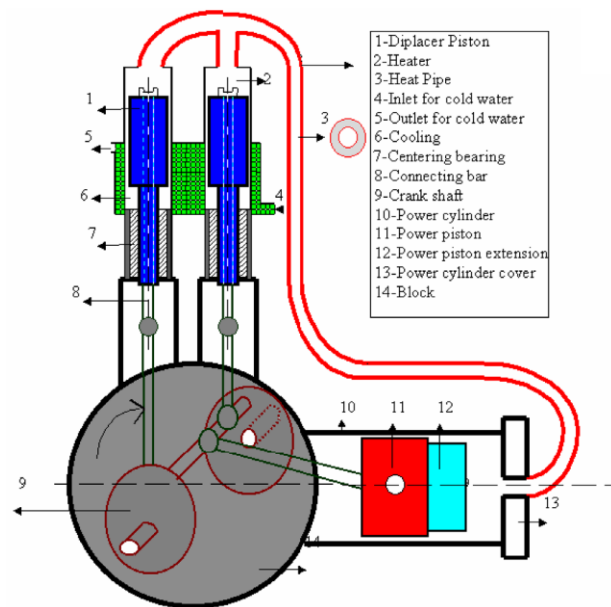


Figure 2.6 A schematic diagram of the manufactured Stirling engine with two displacer pistons [75]

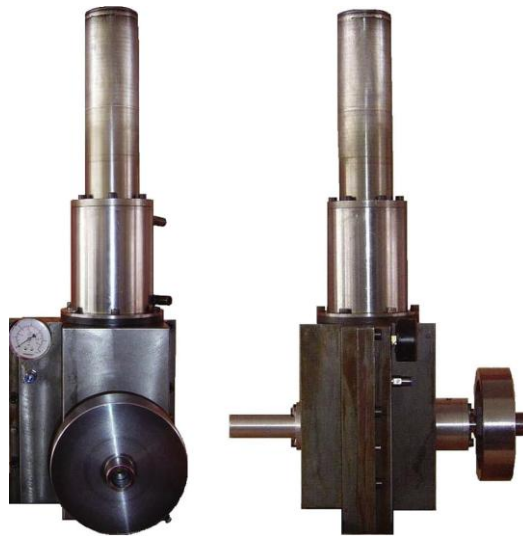


Figure 2.7 A beta-type Stirling engine [78]

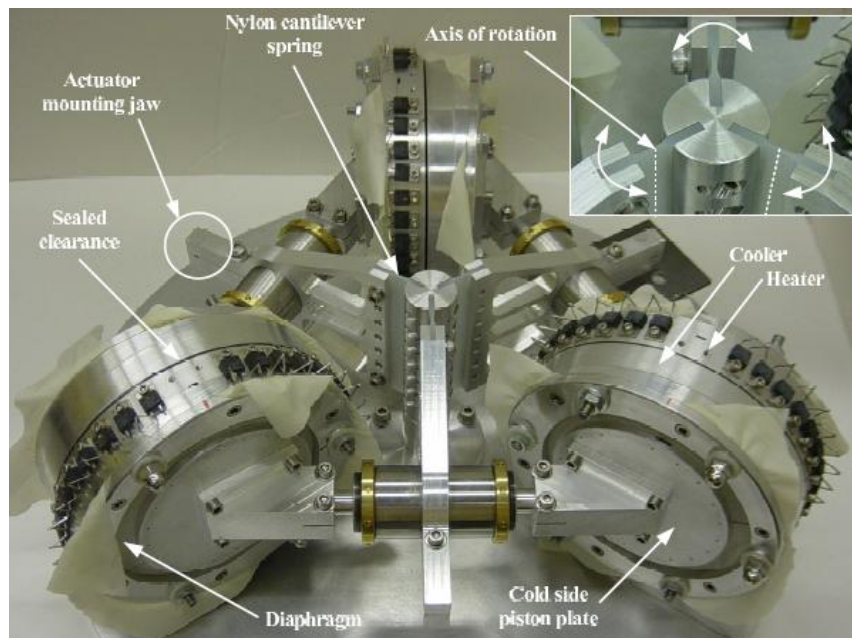


Figure 2.8 A multi-phase free piston Stirling engine [79]

Chapter 2

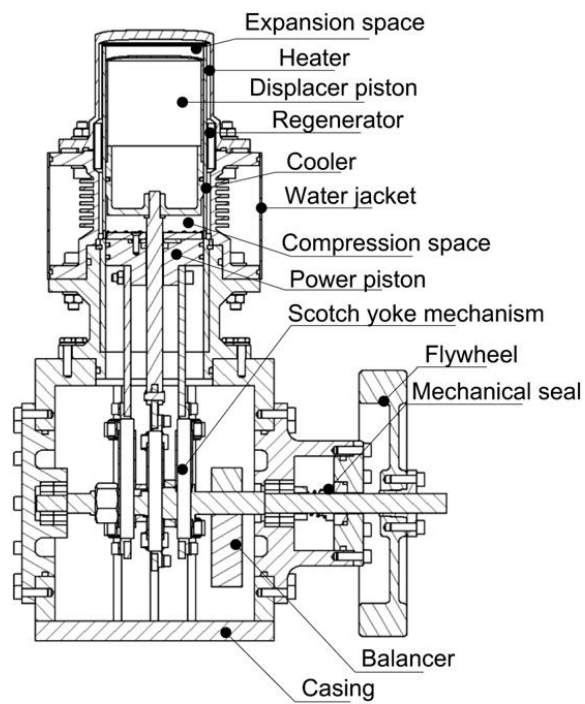


Figure 2.9 Details of a prototype of a Stirling engine [80]

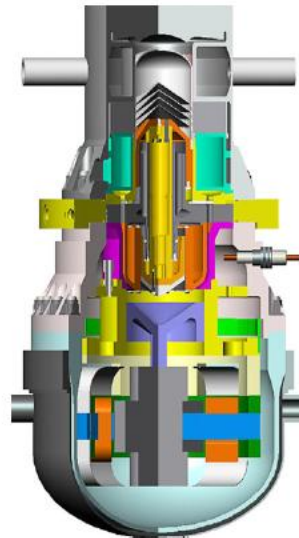


Figure 2.10 Cut-away view of the 5 kW demonstrational Stirling engine convertor

[81]

Chapter 2

2.5 Conclusions

From the literature review performed, it could be concluded that numerous second-order mathematical models were developed and used for the analysis of the working process and the prediction of Stirling engines performance. It can be explained by combination of the acceptable accuracy in prediction of results and the reasonable computing time required in simulations. The application of empirical modelling and the first-order model approach, though requires significantly less computing time, provides only the indicative prediction of engines performance. The third-order models and especially the multi-dimensional CFD modelling might provide much better understanding of the working process and more accurate prediction of the engine performance but these methods require significant computing power and time.

Furthermore, it was also demonstrated that the most of works conducted on the determination of optimal engine parameters used optimisation methods in which the deployed mathematical model provides a closed form solution for the engine power output or efficiency and these parameters then could be used as objective functions. Several studies, however, used the parametric analysis approach to obtain the optimal engine parameter using the high order models. The stochastic optimisation method with the random variables could also be the appropriate technique for engine optimisation when the high order mathematical models were used. It was also shown that the Genetic algorithm optimisation has been commonly used in designing heat engine and heat exchangers.

Chapter 2

A number of studies used the Stirling engine modelling to obtain the engine design specification and to produce engine prototypes. However, only few papers describe the design work for engine prototypes with the use of high order Stirling engine mathematical models which provide better accuracy in prediction of the engine performance. Even fewer are papers describing complete Stirling engine design procedures with the use of optimisation methods. Finally, it should be noted that the design procedures for Stirling engines taking the benefit of 3D CFD modelling were demonstrated only for conventional Stirling engines.

Therefore, in this work the focus will be on the development of advanced mathematical models considering various losses and coupled to the effective optimisation procedure such as GA method for determination of the design parameters of efficient solar-powered LTD and MTD Stirling engines.

In addition, the 3D CFD modelling will be performed for better understanding the working process of Stirling engines, analysis of operation of its components and for more accurate prediction of the engine.

Chapter 3

General principles of the second-order mathematical modelling of the LTD and conventional Stirling engines

In this chapter, the developed thermodynamic models of the LTD and conventional Stirling engines are presented. The physical models of Stirling engines being studied are described. The set of mathematical equations of the second-order modelling and numerical procedures used in simulations are explained.

3.1 The second-order mathematical modelling of the LTD Stirling engine

3.1.1 Physical model

The geometry of a LTD Stirling engine is quite similar to that of a conventional gamma-type Stirling engine. Figure 3.1 shows the schematic diagram of a gamma-type kinematical LTD Stirling engine and gas flow directions. The main components are as follows: the power piston and its cylinder; the displacer which separates the expansion space and the compression space in the hot cylinder; the hot plate installed at the bottom of the displacer cylinder and used to transfer heat from the heat source to the working gas in the expansion space; the cold plate installed at

Chapter 3

the top of the displacer cylinder and which is also a heat exchanger transferring heat from the working gas in the compression space to the heat sink; the regenerator placed inside the displacer; the transmission/drive mechanism; the flywheel. The flow of the gas is induced by the displacements of pistons. In this research, the physical dimensions and experimental data for a twin-power piston LTD Stirling engine described by Kongtragool and Wongwises in [70] are used to obtain and compare numerical results. This engine has two power pistons, each installed in its own cylinder, and one displacer with the built-in regenerator. The regenerator is made of the stainless steel mesh matrix. Two oil grooves are provided on the surface of the power pistons for purpose of lubrication. The displacer rod is equipped with two rubber seals for preventing a gas leakage. The appearance of this engine is shown in Figure 3.2 and the physical dimensions of this twin-power piston LTD Stirling engine are shown in Table 3.1.

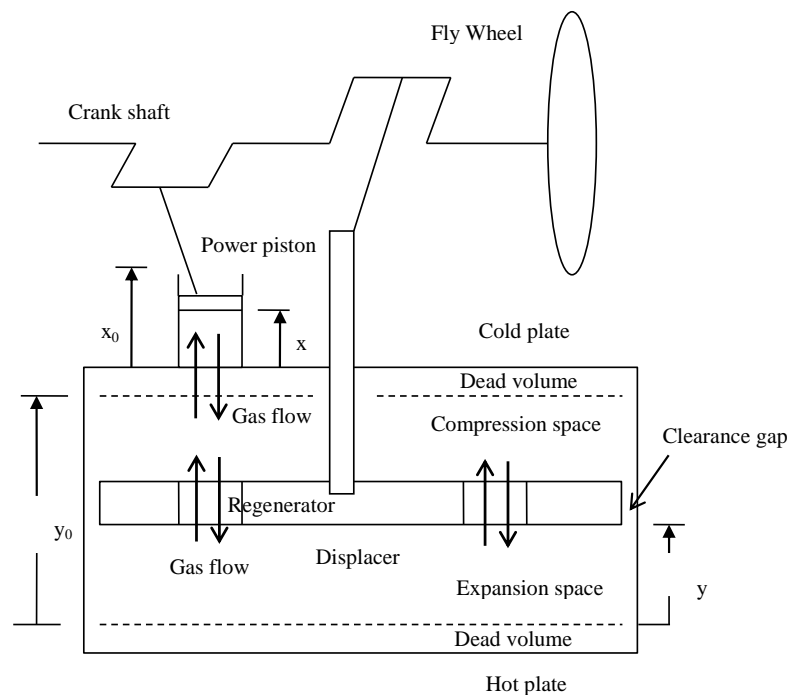


Figure 3.1 The schematic diagram of a gamma-type kinematical LTD Stirling engine

Chapter 3

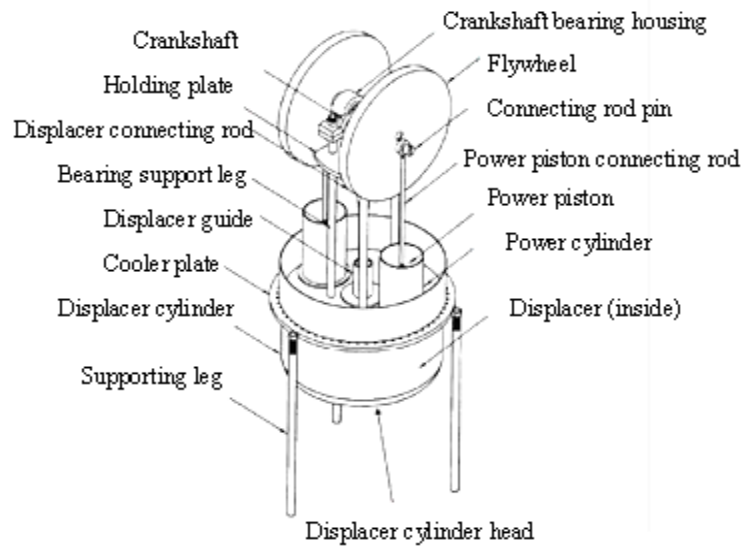


Figure 3.2 The schematic diagram of the twin-power piston LTD Stirling engine from Kongtragool and Wongwisues [70]

Table 3.1 The physical dimensions of the LTD Stirling engine for the numerical analysis from Kongtragool and Wongwisues [70]

The geometric data of the twin-power piston LTD Stirling engine	Value
working piston stroke (m)	0.0826
working piston diameter(m)	0.083
working piston swept volume (m ³)	893.8x10 ⁻⁶
displacer piston stroke (m)	0.0795
displacer piston diameter (m)	0.32
displacer piston swept volume (m ³)	6393.8 x10 ⁻⁶
swept volumes ratio	7.15
piston displacements phase angle (°)	90
displacer thickness (m)	0.075
length of the connecting rod of the power piston (m)	0.265
length of the connecting rod of the displacer (m)	0.185

Chapter 3

3.1.2 The second-order mathematical model

In order to analyse the working process and predict the LTD Stirling engine's performance the engine's internal gas circuit is split into several control volumes and the second-order type mathematical model has been developed which is based on the set of equations of energy and mass conservation and the equation of ideal gas written for each control volume. The thermodynamic model is modified version of that by Timoumi et al. [27] and Urieli [18]. The internal volume of the LTD Stirling engine is divided into three control volumes, namely the expansion space, the regenerator and the compression space, as shown in Figure 3.3. In the thermodynamic model, the work loss due to the pressure drop in the regenerator is taken into account. Moreover, the mechanical losses due to the friction in the mechanical drive mechanism are introduced into the equation of motion of the power piston, the displacer and the crankshaft [82-84].

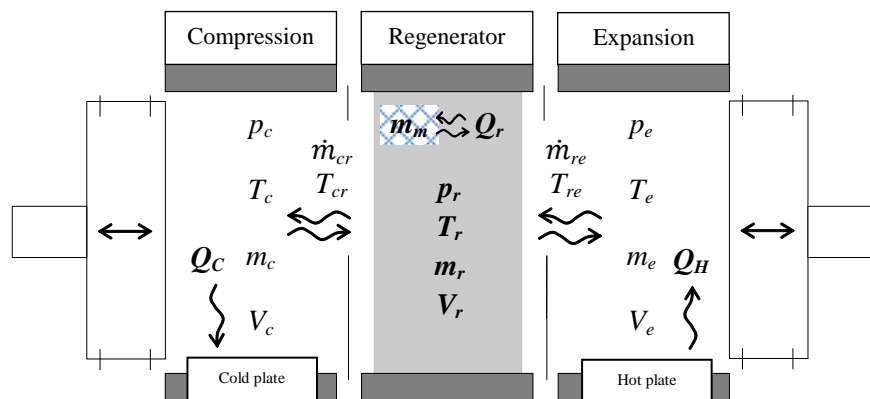


Figure 3.3 The calculation scheme of the LTD Stirling engine

Chapter 3

The main assumptions of the mathematical model are as follows:

1. The pressure in each control volume is identical.
2. There is no gas leakage between the power piston and its cylinder and in the rubber seal of the displacer rod.
3. There is no clearance gap between the displacer and its cylinder and therefore the working gas flows in the cylinder of the displacer only through the built-in regenerator.
4. The working fluid in the engine is considered to be a perfect gas. For the LTD engine the working fluid is air.
5. The side walls of the displacer and the power piston cylinders are insulated.
6. The engine operates under steady state conditions.

Taking into account the above assumptions, it is possible to derive all the equations describing the operation of the engine. The piston and the displacer displacements respectively can be expressed as follows:

$$x = \frac{x_0}{2} (1 + \cos(\theta - \varphi)) \quad (3.1)$$

$$y = \frac{y_0}{2} (1 + \cos \theta) \quad (3.2)$$

Chapter 3

where x is the piston displacement (m); x_0 is piston stroke (m); y is the displacer displacement (m); y_0 is the displacer stroke (m); θ is the piston crank angle and φ is the phase angle.

The volumes of the compression and expansion spaces, respectively, are calculated as

$$V_c = V_{d-c} + xA_P + (y_0 - y)A_D$$
$$V_c = V_{d-c} + \frac{V_{S-P}}{2}(1 + \cos(\theta - \varphi)) + \frac{V_{S-D}}{2}(1 - \cos \theta) \quad (3.3)$$

$$V_e = V_{d-e} + yA_D$$
$$V_e = V_{d-e} + \frac{V_{S-D}}{2}(1 + \cos \theta) \quad (3.4)$$

where V_c is volume of the compression space (m^3); V_{d-c} is dead volume of the compression space (m^3); V_e is volume of the expansion space (m^3); V_{d-e} is dead volume of the expansion space (m^3); V_{S-P} is swept volume of the power piston (m^3); V_{S-D} is swept volume of the displacer (m^3); A_P is contact area of the power piston (m^2); A_D is contact area of the displacer (m^2).

The derivative of volumes can be obtained as

$$\frac{dV_c}{dt} = -\frac{V_{S-P}}{2}\omega \sin(\theta - \varphi) + \frac{V_{S-D}}{2}\omega \sin \theta \quad (3.5)$$

$$\frac{dV_e}{dt} = -\frac{V_{S-D}}{2}\omega \sin \theta \quad (3.6)$$

where ω is angular velocity (rad/s) and t is time.

Chapter 3

The temperature of the gas mass flow between the compression space and the regenerator is defined as follows:

$$T_{c-r} = T_c \quad \text{if} \quad \dot{m}_{c-r} > 0;$$

$$T_{c-r} = T_r \quad \text{if} \quad \dot{m}_{c-r} \leq 0,$$

where \dot{m}_{c-r} is gas mass flow rate between the compression and the regenerator spaces (kg/s); T_c is the temperature of the gas in the compression space (K); T_r is the temperature of the gas in the regenerator space (K); T_{c-r} is the temperature of gas mass flow between the compression and the regenerator spaces (K).

The temperature of the gas mass flow between the regenerator and compression spaces is found in a similar way:

$$T_{r-e} = T_r \quad \text{if} \quad \dot{m}_{r-e} > 0;$$

$$T_{r-e} = T_e \quad \text{if} \quad \dot{m}_{r-e} \leq 0.$$

Here \dot{m}_{r-e} is the gas mass flow rate between the regenerator and compression spaces (kg/s); T_e is the gas temperature in the expansion space (K); T_{r-e} is the temperature of gas mass flow between the regenerator and the expansion spaces (K).

The energy conservation equations

The energy conservation equations for the compression, regenerator and expansion spaces, respectively, can be expressed by the following equations:

Chapter 3

$$C_v \frac{d(m_c T_c)}{dt} = dQ_c - \frac{dW_c}{dt} - \dot{m}_{c-r} C_p T_{c-r} \quad (3.7)$$

$$C_v \frac{d(m_r T_r)}{dt} = dQ_r - dQ_{loss,disip-r} + \dot{m}_{c-r} C_p T_{c-r} - \dot{m}_{r-e} C_p T_{r-e} \quad (3.8)$$

$$C_v \frac{d(m_e T_e)}{dt} = dQ_H - \frac{dW_e}{dt} + \dot{m}_{r-e} C_p T_{r-e} \quad (3.9)$$

Here m_c , m_r , and m_e are the gas masses in the compression, regenerator and expansion spaces, respectively (kg); Q_c , Q_r and Q_H are the heat flow rates in the cooler, the regenerator and the heater, respectively (W); $Q_{loss,disip-r}$ is the heat loss due to the presence of the flow friction in the regenerator (W); W_c and W_e are works done on or by the gas in the compression and expansion spaces, respectively (J).

The work done on or by the working gas inside the compression space and the expansion space can be calculated as $\frac{dW_c}{dt} = p_c \frac{dV_c}{dt}$ and $\frac{dW_e}{dt} = p_e \frac{dV_e}{dt}$, respectively. Using the ideal gas state equation ($pV = mRT$) and the properties of the gas ($R = C_p - C_v$ and $\gamma = \frac{C_p}{C_v}$) Eq. 3.7 and Eq. 3.9 can be used for the determination of gas mass flow rates across the corresponding control volume as follows:

$$\dot{m}_{c-r} = -\frac{1}{RT_{c-r}} \left(-\frac{R}{C_p} dQ_c + p_c \frac{dV_c}{dt} + \frac{V_c}{\gamma} \frac{dp}{dt} \right) \quad (3.10)$$

$$\dot{m}_{r-e} = \frac{1}{RT_{r-e}} \left(-\frac{R}{C_p} dQ_H + p_e \frac{dV_e}{dt} + \frac{V_e}{\gamma} \frac{dp}{dt} \right) \quad (3.11)$$

Chapter 3

Here R is the gas constant; C_p is the specific heat at constant pressure (J/ kgK); C_v is the specific heat at constant volume (J/ kgK); p is the gas pressure inside the engine (Pa); p_c and p_e are the gas pressure in the compression and expansion spaces, respectively (Pa).

If the energy conservation equations for each space are added up then the pressure derivative equation can be expressed as

$$\frac{dp}{dt} = \frac{1}{C_v V_T} \left(R(dQ_H + dQ_r + dQ_C - dQ_{loss,disip-r}) - C_p \left(p_c \frac{dV_c}{dt} + p_e \frac{dV_e}{dt} \right) \right) \quad (3.12)$$

where V_T is the total gas volume of the engine (m³).

In addition to the energy equations written for each space in the engine, the energy conservation equation for the regenerator matrix is used:

$$m_m C_p \frac{dT_m}{dt} = -dQ_r \quad (3.13)$$

The temperature of the regenerator matrix can then be obtained as

$$\frac{dT_m}{dt} = \frac{1}{m_m C_p} (-dQ_r) \quad (3.14)$$

Here m_m and T_m is the mass (kg) and temperature (K) of the regenerator matrix, respectively.

The mass conservation equations

The conservation of mass in each control volume can be written as follows:

Chapter 3

$$\frac{dm_c}{dt} = -\dot{m}_{c-r} \quad (3.15)$$

$$\frac{dm_r}{dt} = \dot{m}_{c-r} - \dot{m}_{r-e} \quad (3.16)$$

$$\frac{dm_e}{dt} = \dot{m}_{r-e} \quad (3.17)$$

The state equation of the ideal gas

From the equation of ideal gas state, the temperature of the gas inside the compression, regenerator and expansion spaces, respectively, can be calculated using the following equations:

$$T_c = \frac{p_c V_c}{Rm_c} \quad (3.18)$$

$$T_r = \frac{p_r V_r}{Rm_r} \quad (3.19)$$

$$T_e = \frac{p_e V_e}{Rm_e} \quad (3.20)$$

where V_r and p_r are the gas volume (m^3) and gas pressure (Pa) in the regenerator space.

The pressure drop occurs as the working gas flows through the regenerator. Such the pressure drop results in the reduction of the work output. The pressure drop in the regenerator can be calculated as in [27, 85]:

$$\Delta p = -\frac{2f_r \mu UV}{A_{free} d_h^2} \quad (3.21)$$

Chapter 3

here Δp is pressure drop (Pa); f_r is Reynolds friction coefficient which is the product of the friction factor, f_c , and the Reynolds number, Re ; μ is the gas dynamic viscosity (Pa.s); U is the fluid velocity (m/s); V is the corresponding volume (m³); A_{free} is the free flow area (m²) and d_h is the hydraulic diameter (m).

The heat generated in the regenerator by the friction flow is given by Tliti et al. [26] and Timoumi et al. [27]:

$$Q_{loss,disip} = \frac{\Delta p \dot{m}}{\rho} \quad (3.22)$$

where $Q_{loss,disip}$ is heat loss due to the flow friction (W); \dot{m} is mass flow rate (kg/s); ρ is density (kg/m³).

In this second-order model, the pressure in the compression space is defined as the pressure calculated using Eq. 3.12. Therefore, the pressure in the regenerator and in the expansion space can be determined as

$$p_r = p_c + \frac{\Delta p_r}{2} \quad (3.23)$$

$$p_e = p_r + \frac{\Delta p_r}{2} \quad (3.24)$$

where Δp_r is pressure drop produced in the regenerator (Pa).

Heat transfer in each space can be calculated as

$$dQ_H = h_H A_{h-H} (T_H - T_e) \quad (3.25)$$

$$dQ_r = e_{eff} h_m A_{h-m} (T_m - T_r) \quad (3.26)$$

Chapter 3

$$dQ_C = h_C A_{h-c} (T_C - T_c) \quad (3.27)$$

where e_{eff} is the effectiveness of the regenerator; h_H , h_m and h_C are the heat transfer coefficient on the surface of the heater, the regenerator matrix and the cooler, respectively ($\text{W}/\text{m}^2\text{K}$); T_H and T_C are the temperature of the heater and cooler, respectively (K); A_{h-H} is the heat transfer area of the heater (m^2); A_{h-C} is the heat transfer area of the cooler (m^2); A_{h-m} is the heat transfer area of the matrix (m^2).

The surface temperature of the thin hot plate heated with the solar irradiation can be determined by the following equation, which takes into account heat losses due to the convection (with the heat transfer coefficient of $4 \text{ W}/\text{m}^2\text{K}$) and the heat radiation into the atmosphere [86]:

$$\alpha \dot{Q}_i = \varepsilon \sigma (T_H^4 - T_0^4) + h_0 (T_H - T_0) + h_H (T_H - T_e) \quad (3.28)$$

where \dot{Q}_i is solar irradiation (W/m^2); $\alpha=0.96$ and $\varepsilon=0.8$ are the absorption and the emissivity of the hot plate with its the surface coated with black lacquer [87]; h_0 is the heat transfer coefficient on the external surface of the heater ($\text{W}/\text{m}^2\text{K}$); T_0 is the ambient temperature (K).

The heat transfer coefficients between the plate and the working gas in the expansion and the compression spaces can be defined in the same way as the heat transfer in the cylinder of a reciprocating engine given by Eichelberg [88]:

$$h = 2.43 V_P^{1/3} (p_{inst} T_g)^{1/2} \quad (3.29)$$

Chapter 3

Here h is the heat transfer coefficient ($\text{W}/\text{m}^2\text{K}$); V_P is the mean piston speed (m/s); p_{inst} is the instantaneous cylinder pressure (bar); T_g is the working gas temperature (K).

The average heat transfer coefficient between the matrix and the working gas in the regenerator is given by Tanaka et al. [85]:

$$\overline{Nu} = 0.33\overline{Re}^{0.67} \quad (3.30)$$

$$NTU = \frac{4\overline{Nu}H_D}{Pr\overline{Re}d_h} \quad (3.31)$$

$$\overline{h}_m = \frac{NTUC_p\overline{m}}{A_{h-m}} \quad (3.32)$$

In Equations 3.30-3.32 \overline{Nu} is the mean Nusselt number; \overline{Re} is the mean Reynolds number based on the mean piston speed; NTU is the number of transfer units; H_D is the thickness of the regenerator (m); Pr is the Prandtl number; \overline{h}_m is the mean heat transfer coefficient on the surface of the matrix ($\text{W}/\text{m}^2\text{K}$); A_{h-m} is the heat transfer area in the matrix (m^2).

The effectiveness of the heat exchange in the regenerator is

$$e_{eff} = \frac{NTU}{NTU + 2} \quad (3.33)$$

The instantaneous indicated work output in the engine can be calculated in the following form:

$$\frac{dW_i}{dt} = \frac{dW_c}{dt} + \frac{dW_e}{dt} = p_c \frac{dV_c}{dt} + p_e \frac{dV_e}{dt} \quad (3.34)$$

Chapter 3

Thus, the cyclic indicated work, W_i (J) is

$$W_i = \oint \left(\frac{dW_i}{dt} \right) dt = \int_0^{\tau} \left(\frac{dW_c}{dt} + \frac{dW_e}{dt} \right) dt = \int_0^{\tau} \left(p_c \frac{dV_c}{dt} + p_e \frac{dV_e}{dt} \right) dt \quad (3.35)$$

The indicated power, P_i (W) is

$$P_i = W_i f \quad (3.36)$$

where f is the frequency (Hz).

In order to calculate the brake cyclic power, the kinetic analysis of the mechanical transmission system of the reciprocating engine given by Hesterman and Stone [82] is used in this work and in order to include the effect of the friction forces acting in the drive mechanism, the kinetic motion equations given by Guzzomi et al. [83, 84] are employed in this study. The free body diagram of the mechanism of the transmission of the reciprocating engine is shown in Figure 3.4. The angle, β , and the angular velocity, $\dot{\beta}$, of crankshaft are defined as

$$\beta = \theta - \pi \quad (3.37)$$

$$\dot{\beta} = \dot{\theta} \quad (3.38)$$

The piston's load along the cylinder axis is

$$Q_{pi}(t) = \left(F_r + \mu_{k-pi} |S_{pi}| + F_{Load} \right) \quad (3.39)$$

Here $Q_{pi}(t)$ is the piston load along the cylinder axis (N); F_r is the friction force in the ring package of the piston (N); μ_{k-pi} is the coefficient of friction in the piston-

Chapter 3

cylinder coupling; S_{pi} is the side force acting on the piston (N); F_{Load} is the external load (N). The external load acting on the piston is defined as

$$F_{Load-P} = p_c A_p - p_a A_p \quad (3.40)$$

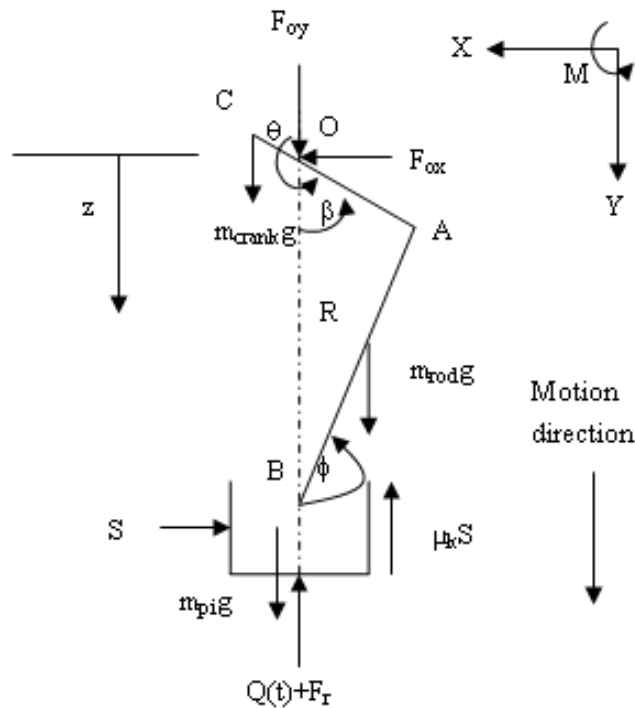


Figure 3.4 The diagram of the power transmission mechanism of a reciprocating engine

And the external load acting on the displacer is

$$F_{Load-D} = p_e A_{D-e} - p_c A_{D-c} \quad (3.41)$$

Here p_a is the ambient pressure (Pa); A_{D-e} and A_{D-c} are the contact areas of the displacer in the expansion and compression spaces, respectively (m^2).

Chapter 3

The radial forces in the crankshaft and the side force on the piston's surface at the constant engine speed can be expressed as in [83]:

$$F_{Ox} = -r\dot{\beta}^2 \sin\beta (m_{crank} h_{pi} - m_{rod}(l-j)) + S_{pi} \quad (3.42)$$

$$F_{Oy} = r\dot{\beta}^2 \left[m_{pi} \left(\frac{r \cos^2 \beta}{l_{rod} \cos^3 \phi} - \sin \beta \tan \phi - \cos \beta \right) + m_{rod} \left(\frac{jr \cos^2 \beta}{l_{rod} \cos^3 \phi} - j \sin \beta \tan \phi - \cos \beta \right) + m_{crank} L \cos \beta \right] - g(m_{pi} + m_{rod} + m_{crank}) + F_r + \mu_{k-pi} |S_{pi}| + p_g A_{pi} - p_a A_{pi} \quad (3.43)$$

$$S_{pi} = \frac{\left\{ \begin{array}{l} -r\dot{\beta}^2 \left[\frac{I_{rod}}{(l_{rod} \cos \phi)^2} \left(\frac{r \cos^2 \beta \tan \phi}{l_{rod} \cos \phi} - \sin \beta \right) \right. \\ \left. + m_{pi} \tan \phi \left(\frac{r \cos^2 \beta}{l_{rod} \cos^3 \phi} - \sin \beta \tan \phi - \cos \beta \right) \right. \\ \left. + j m_{rod} \left(\frac{jr \cos^2 \beta \tan \phi}{l_{rod} \cos^3 \phi} - \cos \beta \tan \phi + \sin \beta - \frac{j \sin \beta}{\cos^2 \phi} \right) \right] \\ \left. + g \tan \phi (m_{pi} + j m_{rod}) - F_r \tan \phi - p_g A_{pi} \tan \phi + p_a A_{pi} \tan \phi \right\}}{D_{pi}} \quad (3.44)$$

Here A_{pi} is the contact area of the piston (m^2); F_{ox} and F_{oy} are the forces acting on the crankshaft in the x- and y-direction, respectively (N); g is the gravitational acceleration (m/s^2); I_{rod} is the inertia of the connecting rod ($kg.m^2$); J is the ratio of the AR and AB lengths (as shown in Figure 3.4); l_{rod} is length of the connecting rod (m); L is the ratio of the OC and OA lengths (as shown in Figure 3.4); m_{pi} is the mass of the piston (kg); m_{crank} is the mass of the crank in the power piston connection (kg); m_{rod} is the mass of the connecting rod in the power piston connection (kg); r is the crank throw (OA) in the piston connection (m).

Chapter 3

D_{pi} can be calculated as

$$D_{pi} = l + \mu_{k-pi} \tan \phi \quad \begin{cases} \dot{z}_{pi} \geq 0, & S_{pi} \geq 0 \\ \dot{z}_{pi} < 0, & S_{pi} < 0 \end{cases}$$

$$D_{pi} = l - \mu_{k-pi} \tan \phi \quad \begin{cases} \dot{z}_{pi} \geq 0, & S_{pi} < 0 \\ \dot{z}_{pi} < 0, & S_{pi} \geq 0 \end{cases}$$

where $\mu_{k-pi} = 0.3$ is the coefficient of friction between the piston surface and the cylinder, lubricated with oil; \dot{z}_{pi} is the velocity of piston stroke (m/s).

The frictional force in the sealing rings of the displacer rod is given by Novikov cited in [29]:

$$F_r = F_{frs1} + F_{frs2} \quad (3.45)$$

in which F_{frs1} and F_{frs2} are the frictional forces (N) in the first and second sealing rings, respectively.

If $p_c \geq p_{br}$

$$F_{frs1} = \mu_{sd} \pi H \left((p_c + p_{spr}) d'_s - 0.9 \bar{p}_{es1} d_s \right) \quad (3.46)$$

if $p_c \leq p_{br}$

$$F_{frs1} = \mu_{sd} \pi H \left((p_{br} + p_{spr}) d'_s - 0.9 \bar{p}_{es1} d_s \right) \quad (3.47)$$

if $p_{br} \geq p_{c-c}$

$$F_{frs2} = \mu_{sd} \pi H \left((p_{br} + p_{spr}) d'_s - 0.9 \bar{p}_{es2} d_s \right) \quad (3.48)$$

if $p_{br} \leq p_{c-c}$

$$F_{frs2} = \mu_{sd} \pi H \left((p_{c-c} + p_{spr}) d'_s - 0.9 \bar{p}_{es2} d_s \right) \quad (3.49)$$

Chapter 3

where d_s is the displacer rod diameter (m); d'_s is the internal diameter of the sealing ring (m); H is the height of the sealing ring (m); p_{br} is the pressure of the gas between the first and second sealing rings (Pa); $p_{spr}=0.005$ MPa is the additional pressure upon the sealing rings; p_{c-c} is the gas pressure in the crankcase (Pa); \bar{p}_{es1} is the average gas pressure on the external surface of the first ring (Pa); \bar{p}_{es2} is the average gas pressure on the external surface of the second ring (Pa); $\mu_{sd} = 0.3$ is the coefficient of the friction between the sealing ring and the displacer rod guide.

The gas pressure between the first and the second seals can be calculated as

$$p_{br} = \frac{1}{2}(p_{c-c} + p_c) \quad (3.50)$$

The pressure on the external side surface of the rings can be assumed to have the linear distribution:

$$\bar{p}_{es1} = \frac{1}{2}(p_c + p_{br}) \quad (3.51)$$

$$\bar{p}_{es2} = \frac{1}{2}(p_{c-c} + p_{br}) \quad (3.52)$$

To determine the brake power of the engine, the total torque on the crank shaft must be calculated. The gamma-type kinematic Stirling engine has two pistons connected to the crankshaft, the power piston and the displacer. The work exerted by the power piston is transferred to the crankshaft and the flywheel. The flywheel then will transfer accumulated energy back to the working gas to maintain its reciprocating with the assistance from the displacer piston. Thus, the total torque in the crankshaft can be calculated as

Chapter 3

$$Tor_T = \Sigma Tor \quad (3.53)$$

where Tor_T and Tor are total and piston torques (Nm), respectively.

The torque from each power piston and displacer (Tor) at the constant engine speed can be obtained using the following equation [84]:

$$Tor = \frac{I}{2} \dot{\beta}^2 I'(\beta) + g(\beta) + Q(t, \beta) \quad (3.54)$$

where $I'(\beta)$ is the rate of change in inertia,

$$\begin{aligned} I'(\beta) = & 2I_{rod} E(\mu_{k-pi}) \left(\frac{r \cos \beta}{l_{rod} \cos \phi} \right)^2 \left(\frac{r \cos \beta}{l_{rod} \cos \phi} \tan \phi - \tan \beta \right) \\ & + 2m_{pi} r^2 (E(\mu_{k-pi}) \cos \beta \tan \phi - \sin \beta) \left(\frac{r \cos^2 \beta}{l_{rod} \cos^3 \phi} - \cos \beta - \sin \beta \tan \phi \right) \\ & - 2m_{rod} r^2 (1-j)^2 \sin \beta \cos \beta + 2m_{rod} r^2 (j E(\mu_{k-pi}) \cos \beta \tan \phi - \sin \beta) \\ & \left(\frac{j r \cos^2 \beta}{l_{rod} \cos^3 \phi} - \cos \beta - j \sin \beta \tan \phi \right) \end{aligned} \quad (3.55)$$

and $g(\beta)$ is the gravity torque:

$$g(\beta) = gr \left[\begin{array}{l} m_{pi} (E(\mu_{k-pi}) \cos \beta \tan \phi - \sin \beta) + m_{rod} (j E(\mu_{k-pi}) \cos \beta \tan \phi - \sin \beta) \\ + m_{crank} L \sin \beta \end{array} \right] \quad (3.56)$$

The gravity torque value is additionally influenced by the value of the friction between piston and cylinder surface which is not zero over the cycle. This results in the cyclic gravity torque to be non-zero.

Chapter 3

The loading torque ($Q(t, \beta)$) on the piston is

$$Q(t, \beta) = (F_r + F_{Load})r (E(\mu_{k-pi}) \cos \beta \tan \phi - \sin \beta) \quad (3.57)$$

Here

$$E(\mu_{k-pi}) = \frac{1 + \mu_{k-pi} \tan \beta}{1 + \mu_{k-pi} \tan \phi} \begin{cases} \dot{z}_{pi} \geq 0, & S_{pi} \geq 0 \\ \dot{z}_{pi} < 0, & S_{pi} < 0 \end{cases}$$

$$E(\mu_{k-pi}) = \frac{1 - \mu_{k-pi} \tan \beta}{1 - \mu_{k-pi} \tan \phi} \begin{cases} \dot{z}_{pi} \geq 0, & S_{pi} < 0 \\ \dot{z}_{pi} < 0, & S_{pi} \geq 0 \end{cases}$$

The method for calculation of the friction force in the seal ring package is presented in [29]. The mechanical loss due to the friction in the rolling bearing is determined as

$$Tor_B = \mu_{k-B} F_O \frac{D_B}{2} \quad (3.58)$$

where Tor_B is loss in the rolling bearing loss (Nm); $\mu_{k-B} = 0.0015$ is the coefficient of the friction in the ball bearing; D_B is the bearing diameter (m); F_O is the absolute force acting upon the ball bearing (N).

Absolute force acting upon the ball bearing can be calculated as

$$\vec{F}_O = \vec{F}_{O-P} + \vec{F}_{O-D} \quad (3.59)$$

Here \vec{F}_{O-P} is the total force vector acting upon the crankshaft from the power piston side (N); \vec{F}_{O-D} is the total force vector acting upon the crankshaft from the displacer side (N).

The cyclic brake work, W_b (J), is then

$$W_b = \oint \left(\frac{dW_b}{dt} \right) dt = \int_0^\tau \left(Tor_T - Tor_B \right) \frac{d\theta}{dt} dt \quad (3.60)$$

Chapter 3

Finally, the cyclic brake power, P_b (W), can be calculated as

$$P_b = W_b f \quad (3.61)$$

3.1.3 Numerical simulation procedure

For the numerical simulations using the above described equations, a computer program was written in MATLAB. The flowchart of numerical simulations is shown in Figure. 3.5. Data on the engine parameters is used as input data in the beginning of calculations. At the start of modelling operating the temperature of the gas in the compression space was set to be equal to that of the constant temperature of the cold plate and the temperature of the gas in the expansion space was set to be equal to the temperature of the hot plate. The classical fourth-order Runge-Kutta method of integration was used for numerical solution of a set of differential equations (Eq.3.12 and Eq.3.14-3.17) in order to obtain the pressure in the compression space and the gas mass in each space and the temperature of the matrix in the regenerator. After that the pressure drop in the regenerator and the heat transfer coefficients on all surfaces such as the hot and cold plates and the matrix were calculated to determine the heat transfer rates. The gas temperature in each space was calculated using the equations of ideal gas (Eq.3.18-3.20). The total torque of crankshaft was obtained using Eq.3.37- Eq.3.61. The calculations with 1000 time steps per cycle were performed continuously until reaching the steady state condition. Finally, the engine performance such as the cyclic indicated power and the cyclic brake power were obtained.

As an example, Appendix A contains MATLAB codes for the second-order mathematical modelling and optimization of LTD Stirling engines.

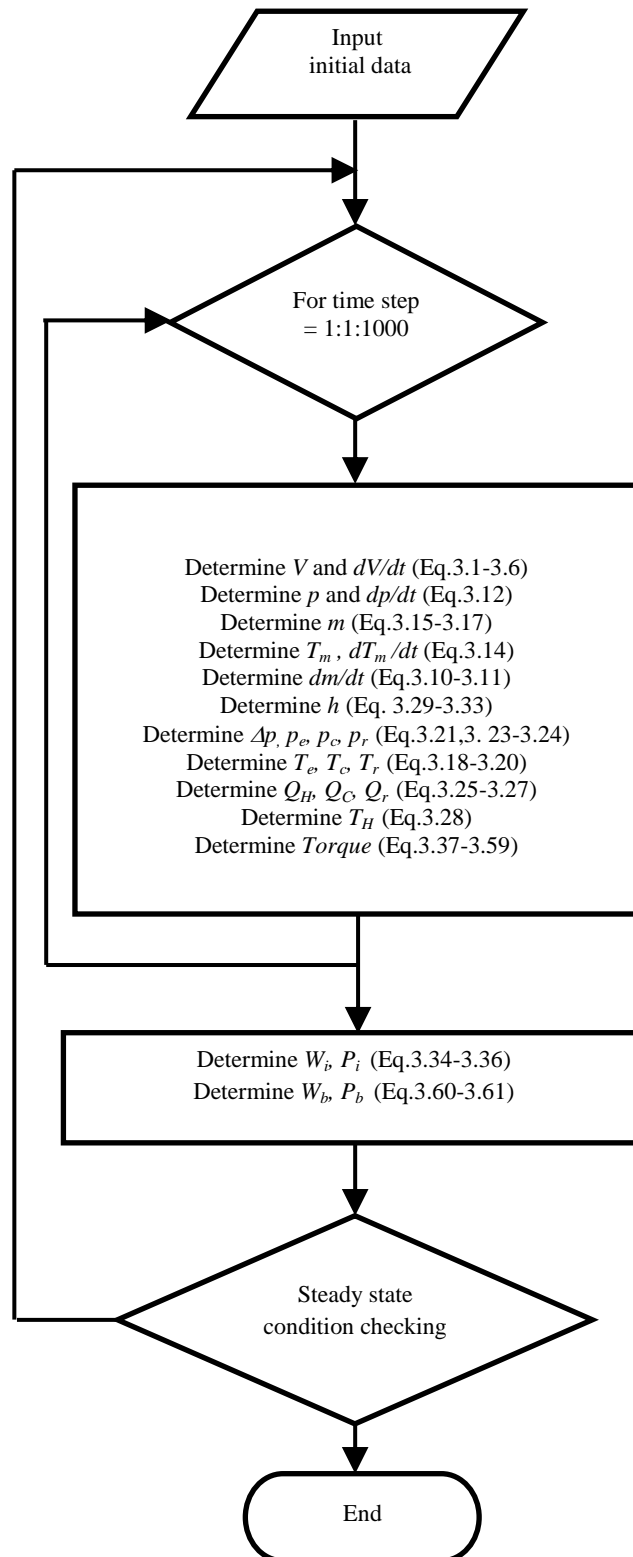


Figure 3.5 The flowchart of the second-order mathematical modelling of the LTD Stirling engine

Chapter 3

3.2 The second-order mathematical model of the conventional Stirling engines

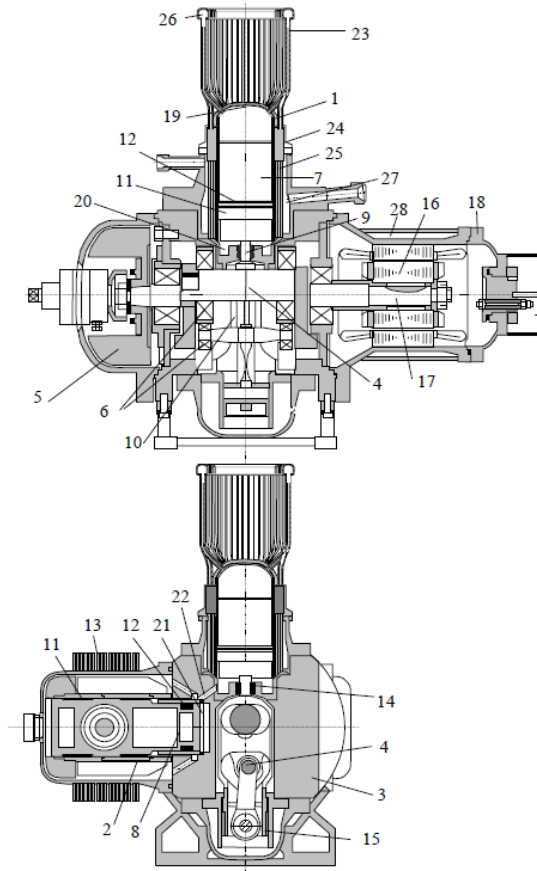
3.2.1 Physical model

The conventional gamma-type Stirling engine is more complicated than the LTD Stirling engine. The heater and cooler sections of the engine are made as the conventional heat exchangers. The small conventional gamma Stirling engine [14] which is installed on the test rig at Northumbria University is used for mathematical modelling purposes. Its cross-section is shown in Figure 3.6. The main parts of this engine are: the power piston made of aluminium alloy; the titanium alloy displacer; the drive mechanism which consists of connecting rods and a crankshaft on the bearings; the tubular basket-type heater; the cooler made of a bank of copper tubes; the co-axial regenerator which contains the stainless steel mesh; the pressurised crankcase which supports the hot and cold cylinders; the water jackets in the casing.

Pistons have guiding and sealing rings which are made of fluoroplastic material. The Stirling engine is coupled to a three-phase induction alternator for the electricity generation of 400 W.

The expansion space is defined to be the volume of the hot cylinder above the displacer. The compression space of the engine is composed of two parts connected to each other through the channels in the crankcase. The first part is formed by the cold cylinder and the power piston. The second part is the volume of the hot cylinder which is located below the displacer. The physical dimensions of the engine are shown in Table 3.2.

Chapter 3



- | | |
|--|---|
| 1-hot cylinder | 17-shaft of the drive mechanism |
| 2-cold cylinder | 18-sealed casing |
| 3-pressurised crankcase | 19-expansion space which is above the displacer |
| 4-crankshaft drive mechanism | 20-first part of the compression space which is below the displacer |
| 5-flywheel | 21-second part of the compression space |
| 6-rolling bearings | 22-connecting channel between two parts of the compression space |
| 7-displacer | 23-turbular basket type heater |
| 8-power piston | 24-axial regenerator |
| 9, 10-connecting rods | 25-tubular cooler |
| 11, 12-sealing rings | 26-collector |
| 13-fins | 27-water jacket for the tubular cooler |
| 14-sealing of the displacer rod | 28-water jacket for the alternator |
| 15-piston for unloading the displacer from side forces | |
| 16-three-phase induction alternator | |

Figure 3.6 The cross-section of the small conventional gamma Stirling engine [14]

Chapter 3

Table 3.2 The physical dimensions of the small conventional gamma Stirling engine

[14]

Parameters	Value
stroke of the power piston (m)	0.025
diameter of the power piston (m)	0.062
swept volume of power piston (m ³)	75.4768x10 ⁻⁶
stroke of the displacer piston (m)	0.025
diameter of the displacer piston (m)	0.062
swept volume of the displacer piston (m ³)	75.4768x10 ⁻⁶
swept volume ratio	1
pistons displacement phase angle (°)	90
diameter of the heater tube (m)	0.003
number of the heater tubes	20
number of the heater tube rows	1
length of the heater tube (m)	0.24
cooler tube diameter (m)	0.0012
number of cooler tubes	154
number of cooler tubes row	2
length of the cooler tube (m)	0.05
diameter of the regenerator chamber (m)	0.08
length of the regenerator (m)	0.04
number of regenerators	1

Chapter 3

3.2.2 The second-order mathematical model

The mathematical model which is used for the description of the working process of the conventional Stirling engines is similar to the developed mathematical model of the LTD Stirling engine. The gas circuit inside the engine is split into several control volumes and the energy and mass conservation equations are applied to each of the control volumes. The system of equations describing the operation of the engine also includes the ideal gas state equation. In this work the second-order mathematical model of Stirling engines developed by Timoumi et al. [27] and Urieli [18] is modified by splitting the regenerator into further several control volumes. The split of the engine's gas circuit into control volumes is shown in Figure 3.7. The control volumes considered are the compression space, the cooler space, ten volumes of the regenerator space, the heater space and the expansion space.

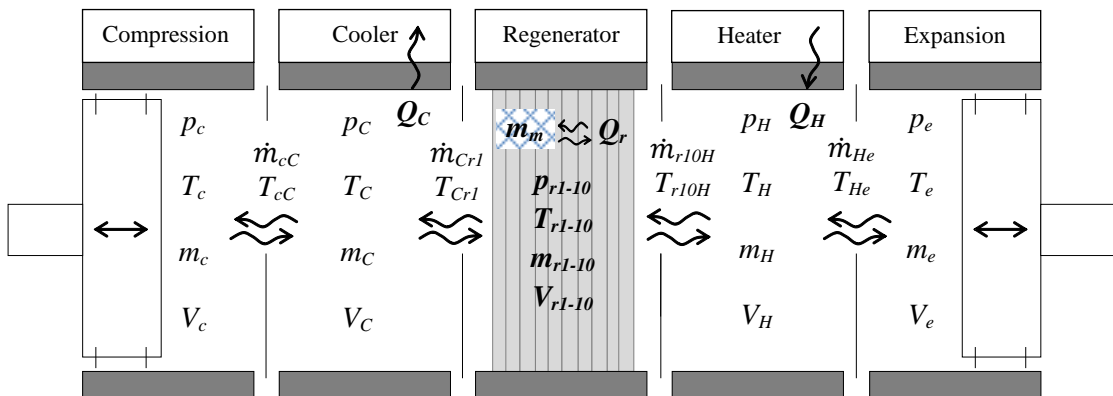


Figure 3.7 The calculation scheme of the conventional Stirling engines

Chapter 3

The performance of the regenerator strongly affects the engine performance, particularly of the conventional Stirling engines operating at the high engine speed. Therefore the regenerator is split into 10 control volumes in order to more accurately describe the working cycle. The developed second-order model also takes into account the hydraulic losses in the heater, cooler and regenerator. The assumptions similar to that in the LTD engine's model are made in this section and are as follows:

1. The derivative pressure in each control volume is the same.
2. There are no gas leakages through sealing rings of the power pistons and of the displacer rod.
3. The working gas in each control volume is considered as a perfect gas.
4. The walls of the displacer and power piston cylinders are thermally insulated.
5. The engine operates at steady state conditions.

The volume of compression and expansion spaces can be calculated as

$$V_c = V_{d-c} + \frac{V_{S-P}}{2}(1 + \cos(\theta - \varphi)) + \frac{V_{S-D}}{2}(1 - \cos \theta) \quad (3.62)$$

$$V_e = V_{d-e} + \frac{V_{S-D}}{2}(1 + \cos \theta) \quad (3.63)$$

The derivatives of volumes are

$$\frac{dV_c}{dt} = -\frac{V_{S-P}}{2} \omega \sin(\theta - \varphi) + \frac{V_{S-D}}{2} \omega \sin \theta \quad (3.64)$$

Chapter 3

$$\frac{dV_e}{dt} = -\frac{V_{S-D}}{2} \omega \sin \theta \quad (3.65)$$

The temperature of the working gas mass flow between the compression space and the cooler can be defined as follows:

$$T_{c-c} = T_c \quad \text{if} \quad \dot{m}_{c-c} > 0,$$

$$T_{c-c} = T_C \quad \text{if} \quad \dot{m}_{c-c} \leq 0,$$

where \dot{m}_{c-c} is gas mass flow between the compression space and the cooler (kg/s); T_{c-c} is the temperature of the gas mass flow between the compression space and the cooler space (K); T_c is the gas temperature in the compression space (K); T_C is gas temperature in the cooler (K).

For the gas mass flow between the cooler and the first part of the regenerator space,

$$T_{c-rl} = T_C \quad \text{if} \quad \dot{m}_{c-rl} > 0,$$

$$T_{c-rl} = T_{r-c} \quad \text{if} \quad \dot{m}_{c-rl} \leq 0,$$

here \dot{m}_{c-rl} is gas mass flow between the cooler space and the first part of the regenerator space (kg/s); T_{c-rl} is the temperature of gas mass flow between the cooler space and the first part of regenerator space (K); T_{r-c} is the gas temperature at boundary between the cooler space and the first part of regenerator space (K) which can be determined as $T_{r-c} = (3T_{rl} - T_{r2})/2$.

Chapter 3

For the temperature of the gas mass flow at the boundaries of the second-ninth control volumes of the regenerator space

$$T_{r(i)-r(i+1)} = (T_{r(i)} + T_{r(i+1)})/2$$

where $T_{r(i)}$ and $T_{r(i+1)}$ are the gas temperatures in the $(i)th$ part and the $(i+1)th$ part of the regenerator space (K), respectively, $i=2-9$.

For the gas mass flow between the tenth part of the regenerator space and the heater:

$$T_{r10-H} = T_{r-H} \quad \text{if} \quad \dot{m}_{r10-H} > 0;$$

$$T_{r10-H} = T_H \quad \text{if} \quad \dot{m}_{r10-H} \leq 0,$$

where \dot{m}_{r10-H} is gas mass flow between the tenth part of the regenerator space and the heater (kg/s); T_{r10-H} is the temperature of the gas mass flow between the tenth part of the regenerator space and the heater space (K); T_{r-H} is the gas temperature at the boundary between the tenth part of the regenerator space and the heater space (K), which can be calculated as $T_{r-H} = (3T_{r10} - T_{r9})/2$.

For the gas mass flow between the heater and expansion spaces

$$T_{H-e} = T_H \quad \text{if} \quad \dot{m}_{H-e} > 0;$$

$$T_{H-e} = T_e \quad \text{if} \quad \dot{m}_{H-e} \leq 0,$$

where \dot{m}_{H-e} is the gas mass flow between the heater and expansion spaces (kg/s); T_{H-e} is the temperature of the gas mass flow between the heater and expansion

Chapter 3

spaces, (K); T_H is the gas temperature in the heater space (K); T_e is the gas temperature in the expansion space (K).

The energy conservation equations

The energy conservation equation is applied to all control volumes (the compression space, the cooler space, ten control volumes of the regenerator space, the heater space and the expansion space).

$$C_v \frac{d(m_c T_c)}{dt} = -\dot{m}_{c-c} C_p T_{c-c} - \frac{dW_c}{dt} \quad (3.66)$$

$$C_v \frac{d(m_c T_c)}{dt} = dQ_C - dQ_{loss,disip-C} + \dot{m}_{c-c} C_p T_{c-c} - \dot{m}_{C-r1} C_p T_{C-r1} \quad (3.67)$$

$$C_v \frac{d(m_{r1} T_{r1})}{dt} = dQ_{r1} - dQ_{loss,disip-r1} + \dot{m}_{C-r1} C_p T_{C-r1} - \dot{m}_{r1-r2} C_p T_{r1-r2} \quad (3.68)$$

For eight volumes of the regenerator (from the second to the ninth) the energy conservation equation is written as

$$C_v \frac{d(m_{r(i)} T_{r(i)})}{dt} = dQ_{r(i)} - dQ_{loss,disip-r(i)} + \dot{m}_{r(i-1)-r(i)} C_p T_{r(i-1)-r(i)} - \dot{m}_{r(i)-r(i+1)} C_p T_{r(i)-r(i+1)} \quad (3.69)$$

here i is number of the regenerator volume (from 2 to 9).

$$C_v \frac{d(m_{r10} T_{r10})}{dt} = dQ_{r10} - dQ_{loss,disip-r10} + \dot{m}_{r9-r10} C_p T_{r9-r10} - \dot{m}_{r10-h} C_p T_{r10-h} \quad (3.70)$$

$$C_v \frac{d(m_H T_H)}{dt} = dQ_H - dQ_{loss,disip-H} + \dot{m}_{r10-H} C_p T_{r10-H} - \dot{m}_{H-e} C_p T_{H-e} \quad (3.71)$$

Chapter 3

$$C_v \frac{d(m_e T_e)}{dt} = \dot{m}_{H-e} C_p T_{H-e} - dQ_{loss,shl} - \frac{dW_e}{dt} \quad (3.72)$$

In the above equations m_C and m_H are the mass of the gas in the cooler and heater spaces, respectively (kg); $Q_{loss,disip-C}$ is the heat loss due to the flow friction in the cooler space (W); $Q_{loss,disip-r1}$ is the heat loss due to the flow friction in the first part of regenerator space (W); $Q_{loss,disip-r(i)}$ is the heat loss due to the flow friction in the $(i)th$ part of the regenerator space, $i=2...9$ (W); $Q_{loss,disip-r10}$ is the heat loss due to the flow friction in the tenth part of regenerator space (W); $Q_{loss,disip-H}$ is the heat loss due to the flow friction in the heater space (W).

The work done on or by the gas in the compression and expansion spaces can be

$$\text{calculated as } \frac{dW_c}{dt} = p_c \frac{dV_c}{dt} \text{ and } \frac{dW_e}{dt} = p_e \frac{dV_e}{dt}.$$

The ideal gas state equation used is $PV = mRT$ and the properties of the gas

$$\text{determined as } R = C_p - C_v \text{ and } \gamma = \frac{C_p}{C_v}.$$

The gas mass flows between the control volumes can be defined as follows:

$$\dot{m}_{cC} = -\frac{1}{RT_{cC}} \left(p_c \frac{dV_c}{dt} + \frac{V_c}{\gamma} \frac{dp}{dt} \right) \quad (3.73)$$

$$\dot{m}_{Cr1} = \frac{1}{RT_{Cr1}} \left(\frac{R}{C_p} dQ_C - \frac{R}{C_p} dQ_{loss,disip-C} - \frac{V_c}{\gamma} \frac{dp}{dt} + R\dot{m}_{cC} T_{cC} \right) \quad (3.74)$$

$$\dot{m}_{r1r2} = \frac{1}{RT_{r1r2}} \left(\frac{R}{C_p} dQ_{r1} - \frac{R}{C_p} dQ_{loss,disip-r1} - \frac{V_{r1}}{\gamma} \frac{dp}{dt} + R\dot{m}_{Cr1} T_{Cr1} \right) \quad (3.75)$$

Chapter 3

For the gas mass flow between volumes in the section of the regenerator between the second and ninth part of the regenerator

$$\dot{m}_{r(i)-r(i+1)} = \frac{I}{RT_{r(i)-r(i+1)}} \left(\frac{R}{C_p} dQ_{r(i)} - \frac{R}{C_p} dQ_{loss,disip-r(i)} - \frac{V_{r(i)}}{\gamma} \frac{dp}{dt} + R\dot{m}_{r(i-1)-r(i)} T_{r(i-1)-r(i)} \right) \quad (3.76)$$

where i is number of the regenerator's part (2...9);

$$\dot{m}_{r10h} = \frac{I}{RT_{r10h}} \left(\frac{R}{C_p} dQ_{r10} - \frac{R}{C_p} dQ_{loss,disip-r10} - \frac{V_{r10}}{\gamma} \frac{dp}{dt} + R\dot{m}_{r9r10} T_{r9r10} \right) \quad (3.77)$$

$$\dot{m}_{He} = \frac{I}{RT_{He}} \left(\frac{R}{C_p} dQ_H - \frac{R}{C_p} dQ_{loss,disip-H} - \frac{V_{r10}}{\gamma} \frac{dp}{dt} + R\dot{m}_{r10H} T_{r10H} \right) \quad (3.78)$$

The pressure derivative can be obtained by adding up all energy conservation equations above:

$$\frac{dp}{dt} = \frac{I}{C_v V_T} \left(R(dQ_H + \sum dQ_r + dQ_C - \sum dQ_{loss,disip} - dQ_{loss,shll}) - C_p \left(p_c \frac{dV_c}{dt} + p_e \frac{dV_e}{dt} \right) \right) \quad (3.79)$$

here $Q_{loss,shll}$ is the shuttle heat loss due to heat transfer from the heater space to cooler space by the reciprocating displacer (W).

Additionally, the energy conservation equation for the regenerator matrix can be written as

$$\dot{m}_m C_p \frac{dT_m}{dt} = -dQ_r \quad (3.80)$$

Chapter 3

Therefore, the temperature derivative in each part of the regenerator matrix can be calculated as

$$\frac{dT_{m(i)}}{dt} = \frac{1}{\dot{m}_{m(i)} C_p} (-dQ_{r(i)}) \quad (3.81)$$

where $i=1 \dots 10$ is the number of the regenerator's part.

The mass conservation equations

The mass conservation equation for the working gas inside each control volume can be presented as follows:

$$\frac{dm_c}{dt} = -\dot{m}_{c-C} \quad (3.82)$$

$$\frac{dm_C}{dt} = \dot{m}_{c-C} - \dot{m}_{C-r1} \quad (3.83)$$

$$\frac{dm_{r1}}{dt} = \dot{m}_{C-r1} - \dot{m}_{r1-r2} \quad (3.84)$$

For the section of the regenerator from its the second to the ninth part

$$\frac{dm_{r(i)}}{dt} = \dot{m}_{r(i-1)-r(i)} - \dot{m}_{r(i)-r(i+1)} \quad (3.85)$$

$$\frac{dm_{r10}}{dt} = \dot{m}_{r9-r10} - \dot{m}_{r10-H} \quad (3.86)$$

$$\frac{dm_H}{dt} = \dot{m}_{r10-H} - \dot{m}_{H-e} \quad (3.87)$$

$$\frac{dm_e}{dt} = \dot{m}_{H-e} \quad (3.88)$$

Chapter 3

The state equation of the ideal gas

The following equations are used for the determination of the temperature of the working gas inside the compression space, cooler, all parts of the regenerator, heater and the expansion space:

$$T_c = \frac{p_c V_c}{Rm_c} \quad (3.89)$$

$$T_C = \frac{p_C V_C}{Rm_C} \quad (3.90)$$

$$T_{r(i)} = \frac{p_{r(i)} V_{r(i)}}{Rm_{r(i)}} \quad (3.91)$$

$$T_H = \frac{p_H V_H}{Rm_H} \quad (3.92)$$

$$T_e = \frac{p_e V_e}{Rm_e} \quad (3.93)$$

In above calculations the pressure drop in the regenerator, heater tubes and cooler tubes of the Stirling engine were taken into account.

For the fluid flow inside the tubes of the heater and cooler, the correlation for the friction coefficient of an unidirectional flow is widely used [79], though the flow in the engine is the oscillating. The equation given by [89] is used for the calculation of pressure drop of the heater and cooler and can be written as

$$\Delta p = - \frac{2 f_r \mu U V}{A_{free} d_h^2} \quad (3.94)$$

$$f_r = f_c Re/4 \quad (3.95)$$

Chapter 3

where friction factor f_c for heater and cooler can be obtained from the following equation

If $Re < 2000$

$$f_c = 64/Re \quad (3.96)$$

If $2000 < Re < 20000$

$$f_c = 0.316Re^{-0.25} \quad (3.97)$$

If $Re > 20000$

$$f_c = 0.184Re^{-0.2} \quad (3.98)$$

For the determination of the pressure drop in the regenerator, a number of correlations obtained from experimental analysis of the oscillating flow through the regenerator have been published. Thomas and Pittman [90] presented the evaluation of different correlations for calculation of the friction factor and the heat transfer coefficient for regenerators. It was demonstrated that the greater pressure drop was obtained using the correlation by Gedeon and Wood. Therefore, f_c for the regenerator can be calculated as

$$f_c = \frac{129}{Re} + \frac{2.91}{Re^{0.103}} \quad (3.99)$$

The energy dissipation due to the friction losses in the flow was studied by Tlili et al. [26] and Timoumi et al. [27] and can be calculated as

$$Q_{loss,disip} = \frac{\Delta p \dot{m}}{\rho} \quad (3.100)$$

Chapter 3

Similar to the procedure used for LTD modelling, the base pressure calculated using Eq. 3.79 is assumed to be the pressure of the gas in the compression space. Therefore, the instantaneous pressure of working gas in each control volume can be calculated as

$$p_C = p_c + \frac{\Delta p_C}{2} \quad (3.101)$$

where Δp_C is the pressure drop in the cooler (Pa);

$$p_{r1} = p_C + \frac{\Delta p_C}{2} + \frac{\Delta p_{r1}}{2}; \quad (3.102)$$

the pressure drop in the section of the regenerator from its second to tenth part is

$$p_{r(i)} = p_{r(i-1)} + \frac{\Delta p_{r(i-1)}}{2} + \frac{\Delta p_{r(i)}}{2} \quad (3.103)$$

where $i = 2, \dots, 10$;

$$p_H = p_{r10} + \frac{\Delta p_{r10}}{2} + \frac{\Delta p_H}{2} \quad (3.104)$$

where Δp_H is pressure drop produced in the heater (Pa);

$$p_e = p_H + \frac{\Delta p_H}{2} \quad (3.105)$$

Heat transfer rate in all recuperative heat exchangers can be calculated as

$$dQ_H = h_H A_{h-H} (T_H - T_e) - dQ_{loss, lir-H} \quad (3.106)$$

Chapter 3

$$dQ_C = h_c A_{h-c} (T_C - T_c) - dQ_{loss,lir-C} \quad (3.107)$$

where $Q_{loss,lir-H}$ is the heat loss due to the heat transfer due to the heat conduction from the hot to cold parts of the heater (W); $Q_{loss,lir-C}$ is the heat loss due to the heat transfer due to the heat conduction from the hot to cold parts of the cooler (W).

The correlation for heat transfer coefficient (h) in the unidirectional flow (Colburn's correlation [91]) is applied in this work for the calculation of the heat transfer coefficients on surfaces of the heater and cooler:

$$J = \frac{hPr^{2/3}}{C_p \dot{m} / A_{free}} \quad (3.108)$$

where

if $Re < 3000$

$$J = \exp(0.337 - 0.812 \log(Re)) \quad (3.109)$$

if $3000 < Re < 4000$

$$J = 0.0021 \quad (3.110)$$

if $4000 < Re < 7000$

$$J = \exp(13.31 - 0.861 \log(Re)) \quad (3.111)$$

if $7000 < Re < 10000$

$$J = 0.0034 \quad (3.112)$$

Chapter 3

if $Re > 10000$

$$J = \exp(-3.575 - 0.229 \log(Re)) \quad (3.113)$$

In the regenerator, the heat transfer rate in its all ten parts is determined as

$$dQ_{r(i)} = e_{eff} h_{m(i)} A_{h-m(i)} (T_{m(i)} - T_{r(i)}) - dQ_{loss,lir-r(i)} \quad (3.114)$$

where $Q_{loss,lir-r(i)}$ is the heat loss due to the heat transfer due to the heat conduction from the hot to cold parts of the regenerator (W) and $i=1 \dots 10$ is the number of the matrix in the corresponding regenerator's part.

Eq.3.30- Eq.3.33 which are the correlations for oscillating flow published by Tanaka et al. [85] are used to calculate the effectiveness of the regenerator and the average heat transfer coefficient between the matrix and the working gas in the regenerator.

In this model, unlike in the model for the LTD engine, the heat dissipation losses due to the pressure drop and internal conduction heat losses and the shuttle heat losses [18, 27] are taken into account.

The internal conduction heat losses are defined as the heat transfer due to the heat conduction from the hot to cold parts of the heat exchanger. The one-dimensional heat conduction equation along the length of the heat exchanger is applied to all heat exchangers of the engine:

$$dQ_{loss,lir} = \frac{kA_l}{l} \Delta T \quad (3.115)$$

Chapter 3

where k is the thermal conductivity of the material (W/mK); A_l is the cross sectional area (m^2); l is the length (m); ΔT is the temperature difference (K).

The reciprocating motion of the displacer causes the heat transfer from the hot to the cold space. A certain amount of heat from the cylinder's body is absorbed by the displacer located at the hot side and then this heat is rejected to cylinder at its cold side. This phenomenon is called shuttle losses and can be calculated as [18, 27]:

$$dQ_{loss,shl} = \frac{0.4Z_D^2 k_D D_D}{\Delta gap l_D} (T_H - T_C) \quad (3.116)$$

where Z_D is the displacer stroke (m); k_D is the thermal conductivity of the working gas (W/mK); D_D is the displacer diameter (m); l_D is the displacer length (m); Δgap is the length of the gap between the displacer and the cylinder (m).

Finally, the cyclic indicated work can be obtained by

$$W_i = \oint \left(\frac{dW_i}{dt} \right) dt = \int_0^\tau \left(\frac{dW_c}{dt} + \frac{dW_e}{dt} \right) dt = \int_0^\tau \left(p_c \frac{dV_c}{dt} + p_e \frac{dV_e}{dt} \right) dt \quad (3.117)$$

and the indicated power is

$$P_i = W_i f \quad (3.118)$$

3.2.3 Numerical simulation procedure

All the described mathematical equations of the second-order model of conventional Stirling engines were used to develop a computer code implemented in MATLAB. The simulations procedure is shown in Figure 3.8 in the form of the flow chart. The

Chapter 3

initial temperatures of the gas in the compression and expansion spaces were defined as corresponding constant temperatures of the cooler and heater. The range of temperature from the cooler temperature to the heater temperature was used for defining the initial temperature of the gas and matrix in all parts of the regenerator. The input data consisting of the engine physical dimensions and the working fluid parameters was used for the numerical simulations and then a set of differential equations was solved using the classical fourth-order Runge-Kutta method. Then heat transfers and the pressure drops in all heat exchangers were calculated. The pressure of the gas in each control volume was calculated using Eq.3.101-Eq.3.105 and then all heat losses were obtained at this stage of the modelling. The simulations were run until the steady state condition was reached. Temperature and pressure variations and also the heat balance of the engine were used to determine whether the steady state condition was reached. The temperature of the matrix inside the regenerator was automatically adjusted every cycle until the sum of the cyclic heat transfer in the regenerator and its cyclic heat losses was approximately equal to zero. Finally, the values of the cyclic work and power were calculated in the last stages of simulations.

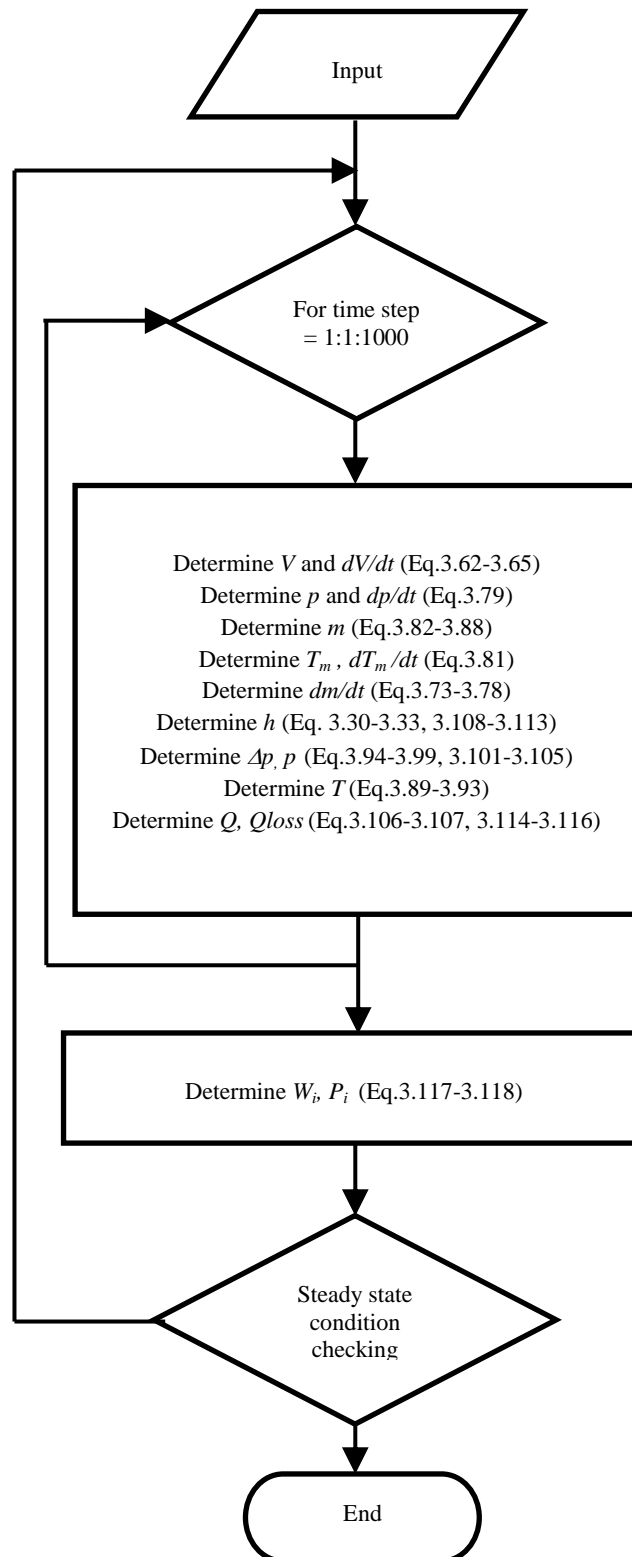


Figure 3.8 The flowchart of the second-order modelling of the conventional Stirling engines

Chapter 4

General principles of three-dimensional CFD modelling

Chapter 4 presents the governing equations of computational fluid dynamics (CFD) modelling for the analysis of the working process inside the Stirling engine's gas circuit.

4.1 Three-dimensional CFD modelling background

To achieve better understanding of the working process of Stirling engines and also to improve the accuracy of predictions of the engine performance, the three-dimensional computational fluid dynamics model with the use of the standard $k-\varepsilon$ two-equation turbulence model for a compressible flow has been used for the simulation of the working process of Stirling engines. The numerical analysis of the internal flow in the engine has been carried out with application of the governing equations such as the conservation of mass, momentum and energy and the $k-\varepsilon$ turbulence model equations taking into account the compressibility correction term described by Hirsch [92] and Hoffman and Chiang [93] as follows:

The mass conservation equation

$$\frac{\partial \rho}{\partial t} + \frac{\partial}{\partial x}(\rho u) + \frac{\partial}{\partial y}(\rho v) + \frac{\partial}{\partial z}(\rho w) = 0 \quad (4.1)$$

Chapter 4

The momentum conservation equation

$$\begin{aligned} \frac{\partial(\rho u)}{\partial t} + \frac{\partial(\rho u^2 + p)}{\partial x} + \frac{\partial(\rho uv)}{\partial y} + \frac{\partial(\rho uw)}{\partial z} &= \frac{\partial\tau_{xx}}{\partial x} + \frac{\partial\tau_{xy}}{\partial y} + \frac{\partial\tau_{xz}}{\partial z} \\ + \frac{\partial(-\rho\overline{u'^2})}{\partial x} + \frac{\partial(-\rho\overline{u'v'})}{\partial y} + \frac{\partial(-\rho\overline{u'w'})}{\partial z} \end{aligned} \quad (4.2)$$

$$\begin{aligned} \frac{\partial(\rho v)}{\partial t} + \frac{\partial(\rho uv)}{\partial x} + \frac{\partial(\rho v^2 + p)}{\partial y} + \frac{\partial(\rho vw)}{\partial z} &= \frac{\partial\tau_{xy}}{\partial x} + \frac{\partial\tau_{yy}}{\partial y} + \frac{\partial\tau_{zy}}{\partial z} \\ + \frac{\partial(-\rho\overline{u'v'})}{\partial x} + \frac{\partial(-\rho\overline{v'^2})}{\partial y} + \frac{\partial(-\rho\overline{v'w'})}{\partial z} \end{aligned} \quad (4.3)$$

$$\begin{aligned} \frac{\partial(\rho w)}{\partial t} + \frac{\partial(\rho uw)}{\partial x} + \frac{\partial(\rho vw)}{\partial y} + \frac{\partial(\rho w^2 + p)}{\partial z} &= \frac{\partial\tau_{xz}}{\partial x} + \frac{\partial\tau_{yz}}{\partial y} + \frac{\partial\tau_{zz}}{\partial z} \\ + \frac{\partial(-\rho\overline{u'w'})}{\partial x} + \frac{\partial(-\rho\overline{v'w'})}{\partial y} + \frac{\partial(-\rho\overline{w'^2})}{\partial z} \end{aligned} \quad (4.4)$$

The energy conservation equation

$$\begin{aligned} \frac{\partial(\rho e)}{\partial t} + \frac{\partial(u(\rho e + p))}{\partial x} + \frac{\partial(v(\rho e + p))}{\partial y} + \frac{\partial(w(\rho e + p))}{\partial z} &= \frac{\partial}{\partial x} \left[\left(\lambda + \frac{C_p \mu_t}{Pr_t} \right) \frac{\partial T}{\partial x} \right] \\ + \frac{\partial}{\partial y} \left[\left(\lambda + \frac{C_p \mu_t}{Pr_t} \right) \frac{\partial T}{\partial y} \right] + \frac{\partial}{\partial z} \left[\left(\lambda + \frac{C_p \mu_t}{Pr_t} \right) \frac{\partial T}{\partial z} \right] \end{aligned} \quad (4.5)$$

The turbulent kinetic energy equation

$$\begin{aligned} \frac{\partial(\rho k)}{\partial t} + \frac{\partial(\rho uk)}{\partial x} + \frac{\partial(\rho vk)}{\partial y} + \frac{\partial(\rho wk)}{\partial z} &= \frac{\partial}{\partial x} \left[\left(\mu + \frac{\mu_t}{\sigma_k} \right) \frac{\partial k}{\partial x} \right] \\ + \frac{\partial}{\partial y} \left[\left(\mu + \frac{\mu_t}{\sigma_k} \right) \frac{\partial k}{\partial y} \right] + \frac{\partial}{\partial z} \left[\left(\mu + \frac{\mu_t}{\sigma_k} \right) \frac{\partial k}{\partial z} \right] &+ P_k - \rho(\varepsilon + \varepsilon_c) + \overline{p''d''} \end{aligned} \quad (4.6)$$

Chapter 4

The dissipation rate equation

$$\begin{aligned} \frac{\partial(\rho\varepsilon)}{\partial t} + \frac{\partial}{\partial x}(\rho u\varepsilon) + \frac{\partial}{\partial y}(\rho v\varepsilon) + \frac{\partial}{\partial z}(\rho w\varepsilon) = \frac{\partial}{\partial x} \left[\left(\mu + \frac{\mu_t}{\sigma_\varepsilon} \right) \frac{\partial\varepsilon}{\partial x} \right] \\ + \frac{\partial}{\partial y} \left[\left(\mu + \frac{\mu_t}{\sigma_\varepsilon} \right) \frac{\partial\varepsilon}{\partial y} \right] + \frac{\partial}{\partial z} \left[\left(\mu + \frac{\mu_t}{\sigma_\varepsilon} \right) \frac{\partial\varepsilon}{\partial z} \right] + c_{\varepsilon 1} P_k \frac{\varepsilon}{k} - c_{\varepsilon 2} \rho \frac{\varepsilon^2}{k} \end{aligned} \quad (4.7)$$

In the above equations x , y and z are directions of three dimension (m); u , v and w are velocity in x , y and z directions, respectively (m/s); p is pressure (Pa); Pr_t is turbulent Prandtl number; t is time (sec); ρ is density (kg/m^3); k is turbulent kinetic energy (m^2/s^2); ε is turbulent dissipation (m^2/s^2); μ is dynamic viscosity (Pa s).

The shear stress terms τ_{xx} , τ_{xy} , τ_{xz} , τ_{yx} , τ_{yy} , τ_{yz} , τ_{zx} , τ_{zz} and τ_{zy} are defined as

$$\tau_{xx} = \mu \left(\frac{4}{3} \frac{\partial u}{\partial x} - \frac{2}{3} \frac{\partial v}{\partial y} - \frac{2}{3} \frac{\partial w}{\partial z} \right) \quad (4.8)$$

$$\tau_{yy} = \mu \left(\frac{4}{3} \frac{\partial v}{\partial y} - \frac{2}{3} \frac{\partial u}{\partial x} - \frac{2}{3} \frac{\partial w}{\partial z} \right) \quad (4.9)$$

$$\tau_{zz} = \mu \left(\frac{4}{3} \frac{\partial w}{\partial z} - \frac{2}{3} \frac{\partial u}{\partial x} - \frac{2}{3} \frac{\partial v}{\partial y} \right) \quad (4.10)$$

$$\tau_{xy} = \tau_{yx} = \mu \left(\frac{\partial v}{\partial x} + \frac{\partial u}{\partial y} \right) \quad (4.11)$$

$$\tau_{xz} = \tau_{zx} = \mu \left(\frac{\partial w}{\partial x} + \frac{\partial u}{\partial z} \right) \quad (4.12)$$

$$\tau_{yz} = \tau_{zy} = \mu \left(\frac{\partial w}{\partial y} + \frac{\partial v}{\partial z} \right) \quad (4.13)$$

Chapter 4

The production of turbulence P_k is defined as

$$P_k = \mu_t \left\{ \begin{aligned} & \left(\frac{4}{3} \frac{\partial u}{\partial x} - \frac{2}{3} \frac{\partial v}{\partial y} - \frac{2}{3} \frac{\partial w}{\partial z} \right) \left(\frac{\partial u}{\partial x} \right) + \left(\frac{4}{3} \frac{\partial v}{\partial y} - \frac{2}{3} \frac{\partial u}{\partial x} - \frac{2}{3} \frac{\partial w}{\partial z} \right) \left(\frac{\partial v}{\partial y} \right) \\ & + \left(\frac{4}{3} \frac{\partial w}{\partial z} - \frac{2}{3} \frac{\partial u}{\partial x} - \frac{2}{3} \frac{\partial v}{\partial y} \right) \left(\frac{\partial w}{\partial z} \right) + \left(\frac{\partial u}{\partial y} + \frac{\partial v}{\partial x} \right) \left(\frac{\partial u}{\partial y} \right) + \left(\frac{\partial u}{\partial z} + \frac{\partial w}{\partial x} \right) \left(\frac{\partial u}{\partial z} \right) \\ & + \left(\frac{\partial v}{\partial x} + \frac{\partial u}{\partial y} \right) \left(\frac{\partial v}{\partial x} \right) + \left(\frac{\partial v}{\partial z} + \frac{\partial w}{\partial y} \right) \left(\frac{\partial v}{\partial z} \right) + \left(\frac{\partial w}{\partial x} + \frac{\partial u}{\partial z} \right) \left(\frac{\partial w}{\partial x} \right) \\ & + \left(\frac{\partial w}{\partial y} + \frac{\partial v}{\partial z} \right) \left(\frac{\partial w}{\partial y} \right) \end{aligned} \right\} \quad (4.14)$$

The typical constants in equations (4.5) and (4.6) are $\sigma_k = 1.0$, $\sigma_\varepsilon = 1.3$, $c_{\varepsilon l} = 1.44$ and $c_{\varepsilon 2} = 1.92$. In addition, the turbulent viscosity is expressed as

$$\mu_t = \rho c_\mu \frac{k^2}{\varepsilon} \quad (4.15)$$

where c_μ is equal to 0.09.

The semi-empirical correlations to determine the values $\overline{u'^2}$, $\overline{v'^2}$ and $\overline{w'^2}$ are used:

$$\overline{u'^2} = 2\alpha_2 k \quad (4.16)$$

$$\overline{v'^2} = 2\alpha_3 k \quad (4.17)$$

$$\overline{w'^2} = 2\alpha_4 k \quad (4.18)$$

where α_2 , α_3 and α_4 are structural scale constants.

Chapter 4

The Reynolds stress terms $-\rho\overline{u'v'}$, $-\rho\overline{u'w'}$ and $-\rho\overline{v'w'}$ are given as

$$-\rho\overline{u'v'} = \mu_t \left(\frac{\partial u}{\partial y} + \frac{\partial v}{\partial x} \right) \quad (4.19)$$

$$-\rho\overline{u'w'} = \mu_t \left(\frac{\partial u}{\partial z} + \frac{\partial w}{\partial x} \right) \quad (4.20)$$

$$-\rho\overline{v'w'} = \mu_t \left(\frac{\partial v}{\partial z} + \frac{\partial w}{\partial y} \right) \quad (4.21)$$

The term ε_c and the pressure dilatation term $\overline{p''d''}$ present the compressibility correction in the k - ε turbulence model and are expressed as

$$\varepsilon_c = \gamma_1 M_t^2 \varepsilon \quad (4.22)$$

$$\overline{p''d''} = -\gamma_2 P_k M_t^2 + \gamma_3 \rho \varepsilon M_t^2 \quad (4.23)$$

Here the turbulent Mach number $M_t = \sqrt{2k/a_s^2}$ in which a_s is the speed of the sound (m/s) and the constant values are $\gamma_1=1.0$, $\gamma_2=0.4$ and $\gamma_3=0.2$.

For the compression space and the expansion space, it is essentially considered that the velocity of the working gas is induced by the piston movement in the direction of x axis which is defined by the kinematical motion of the piston. The velocity u in the above equations will be replaced by the term of $u-u_p$ where u_p is the velocity of the piston along the x axis.

For the regenerator of the engine, the matrix of the regenerator is considered to be a porous media and the regenerator is assumed to be homogenous. The momentum equations of the fluid flow are modified with the additional term which composed of

Chapter 4

a viscous loss term and an inertial loss term. The extra terms are presented as follows:

$$S_x = u \left(\frac{\mu}{\alpha} \right) + \frac{1}{2} C \rho |u| u \quad (4.24)$$

$$S_y = v \left(\frac{\mu}{\alpha} \right) + \frac{1}{2} C \rho |v| v \quad (4.25)$$

$$S_z = w \left(\frac{\mu}{\alpha} \right) + \frac{1}{2} C \rho |w| w \quad (4.26)$$

where α is the permeability of the matrix and C is the inertial resistance.

Values of the permeability of the matrix and the inertial resistance coefficient are usually calculated from the information on the geometry and material of the matrix or are determined experimentally from flow tests.

In addition, the heat conduction between the matrix and the working fluid which flows through the regenerator is introduced into the energy equation as follows:

$$\begin{aligned} & \frac{\partial [\rho \Pi e + (1 - \Pi) \rho_M e_M]}{\partial t} + \frac{\partial [u(\rho e + p)]}{\partial x} + \frac{\partial [v(\rho e + p)]}{\partial y} + \frac{\partial [w(\rho e + p)]}{\partial z} \\ & = \frac{\partial}{\partial x} \left[\left(\lambda_{\Pi} + \frac{c_p \mu_t}{Pr_t} \right) \frac{\partial T}{\partial x} \right] + \frac{\partial}{\partial y} \left[\left(\lambda_{\Pi} + \frac{c_p \mu_t}{Pr_t} \right) \frac{\partial T}{\partial y} \right] + \frac{\partial}{\partial z} \left[\left(\lambda_{\Pi} + \frac{c_p \mu_t}{Pr_t} \right) \frac{\partial T}{\partial z} \right] \end{aligned} \quad (4.27)$$

Here Π is the porosity of the matrix, ρ_M is the density of the matrix and e_M is the energy of the matrix. λ_{Π} is the effective conductivity of the matrix which is determined as $\lambda_{\Pi} = \Pi \lambda + \lambda_M (1 - \Pi)$ where λ_M is the thermal conductivity of the matrix.

Chapter 4

4.2 Numerical simulation procedure

For the numerical 3D simulation process, commercial CFD software, namely ANSYS, was used to solve the governing equations of the working process described above. A computational mesh was created in the three-dimensional geometry of the gas volume inside the engine. Since the oscillating flow caused by the reciprocating movement of the power piston and the displacer was formed inside the engine circuit, the moving mesh or dynamic mesh model was applied for these simulations.

The “Dynamic Layering Method” [94] option in CFD code was deployed for modelling piston displacements in the prismatic (hexahedral and/or wedge) computational mesh of the engine. This method adds or removes layers of cells adjacent to a moving boundary, based on the specified ideal height of the layer adjacent to the moving surface.

The subroutine describing the piston and displacer motions was written in the C computer language and compiled and added to the main body of the ANSYS software. Then the material of the regenerator matrix was defined. The suitable initial temperatures in each space were defined to avoid an excessive computing time.

In computing process, a number of iterations were run using the standard $k-\varepsilon$ turbulence model for a compressible flow until the steady condition found in each time step. In these simulations the cyclic operation of the LTD Stirling engine was divided into 500 time steps. The simulations were performed using a high performance PC. The average gas temperature and pressure in each space were

Chapter 4

monitored during modelling to decide whether the steady operation conditions were reached in the modelling.

Chapter 5

General principles of the Genetic Algorithm method

A description of general principles of Genetic algorithm (GA) method applied for the determination of optimal design parameter of Stirling engines is provided in this chapter. Optimisation procedure based on GA was used for the LTD Stirling engine and the conventional Stirling engine for MTD and HTD applications.

5.1 Introduction to the Genetic algorithms

Genetic algorithms (GAs) are stochastic optimisation methods based on the biological mechanism of survival in nature. The GA theory was firstly published by Holland in 1975 and was successfully applied in practice by Goldberg in 1989. The rule of survival of the fittest worked on a population of variables to produce a new population with better individuals. The global optimum for the problem solution can be obtained because GAs are operating with an initial random population and using the stochastic operator, whilst the local optimum may be found by using other optimisation methods such as the calculus-based methods. Additionally, there are many advantages of GAs over other optimisation methods [95]:

Chapter 5

1. Continuous or discrete variables can be used in GAs.
2. There are no requirements for the derivative information in the GA procedure.
3. A large number of variables are allowed in GAs.
4. There is a benefit of time saving when using parallel computing facilities.
5. The objective function in GAs can be not only an analytical function but also in the form of numerical or experimental data.

The simple procedure for implementing GAs is described in [96]. The natural selection process is introduced as the optimisation procedure. A set of individuals called population is randomly formed as an initial population. Each individual or chromosome contains various parameters that are the solution of the problem. The evaluation of each chromosome inside the initial population affects the fitness function. The objective function is defined to measure the fitness value. The fitness value ranking is used for the selection procedure. In the natural process to obtain the next generation, the natural selection is applied to determine the parents for the reproduction. Some offsprings, or newly generated chromosomes, are created through the recombination with the crossover and the mutation operations. Then the fitness evaluation is applied to the new population. Such the algorithm is used to create several generations until the solution is found satisfying the termination condition.

Chapter 5

5.2 Genetic algorithm procedure for finding the optimal design parameters of Stirling engines

The commonly used GA is the binary GA, in which the variable is converted into the bit number with the encoding process and reverted with decoding process. The binary GA with a large number of variables in each chromosome will face the requirement of using many bits and a significant computing time is needed for the encoding and decoding procedures. Therefore, the continuous GA or the real-value GA, in which the variables are represented by single floating point numbers, is applied in this work in order to avoid the quantitative limitations and to reduce the computing time [95]. A diagram of the continuous GA for the determination of the optimal design parameters of the LTD and conventional Stirling engines with the procedures arranged as a flow chart is shown in Figure 5.1. The details of each procedure are discussed below.

5.2.1 Definition of the objective function and variables

A set of engine design parameters is defined as a solution of the optimisation procedure and forms the vector which represents GA variables contained in each chromosome of the population.

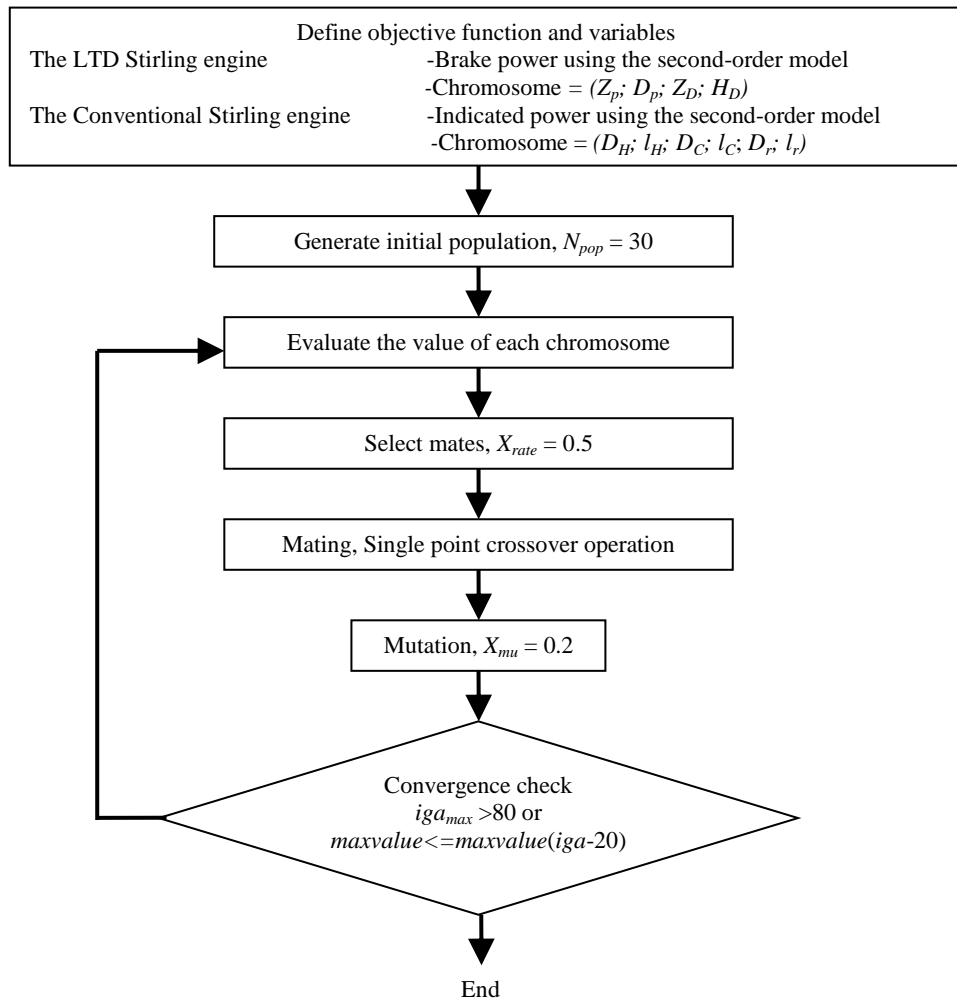


Figure 5.1 A diagram of the continuous GA for the determination of the optimal design parameters of the LTD and conventional Stirling engines

5.2.1.1 Definition of the objective function and variables for finding the optimal design of a LTD Stirling engine

For a LTD Stirling engine, all numerical simulations are run under conditions identical to those for experimental tests of the twin power-piston LTD Stirling

Chapter 5

engine prototype. Most of the engine parameters were kept to be the constant during simulations. There are only four engine parameters which are defined as variables of chromosome, namely the diameter and the stroke of the power piston, the stroke of the displacer and the thickness of the regenerator. Thus, the chromosome can be presented as

$$\text{Chromosome} = (Z_p; D_p; Z_D; H_D) \quad (5.1)$$

where Z_p is stroke of piston (m); D_p is diameter of piston (m); Z_D is stroke of displacer (m); H_D is thickness of regenerator (m).

The appropriate upper and lower boundaries for each variable are as follows:

1. $0.04 < Z_p < 0.3$; Z_p is stroke of piston (m)
2. $0.02 < D_p < 0.13$; D_p is diameter of piston (m)
3. $0.04 < Z_D < 0.3$; Z_D is stroke of displacer (m)
4. $0.01 < H_D < 0.2$; H_D is thickness of regenerator (m)

Boundaries present the constrain function for the variable space of the problem chosen based on the practical manufacture requirements. The diameter of both the power pistons is limited by the diameter of the cold plate which is equal to the displacer diameter. The use of the short piston stroke and the large diameter is recommended for the displacer of a LTD Stirling engine in order to obtain the large swept volume which in turn results in the high volumetric ratio [97]. The engine performance parameter, namely the brake power, is defined to be a chromosome value. The efficiency is considered to be a non-primary parameter since the engine is

Chapter 5

run using solar energy as a heat source. The value of the brake power is determined deploying the developed second-order mathematical model of a LTD Stirling engine (Chapter 3). The objective is used in the following form:

$$\text{Brake power} = f(\text{chromosome}) = f(Z_p; D_p; Z_D; H_D) \quad (5.2)$$

5.2.1.2 Definition of the objective function and variables for the optimal design of a conventional Stirling engine

All heat exchangers of a conventional Stirling engine, namely a heater, a cooler and a regenerator should be carefully designed because these greatly affect the engine performance. Any departure from optimal design dimensions, particularly of the regenerator, may result in a significant drop in the engine's power output [59]. The change in the geometry of heat exchangers leads to the change in the value of the dead volume, pressure drop and heat transfer area which have the main influence on the engine performance. The optimal design search for the small conventional gamma-type Stirling engine located at Northumbria University is only focused on dimensions of its heat exchangers whilst the stroke and the diameter of both the power piston and displacer are kept constant in this study. Six engine parameters defined as variables are as follows: the diameter and the length of heater tube, the diameter and the length of the cooler tube and the diameter and the length of the regenerator:

$$\text{Chromosome} = (D_H; l_H; D_C; l_C; D_r; l_r) \quad (5.3)$$

Chapter 5

where D_H is diameter of heater tube (m); l_H is length of heater tube (m); D_C is diameter of cooler tube (m); l_C is length of cooler tube (m); D_r is diameter of regenerator chamber (m); l_r is length of regenerator chamber (m).

Additionally, the number of tubes of heat exchangers is recalculated by using the pattern of tubes arrangement in each heat exchanger for the 400 Watt small gamma-type Stirling engine.

The choice of boundaries for the value range of variables is based on the practical manufacturing requirements. The upper and the lower boundaries for each variable are as follows:

1. $0.001 < D_H < 0.007$; D_H is diameter of heater tube (m)
2. $0.2 < l_H < 0.8$; l_H is length of heater tube (m)
3. $0.0005 < D_C < 0.01$; D_C is diameter of cooler tube (m)
4. $0.01 < l_C < 0.1$; l_C is length of cooler tube (m)
5. $0.073 < D_r < 0.12$; D_r is diameter of regenerator chamber (m)
6. $0.01 < l_r < 0.15$; l_r is length of regenerator chamber (m)

As in the case of the LTD Stirling engine, the indicated power is used as the objective function and is calculated using the developed second-order mathematical model for conventional Stirling engines (Chapter 3):

$$\text{Indicated power} = f(\text{chromosome}) = f(D_H; l_H; D_C; l_C; D_r; l_r) \quad (5.4)$$

Chapter 5

5.2.2 Generation of the initial population

The initial population (the set of design parameters) is formed in the absolutely random way and presents the matrix formation of various chromosomes:

$$\text{population} = \text{rand} (N_{pop}; N_{var}) \quad (5.5)$$

where N_{pop} is number of chromosomes and N_{var} is number of variables.

The size of the population strongly effects on the speed of the convergence of the problem solution and therefore should be carefully defined. It is recommended that the number of chromosomes should be between 30 and 100 when using GA optimisation [98]. The number of chromosomes (N_{pop}) of 30 per generation is used for optimisation of both LTD and conventional Stirling engines.

5.2.3 Evaluation

The developed second-order mathematical models of a LTD Stirling engine and of conventional MTD and HTD Stirling engines are used to calculate the brake power and the indicated power, respectively. The chromosome values which are the brake power for the LTD Stirling engine and the indicated power of the conventional MTD and HTD Stirling engines are evaluated by the fitness functions. The fitness value then is calculated and ranked in the value map for each generation [99]:

$$\text{Fitnessvalue} = \frac{1}{1 + \text{maxvalue} - \text{value}} \quad (5.6)$$

where maxvalue is the maximum value of chromosome and value is the value of chromosome.

Chapter 5

5.2.4 Selection process

The fitness value of each chromosome is ranked in the descending order to determine survival chromosomes to form the next generation:

$$N_{keep} = X_{rate}N_{pop} \quad (5.7)$$

where X_{rate} is the selection rate of 0.5 and N_{keep} is the number of survival chromosomes. Fittest chromosomes in the ranking list are randomly selected using the weighted random pairing selection procedure using the rank weighting technique described in [94] to be the parents for the reproduction operation.

5.2.5 Mating process

Mating is the process in which the parents are used by the reproduction operator to produce some offsprings for the next generation. The crossover operator is usually the simplest operator used for this process. The single point crossover is the operator with a random position and is applied to a couple of chromosome parents. Design parameters on the different sides from the selected crossover point are swapped between two parents to form two new chromosomes.

5.2.6 Mutation process

If excessively fast convergence occurs in the optimization procedure then the solution found might be a localized maximum or minimum and not the global solution. Therefore, the second operator of the reproduction called the mutation is used as a tool to avoid finding only the local solutions. The mutation initiates the random selection to change the value of some selected parameters in the

Chapter 5

chromosome. Although the high mutation rate of 0.2 results in the relatively slow and gradual convergence, this value is acted to ensure that the global solution is obtained [95].

5.2.7 Convergence check

This procedure finds whether the termination condition of numerical calculation is met. Firstly, the number of the current generation is examined. The maximum number of the generation in the computing process of 80 is specified to ensure the convergence in this algorithm. Secondly, the constant small differences in the values of the best brake power in the case of a LTD Stirling engine or the best indicated power in the case of a conventional Stirling engine for the last twenty generations is used to terminate numerical calculations before the computing process reaches the maximum number of generations. If the convergence in the solution is not reached, then the population of chromosomes of new generation is formed using the fitness selection process.

The optimisation code developed for this study was modified from a simple continuous GA code presented in [94]. All procedures described above were implemented in MATLAB. The developed continuous GA code was coupled to the second-order mathematical model of a LTD Stirling engine and that of a conventional Stirling engine. The optimisation was carried out for the same operating conditions for which experimental data was obtained for both LTD and conventional Stirling engines.

Chapter 5

Finally, the solutions obtained from optimisation computing were used to create the engine computational mesh for 3D CFD simulations to more accurately predict the engine's power.

Chapter 6

Mathematical modelling and optimisation of the design of a LTD Stirling engine

This chapter presents results on the second-order mathematical modelling and optimisation of the design of a LTD Stirling engine. Analysis of the working process of the engine was carried out using the developed second-order mathematical model and the 3D CFD modelling. The optimisation calculations were performed using the GA method. The first section presents results obtained from the numerical simulation of the working process of the twin-power piston LTD Stirling engine described in [70] using the developed second-order mathematical model. Results concerning the working process of the engine are discussed in details. The results obtained from 3D CFD modelling of the LTD Stirling engine are described in the second section of this chapter. The last section presents the results obtained from the GA optimisation method coupled to the developed second-order mathematical model of the LTD Stirling engine. Two sets of the optimal engine design parameters are presented and the 3D CFD modelling was applied to the optimal design of the engine for obtaining better accuracy in the prediction of the engine performance.

Chapter 6

6.1 Results obtained using the second-order mathematical model

The numerical results were obtained by modelling the working process of the twin-power piston LTD Stirling engine for the operating conditions described by Kongtragool and Wongwises in [70]. For numerical simulations of the engine the developed second-order mathematical model was used. The geometry and information on the engines' prototype was presented in Chapter 3 and in Table 3.1. The LTD Stirling engine was run with the use of the constant irradiation flux generated by the solar simulator. The water cooling system was used as a heat sink. The hot plate of the engine was exposed to the intensive irradiation of $5,097 \text{ W/m}^2$ whilst the cold plate was constantly kept at the temperature level of 307 K. Air at the atmospheric pressure was used as the working gas in the engine. Atmospheric pressure and atmospheric temperature were defined as 1 bar and 305.5 K, respectively. Furthermore, the matrix in the regenerator was assumed to be made of the SM 15 metal sponge with the wire diameter of 0.0003 m and the porosity of the regenerator was 0.956 [85]. The LTD engine ran at the speed of 46.5 rpm. The heat input to the engine was determined experimentally to be 230.2 W [70].

6.1.1 Analysis of the working process

The parameters of the working cycle inside the engine, namely the variation of volumes, pressure and temperature of the gas and the engine performance in terms of the brake power and efficiency are presented below in the form of diagrams.

Thus, the volume variation of the expansion and compression spaces and also that of the total volume inside the engine are presented in Figure 6.1 as functions of the crank angle. It can be seen that the sinusoidal lines for volumes of the expansion and

Chapter 6

compression spaces are almost in anti-phase. The amplitude in the change of the total volume inside the engine is relatively small since it is defined by the volumes of the power pistons only. The volume of the compression space is calculated by summation of the volume swept by power piston and the dead volume at the top of the displacer chamber (above the displacer). The volume located under the displacer is defined to be the volume of the expansion space. The volume ratio of 7.15 was obtained for this particular LTD Stirling engine which is thought to be a good value for the engine [96].

Figure 6.2 shows the variation of the pressure inside the engine with respect to the crankshaft angle. All pressure lines are close to each other and of a sinusoidal form. The maximum operating pressure inside the engine over the cycle is 103,647 Pa at 292° of the crankshaft angle. The pressure ratio in the cycle, which is the ratio of the maximum and minimum pressures, is 1.071. It can be seen that there is the very little difference in the pressure values in each space of the engine. Such the small difference of pressures in each part is due to a small pressure drop in the regenerator which is only a heat exchanger installed in the LTD Stirling engine. The variation of the pressure drop when the working gas flows through the matrix of the regenerator is presented in Figure 6.3. The peak value is only about 10 Pa. This is due to the high porosity of the regenerator (0.956) and the low engine speed of 46.5 rpm. The maximum pressure drop is approximately 0.01 % of the operating pressure and it can be seen that the pressure drop has an insignificant effect on the engine performance.

The variations of the gas temperature in each space are presented in Figure 6.4. The gas temperature in the expansion space slowly increases in the first third of the cycle

Chapter 6

and then rapidly rises when the displacer approaches the top dead centre peaking at 491.29 K at the crankshaft angle of 187° . Then the temperature of the gas rapidly reduces with displacer moving towards the bottom dead centre (from 187 and 270 degrees of the crankshaft angle). For the rest of the cycle there is only slow reduction in the temperature of the gas in the expansion space. The magnitude of the temperature variation in the expansion space is about 50 K. In the compression space the temperature variation is also mainly determined by the movement of the displacer. The gas temperature has the lowest value of 375.73 K when the displacer is at the bottom dead centre and the temperature range in this part of the engine is also about 50 K. The temperature variation in the working gas in the regenerator is of a sinusoidal form and is between the temperatures of the working gas in the expansion and compression spaces whilst the matrix temperature is almost constant at about 430 K. The constant temperature of the regenerator matrix can be explained by its large heat capacity. Temperatures of the gas and in the matrix are very similar to the behavior of the gas and matrix temperatures in the simple stationary regenerator of conventional Stirling engines although the matrix of the regenerator in the LTD Stirling engine is contained in the moving displacer. Overall, the gas temperature variation in each part of the LTD Stirling engine depends on the change in the corresponding volume and the heat flow rate.

Chapter 6

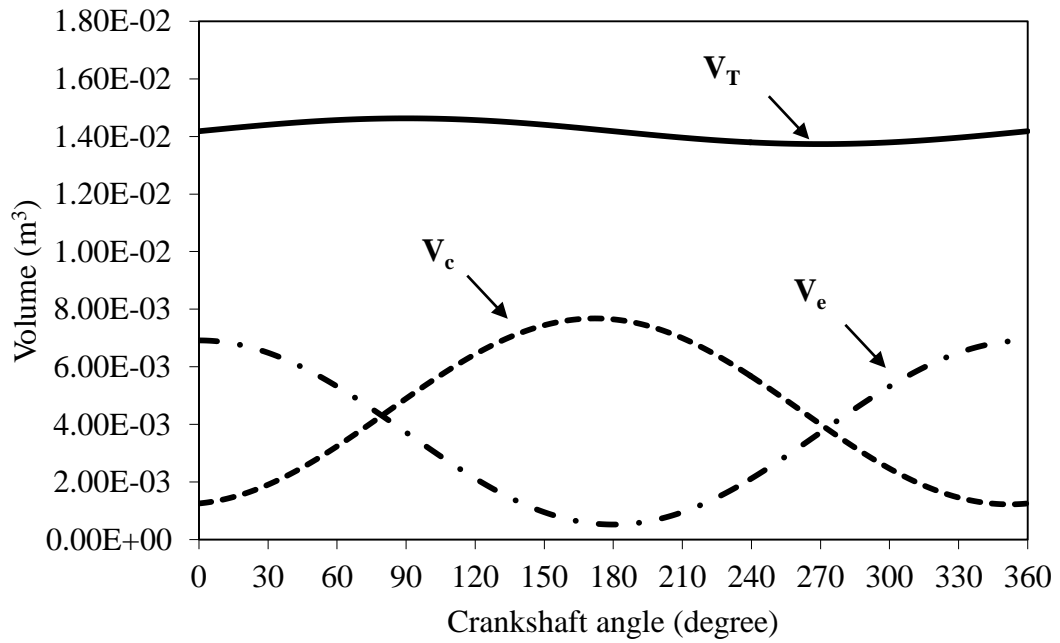


Figure 6.1 The variation of the volumes in the engine

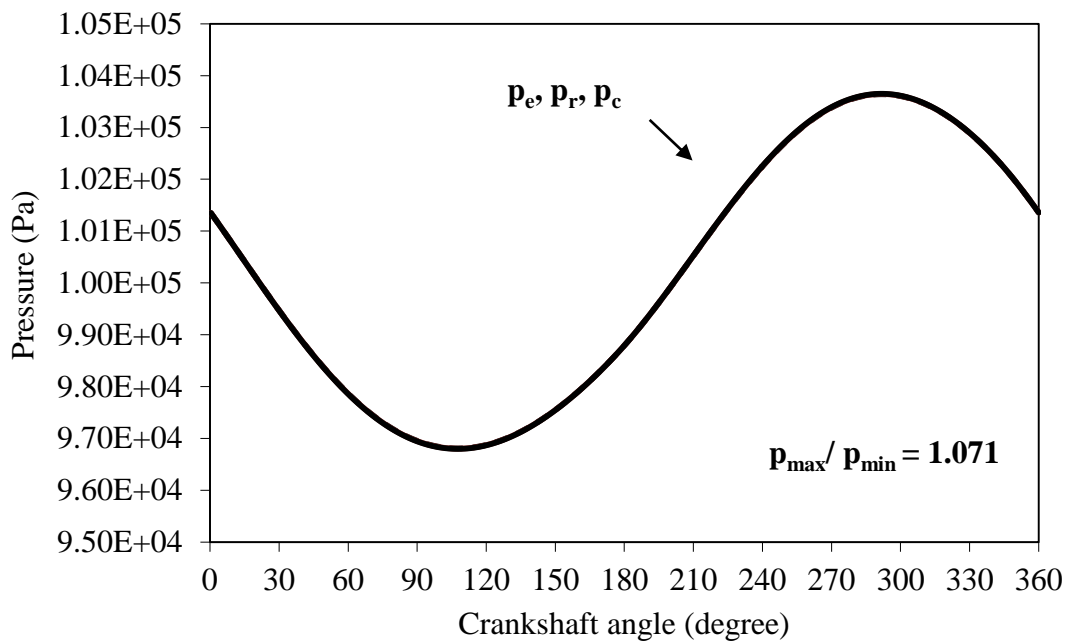


Figure 6.2 The variation of the pressures in the engine

Chapter 6

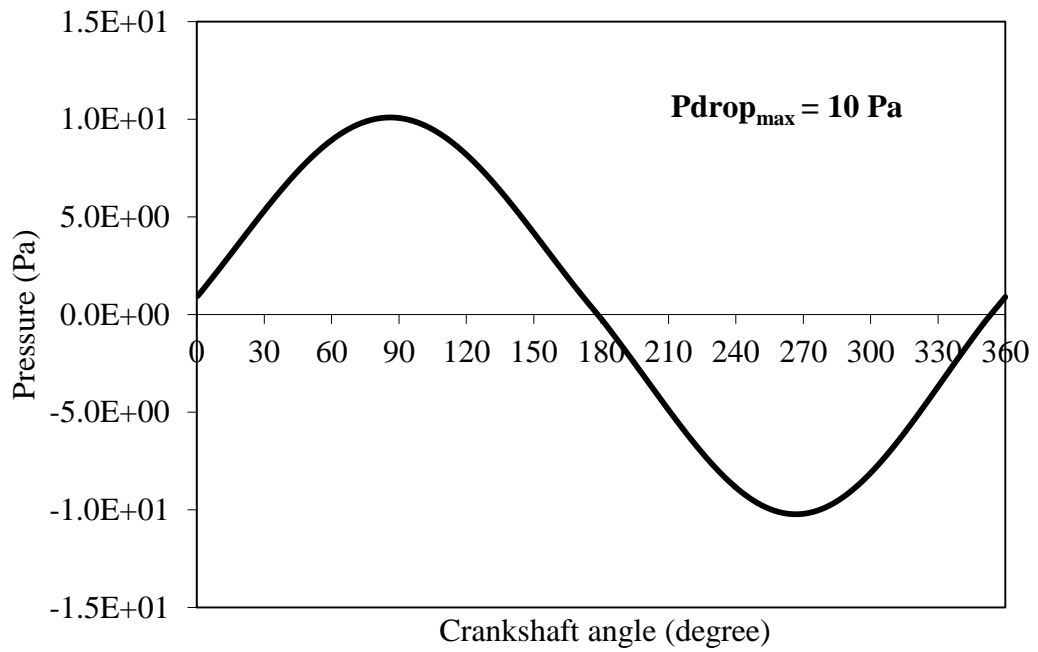


Figure 6.3 The variation of the pressure drop in the engine

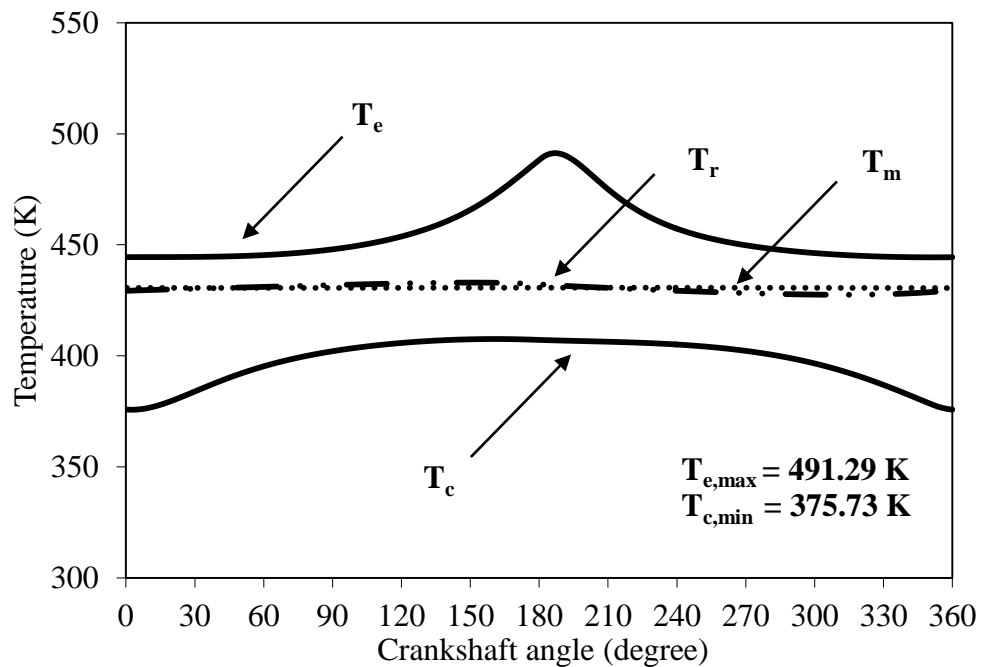


Figure 6.4 The variation of the temperatures in the engine

Chapter 6

The variations in the heat flow rates in different parts of the engine are presented in Figure 6.5. It can be seen that the lowest values of the absorbed heat flow rate in the expansion space and of the rejected heat flow rate in the compression space occur when the displacer is at the top and the bottom dead center positions. At these positions when direction of piston motion is reversed, the velocity of the displacer is zero and it affects the heat transfer coefficient at the hot and cold plates. Such behavior in the heat transfer differs from that in the heater and cooler of a conventional Stirling engine. In addition, the heat dissipation due to the friction flow throughout the regenerator is very small because of the low pressure drop in the cycle.

Although the absorbed and the rejected heat flow rates on the heat transfer surfaces at the moment of the cycle corresponding to the piston top and bottom dead centers in both spaces are low, it can be seen in Figure 6.4 that the gas temperatures have the maximum and minimum values, respectively, and the temperature rapid rise or drop is because of very small volumes at those positions which indicates the dominant influence of the volume on the temperature change in the gas. For the regenerator space, mainly the heat flow rate between the matrix and the working gas affects the gas temperature variation in the regenerator.

P-V diagrams for the engine are shown in Figure 6.6. The calculated area of the P-V diagram of the expansion space represents the positive work whilst the negative cyclic work is found from the calculation of the area of the P-V diagram of the compression space. The net calculated indicated power is found as a difference of

Chapter 6

PV diagrams areas multiplied by a number of cycles per second and it is 1.276 W for this particular engine.

From analysis of the mechanical transmission mechanism, the values of the positive and negative torques are obtained exerted by the power and displacer pistons. The simulation shows the LTD Stirling engine generates the total brake power of 1.117 W while the overall efficiency of the engine is 0.486 %.

It could be established that there is a close correlation between the numerical results of the working process described above and the results from the mathematical modelling presented in [72]. Thus, it can be concluded that the numerical results obtained using the second-order mathematical model developed in this work are closely describe the operation and the working process of the LTD Stirling engine.

6.1.2 Validation of the developed second-order mathematical model of a LTD Stirling engine

Figure 6.7 and Figure 6.8 illustrate the engine performance results obtained using the developed second-order mathematical model and those obtained from the experiments presented by Kongtragool and Wongwises in [70]. It can be seen in Figure 6.7 that the predicted indicated and brake powers first rise to its maximum point at the speed equal to about 50 rpm and then drop with the further increase in the engine speed. The trend in variation of the theoretical brake and indicated power curves is similar to that from the experiments. The experimental power output obtained in [70] first rapidly increases with the rise of the speed peaking at 0.969 W at the speed of 46.5 rpm and then with further rise of the shaft speed it decreases.

Chapter 6

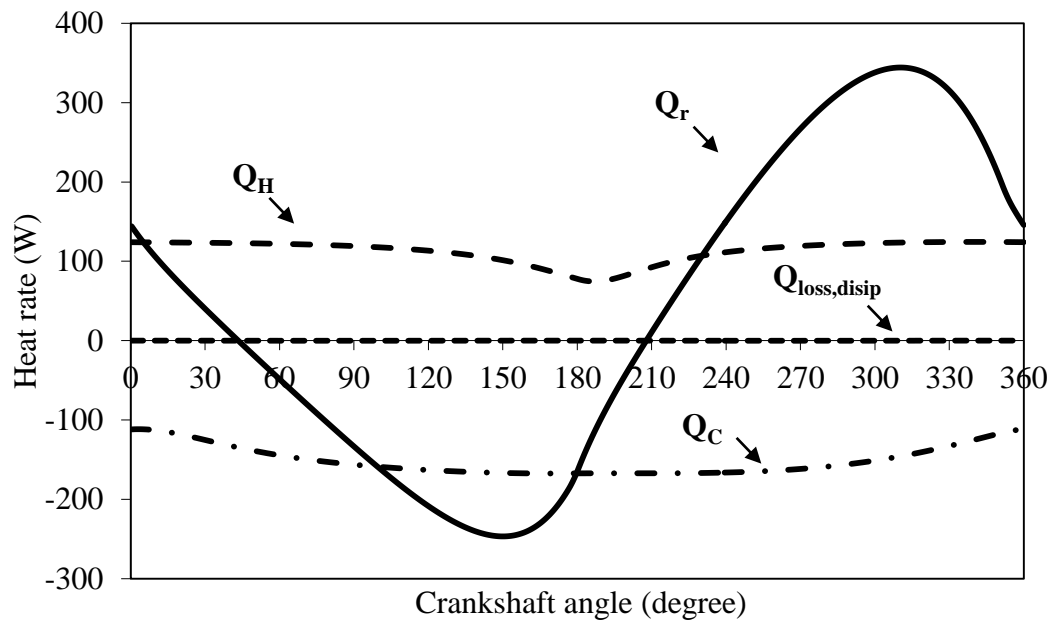


Figure 6.5 The variation of the heat rates in the engine

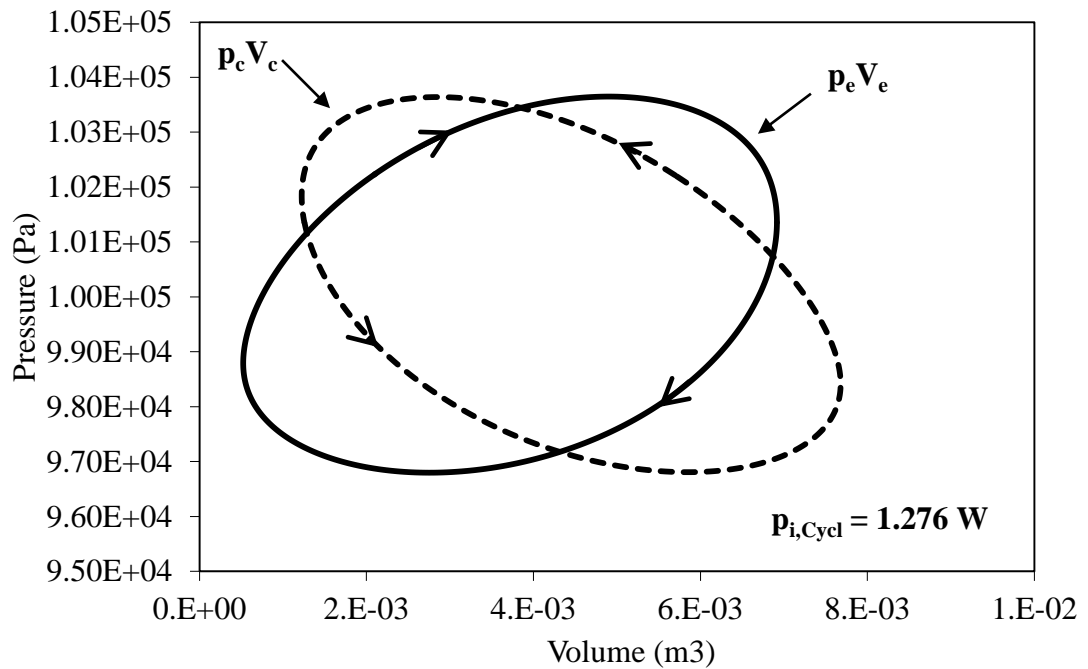


Figure 6.6 P-V diagrams

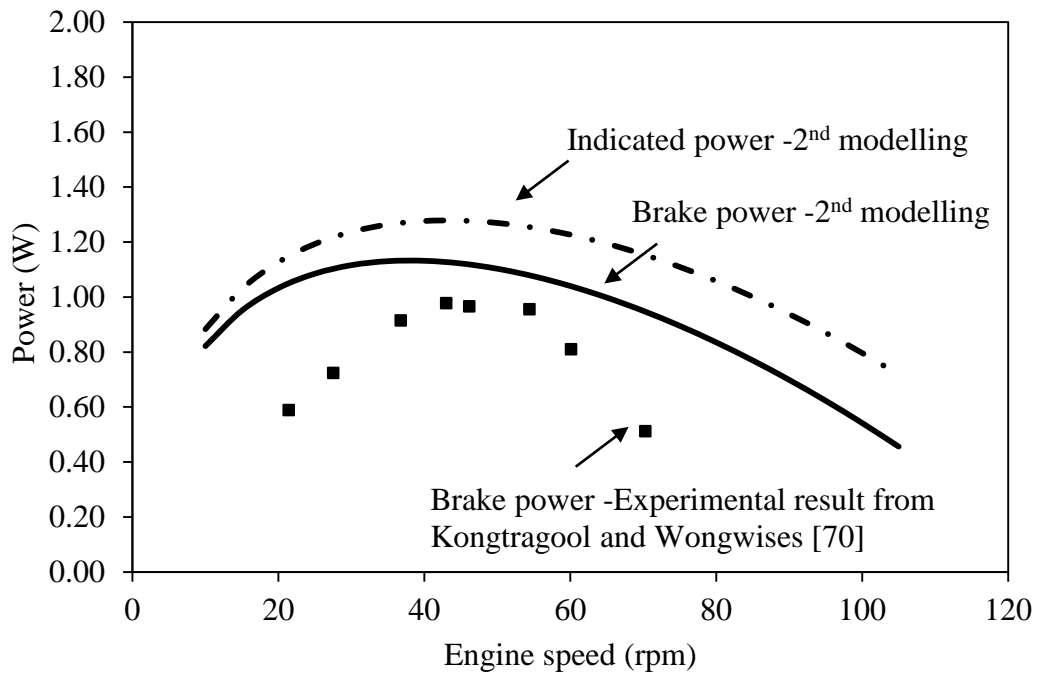


Figure 6.7 The predicted brake power with respect to the engine speed

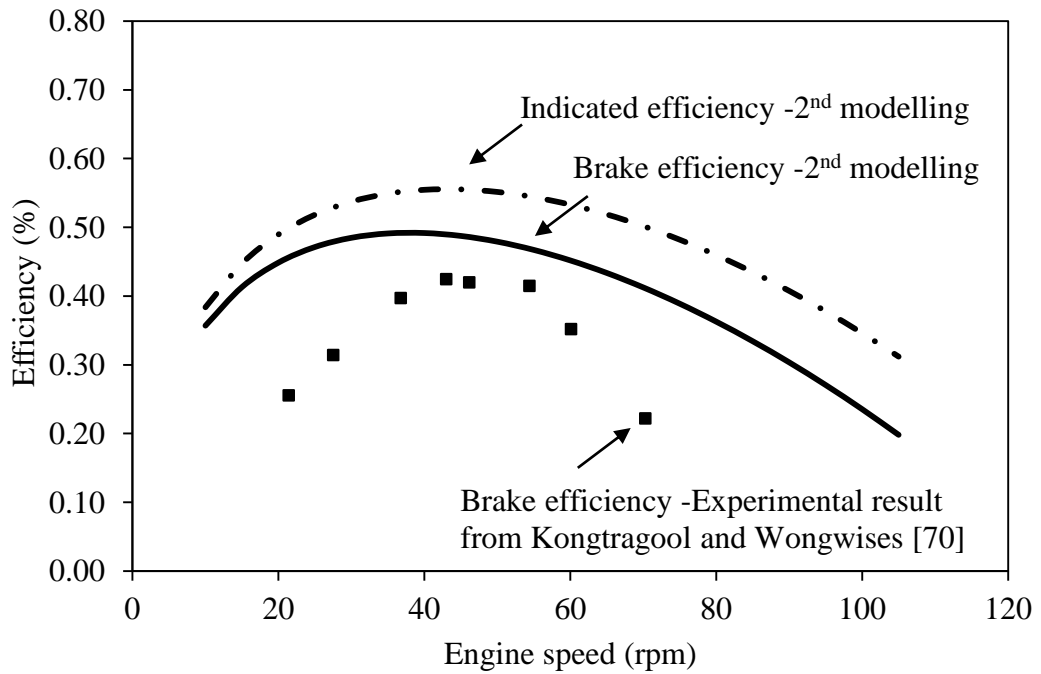


Figure 6.8 The predicted overall efficiency of the engine with respect to the engine speed

Chapter 6

Furthermore, the numerical results show that the range of the mechanical efficiency of the transmission mechanism is between 75-92 %. It is because there are frictional losses in the rubber seals of the displacer rod and of the crankshaft of this engine. The mechanical efficiency is overall high because the engine is operated at a low speed compared to the engine speed of conventional Stirling engines. The predicted overall efficiency curve as a function of the engine speed is shown in Figure 6.8.

Its value is determined as the engine's power divided by the heat input of 230.2 W in the experiments described in [70]. Figure 6.8 shows that the theoretical overall efficiency curve has the same trend as in experimental data.

The maximum brake power and the overall efficiency from the experimental results are 0.969 W and 0.421 % at the engine speed of 46.5 rpm [70], respectively whilst the theoretically predicted brake power and the overall efficiency are 1.117 W and 0.486 %, respectively. The predicted brake power has the error of 15 % when compared to the experimental result at the engine speed of 46.5 rpm. Accuracy of 15% in numerical predicting of the engine's power output in designing of Stirling engines is considered to be acceptable. The models developed in this study provide the improved accuracy in numerical simulations compared to previously published results. For example, in [43] it was demonstrated that the second-order mathematical model had an error of 30 % in predicting of the performance of the engine.

Therefore, it could be said that there is an acceptable agreement between the experimental and the predicted results. The best correlation is achieved at the middle zone of the engine speed at which the maximum value of the actual brake power is achieved. Diagrams, however, show the significant difference between the predicted

Chapter 6

brake power and the experimental result at the lower engine and higher engine speeds. It might be caused by application in the second-order mathematical model the heat transfer coefficient calculations using the heat transfer correlation derived for the high speed reciprocating engine whilst the LTD Stirling engine operates at low speeds. It is possible also that the prediction of the flow friction in the regenerator is calculated using correlations derived for high engine speeds. Therefore, more appropriate heat transfer and friction correlations should be derived and applied in the mathematical model of a LTD Stirling engine in order to obtain better accuracy in predictions.

However, it might be concluded that the developed second-order mathematical model can be used for the analysis of the working process and the acceptable prediction of the performance of LTD Stirling engines.

6.2 Results obtained using 3D CFD modelling

A 286,852 cell computational mesh for the simplified geometry of the LTD Stirling engine was created using ANSYS, see Figure 6.9. This 3D simplified geometry consists of the twin-power piston LTD engine with two compression spaces in the piston cylinders, the expansion space and the gap between the displacer and its cylinder and the regenerator space. The boundary conditions applied in CFD modelling are similar to that observed in experimental tests described in [70]. The constant solar irradiation flux of $5,097 \text{ W/m}^2$ was applied on the surface of the hot plate by using the solar model in ANSYS. The heat convection losses to the free air stream with the constant velocity of 4 m/s and the constant temperature of 305.5 K were defined as the boundary conditions on the surface of the hot plate.

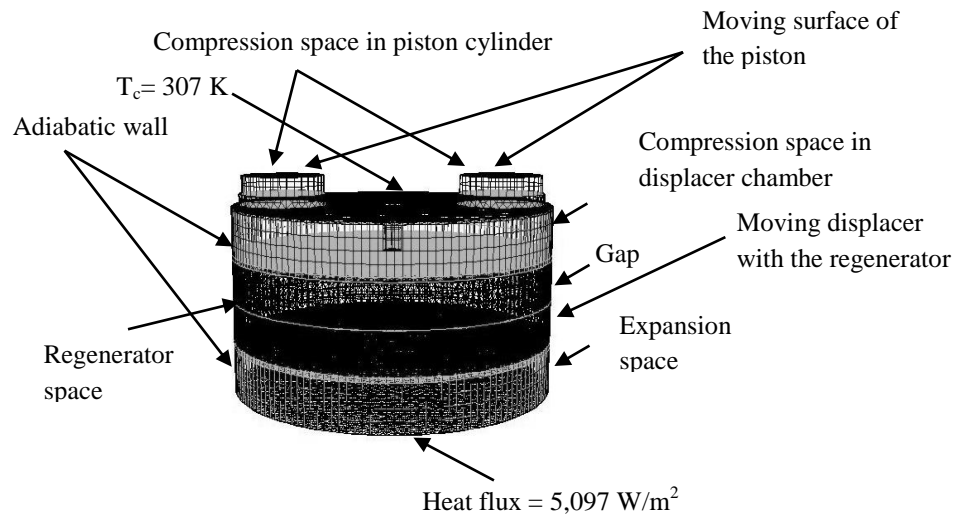


Figure 6.9 A simplified geometry and computational mesh of the LTD Stirling engine

Also heat losses due to re-radiation from the hot plate to the environment were considered in order to closely simulate the laboratory test conditions. For the cold plate the constant temperature of 307 K was defined on its surface. The cylinders of power pistons and of the displacer were assumed to be adiabatic. The space in the regenerator was defined as a porous media zone with properties of the SM 15 metal sponge. The values of the inertial and viscosity resistant factors were to be defined in the porous zone. These could be obtained by using the empirical correlations of pressure drop presented in [85] and the method described in the ANSYS manual [99]. The initial gas temperatures in the expansion and compression spaces were set to be equal to the wall temperatures of the heater and cooler. The initial gas temperature in the porous zone was set as the average value of the heater and cooler temperatures. These simulations were performed with the initial operating pressure of 1 bar and the engine speed of 46.5 rpm.

Chapter 6

The first cycle was run with allocation of 300 iterations per each with the under-relaxation factors for the pressure, momentum, density, body forces and energy set at 0.3. Less than 100 iterations in each time step were requested to achieve the convergence during the second cycle. The simulations were run until the steady condition operation was reached so that the temperature and pressure variations in each space in the last cycles stay approximately the same.

The results obtained from the 3D CFD modelling procedure are presented as velocity, pressure and temperature distributions in the working gas inside the engine.

6.2.1 Analysis of the CFD modelling results

The gas velocity vectors inside the engine in the vertical plane passing through the axes of the displacer and power pistons for the instances of the cycle when the crankshaft angle is 90, 180, 270 and 360° are shown in Figures 6.10 - 6.13. Every figure clearly shows the flow patterns and the gas velocity range is between 0.0002-0.0623 m/s. The middle and upper ranges of the velocity are observed in the expansion and compression spaces. The relatively high velocities affect the heat transfer rates on the surfaces of the hot and cold plates. The average heat transfer coefficients on the heater and cooler surfaces are 2.77-7.70 W/m²K. It is worth noticing that the average heat transfer coefficient obtained from 3D CFD modelling is less than that obtained from the second-order mathematical modelling. These results are consistent with the discussion presented in the previous section that the more suitable heat transfer correlations should be derived for the reciprocating flow in LTD Stirling engines.

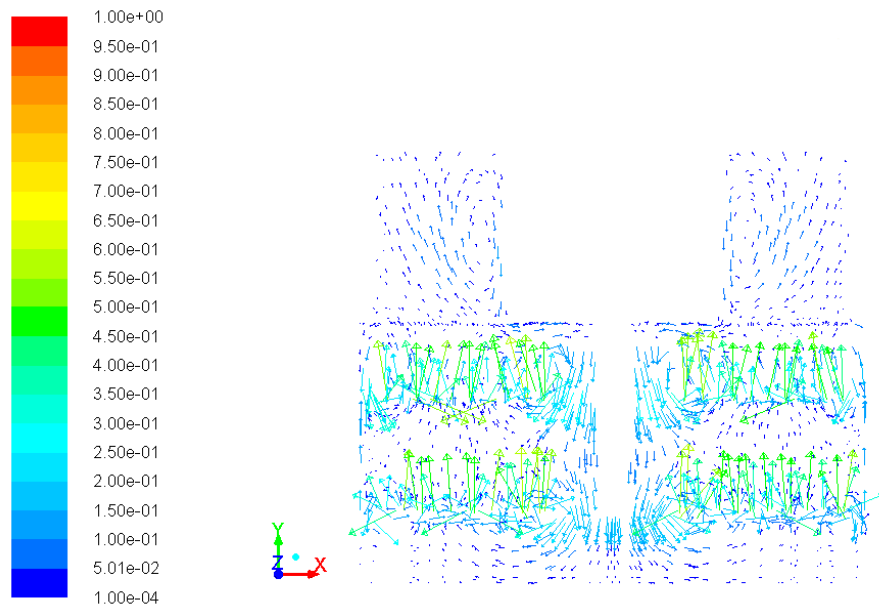


Figure 6.10 The velocity distribution of the gas inside the engine at the instance of cycle when the crankshaft angle is 90°

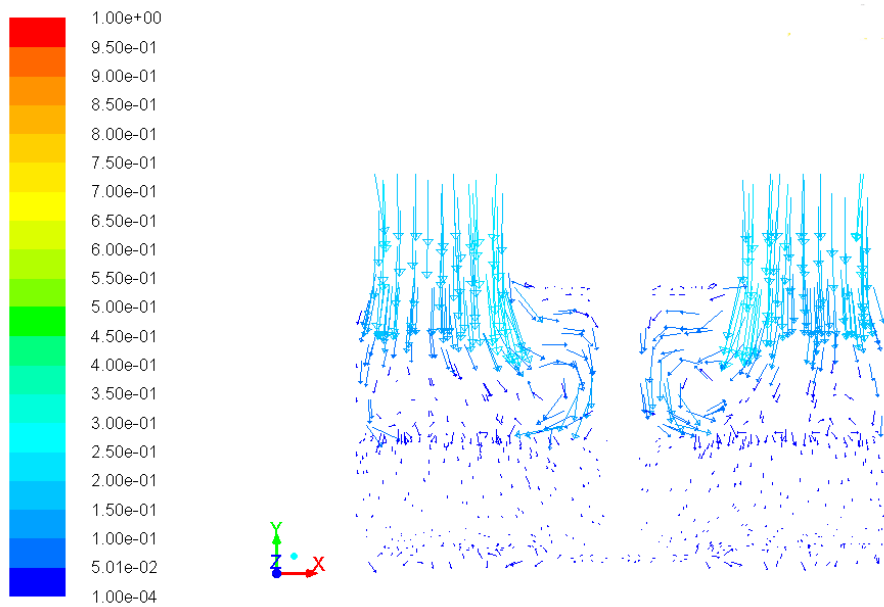


Figure 6.11 The velocity distribution of the gas inside the engine at the instance of cycle when the crankshaft angle is 180°

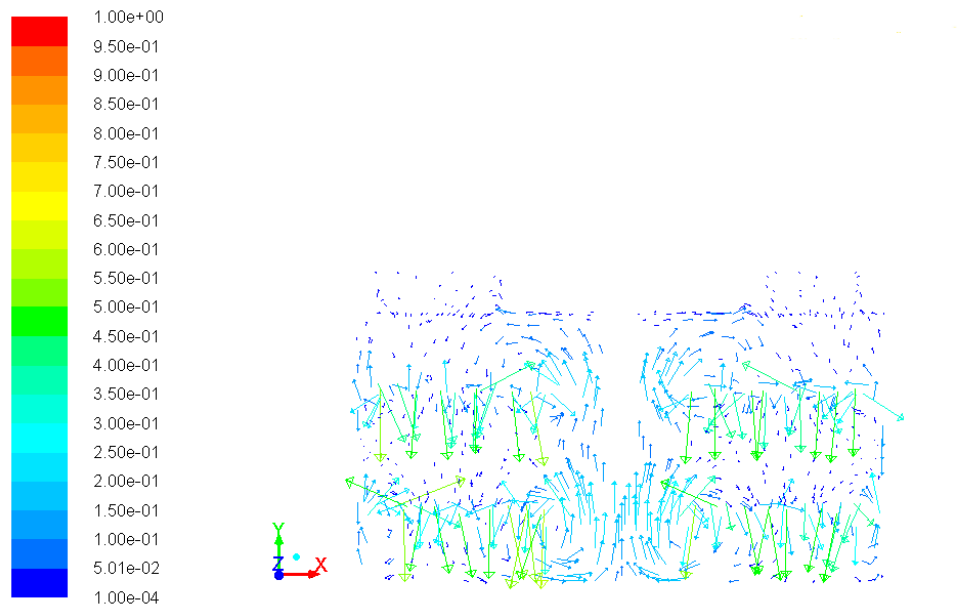


Figure 6.12 The velocity distribution of the gas inside the engine at the instance of cycle when the crankshaft angle is 270°

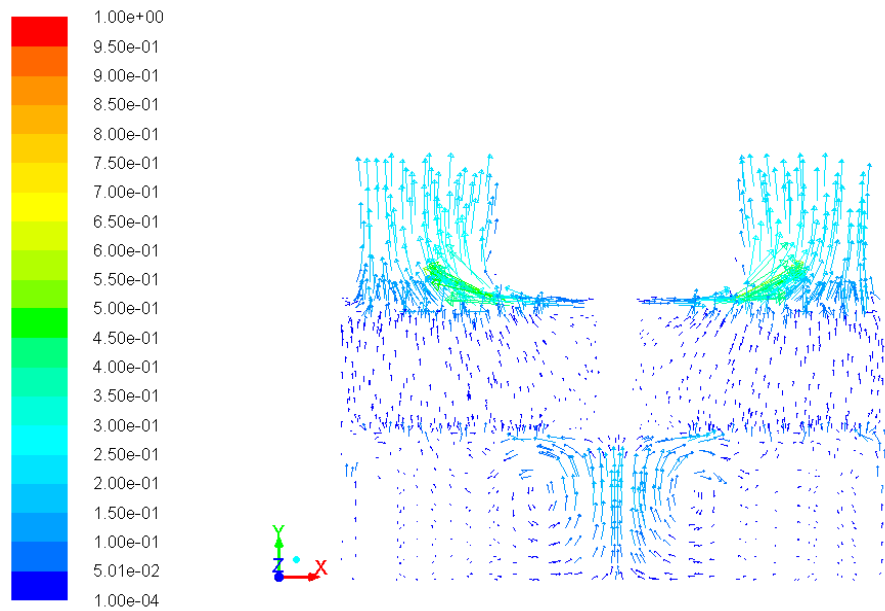


Figure 6.13 The velocity distribution of the gas inside the engine at the instance of cycle when the crankshaft angle is 360°

Chapter 6

The casing of the regenerator is made from a round sheet with a number of round 1/8" perforated holes. The velocity vector figures demonstrate that there are low gas velocities in the moving regenerator. This is because there is resistance to the gas flow through the regenerator matrix.

Figures 6.14-6.17 present the temperature distributions of the gas inside the engine for four instances of the cycle. It could clearly be seen that there is a significant difference in the temperature between all spaces over the whole engine cycle. The gas temperature is high at the bottom part of the engine and is lower at its top part. The gas in the space under the displacer core in the expansion space has the highest temperature and it is because of the hot plate located at the bottom part of the displacer chamber. The temperature in this space peaks around the cylinder axis. The temperature of the gas gradually decreases across the regenerator from the bottom to upper part of the engine. The temperature is reduced in the compression space due to the heat rejection to the cold plate at the top of the displacer chamber. The temperature distribution in the compression and expansion spaces at different instances of the cycle is caused by the gas flow patterns. The small variation of the temperature of the gas in the regenerator is because of very low gas flow velocities inside the regenerator. In calculations the average gas temperature in each space was found and plotted to more clearly present the variation of the gas temperature as a function of the crankshaft angle, see Figure 6.18. It can be seen that there is an increase in the average gas temperature in the expansion space while displacer is moving towards the hot plate. The peak temperature in the cycle is about 480.52 K and this value is lower than the result from the second-order modelling. This is

Chapter 6

because the heat transfer coefficient value for heat exchange between the hot plate and the working fluid in the 3D CFD modelling is lower. The average gas temperature in the compression space in the displacer cylinder rises to the maximum point at 410.73 K and then drops to the minimum point at about 366.84 K whilst the average temperature in the compression spaces in the piston cylinders has a low fluctuation at the temperature of 376.86 K.

The pressure contours inside the engine for four instances are shown in Figure 6.19-6.22. It can be seen that there is a very little (often undetectable) difference in the gas pressure across the working space of the engine for any instance of the cycle. The pressure difference across the gas circuit is up to 5 Pa. It is because of the small pressure drop while the gas travels inside the engine and this result is very similar to that obtained from the second-order mathematical modelling. This is clearly seen in Figure 6.23 which shows the average gas pressures in each space over the operating cycle. The maximum average pressure of about 103,682 Pa in the engine is achieved when the crankshaft angle is 288° and the minimum average pressure is 96,207 Pa at the crankshaft angle of 100° . The pressure ratio in the cycle of 1.078 which is close to that obtained from the thermodynamic modelling.

Figure 6.24 shows P-V diagrams for the expansion space and the compression space in the displacer chamber and for the compression spaces in the piston cylinders. It is found that the positive works are produced in the expansion space and the compression spaces in the piston cylinders while the negative work is done on the gas in the compression space of the displacer chamber. The net indicated power of the engine is 1.162 W at the engine speed of 46.5 rpm.

Chapter 6

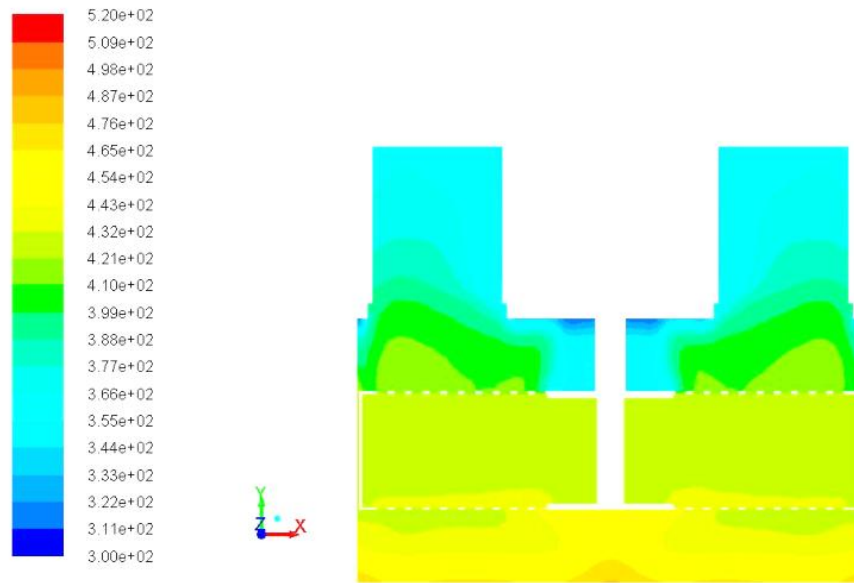


Figure 6.14 The temperature distribution of the gas inside the engine at the instance of cycle when the crankshaft angle is 90°

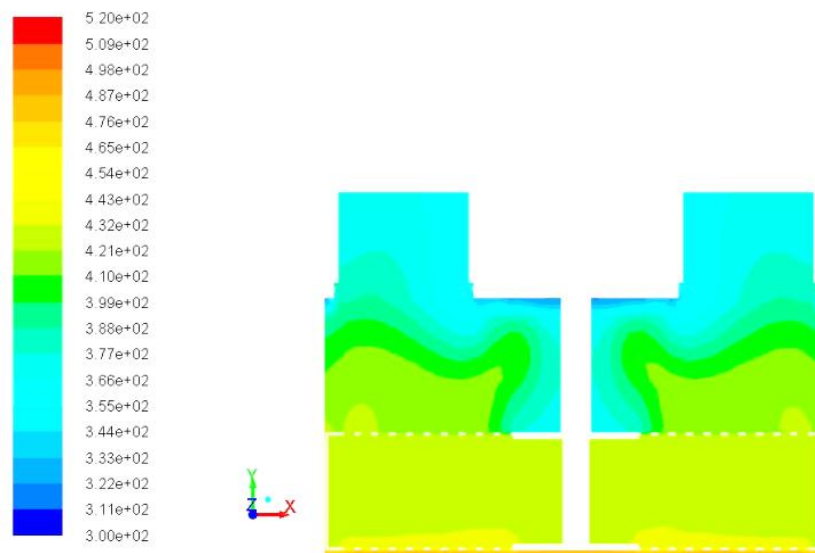


Figure 6.15 The temperature distribution of the gas inside the engine at the instance of cycle when the crankshaft angle is 180°

Chapter 6

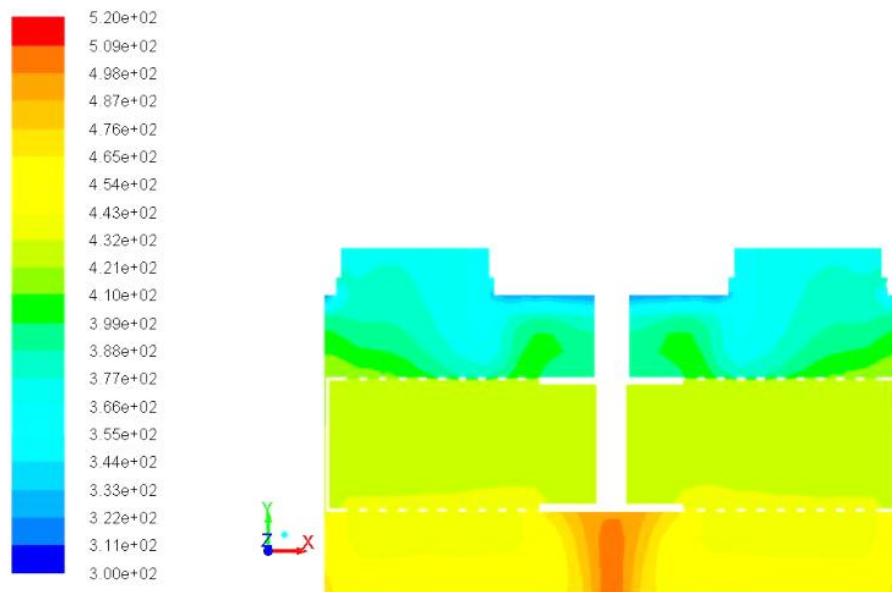


Figure 6.16 The temperature distribution of the gas inside the engine at the instance of cycle when the crankshaft angle is 270°

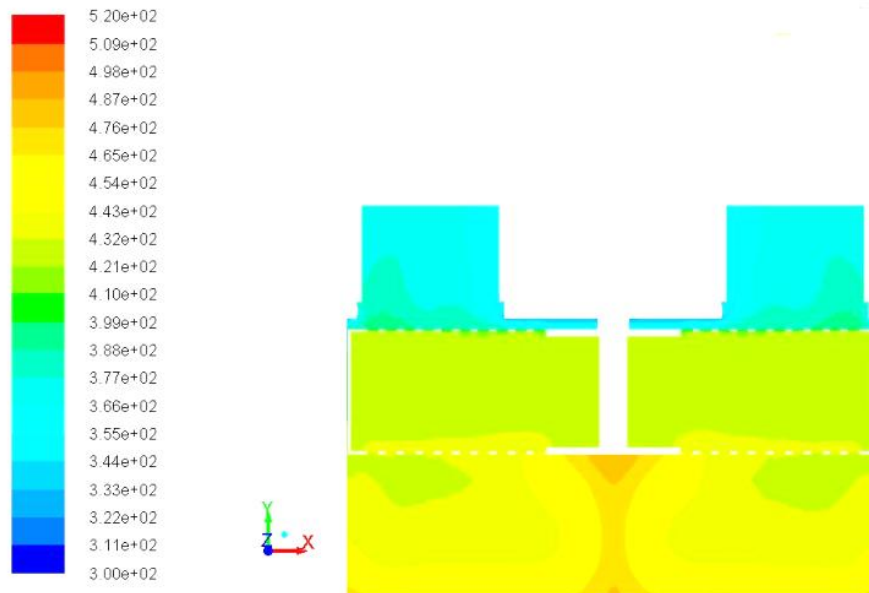


Figure 6.17 The temperature distribution of the gas inside the engine at the instance of cycle when the crankshaft angle is 360°

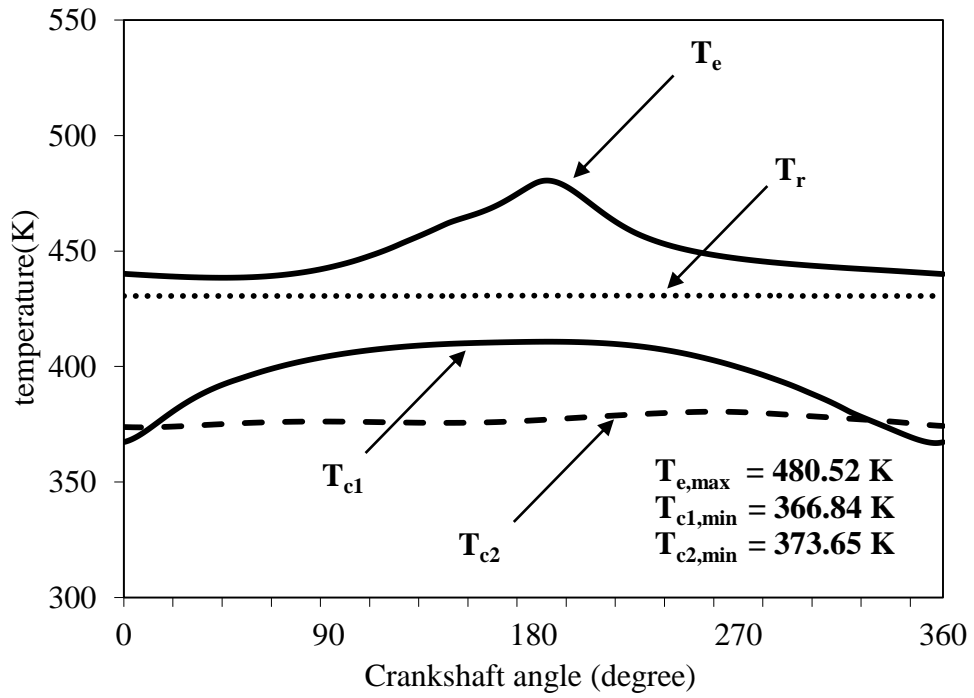


Figure 6.18 The average gas temperatures in each space of the engine over its cycle

Chapter 6

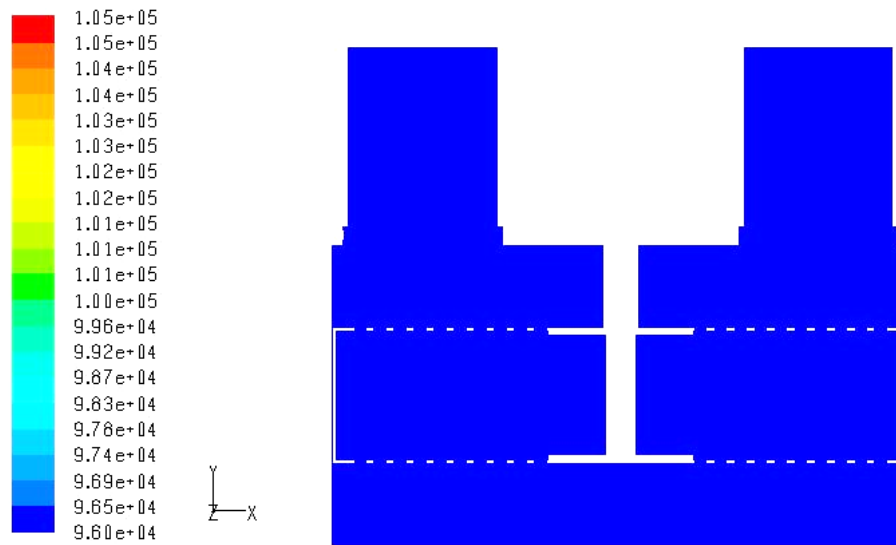


Figure 6.19 The pressure distribution of the gas inside the engine at the instance of the cycle when the crankshaft angle is 90°

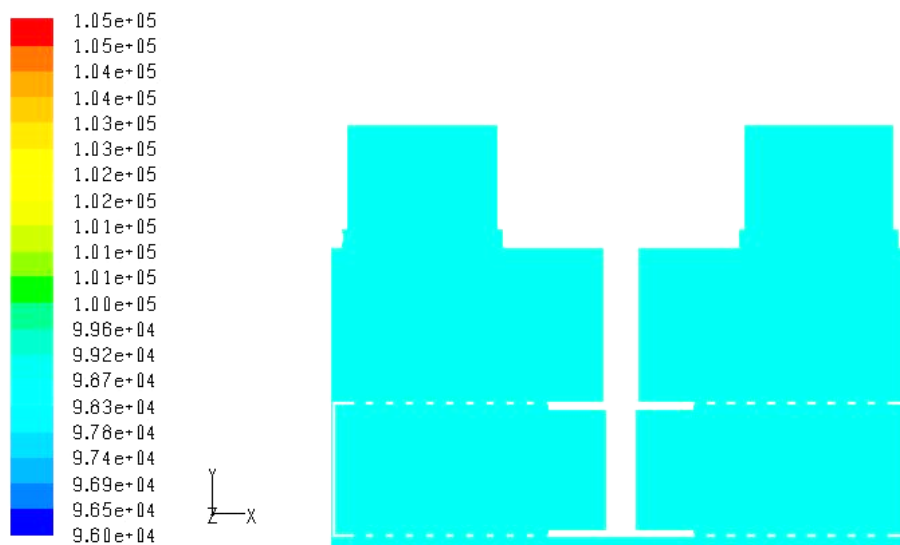


Figure 6.20 The pressure distribution of the gas inside the engine at the instance of the cycle when the crankshaft angle is 180°

Chapter 6

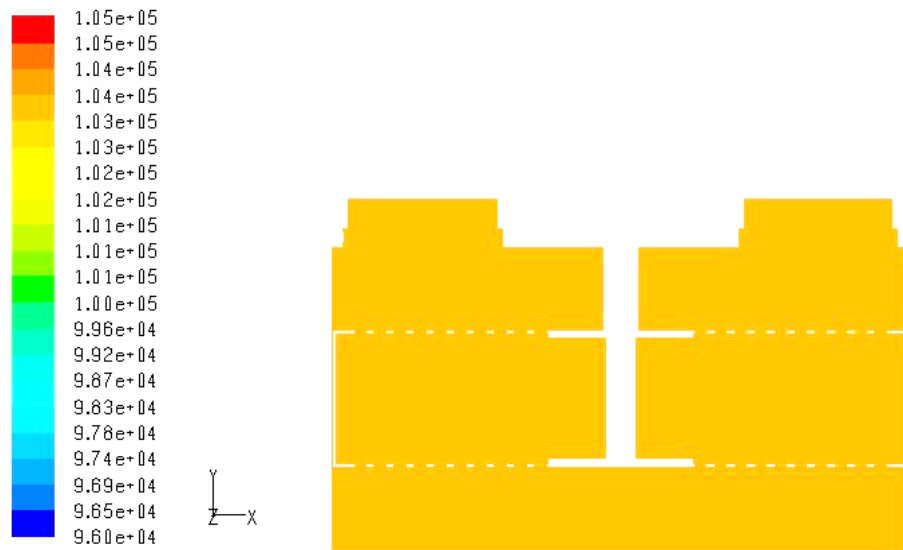


Figure 6.21 The pressure distribution of the gas inside the engine at the instance of the cycle when the crankshaft angle is 270°

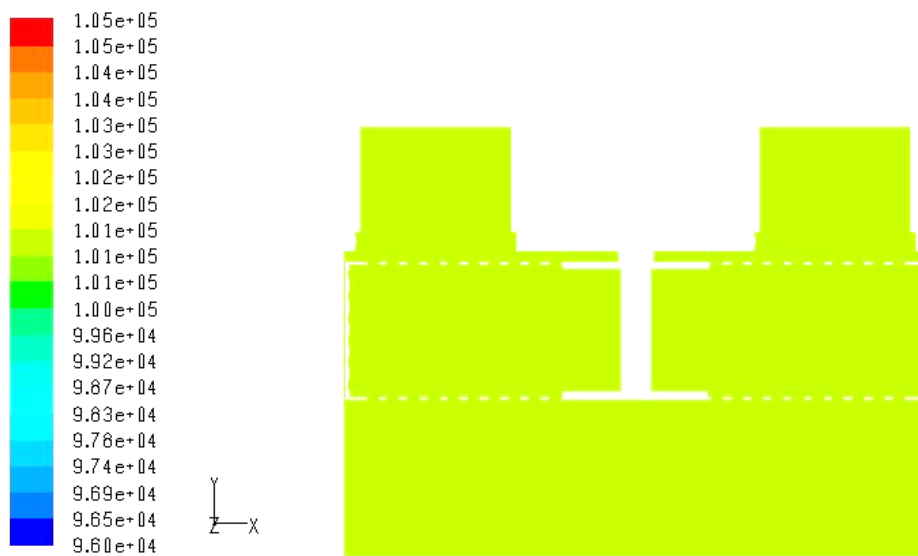


Figure 6.22 The pressure distribution of the gas inside the engine at the instance of the cycle when the crankshaft angle is 360°

Chapter 6

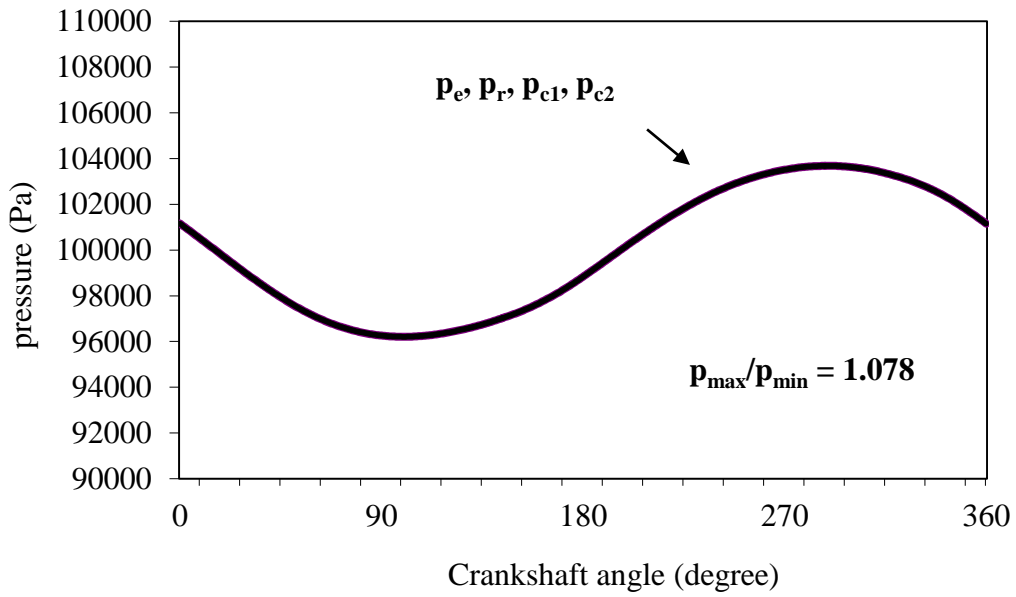


Figure 6.23 The average pressures in each space of the engine over its operating cycle

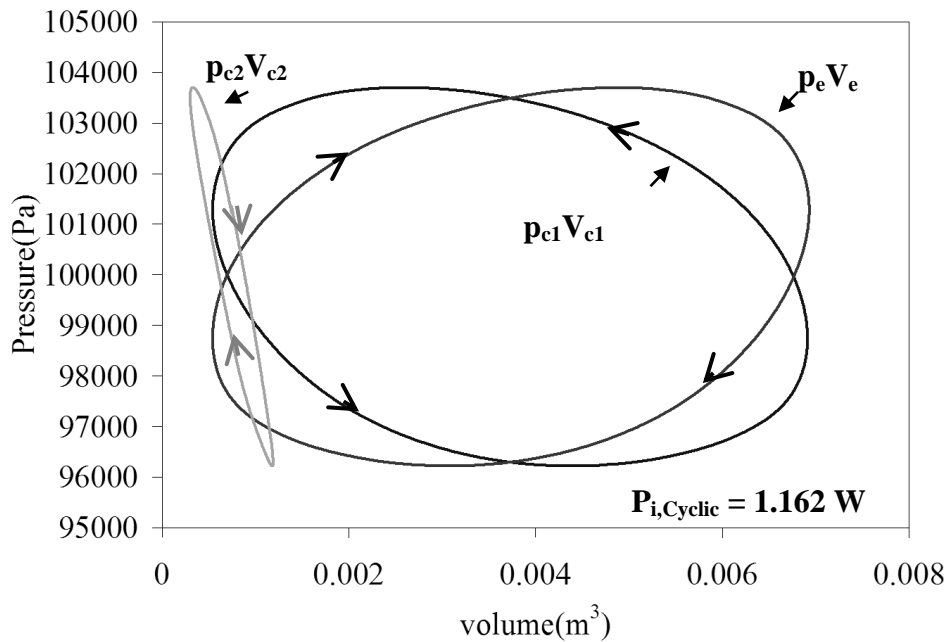


Figure 6.24 P-V diagrams of the engine obtained using the 3D CFD modelling

Chapter 6

Overall, the 3D CFD modelling provide very detailed information on the heat transfer and gas flow processes inside the engine and this data can be used for refinement of the design LTD Stirling engines.

6.2.2 Validation of CFD modelling

The predicted engine performance obtained from the 3D CFD modelling was validated with the use of experimental results published by Kongtragool and Wongwises in [70]. Table 6.1 compares results obtained using the second-order modelling, the CFD theoretical results and experimental results from the laboratory testing. The indicated power of 1.162 W is obtained using the 3D CFD modelling and this value is close to the experimental data than 1.276 W obtained from the developed second-order mathematical model. Overall results in this work are consistent with conclusions made in several published works stating better accuracy of results obtained using 3D CFD modelling [43]. Although the better results are obtained using 3D CFD simulations, the complicated procedure for mesh generation, the preparation time and also the computing time should be carefully considered in design the procedure.

From analysis of results, it might be concluded that the developed second-order mathematical model which provides the acceptable accuracy in the prediction of the engine performance can be efficiently used for coupling with an optimisation code in order to determine the optimal design parameters of Stirling engines.

Chapter 6

Table 6.1 Comparison of the theoretical and experimental results on the LTD

Stirling engine's power production

Results	Experimental result	The developed second-order model result	3D CFD result
Indicated power (W)	-	1.276	1.162
Brake power (W)	0.969	1.117	-
Overall Efficiency (%)	0.421	0.486	-

6.3 Optimization of the design parameters of the LTD Stirling engine

This section presents results obtained using the continuous GA optimization procedure coupled to the developed second-order mathematical model. The brake power was used as the objective function. The engine with the SM15-matrix regenerator was operated at the engine speed of 46.5 rpm. Air at 1 bar pressure was used as the working fluid. The size of the population was chosen to be 30 chromosomes and the selection rate for keeping the survival chromosome was 0.5. The mutation rate of 0.2 was used in the numerical calculations.

Figure 6.25 shows the best brake power for each generation as a function of generations. The best brake power for each generation first rapidly increases and then reaches the convergence after about 10-15 generations. The best brake power was found for the 80th generation and was 1.515 W with the optimal design parameters as shown in Table 6.2. The indicated power at the maximum brake power

Chapter 6

point was 1.668 W. This is the performance improvement when compared to the indicated power of 1.276 W of the original engine.

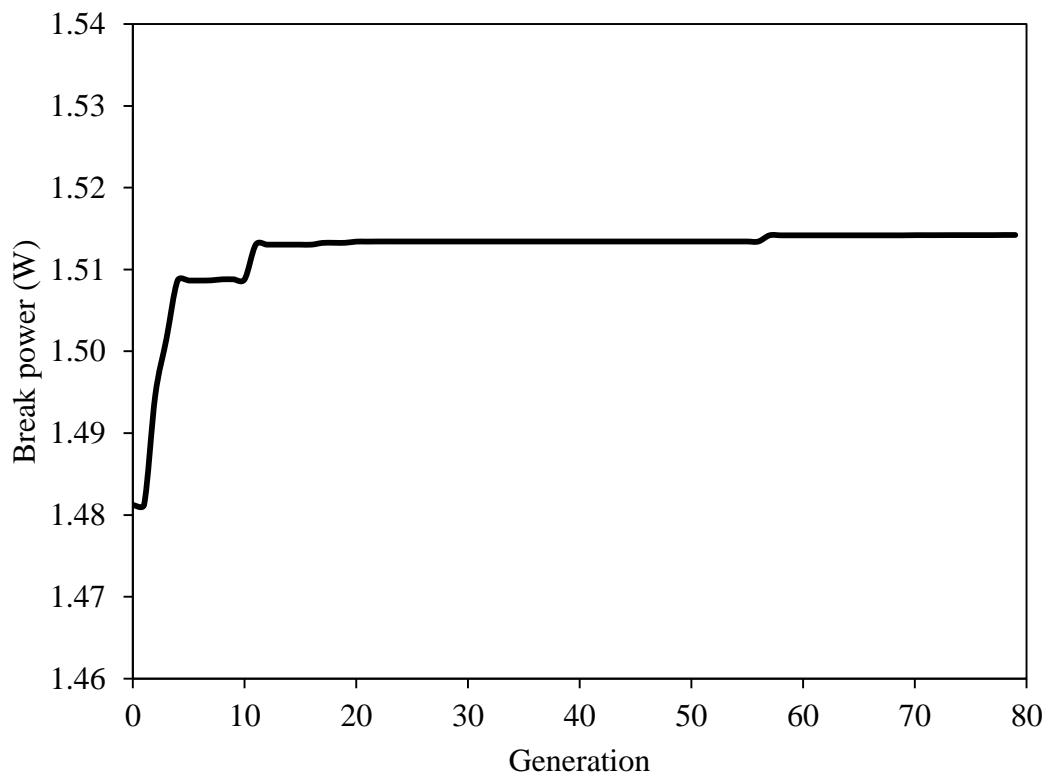


Figure 6.25 The best value of the brake power for each generation

Chapter 6

Table 6.2 The first set of the optimal engine design parameters obtained using the optimization procedure

Optimal engine design parameters	
working piston stroke (m)	0.228
working piston diameter(m)	0.065
displacer piston stroke (m)	0.074
displacer thickness (m)	0.056

To ensure that the optimal engine design parameters was obtained using the GA optimization, the parametric analysis of influence of four GA variables was analyzed using the developed second-order model and results are shown in Figures 6.26-6.29. It can be seen that each of the optimal engine design parameters provides the brake power value at around the area of the peak point. Figure 6.26 and Figure 6.28 demonstrate that a change in values of strokes of pistons results in a relatively small variation in the brake power of the engine. On the contrary the change in the value of the power piston diameter and in the value of the displacer thickness cause a significant variation in the magnitude of the brake power, see Figures 6.27 and 6.29. The power increases dramatically until reaching the peak and then reduces rapidly against the rise in the power piston diameter. The size of the piston diameter also affects the size of the heat transfer area on the cold plate. However, it is the rise of the volume in the compression space which plays the dominant role in this effect. The rise in the thickness of the displacer results in the increase of the mass of the matrix in the regenerator. This means that the heat transfer surface also sharply

Chapter 6

increases and this explains the rise in the brake power at the first. But after that the pressure drop and the dead volume increase starts to play a dominant role.

However, it is obvious that the value of the stroke of the power piston equal to 0.228 m, which is much greater than the stroke of the displacer of 0.074 m, may be unsuitable for the practical engine. In the engine production process it is more convenient if strokes of pistons are identical which provides the simplicity in the design of the crankshaft and reduces production costs. Thus, this value should be modified in accordance with practical manufacturing and design requirements. It was assumed that the power piston stroke and the displacer stroke up to 0.1 m will be appropriate for the practical engine. A new set of optimal engine parameters from the new optimization procedure with two variables is shown in Table 6.3. The maximum brake power this time is 1.346 W and the indicated power is 1.47 W at the maximum brake power point. There is only the 11.13% reduction compared in the brake power compared to the first set of the optimal design parameters but in this second set all the design parameters are suitable from the practical manufacturing point of view.

Table 6.3 The second set the of optimal engine design parameters obtained using the optimisation procedure

Optimal engine design parameters	
working piston stroke (m)	0.1
working piston diameter (m)	0.095
displacer piston stroke (m)	0.1
displacer thickness (m)	0.058

Chapter 6

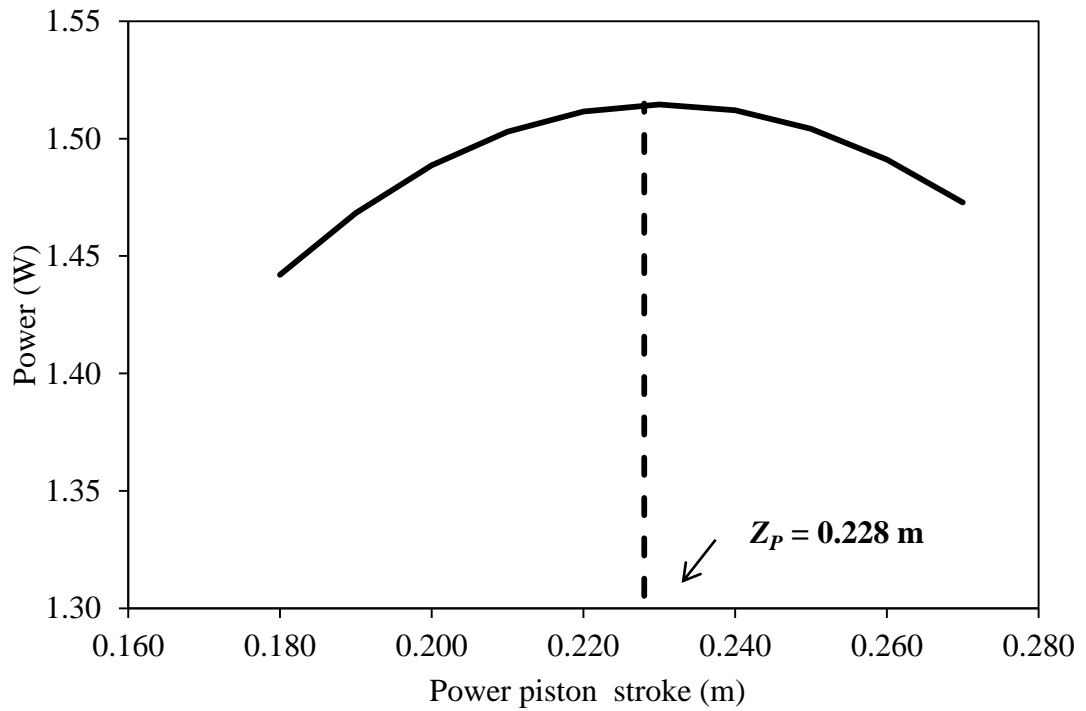


Figure 6.26 The brake power as a function of the power piston stroke

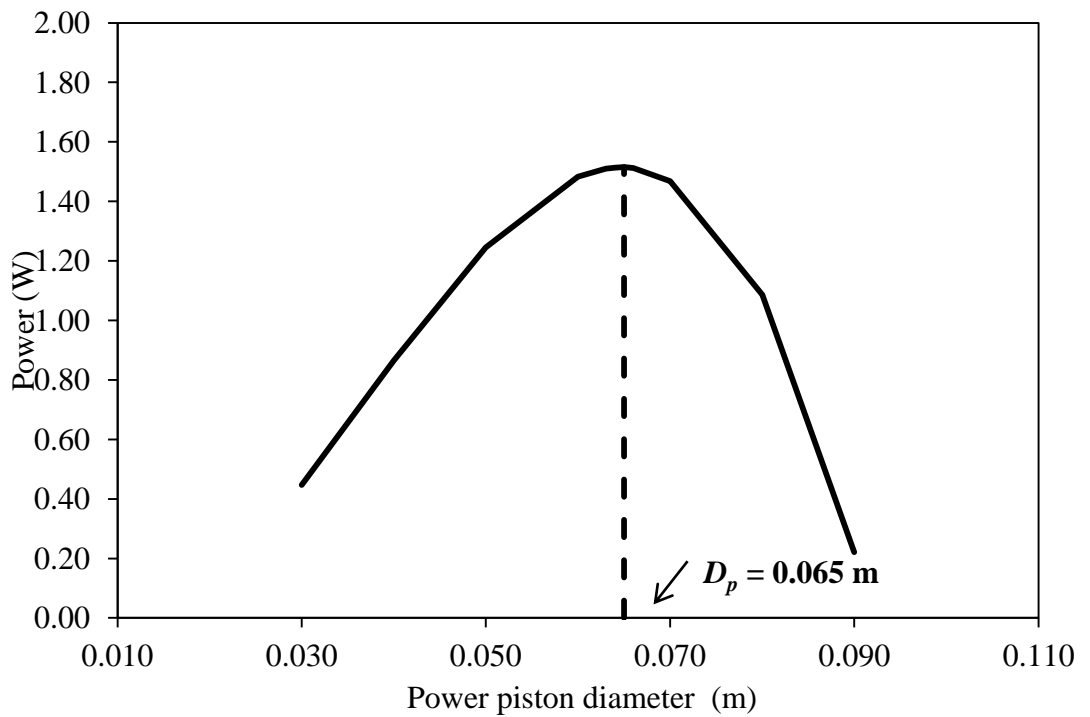


Figure 6.27 The brake power as a function of the power piston diameter

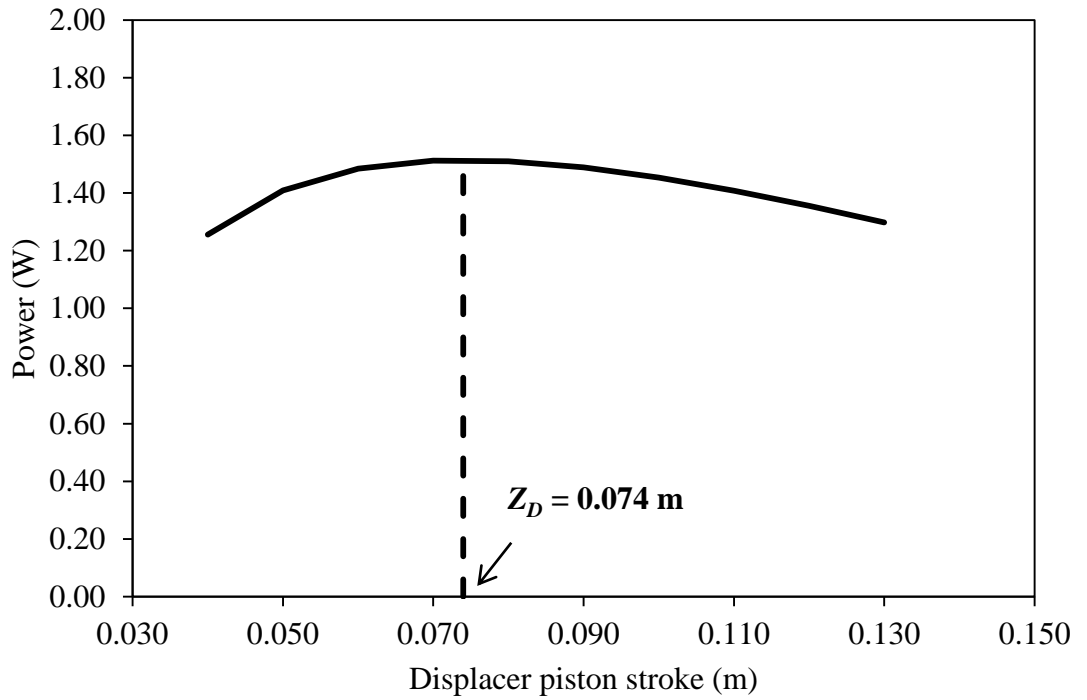


Figure 6.28 The brake power as a function of the displacer stroke

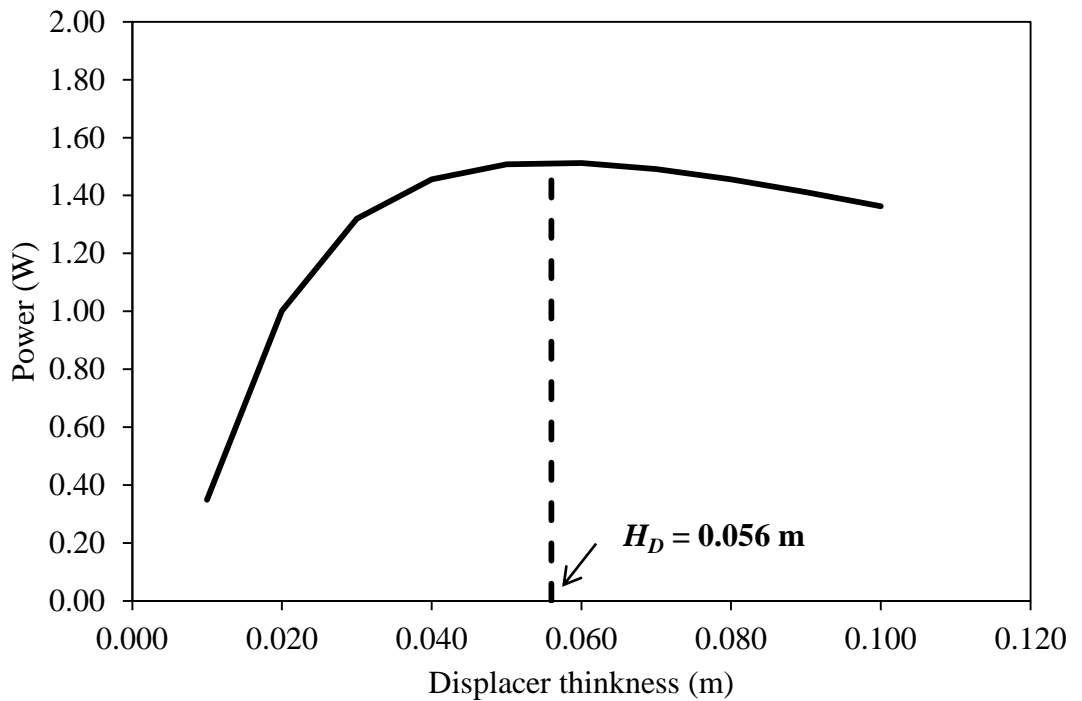


Figure 6.29 The brake power as a function of the displacer thickness

Chapter 6

Finally, the engines with the above two sets of the optimal engine parameters were simulated using 3D CFD modelling. The indicated powers of the engine with the first and second sets of the optimal engine parameters were calculated from P-V diagrams shown in Figure 6.30 and Figure 6.31 and are 1.427 W and 1.352 W, respectively. It was found that both the indicated powers obtained using 3D CFD modelling were consistent with results obtained application of the developed second-order mathematical model but 3D CFD modelling provided a better accuracy in the prediction of the engine performance.

In conclusion, in this Chapter it was demonstrated that the optimal design parameters of a LTD Stirling engine can be determined using the GA optimization procedure. In this procedure the developed second-order mathematical model of a LTD Stirling engine which includes heat and hydraulic losses and also the mechanical losses is coupled to the GA optimization code. As a result of optimization calculations it was possible to determine the optimal design parameters of the twin-power piston LTD Stirling engine which provides the increase in the brake power, compared to the original design. At the final stage the results of optimization calculations were checked with the use more advanced 3D CFD modelling technique.

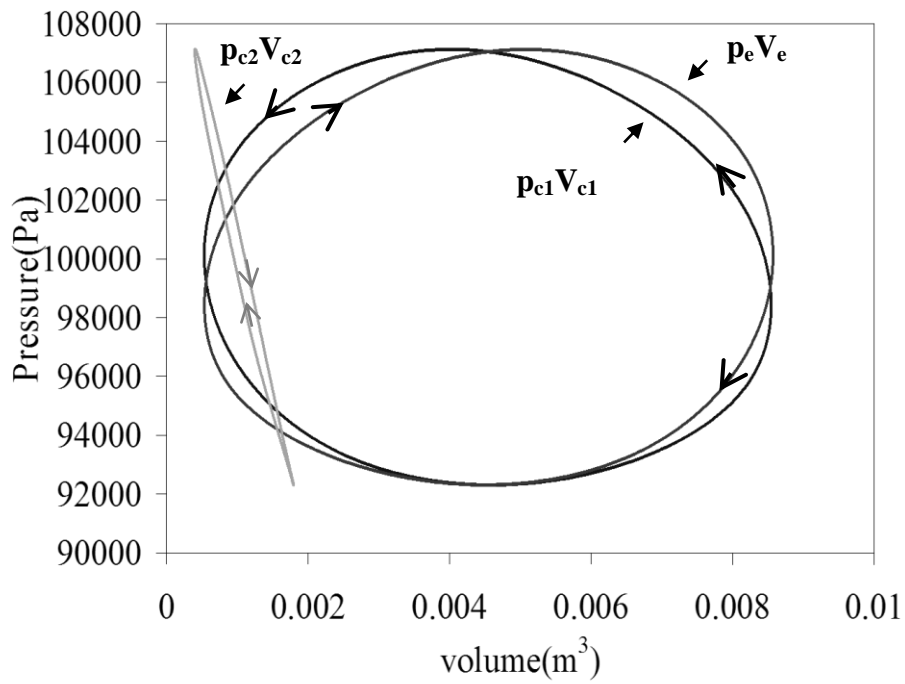


Figure 6.30 P-V diagrams of the first optimal design using the 3D CFD modelling

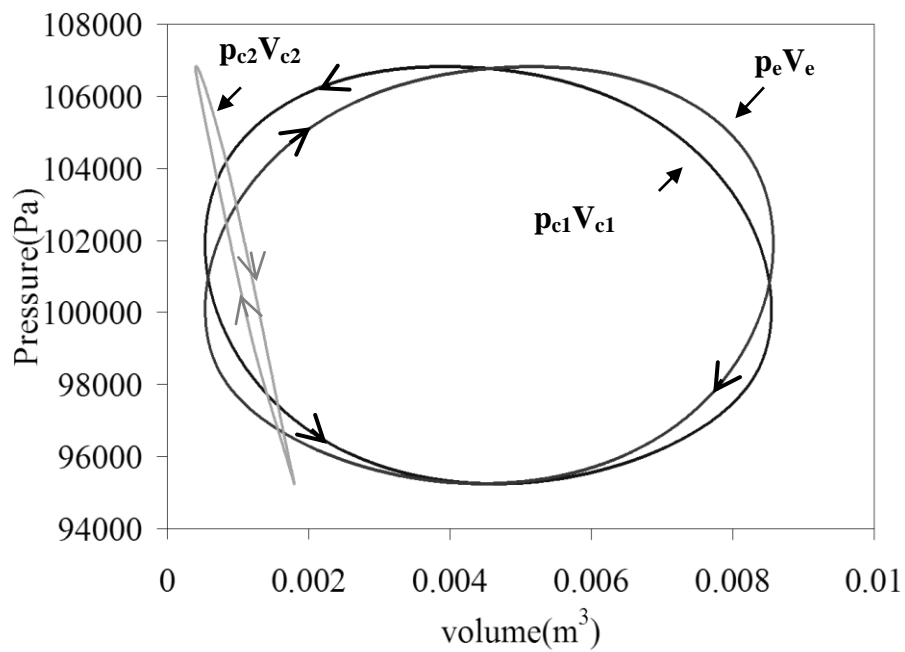


Figure 6.31 P-V diagrams of the second optimal design using the 3D CFD modell

Chapter 7

Mathematical modelling and optimisation of the design of conventional Stirling engines

Results of study on the mathematical modelling and optimisation of conventional Stirling engines are presented in this chapter. Analysis of the working process of the small conventional Stirling engine using the new developed second-order mathematical model is carried out and presented in the first section of the chapter. The theoretical results obtained from numerical simulations are discussed in details. The new developed second-order mathematical model is validated with the use of numerical results from 3D CFD modelling published in [14] and the experimental results published in [14]. The last section of the chapter presents results obtained from the GA optimisation of the engine design and also of the parametric analysis of the GA outcomes.

7.1 Results obtained from the new developed second-order mathematical model

The working process of the small conventional Stirling engine with a gamma configuration which is installed at Northumbria University was numerically simulated using the new developed second-order mathematical model (described in Chapter 3). Information on the geometry of the engine and its parameters presented

Chapter 7

in Table 3.2 was used as input data for numerical simulations. The experimental tests conditions were described in [14] and used to run numerical simulations of the engine. Thus, the heater and cooler temperatures of 913 and 290 K were specified in simulations. Helium was the working fluid for the engine with the maximum operating pressure of 58 bar. The matrix of the regenerator was made of stainless wire mesh with diameter of wire of 0.0001 m and the porosity of the regenerator was 0.75. The Stirling engine was operated at the frequency of 23.85 Hz which corresponds to the engine speed of 1,431 rpm.

7.1.1 Analysis of the working process

Figures 7.1-7.7 present information on the variation of volumes, gas pressures, pressure drops, temperatures and heat flow rates over the engine's cycle and also P-V diagrams for the compression and expansion spaces obtained using the new developed second-order mathematical model.

Figure 7.1 shows variations in the gas volume in the compression and expansion spaces. It can be seen that the swept total volume of this conventional Stirling engine significantly exceeds that of the LTD Stirling engine, analysed in Chapter 6. This means that the power output from the engine also will be much higher. The design of this engine is such that diameters and strokes of both the pistons are the same. The gamma configuration of the engine results in the greater swept volume in the compression space compared to that in the expansion space.

Chapter 7

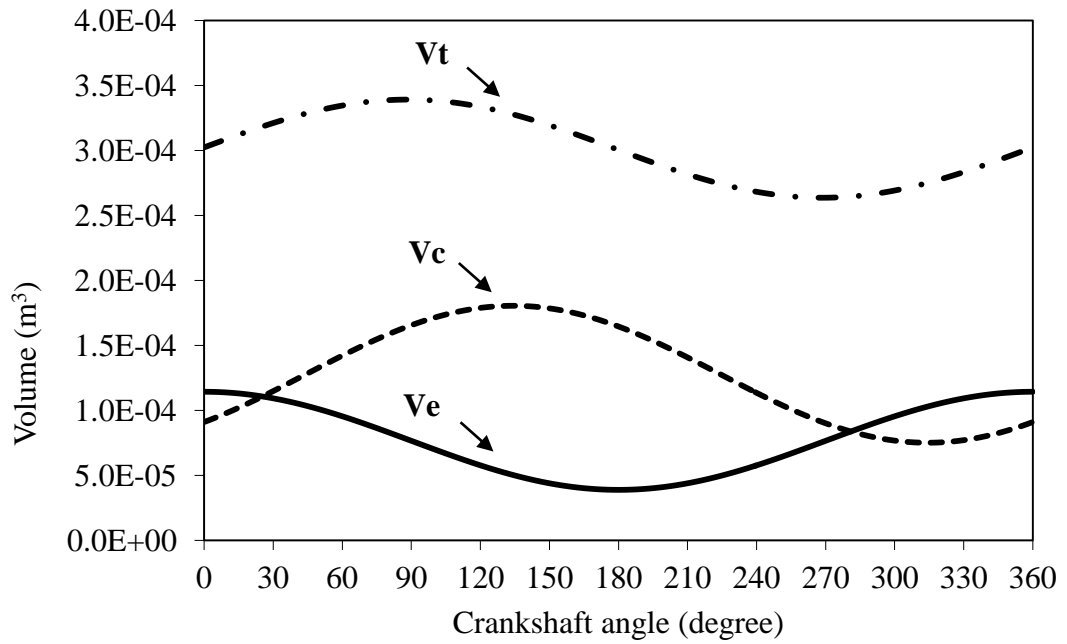


Figure 7.1 The variation of the volumes in the engine

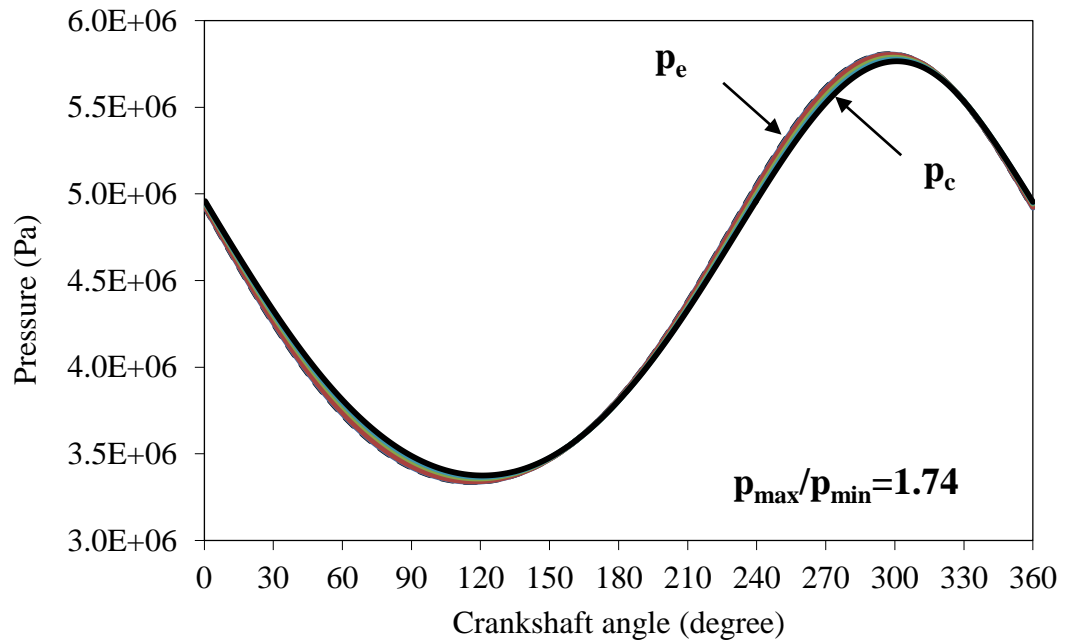


Figure 7.2 The variation of the gas pressures in the engine

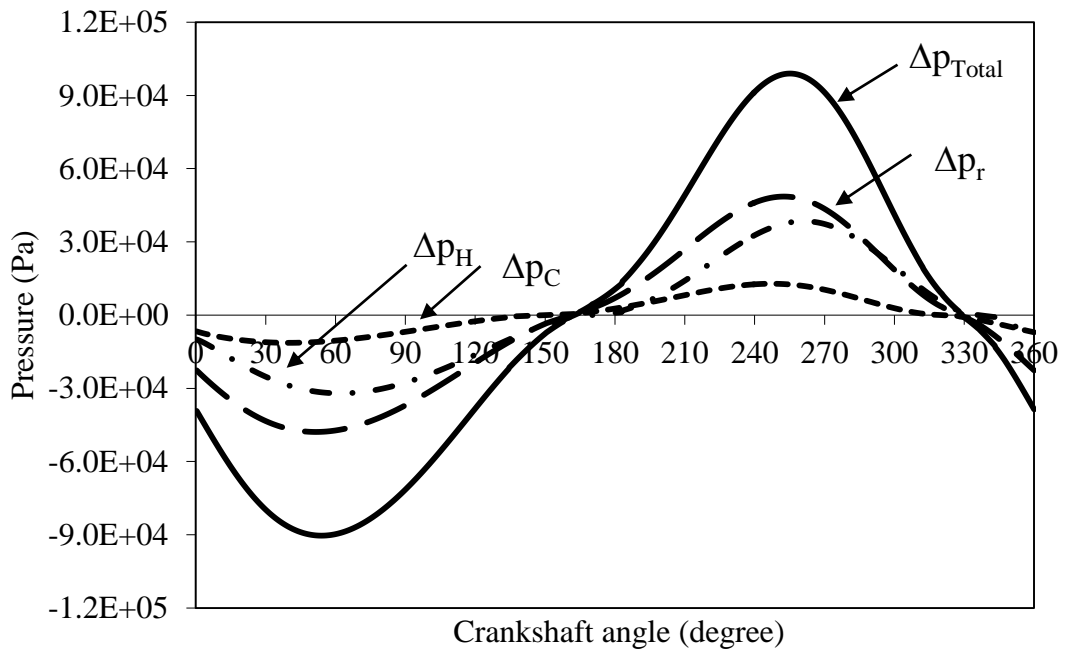


Figure 7.3 The variation of the pressure drops in the engine

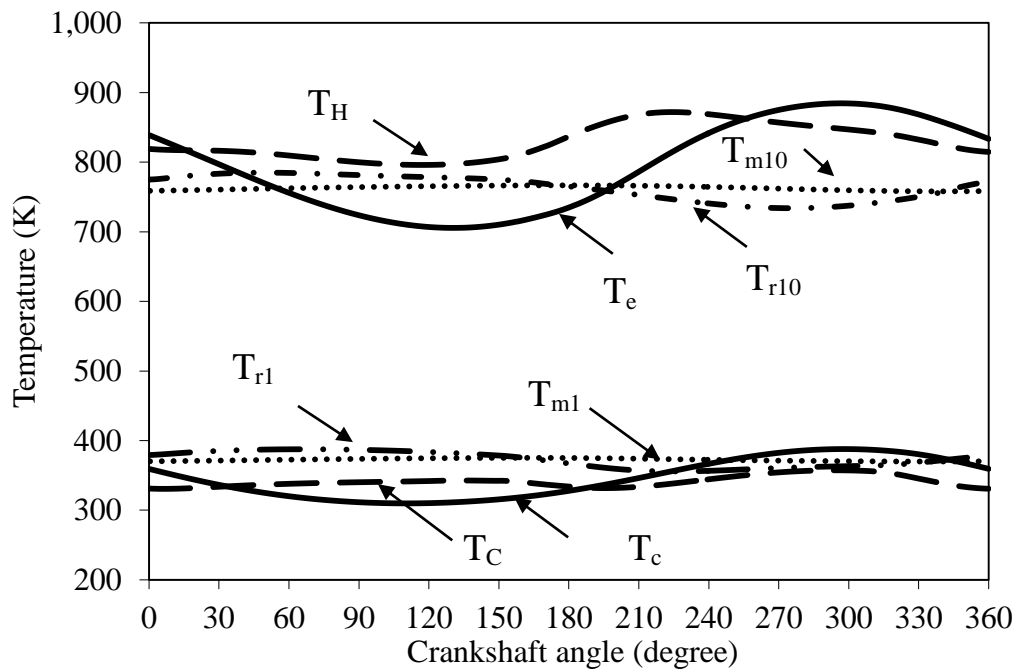


Figure 7.4 The variation of the gas temperatures in the engine

Chapter 7

However, in general the pattern in the variation of volumes in the compression and expansion spaces are similar to that for the LTD Stirling engine. There specific feature is that in the conventional Stirling engine there is a considerable offset between the maximum and minimum points of the volume lines for the expansion and compression spaces. This is because the gas volume in the compression space of the gamma Stirling engine is split into two parts which are swept by different pistons displacement of which takes place with 90° angle shift.

The variation of gas pressures inside the engine is presented in Figure 7.2. The gas pressure in the expansion space, compression space, the heater, ten parts of the regenerator and the cooler are plotted as functions of the crankshaft angle. It can be seen that all pressure lines are of a sinusoidal form. The operating pressure has a maximum of 5,806,228 Pa at the crankshaft position of 297° and the pressure minimum of 3,337,048 Pa is achieved at the crankshaft position of 116° . The pressure ratio in the cycle is 1.74. There is a noticeable difference between the pressure lines in the compression and expansion spaces. This is caused by the pressure drop in three heat exchangers of the Stirling engine when the working gas flows through these components, especially at the high engine speed. As described in Chapter 3, the heater and the cooler of the conventional Stirling engine are of tubular-basket and shell-tube types, respectively. The oscillating gas flow through each small tube inside the heat exchanger produces a considerable pressure drop. Figure 7.3 presents the value of pressure drops which occur in each heat exchange of the engine. The maximum total pressure drop is 98,960 Pa. The maximum pressure drops which occur in the heater, cooler and regenerator are 38,464 Pa, 12,847 Pa and 48,562 Pa, respectively. The most of the pressure drop occurs when the working gas

Chapter 7

flows through the matrix inside the regenerator. The hydraulic resistance in the regenerator may strongly affect the power output of the conventional Stirling engine. Therefore, a number of studies were conducted to optimise the regenerator [52, 59]. In general, not only the regenerator but also the heater and cooler, are studied for optimisation purposes in order to provide the high performance of the whole engine [59].

Figure 7.4 presents information on the variation of the gas temperatures in each space of the engine. The minimum temperature in the expansion space is 706 K and its maximum value is 885 K. The pattern in the change in the gas temperature in the compression space is similar to that in the expansion space and the maximum and minimum values are 388 and 310 K, respectively. In calculations it was assumed that there is a perfect thermal insulation on outer surfaces of the hot and cold cylinders so there is no heat transfer flows through the walls of these cylinders. Only the volume and pressure changes and mass transfer cause the variation of the temperature in the cylinders.

It can be seen in this figure that the maximum and minimum gas temperatures in the heater space are 872 K and 796 K, respectively. For the cooler, the gas temperature varies between 357 and 330 K. The gas temperatures for only two parts of the regenerator next to the heater and cooler, respectively, are presented in Figure 7.4. Overall, the gas temperature in the regenerator varies between the heater and the cooler temperatures. The gas temperature in the part of the regenerator next to the cooler is very close to the cooler's temperature at the crankshaft position of 286° whilst the temperature in the part of the regenerator next to the heater nearly reaches

Chapter 7

the heater's temperature at the crankshaft position of 109° . The average gas temperature in all ten parts of the regenerator is about 567.89 K. The volume of all heat exchangers is constant and their surfaces are used for heat transfer. Figure 7.5 presents information on the variation of heat transfer flows on the surface of heat exchangers. The maximum values of heat transfer rates on the surfaces of the heater and cooler are 7,829 W and 4,955 W, respectively. The heat transfer rates are proportional to the magnitude of heat transfer coefficients and the minimum heat transfer rates correspond to the instances in the cycle at which the gas velocity is lowest. The heat flow from the working gas to the matrix in the regenerator occurs at the first half cycle and the reverse heat flow occurs at the second half cycle. The external heat loss in the regenerator over the cycle is found to be only 45.72 W. Figure 7.6 presents information on other heat losses in the cycle, such as the internal conduction heat loss, the dissipation heat loss and the shuttle loss. It can be seen that the internal conduction heat loss is the largest term in the total heat losses whilst the shuttle heat loss is the smallest one. There is a large amount of heat being transferred from the hot to cold side of the heat exchanger. The dissipation heat loss due to the pressure drop in the conventional Stirling engine is also significant compared to that in the LTD engine. This is because the conventional Stirling engine has a full set of heat exchangers and operates with the high pressure and at the high speed. The indicated power of the engine can be calculated using P-V diagrams shown in Figure 7.7. The indicated power produced by this Stirling engine is 1,457 W at the engine speed of 1,431 rpm. The engine's efficiency is calculated to be 33.27 %.

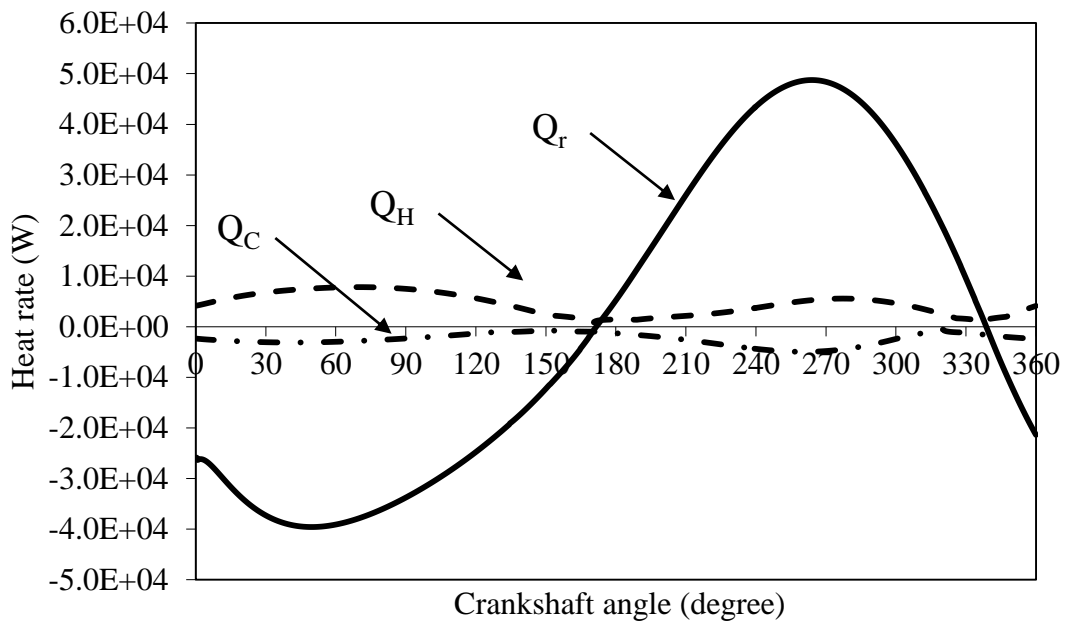


Figure 7.5 The variation of the heat transfer rates in the engine

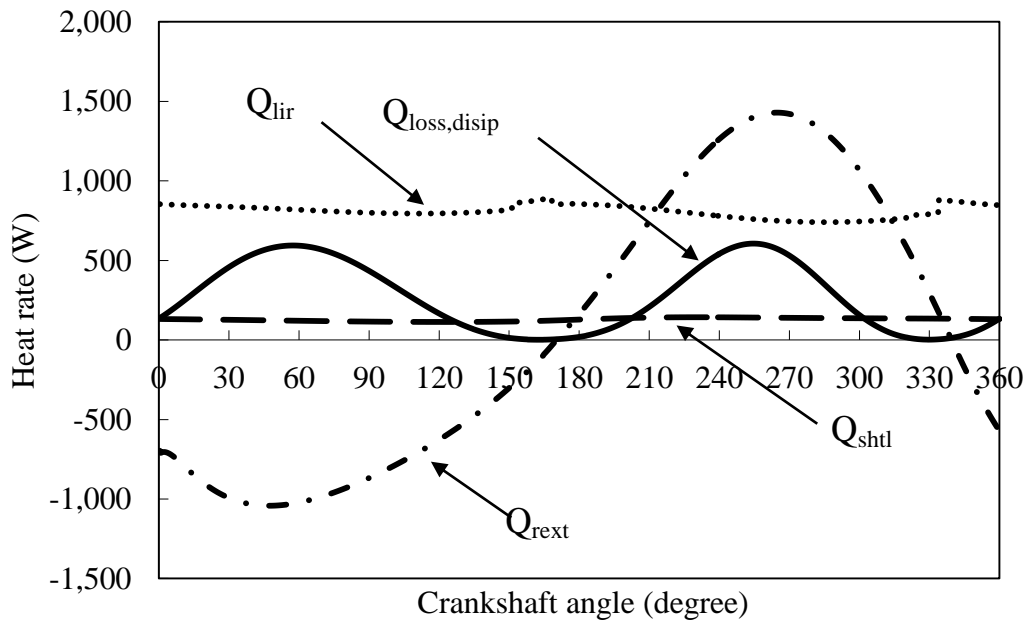


Figure 7.6 The variation of the heat loss rates in the engine

Chapter 7

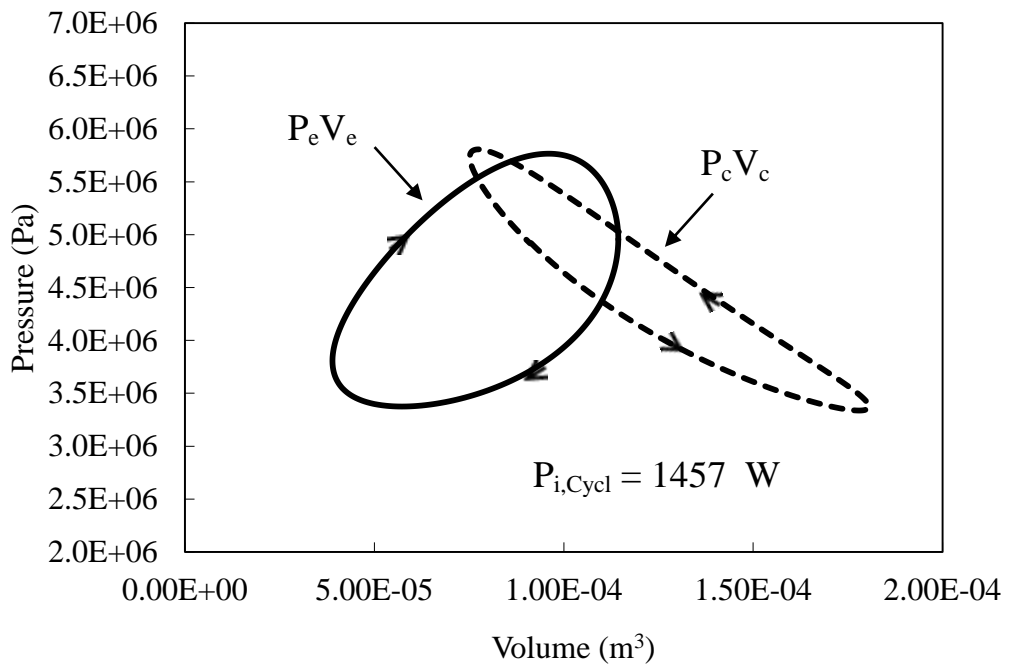


Figure 7.7 P-V diagrams for the conventional Stirling engine

Table 7.1 Comparison of theoretical and experimental results on the engine's power production

Results	Experiment [14]	3D CFD [14]	The new developed second-order model	SOPRANOS [14]
Indicated power (W)	844.34	1,159.04	1,457.06	1,474.2

Chapter 7

7.1.2 Validation of the new developed second-order mathematical model of conventional Stirling engines

The numerical results obtained using the new developed second-order mathematical model are compared to the results published by Makhamov in [14] namely to theoretical results from SOPRANOS program (based on the second-order mathematical model developed by Mahkamov), and the results from 3D CFD modelling presented by Makhamov in [14] and also the experimental results from tests performed by Mahkamov [14].

Table 7.1 presents the comparison of results on the power production in terms of the indicated power obtained from the new developed second-order mathematical model, SOPRANO [14], the 3D CFD modelling [14] and the laboratory tests [14]. Using the model developed in this work it was predicted that indicated power was 1457.06 W. This value is slightly more accurate than that obtained using SOPRANOS code (1474.20 W) but still much greater than the indicated power of 844.34 W obtained during experimental tests [14]. The error in prediction using the new developed mathematical model is 72 %. However, such the error is consistent with results of other studies with the use of various second-order mathematical models [27, 43]. From the numerical simulations of GPU-3 Stirling engine presented by Timouni et al. in [27], the best accuracy from the use of the second-order mathematical model including several heat and hydraulic losses was calculated to be 8 %. But without including the gas hysteresis losses the accuracy was 47 %. There is a contradiction in published literature concerning the influence of the gas hysteresis losses (which is heat transfer between the working gas and the cylinder wall in the compression space

Chapter 7

of the power piston cylinder) on the indicated power. For example, Urielli states that the gas hysteresis losses make only very small part of total heat losses [18]. Therefore, the gas hysteresis losses were not included in the model developed in this work.

Table 7.1 shows the best accurate prediction is made by using 3D CFD modelling. However, to obtain such numerical results a very significant computing time is needed [41, 42, and 43].

The results of the gas working process modelling from the use of the new developed second-order model are compared to those from the 3D CFD modelling and the laboratory tests, seen in Figures 7.8-7.13. The comparison of the gas temperatures obtained from the new developed second-order mathematical model, the 3D CFD modelling and the testing is shown in Figure 7.8. It can be seen that the gas temperature lines in the compression and expansion spaces of the experimental results are below the lines of the new developed second-order mathematical model and from 3D CFD modelling but all lines have the same pattern in the variations.

Figure 7.9 shows the gas pressures in the compression space obtained from the new developed second-order mathematical model, 3D CFD modelling and the laboratory tests. It can be seen that the maximum pressure obtained from the new mathematical model is greater than other results. The minimum pressure in the cycle obtained from the second-order mathematical model is also lower than results from CFD modelling and the experiments. This larger magnitude of the pressure wave from the new developed second-order mathematical model is the cause for over prediction in the indicated power of the engine.

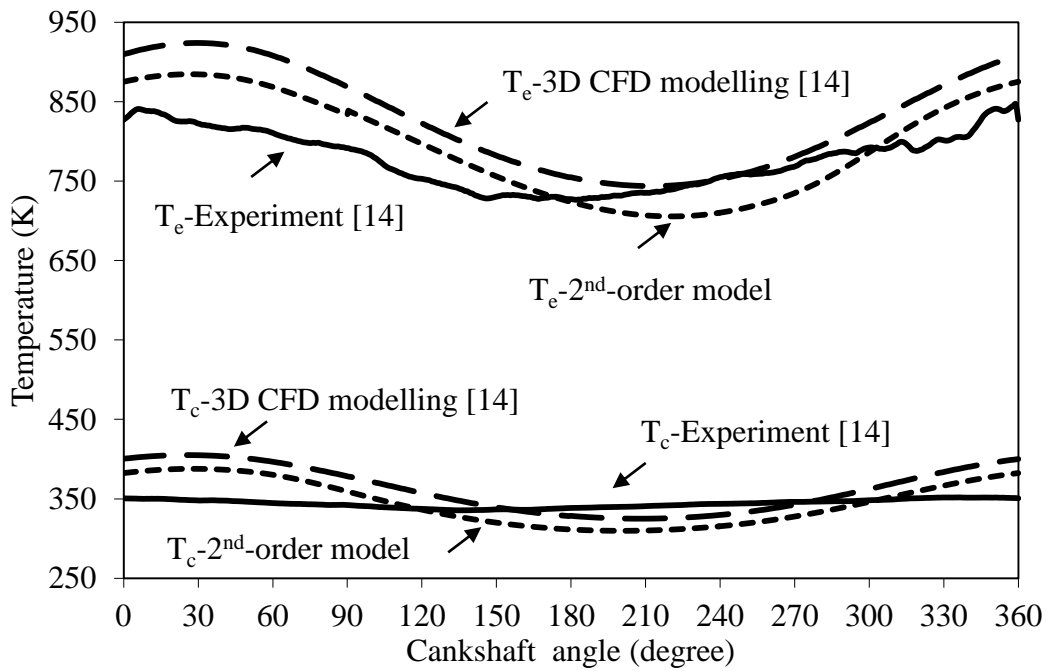


Figure 7.8 Comparison of the gas temperatures

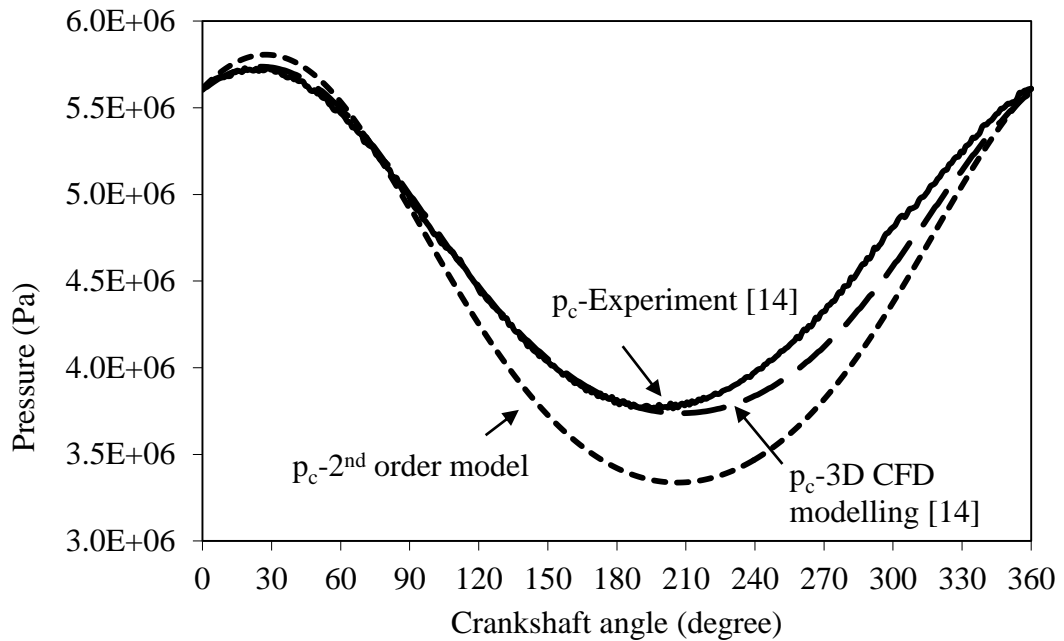


Figure 7.9 Comparison of the gas pressures in the compression space

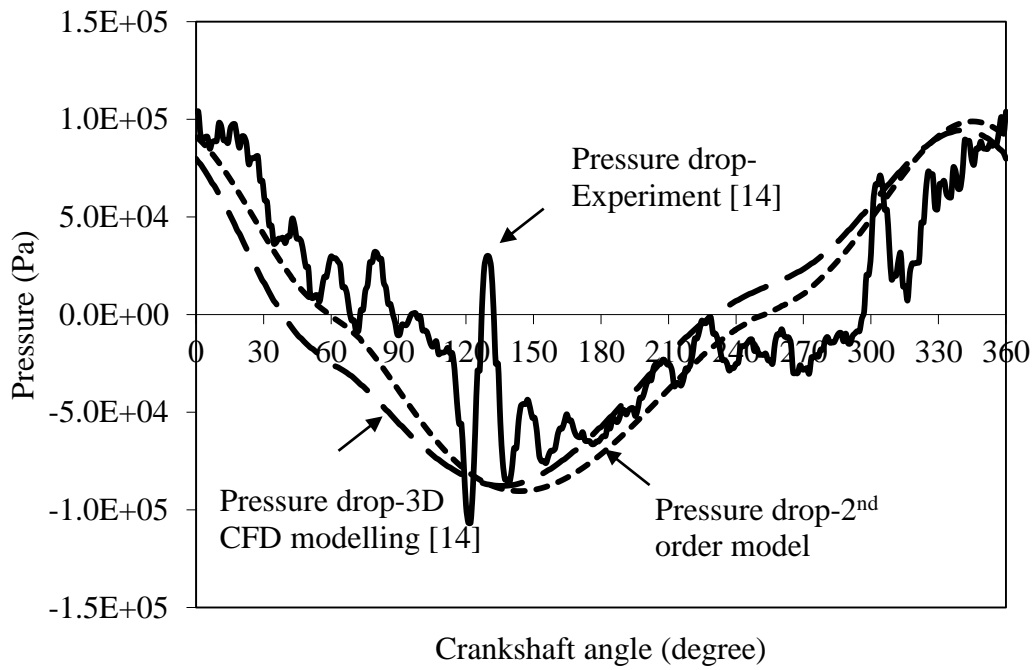


Figure 7.10 Comparison of the total pressure drops

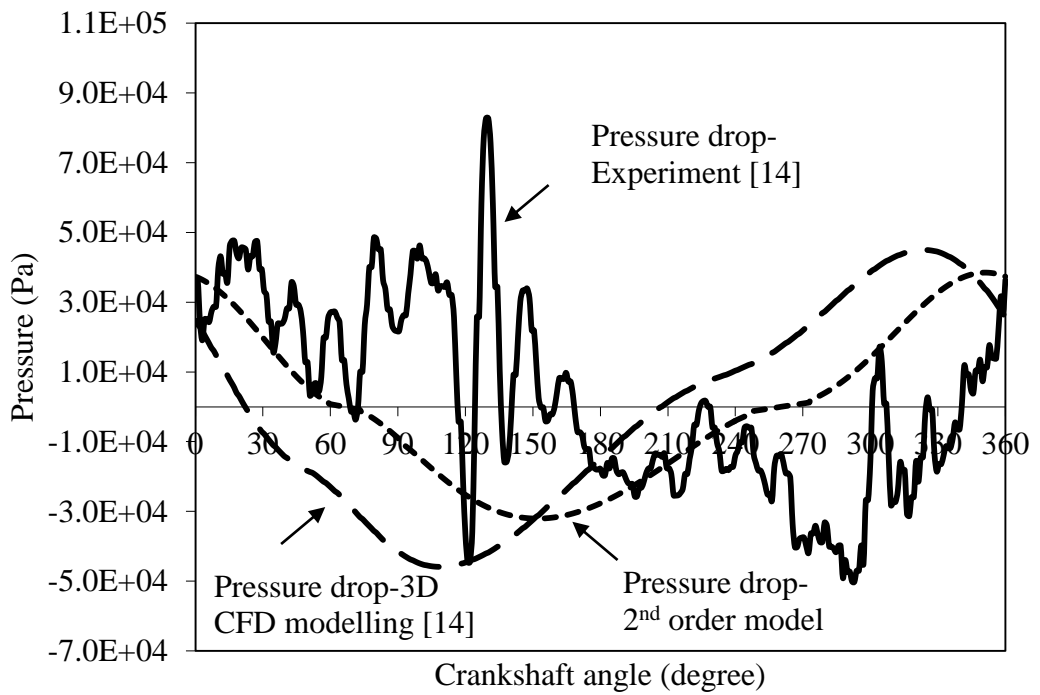


Figure 7.11 Comparison of the pressure drops in the heater

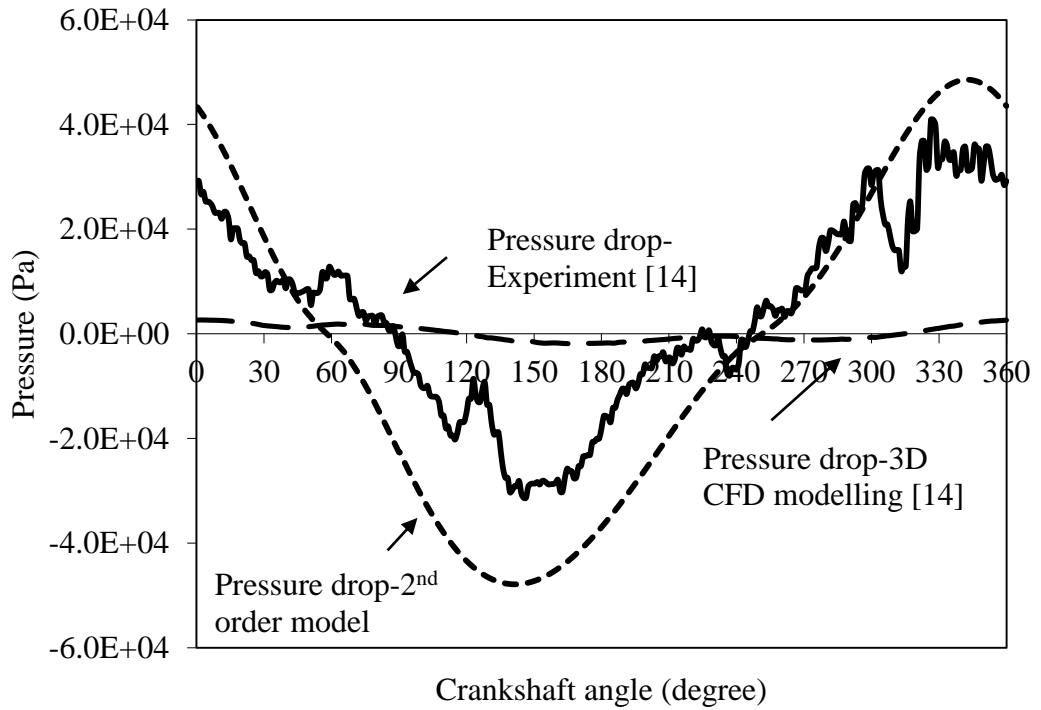


Figure 7.12 Comparison of the pressure drops in the regenerator

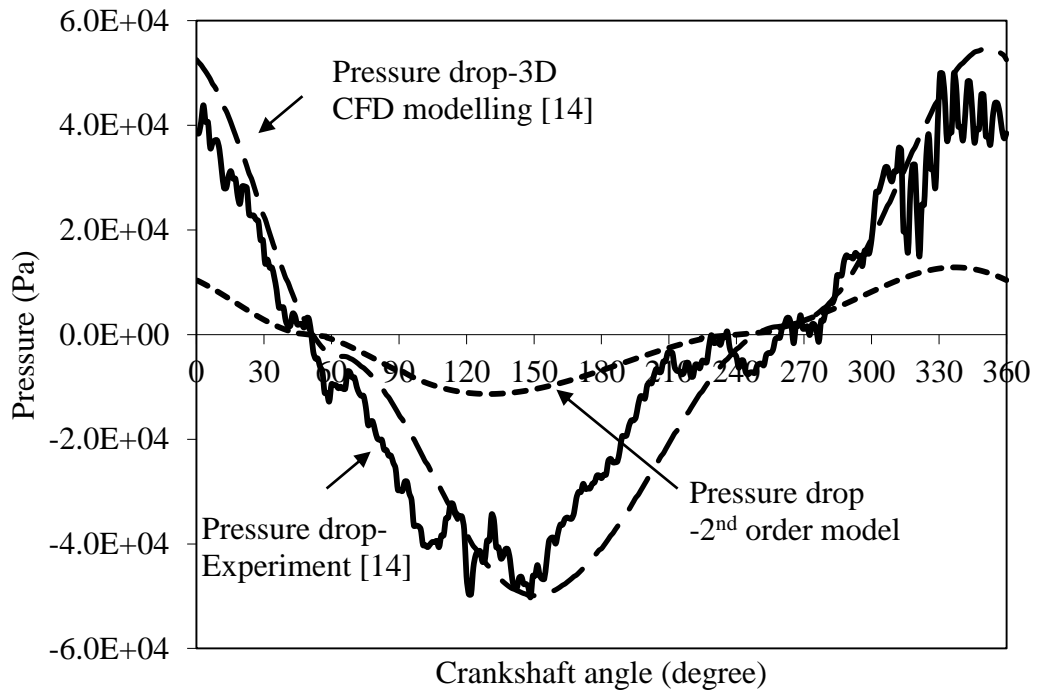


Figure 7.13 Comparison of the pressure drops in the cooler

Chapter 7

In Figures 7.10 and 7.11 results are strongly affected by fluctuations in the experimental pressure drop curve for the heater and this is caused by insufficient cooling of the working gas acting on the membrane of the differential pressure transducer. The pressure transducer was checked when engine was run by the electrical motor without heat input and for such “cold” run conditions it produces a smooth pressure drop curve.

Figure 7.10 shows that the peak of the total pressure drop of the experimental results is more than those from 3D CFD modelling and the new second-order mathematical model. The total pressure drop peak point in the experimental results is 104,008 Pa whilst that from 3D CFD modelling is 94,411 Pa and that from the new developed second-order mathematical model is 98,960 Pa. The results for pressure drops in each heat exchanger are presented in Figure 7.11-7.13. There is a significant difference between the results on the pressure drops in the heater, cooler and regenerator spaces. This means that the friction correlations which were used for the pressure drop calculation in the heater, cooler and regenerator might be not suitable for prediction of the actual physical phenomena in the working process. Figure 7.11 shows that there is a significant difference in results for the maximum pressure drop in the heater space from the experiments and the mathematical and CFD models. However, it should be noted that there is a significant fluctuations in the pressure drop line obtained from the experimental tests. The pressure drop in the regenerator space from the developed second-order model is close to the experimental result as shown in Figure 7.12. From Figure 7.13, it can be seen that the pressure drop obtained from the developed second-order model is much lower than that obtained from 3D CFD modelling and the experiment.

Chapter 7

A comparison of the results was carried out in this work using the new developed mathematical model with various flow friction and heat transfer correlations for the calculation of the pressure drops and the heat transfer coefficients in all heat exchangers of the engine. Three optional heat transfer correlations used for the heater and cooler were the unidirectional flow friction correlations commonly applied in modelling of conventional Stirling engines. There have been not many works regarding the investigation of the oscillating flow in the recuperative heat exchangers but there have been a number of studies on the oscillating flow in regenerative heat exchangers. For the flow friction correlations the unidirectional flows and the oscillating flows were applied for the calculation of the pressure drop in the recuperative heat exchangers and the regenerative heat exchanger, respectively, in this work. Table 7.2 presents results on the indicated power calculated with the use of various correlations in the new developed second-order mathematical model. The best case in Table 7.2 was used to report in this Chapter.

In conclusion, it could be highlighted that the new developed second-order mathematical model provides acceptable accuracy in the prediction of conventional Stirling engines performance and in the description of their working process with relatively low requirements to the computing time and computing power and therefore can be efficiently used for engine optimization procedures.

Chapter 7

Table 7.2 The indicated power obtained by using the various correlations in the new developed second-order mathematical model

The correlation for heat transfer in the heater and cooler	The correlation for flow friction in the heater and cooler	The correlation for heat transfer in the regenerator	The correlation for flow friction in the regenerator	Indicated Power (W)
Dittus-Boelter cited in [89]	Incorpera et al. [89]	Tanaka et al. [85]	Gedeon & Wood cited in [90]	1,624.60
Colburn cited in [91]	Incorpera et al. [89]	Tanaka et al. [85]	Gedeon & Wood cited in [90]	1,457.06
Kays & London [91]	Incorpera et al. [89]	Tanaka et al. [85]	Gedeon & Wood cited in [90]	1,789.50
Colburn cited in [91]	Kay & London [91]	Tanaka et al. [85]	Gedeon & Wood cited in [90]	1,515.60
Colburn cited in [91]	Incorpera et al. [89]	Tanaka et al. [85]	Tanaka et al. [85]	1,510.57
Colburn cited in [91]	Incorpera et al. [89]	Gedeon & Wood cited in [90]	Gedeon & Wood cited in [90]	1,552.36
Colburn cited in [91]	Incorpera et al. [89]	Gedeon & Wood cited in [90]	Tanaka et al. [85]	1,609.06

Chapter 7

7.2 Optimization of the design parameters of the conventional Stirling engine

The numerical results obtained from the optimization of design parameters of the conventional Stirling engine using the developed GA optimization code coupled to the new developed second-order mathematical model are presented in this section. The obtained set of optimal design parameters of the engine provides the maximum indicated power for a given set of restrictions. In the final part the parametric analysis of the obtained optimal design parameters was performed for the confirmation results of GA optimization.

The indicated power was defined as the objective function of the GA optimization. The conventional Stirling engine operated with helium as the working fluid and the maximum pressure of 58 bar in the cycle and the engine speed of 1,431 rpm were specified for numerical simulations of the working process using the developed second-order mathematical model. For the GA optimization, the population of 30, the selection rate of 50% and the mutation rate of 0.2 were used. The optimal values of six engine parameters were found at the 80th generation.

Information on the best indicated power of each generation against the number of generation is presented in Figure 7.14. It can be seen that the indicated power sharply rises for the first several generations and then slowly increases until the termination criteria is met. The maximum indicated power reached is 1,577.93 W at the 80th generation and it is the 8 % improvement when compared to the original design. The optimal engine design parameters defined at the 80th generation are shown and compared to the original engine parameters in Table 7.3.

Chapter 7

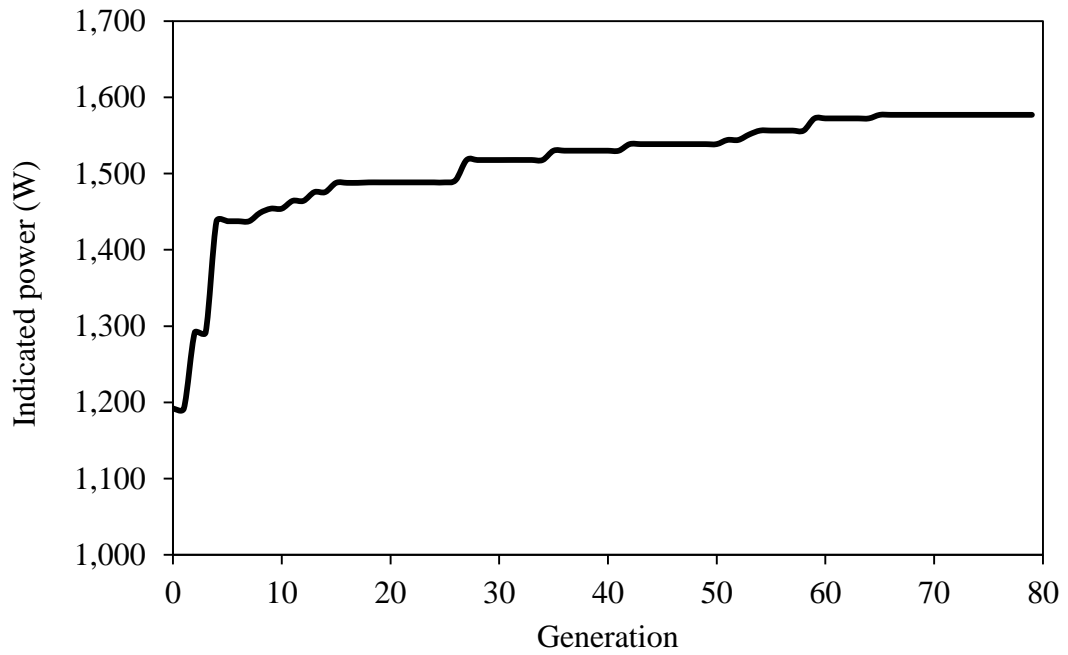


Figure 7.14 The best indicated power of each generation against the number of generations

Table 7.3 The engine design parameters obtained from the GA optimization

Engine parameter	Engine parameters of the original conventional Stirling engine	Optimal engine parameters
diameter of heater tube (m)	0.003	0.0031
length of heater tube (m)	0.24	0.233
diameter of cooler tube (m)	0.0012	0.0008
length of cooler tube (m)	0.05	0.0758
diameter of regenerator chamber (m)	0.08	0.091
length of regenerator chamber (m)	0.04	0.022

Chapter 7

It can be seen in Table 7.3 that there is a considerable change in values of considered design parameters except the diameter of the heater tube.

To corroborate optimization results, a parametric analysis of the above six engine parameters was performed and results are presented in Figures 7.15-7.20. These diagrams show that the indicated power is very sensitive to the values of all six parameters. Figure 7.15 shows that the indicated power first sharply increases with the growth of the diameter of the heater tube and then gradually decreases. It is caused by first increase in the heat transfer area and then by increase in the dead volume of the heater. The increase in the length of the tubes of the heater results in the rise of flow frictional losses and also in the increase of the heater's dead volume shown in Figure 7.16. The same pattern can be observed for the cooler and regenerator in Figures 7.17-7.20.

All the above figures indicate that the indicated power obtained using the GA optimization is slightly different from the possible maximum value. Although the GA optimization is unable to precisely locate the point with the possible maximum indicated power, it provides overall very good accuracy in finding an optimal set of design parameters of the engine.

In conclusion, it could be highlighted that the new developed second-order mathematical model of conventional Stirling engines and the developed GA based optimization code now could be used by manufacturers and developers for creating the high performance conventional Stirling engines for HTD and MTD applications.

Chapter 7

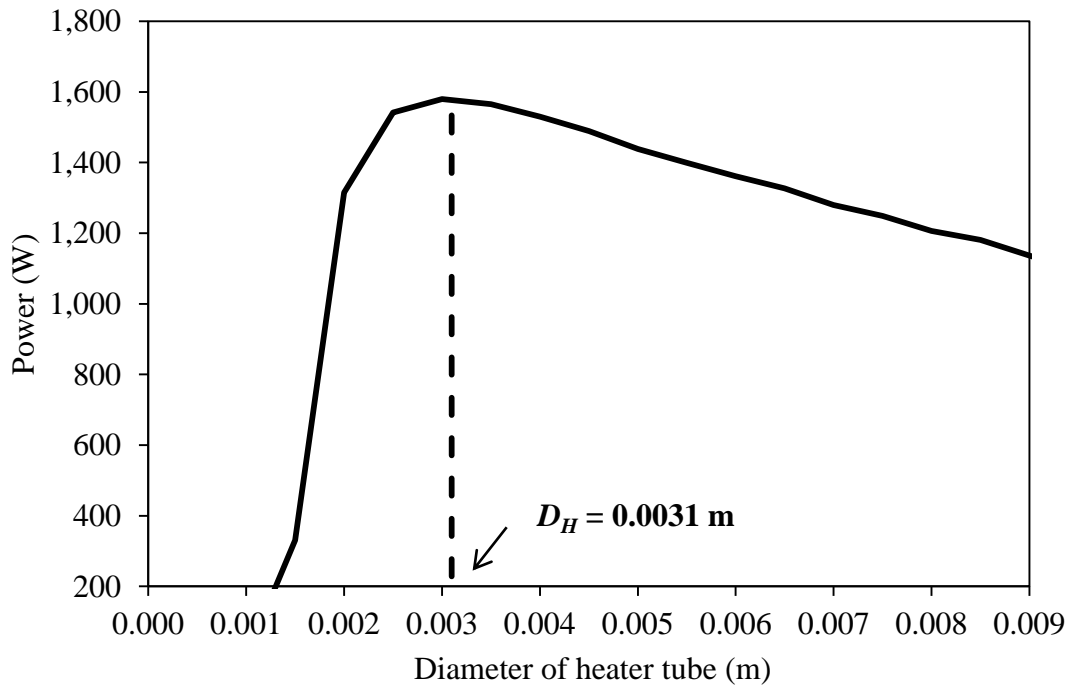


Figure 7.15 The indicated power against the diameter of the heater tube

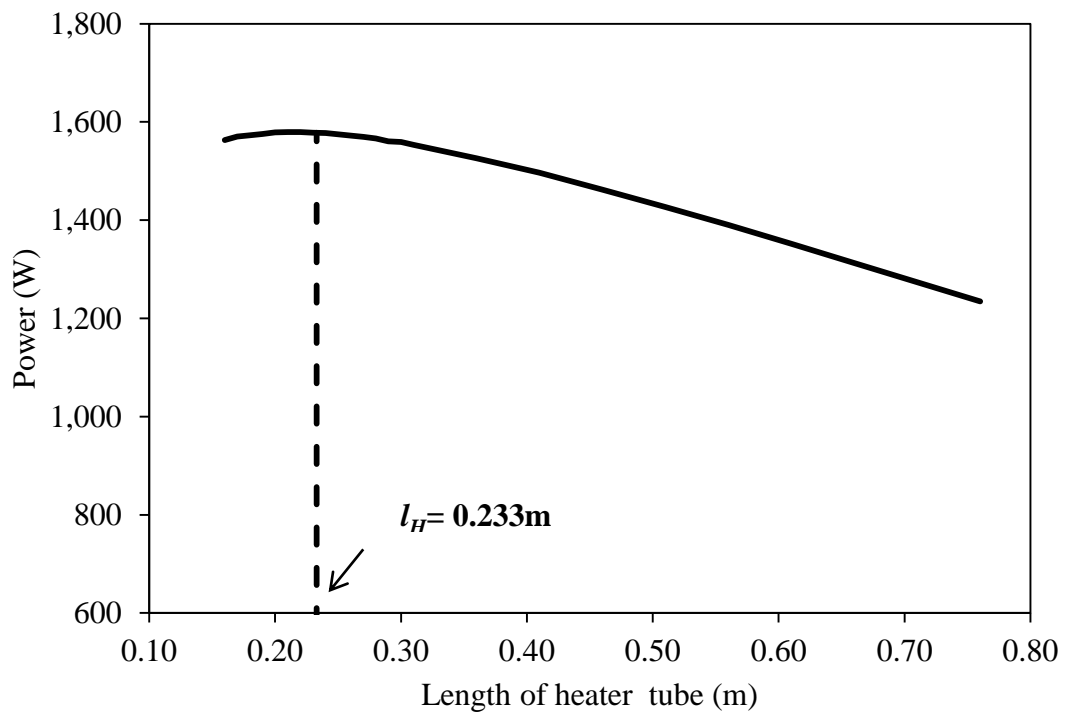


Figure 7.16 The indicated power against the length of the heater tube

Chapter 7

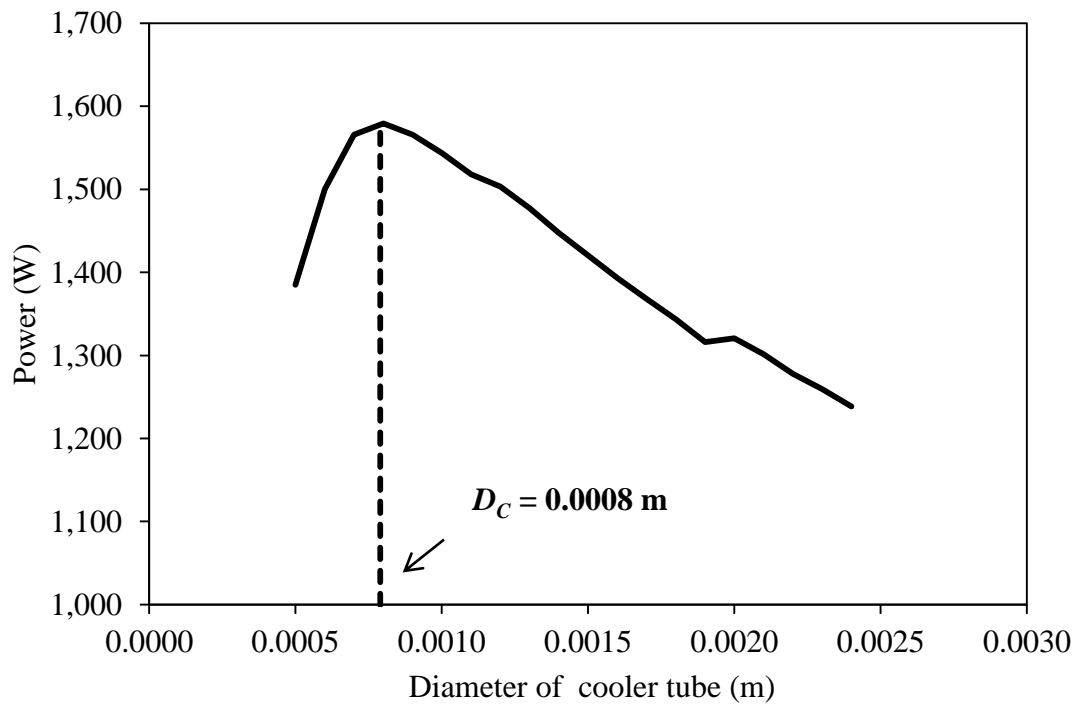


Figure 7.17 The indicated power against the diameter of the cooler tube

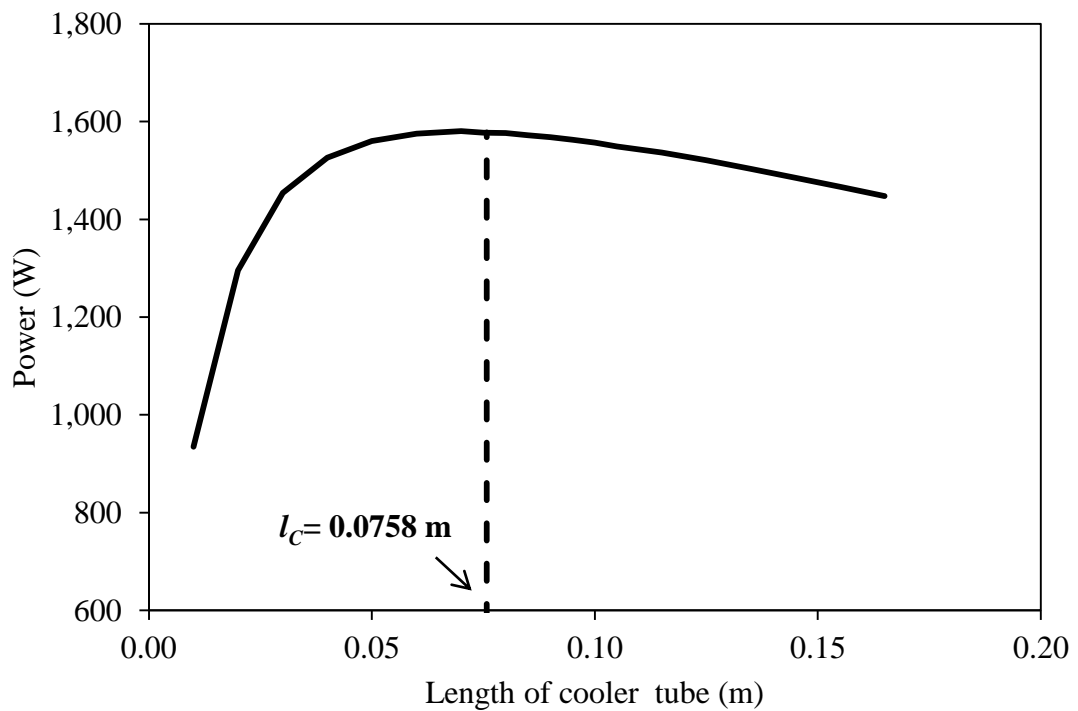


Figure 7.18 The indicated power against the length of the cooler tube

Chapter 7

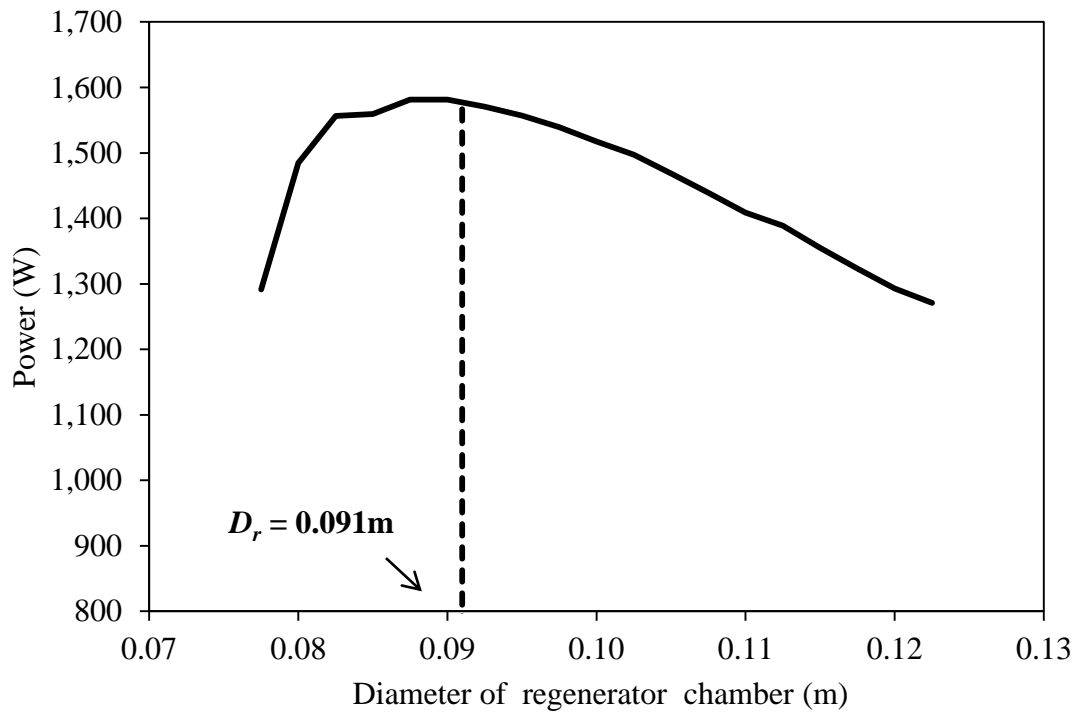


Figure 7.19 The indicated power against the diameter of the regenerator chamber

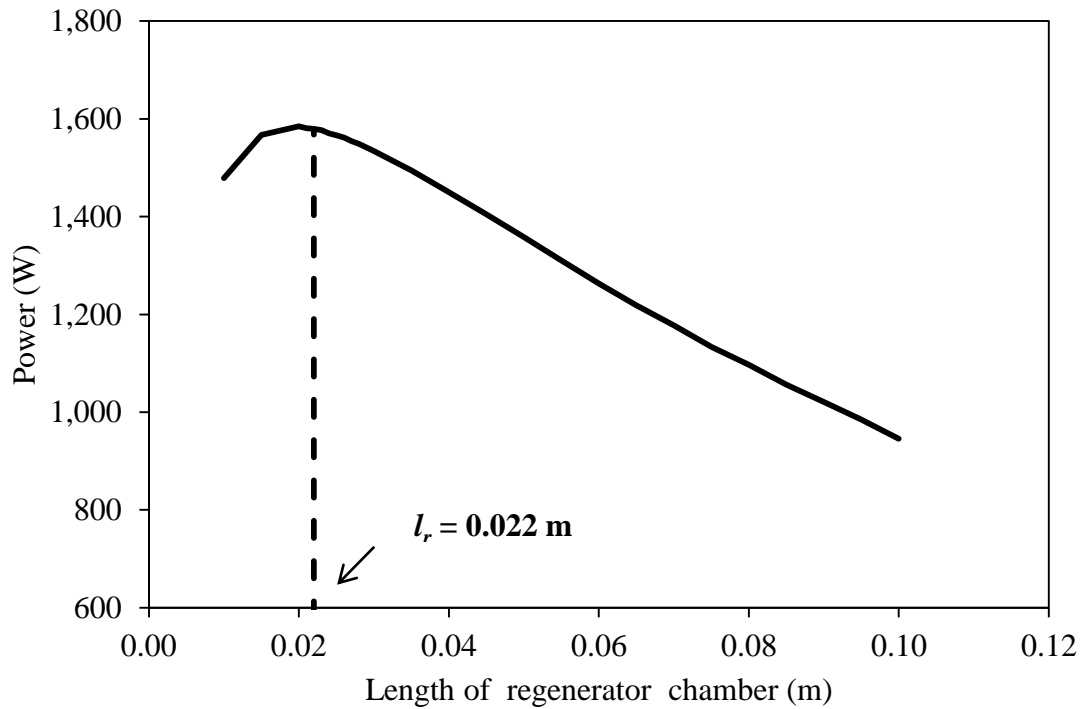


Figure 7.20 The indicated power against the length of the regenerator chamber

Chapter 8

Conclusions and recommendations for future work

This chapter presents main conclusions from research carried out in this work and recommendations for future work.

8.1 Conclusions

Conclusions from investigations of both the LTD and conventional Stirling engines are summarised in the following section.

8.1.1 Conclusions from research work on the development of the optimal design of the LTD Stirling engine

In this study, the second-order mathematical model of the gamma-type LTD Stirling engine was developed which takes into account the hydraulic losses, due to the flow friction in the regenerator, and mechanical losses due to the frictions between the piston and displacer and cylinders and other sealing components. Moreover, the 3D CFD simulation of the engine with the use of the standard $k-\varepsilon$ turbulence model was performed for better understanding the engine operation. Work on the optimisation of the design of the LTD Stirling engine based on the GA method was also conducted. The obtained results can be summarised as follows:

Chapter 8

1. The analysis of the working process of the LTD Stirling engine using the developed second-order mathematical model provided information on the variation of volumes, pressure, temperature and heat flow rate as functions of the crankshaft angle. Results of simulations showed that there was a low pressure drop in the regenerator of the engine because of a small hydraulic resistance in the high porosity matrix and the low engine speed. The movement of the displacer strongly affected the gas flow patterns in the displacer chamber and magnitude of the heat transfer rate on the surfaces of the hot and cold plates of the engine.

2. Experimental data obtained from testing the twin-power piston LTD Stirling engine manufactured by Kongtragool and Wongwiset [70] was used to calibrate the developed second-order mathematical model. It was found that the developed second-order mathematical model was capable to produce acceptable results in terms of the predicted brake power and overall efficiency of the engine.

3. Further information on the temperature and pressure distributions in the engine and gas flow patterns were obtained using 3D CFD modelling for better understanding the working process.

4. The use of the 3D CFD modelling provided a better accuracy in prediction of the engine's indicated power compared to the second-order mathematical model.

5. The set of optimal design parameters for the LTD Stirling engine described in [70] was obtained using the GA optimisation code coupled to the developed second-order model of the engine. The new optimised design parameters of the twin-power piston LTD Stirling engine provided a noticeable improvement in the value of the brake power of the engine.

Chapter 8

The developed second-order mathematical model of a LTD Stirling engine and also the developed GA optimisation code can now be used by manufacturers and developers in the designing process of LTD Stirling engines of different configurations.

8.1.2 Conclusions from research work on the development of the optimal design of conventional Stirling engines

The new second-order mathematical model was developed for conventional Stirling engines which include heat losses, such as internal conduction losses, shuttle losses and external heat losses, and also hydraulic losses due to the flow friction in all heat exchangers. In this model the regenerator of an engine was split into ten control volumes. The developed second-order mathematical model was used to analyze the performance of the conventional gamma-type Stirling engine. Additionally, the optimisation code based on the GA method was developed and coupled to the developed second-order mathematical model to find the optimal set of engine design parameters. The results of conducted study can be summarized as follows:

1. The new developed second-order mathematical model was used to analyse the working process of the conventional Stirling engine at Northumbria University. Information on the variation of volumes, pressure, pressure drops, temperatures and heat flow rates over the engine cycle and also P-V diagrams for the compression and expansion spaces was obtained, figured and discussed. It was found that there were small external heat losses in the cycle and in the regenerator. The greatest heat loss was due to the internal heat conduction. The heat loss due the

Chapter 8

shuttle heat loss mechanism was the smallest one. In addition, it was found that there was a large pressure drop in the regenerator of the engine.

2. The validation of the new developed second-order mathematical model was performed by comparison with results obtained using the second-order mathematical program SOPRANOS, 3D CFD modelling and the laboratory tests of the small conventional gamma-type Stirling engine presented and analysed by K Mahkamov in [14]. The predicted indicated power obtained using the new developed mathematical model was slightly more accurate than that obtained using SOPRANOS program. When compared to 3D CFD modelling the new developed second-order model demonstrated the less accuracy. However, when compared to the experimental results the new developed second-order mathematical model produced results which were in a good agreement with physical tests.

3. The optimal set of design parameters was obtained for the small conventional gamma-type Stirling engine described by Mahkamov in [14]. It was carried out by using the new developed second-order mathematical model coupled to the developed GA based optimization code. The optimal set of design parameters provided a considerable improvement in the value of indicated power when compared to the original engine prototype.

The new developed second-order mathematical model of conventional Stirling engines and the developed GA optimization code can now be used by manufacturers and developers to find optimal design parameters such as the dimensions and configuration of heat exchangers and to create a high performance conventional Stirling engines.

Chapter 8

8.2 Recommendations for future work

The modelling and optimization methodology developed in this study can be effectively used for the development and improvement of LTD Stirling engines and conventional Stirling engines for MTD and HTD applications. The models and optimization codes developed in this work, however, can be improved to provide a better accuracy in predictions and be more efficient in terms of computing time. Recommendations on improvements of the developed models and the optimization procedures to be used for the development of Stirling engines are as follows:

1. The more accurate correlation equations for the heat transfer in the oscillating flow are required for more precise calculations of the heat transfer in the heat exchangers and cylinders of Stirling engines, especially LTD engines. Additionally, physical investigations on the heat transfer in reciprocating flow for low engine speeds would be useful in order to derive the empirical heat transfer correlation to be used for LTD Stirling engines modelling.
2. There is need for more accurate flow friction correlations for determining the pressure drop in modelling of high speed Stirling engines.
3. More advanced numerical solving methods are need to be deployed for solving the ordinary differential equations in Stirling engine mathematical models which are capable to reduce the computing time in numerical simulations.
4. The more advanced GA techniques could be used for optimization of design parameters of Stirling engines which are capable to reduce the computational time in the optimization simulations. The multi-objective optimization methods

Chapter 8

should be developed to be coupled with Stirling engine models for the optimization of the engine which is capable to achieve both the high power output and efficiency.

References

- [1] B. Kongtragool, S. Wongwises. A review of solar-powered Stirling engines and low temperature differential Stirling engines. *Renewable and Sustainable Energy Reviews*, 7 (2003):131-154.
- [2] D. Mills. Advances in solar thermal electricity technology. *Solar Energy*, 76 (2004):19-31.
- [3] G. Brakmann, R. Aringhoff, M. Geyer, S. Teske. Concentrated Solar Thermal Power –Now! Online report, 2005. Available at <http://www.greenpeace.org/international/en/press/reports/Concentrated-Solar-Thermal-Power> (accessed on 12 June 2010).
- [4] D.G. Thombare, S.K. Verma. Technological development in the Stirling cycle engines. *Renewable and Sustainable Energy Reviews*, 12 (2008):1-38.
- [5] C.D. West. Principles and applications of Stirling engines. Van Nostrand Reinhold, 1986.
- [6] J.R. Senft. Ringbom stirling engines. Oxford University Press, 1993.
- [7] B. Kongtragool, S. Wongwises. Investigation on power output of the gamma-configuration low temperature differential Stirling engines. *Renewable Energy*, 30 (2005):465-476.
- [8] J.I. Prieto, J. Fano, C. González, M.A. González, R. Diaz. Preliminary design of the kinematic Stirling engine using dynamic similarity and quasi-static simulation. *Proceedings of the Institution of Mechanical Engineers, Part C: Journal of Mechanical Engineering Science*, 211 (1997):229-238.
- [9] J.I. Prieto, A.B. Stefanovskiy. Dimensional analysis of leakage and mechanical power losses of kinematic Stirling engines. *Proceedings of the Institution of*

References

- Mechanical Engineers, Part C: Journal of Mechanical Engineering Science, 217 (2003):917-934.
- [10] J.I. Prieto, M.A. González, C. González, J. Fano. A new equation representing the performance of kinematic Stirling engines. Proceedings of the Institution of Mechanical Engineers, Part C: Journal of Mechanical Engineering Science, 214 (2000):449-464.
- [11] J. Prieto, D. Garcia. Comparison between Kolin's cube law for power and other criteria for preliminary design of kinematic Stirling engines. Proceeding of 12th international Stirling engine conference, Durham UK, 2005, pp. 389-397.
- [12] W.R. Martini. Stirling Engine Design Manual. Arch, 1978.
- [13] N.C.L. Chen, F.P. Griffin. A review of Stirling engine mathematical models. Report No ORNL/CON 135, OAK Ridge National Laboratory, Tennessee, 1983.
- [14] K. Mahkamov. Stirling Engine Based Micro-Energy Systems. In: R. Beith, I.P. Burdon, M. Knowles (Eds.). Micro-Energy Systems. John Wiley & Sons, 2004, pp. 101-144.
- [15] G. Walker. Stirling engines. Clarendon Press, 1980.
- [16] G. Walker, J.R. Senft. Free Piston Stirling Engines. Springer, 1985.
- [17] F. Toda, S. Iwamoto, K. Nagajima. Development of Low-Temperature Difference Stirling engine- Behaviour of the mechanism effectiveness for the performance prediction method. Proceeding of 13th international Stirling engine conference, Tokyo, 2007, pp. 49-51.
- [18] I. Urieli, D.M. Berchowitz. Stirling cycle engine analysis, A. Hilger, 1984.
- [19] M. Abbas, N. Said, B. Boumeddane. Thermal analysis of Stirling engine solar driven. Revue des Energies Renouvelables, 11 (2008):503 - 514.

References

- [20] J.M. Strauss, R.T. Dobson. Evaluation of a second order simulation for Sterling engine design and optimisation. *Journal of Energy in Southern Africa*, 21 (2010):17-29.
- [21] I. Urieli. Stirling cycle machine analysis. Available at <http://www.ent.ohiou.edu/urieli/stirling/me422.html> (accessed on 17 November 2008)
- [22] F.J.G. Granados, M.A.S. Perez, V. Ruiz-Hernandez. Thermal Model of the EuroDish Solar Stirling Engine. *Journal of Solar Energy Engineering*, 130 (2008):011014-011018.
- [23] F. Nepveu, A. Ferriere, F. Bataille. Thermal model of a dish/Stirling systems. *Solar Energy*, 83 (2009):81-89.
- [24] W. Reinalter, S. Ulmer, P. Heller, T. Rauch, J.-M. Gineste, A. Ferriere, F. Nepveu. Detailed performance analysis of the 10 kW CNRS-PROMES dish/stirling system. *Proceedings of the 13th SolarPACES International Symposium, Seville Spain, 2006.*
- [25] N. Parlak, A. Wagner, M. Elsner, H.S. Soyhan. Thermodynamic analysis of a gamma type Stirling engine in non-ideal adiabatic conditions. *Renewable Energy*, 34 (2009):266-273.
- [26] I. Tlili, Y. Timoumi, S.B. Nasrallah. Analysis and design consideration of mean temperature differential Stirling engine for solar application. *Renewable Energy*, 33 (2008):1911-1921.
- [27] Y. Timoumi, I. Tlili, S. Ben Nasrallah. Design and performance optimization of GPU-3 Stirling engines. *Energy*, 33 (2008):1100-1114.
- [28] S. Schulz, F. Schwendig. A General Simulation Model for Stirling Cycles. *Journal of Engineering for Gas Turbines and Power*, 118 (1996):1-7.

References

- [29] K.K. Makhkamov, D.B. Ingham. Analysis of the Working Process and Mechanical Losses in a Stirling Engine for a Solar Power Unit. *Journal of Solar Energy Engineering*, 121 (1999):121-127.
- [30] Ö. Ercan Ataer, H. Karabulut. Thermodynamic analysis of the V-type Stirling-cycle refrigerator. *International Journal of Refrigeration*, 28 (2005):183-189.
- [31] H. Karabulut, H.S. Yücesu, C. Çınar. Nodal analysis of a Stirling engine with concentric piston and displacer. *Renewable Energy*, 31 (2006):2188-2197.
- [32] S.K. Andersen, H. Carlsen, P.G. Thomsen. Preliminary results from simulations of temperature oscillations in Stirling engine regenerator matrices. *Energy*, 31 (2006):1371-1383.
- [33] N. Martaj, L. Grosu, P. Rochelle. Thermodynamic Study of a Low Temperature Difference Stirling Engine at Steady State Operation. *International Journal of Thermodynamics*, 10 (2007):165-176.
- [34] A. Robson, T. Grassie, J. Kubie. Modelling of a low-temperature differential Stirling engine, *Proceedings of the Institution of Mechanical Engineers, Part C: Journal of Mechanical Engineering Science*, 221 (2007):927-943.
- [35] R.W. Dyson, S.D. Wilson, R.C. Tew. Review of Computational Stirling Analysis Methods. *Proceedings of 2nd International Energy Conversion Engineering Conference*, Paper No AIAA20045582, Providence RI, (2004) 1-21.
- [36] S.K. Andersen. Numerical Simulation of Cyclic Thermodynamic Processes. PhD Thesis (2006). Department of Mechanical Engineering, Technical University of Denmark.
- [37] R.C. Tew, R.W. Dyson, S.D. Wilson, R. Demko. Overview 2004 of NASA-Stirling Convertor CFD Model Development and Regenerator R&D Efforts. Report No NASA/TM-2004-213404, NASA, 2004.

References

- [38] S.K. Andersen, H. Carlsen, P.G. Thomsen. Control volume based modelling in one space dimension of oscillating, compressible flow in reciprocating machines. *Simulation Modelling Practice and Theory*, 14 (2006):1073-1086.
- [39] K. Mahkamov. An Axisymmetric Computational Fluid Dynamics Approach to the Analysis of the Working Process of a Solar Stirling Engine. *Journal of Solar Energy Engineering*, 128 (2006):45-53.
- [40] M.B. Ibrahim, R.C. Tew, Z. Zhang, D. Gedeon, T. Simon. CFD modeling of free-piston Stirling engines. Report No NASA/TM-2001-211132, NASA, 2001.
- [41] K. Mahkamov, D. Djumanov. Three- Dimensional CFD Modelling of a Stirling Engine. *Proceeding of 11th International Stirling Engine Conference*, Rome, Italy, 2003, pp. 96-107.
- [42] R. Tan, K. Mahkamov, D. Djumanov. Experimental and numerical investigations on a small physical Model of a solar Stirling engine. *Proceeding of 12th International Stirling Engine Conference*, Durham, UK, 2005, pp. 74-85.
- [43] K. Mahkamov. Design Improvements to a Biomass Stirling Engine Using Mathematical Analysis and 3D CFD Modeling. *Journal of Energy Resources Technology*, 128 (2006):203-215.
- [44] K. Mahkamov, E. Eid. Technical feasibility study of a concept of a medium temperature Stirling engine solar power unit. *Proceeding of 14th International Stirling Engine Conference (on CD only)*, Groningen, The Netherlands, 2009.
- [45] R.W. Dyson, S.D. Wilson, R.C. Tew, R. Demko. Fast whole-engine Stirling analysis. Report No NASA/TM—2005-213960, NASA, 2005.
- [46] D.A. Blank, C. Wu. Power optimization of an extra-terrestrial, solar-radiant stirling heat engine. *Energy*, 20 (1995):523-530.

References

- [47] L.B. Erbay, H. Yavuz. Analysis of the stirling heat engine at maximum power conditions. *Energy*, 22 (1997):645-650.
- [48] M. Costea, S. Petrescu, C. Harman. The effect of irreversibilities on solar Stirling engine cycle performance. *Energy Conversion and Management*, 40 (1999):1723-1731.
- [49] S.T. Hsu, F.Y. Lin, J.S. Chiou. Heat-transfer aspects of Stirling power generation using incinerator waste energy. *Renewable Energy*, 28 (2003):59-69.
- [50] Y.C. Hsieh, T.C. Hsu, J.S. Chiou. Integration of a free-piston Stirling engine and a moving grate incinerator. *Renewable Energy*, 33 (2008):48-54.
- [51] N. Martaj, L. Grosu, P. Rochelle. Exergetical analysis and design optimisation of the Stirling engine. *International Journal of Exergy*, 3 (2006):45-67.
- [52] P.C.T. de Boer. Optimal regenerator performance in Stirling engines. *International Journal of Energy Research*, 33 (2009):813-832.
- [53] L. Yaqi, H. Yaling, W. Weiwei. Optimization of solar-powered Stirling heat engine with finite-time thermodynamics. *Renewable Energy*, 36 (2011):421-427.
- [54] J.R. Senft. Optimum Stirling engine geometry. *International Journal of Energy Research*, 26 (2002):1087-1101.
- [55] B. Cullen, J. McGovern. Development of a theoretical decoupled Stirling cycle engine. *Simulation Modelling Practice and Theory*, 19 (2011):1227-1234.
- [56] F. Formosa, G. Despesse. Analytical model for Stirling cycle machine design. *Energy Conversion and Management*, 51 (2010):1855-1863.
- [57] A. Altman. SNAPpro: Stirling numerical analysis program (2004). Available at <http://home.comcast.net/snapburner/SNAPpro> (accessed on 13 March 2009).

References

- [58] B. Orunov, V.T. Krykov, A.P. Korobkov, K. Mahkamov, D. Djumanov. The first stage of the development of a small Stirling tri-generation power unit. Proceeding of 12th international Stirling engine conference, Durham, UK, 2005, pp. 416-423.
- [59] J. Zarinchang, A. Yarmahmoudi. Optimization of Thermal Components in a Stirling Engine. WSEA Transactions on Heat and Mass Transfer, 4(2009):1-10.
- [60] P. Rochelle. LTD Stirling engine simulation and optimization using Finite dimension thermodynamics. Proceeding of 12th international Stirling engine conference, Durham, UK, 2005, pp. 358-366.
- [61] S. Abdullah, B.F. Yousif, K. Sopian. Design consideration of low temperature differential double-acting Stirling engine for solar application. Renewable Energy, 30 (2005):1923-1941.
- [62] A. Homaifar, H.Y. Lai, E. McCormick. System optimization of turbofan engines using genetic algorithms. Applied Mathematical Modelling, 18 (1994): 72-83.
- [63] U. Kesgin. Genetic algorithm and artificial neural network for engine optimisation of efficiency and NOx emission. Fuel, 83 (2004):885-895.
- [64] M.C. Tayal, Y. Fu, U.M. Diwekar. Optimal Design of Heat Exchangers: A Genetic Algorithm Framework. Industrial & Engineering Chemistry Research, 38 (1998):456-467.
- [65] M. Mohagheghi, J. Shayegan. Thermodynamic optimization of design variables and heat exchangers layout in HRSGs for CCGT using genetic algorithm. Applied Thermal Engineering, 29 (2009):290-299.
- [66] J.M. Ponce-Ortega, M. Serna-González, A. Jiménez-Gutiérrez. Use of genetic algorithms for the optimal design of shell-and-tube heat exchangers. Applied Thermal Engineering, 29 (2009):203-209.

References

- [67] L. Gosselin, M. Tye-Gingras, F. Mathieu-Potvin. Review of utilization of genetic algorithms in heat transfer problems. *International Journal of Heat and Mass Transfer*, 52 (2009):2169-2188.
- [68] S. Hongprapas, S. Ewasakul, A. Lee. Low-temperature differential stirling engine prototype powered by a flat-plate solar collector. *The 20th Conference of the Mechanical Engineering Network of Thailand*, Thailand, 2006, pp. 74-85.
- [69] B. Kongtragool, S. Wongwises. Performance of low-temperature differential Stirling engines. *Renewable Energy*, 32 (2007):547-566.
- [70] B. Kongtragool, S. Wongwises. Performance of a twin power piston low temperature differential Stirling engine powered by a solar simulator. *Solar Energy*, 81 (2007):884-895.
- [71] B. Kongtragool, S. Wongwises. A four power-piston low-temperature differential Stirling engine using simulated solar energy as a heat source. *Solar Energy*, 82 (2008):493-500.
- [72] A.R. Tavakolpour, A. Zomorodian, A. Akbar Golneshan. Simulation, construction and testing of a two-cylinder solar Stirling engine powered by a flat-plate solar collector without regenerator. *Renewable Energy*, 33 (2008):77-87.
- [73] C. Çınar, H. Karabulut. Manufacturing and testing of a gamma type Stirling engine. *Renewable Energy*, 30 (2005):57-66.
- [74] C. Cinar, S. Yucesu, T. Topgul, M. Okur. Beta-type Stirling engine operating at atmospheric pressure. *Applied Energy*, 81 (2005):351-357.
- [75] İ. Batmaz, S. Üstün. Design and manufacturing of a V-type Stirling engine with double heaters. *Applied Energy*, 85 (2008):1041-1049.

References

- [76] H. Karabulut, F. Aksoy, E. Öztürk. Thermodynamic analysis of a type Stirling engine with a displacer driving mechanism by means of a lever. *Renewable Energy*, 34 (2009):202-208.
- [77] H. Karabulut, H.S. Yücesu, C. Çınar, F. Aksoy. An experimental study on the development of a β -type Stirling engine for low and moderate temperature heat sources. *Applied Energy*, 86 (2009):68-73.
- [78] H. Karabulut, C. Çınar, E. Öztürk, H.S. Yücesu. Torque and power characteristics of a helium charged Stirling engine with a lever controlled displacer driving mechanism. *Renewable Energy*, 35 (2010):138-143.
- [79] A. Der Minassians. Stirling Engines for Low-temperature Solar-thermal-electric Power Generation. PhD Thesis (2007), University of California, Berkeley.
- [80] A. Sripakagorn, C. Srikan. Design and performance of a moderate temperature difference Stirling engine. *Renewable Energy*, 36 (2011):1728-1733.
- [81] H.W. Brandhorst Jr, P.A. Chapman Jr. New 5kW free-piston Stirling space convertor developments. *Acta Astronautica*, 63 (2008):342-347.
- [82] D.C. Hesterman, B.J. Stone. A Systems Approach to the Torsional Vibration of Multi-Cylinder Reciprocating Engines and Pumps. *Proceedings of the Institution of Mechanical Engineers, Part C: Journal of Mechanical Engineering Science*, 208 (1994):395-408.
- [83] A.L. Guzzomi, D.C. Hesterman, B.J. Stone. The effect of piston friction on engine block dynamics. *Proceedings of the Institution of Mechanical Engineers, Part K: Journal of Multi-body Dynamics*, 221 (2007):277-289.
- [84] A.L. Guzzomi, D.C. Hesterman, B.J. Stone. Variable inertia effects of an engine including piston friction and a crank or gudgeon pin offset. *Proceedings of the Institution of Mechanical Engineers, Part D: Journal of Automobile Engineering*, 222 (2008):397-414.

References

- [85] M. Tanaka, I. Yamashita, F. Chisaka. Flow and Heat Transfer Characteristics of the Stirling Engine Regenerator in an Oscillating Flow. *JSME international journal, Ser. 2, Fluids engineering, heat transfer, power, combustion, thermophysical properties*, 33 (1990):283-289.
- [86] B. Kongtragool, S. Wongwises. Optimum absorber temperature of a once-reflecting full conical concentrator of a low temperature differential Stirling engine. *Renewable Energy*, 30 (2005):1671-1687.
- [87] J.P. Holman. *Heat transfer*. McGraw-Hill, 2002.
- [88] C.A. Finol, K. Robinson. Thermal modelling of modern engines: A review of empirical correlations to estimate the in-cylinder heat transfer coefficient. *Proceedings of the Institution of Mechanical Engineers, Part D: Journal of Automobile Engineering*, 220 (2006):1765-1781.
- [89] F.P. Incropera, D.P. DeWitt. *Fundamentals of heat and mass transfer*. John Wiley, 2007.
- [90] B. Thomas, D. Pittman. Update on the evaluation of different correlations for the flow friction factor and heat transfer of Stirling engine regenerators. *Proceedings of the 35th Intersociety Energy Conversion Engineering Conference and Exhibition, Las-Vegas, USA, 2000*, pp. 76-84 vol.71.
- [91] W.M. Kays, A.L. London. *Compact Heat Exchangers*. McGraw-Hill Book Company, 1964.
- [92] C. Hirsch. *Numerical Computation of Internal and External Flows: Computational methods for inviscid and viscous flows*. Wiley, 1990.
- [93] K.A. Hoffmann, S.T. Chiang. *Computational Fluid Dynamics*. Engineering Education System, 2000.
- [94] *Fluent 6.3 User's Guide Manual*, ANSYS Inc, 2006.
- [95] R.L. Haupt, S.E. Haupt. *Practical Genetic Algorithms*. John Wiley, 2004.

References

- [96] D.E. Goldberg. Genetic algorithms in search, optimization, and machine learning. Addison-Wesley Pub. Co., 1989.
- [97] J.R. Senft. An introduction to low temperature differential Stirling engines. Moriya Press, 1996.
- [98] A.M.S. Zalzal, P.J. Fleming. Genetic Algorithms in Engineering Systems. Institution of Electrical Engineers, 1997.
- [99] E.G. Shopova, N.G. Vaklieva-Bancheva. BASIC—A genetic algorithm for engineering problems solution. Computers & Chemical Engineering, 30 (2006):1293-1309.

Appendix A

MATLAB codes for the second-order mathematical modelling and optimisation of LTD Stirling engines

The code consists of the following subprograms:

inputdata_GA_LTD	Reynolds_number
global_file_LTD	heatcoff_Heat
define_y_parameter_LTD	heatcoff_Cool
GA_optimisation_LTD_Stirling_engine	foil
objective_function_LTD	calTw
LTD_modelling	newton_method
cal_function_LTD	rk4

Appendix A

inputdata_GA_LTD

```
*****
inputdata_GA_LTD.m
*****
%global_file_LTD
%constant values
g=9.806;          %gravitation accerelation[ m/s2]
R=287;           %gas constant
Cap=1005;        %specific heat capacity at constant pressure of gas
[J/kg.K]
Cav=718;         %specific heat capacity at constant volume of gas
[J/kg.K]
*****
TA=305.5;        %Ambient temperature
pO=101325;       %operating pressure, Pa
pA=101325;       %ambient presure, Pa
hA=4;           %heat convection coefficient at atmosphere [W/m2K]
sigma = 5.667e-8; %Stefan-boltzmann constant
emit = 0.8;      %emissivity
Plr=0.7;         %Prandtl number
% operating condition
qs=5097;
TC=307;          %Temperature of the chamber wall inside cooler space in
the beginning of the cycle, [K]
N=46.5;          % engine speed, [rpm]
f=N/60;          %frequency, [Hz]
*****
%marix
n=1;             %Number of regenerator
poros = 0.956;   %porosity of matrix in the regenerator
dM=0.0003;       %wire diameter, [m]
Capm=500;        % Heat capacity of matrix
fshp = 6.9;      % shape factor -wire
*****
num=1000;        %number of time step per cycle
*****
kD=36;           % thermal conductivity of displacer, [W/mK]
kr=16.3;         % thermal conductivity of matrix, [W/mK]
kH=36;           % thermal conductivity of heater tube, [W/mK]
kC=36;           % thermal conductivity of cooler tube, [W/mK]
*****
%GA parameters
popsize=30;      % set population size
mutrate=.2;     % set mutation rate
selection=0.5;   % fraction of population kept
maxit=80;       % max number of iterations
*****
%geometric data
DD=0.32;         %diameter of displacer [m]
DrodD=0.019;    %diameter of rod of displacer [m]
Dsh=0.05;       %diameter of bearing [m]
Dr=0.32;        %diameter of regenerator [m]
mp=0.1;         % mass of power piston [kg]
hp=0;           % ratio of length OC to OA in the piston connection
hD=0;           % ratio of length OC to OA in the displacer
connection
lp= 0.2645;     % length of power piston connecting rod [m]
lD= 0.1845;     % length of displacer conecting rod [m]
jp=0.5;         % ratio of length AR to AB in the piston connection
jD=0.5;         % ratio of length AR to AB in the displacer
connection
muf=0.3;        % friction coefficient on the piston surface
```

Appendix A

```
mus=0.3; % friction coefficient on the displacer surface
H=0.005; % height of sealing ring [m]
dirod=0.01; % internal diameter of sealing ring [m]
Pspr=0.005e6; % additional pressure due to the sealing ring [Pa]

%disp ('Choose optimal engine parameters and define upper and lower
bounds')
%stroke of displacer piston
M_Z=1;
%diameter of power piston , m
M_Dp=1;
%stroke of power piston
M_Zp=1;
%Thickness of regenerator
M_HD=1;
M=[M_Z M_Dp M_Zp M_HD];
npar=sum(M);
var_hi=zeros(1,npar);
var_lo=zeros(1,npar);
sign=zeros(1,npar);
%Z=input('Stroke of displacer[m]');
%var_hi(1,sum(sign)+1)=input('stroke of displacer-upper bound[m]');
var_hi(1,sum(sign)+1)=0.3; % upper bound
%var_lo(1,sum(sign)+1)=input('stroke of displacer-lower bound[m]');
var_lo(1,sum(sign)+1)=0.04; % lower bound
sign(1,sum(sign)+1)=1;
signZ=sum(sign);
%Dp[=input('diameter of power piston[m]');
%var_hi(1,sum(sign)+1)=input('stroke of power piston-upper bound[m]');
var_hi(1,sum(sign)+1)=0.13; % upper bound
%var_lo(1,sum(sign)+1,npar)=input('stroke of power piston-lower
bound[m]');
var_lo(1,sum(sign)+1)=0.02; % lower bound
sign(1,sum(sign)+1)=1;
signDp=sum(sign);
%Zc=input('Stroke of power piston[m]');
%var_hi(1,sum(sign)+1)=input('stroke of power piston-upper bound[m]');
var_hi(1,sum(sign)+1)=0.3; % upper bound
%var_lo(1,sum(sign)+1)=input('stroke of power piston-lower bound[m]');
var_lo(1,sum(sign)+1)=0.04; % lower bound
sign(1,sum(sign)+1)=1;
signZp=sum(sign);
%HD=input('Thickness of regenerator[m]');
%var_hi(1,sum(sign)+1)=input('Thickness of regenerator-upper
bound[m]');
var_hi(1,sum(sign)+1)=0.2; % upper bound
%var_lo(1,sum(sign)+1)=input('Thickness of regenerator-lower
bound[m]');
var_lo(1,sum(sign)+1)=0.01; % lower bound
sign(1,sum(sign)+1)=1;
signHD=sum(sign);
%*****
```

Appendix A

global_file_LTD

```
%global_file_LTD.m

global check % parameter for steady state status
global popsize % set population size
global maxit % maximum number of the generation
global mutrate % set mutation rate
global selection % fraction of population kept
global pA % ambient pressure [Pa]
global Dcyl % diameter of cyclinder [m]
global DD % diameter of displacer [m]
global DrodD % diameter of displacer rod [m]
global Ae % Heat transfer area of heat source[m2]
global Ak % Heat transfer area of heat sink [m2]
global Awgr % Heat transfer area of regenerator [m2]
global Ar % cross section area of regenerator [m]
global Acr % cross section area of gas in the regenerator [m]
global epsilon % effectiveness of regenerator
global R % gas constant [J/kg.K]
global Cap % specific heat capacity at constant pressure of gas [J/kg.K]
global Cav % specific heat capacity at constant volume of gas [J/kg.K]
global Capm % specific heat capacity at constant volume of matrix [J/kg.K]
global M % total mass of gas [kg]
global Vcle % dead volume of the expansion space [m3]
global Vclk % dead volume of the compression space [m3]
global VswD % swept volume of displacer [m3]
global VswP % swept volume of power piston [m3]
global TH TC % cold and hot plates temperatures [K]
global TA % ambient temperature [K]
global f % frequency [Hz]
global timestep % time per time step
global theta % crank angle [rad]
global degree % crank angle [degree]
global dirod % outside diameter of rod [m]
global Dcylp % diameter of power piston cylinder [m]
global it % iteration
global num %number of time step
global N % engine speed [rpm]
global Vr % volume of regenerator [m3]
global Vcr % gas volume in the regenerator [m3]
global qs % solar irradiation [w/m2]
global hA % heat transfer coefficient of ambient [W/m2K]
global sigma % Stefan-boltzmann constant
global p0 % operating pressure [Pa]
global poros % porosity of matrix in the regenerator
global mm % mass of matrix [kg]
global n % number of regenerator
global Dr % diameter of regenerator [m]
global Plr % Prandtl number
global lr % length of regenerator [m]
global dM % wire diameter [m]
global fshp % shape factor
global kD % thermal conductivity of displacer [W/mK]
global kr % thermal conductivity of matrix [W/mK]
global kC % thermal conductivity of cooler [W/mK]
global kH % thermal conductivity of heater [W/mK]
global Dp % diameter of power piston [m]
global Z % stroke of displacer [m]
global Zp % stroke of power piston [m]
global HD % displacer thickness [m]
global lp % length of power piston connecting rod [m]
global lD % length of displacer connecting rod [m]
```

Appendix A

```
global mp % mass of power piston [kg]
global mD % mass of displacer [kg]
global Ap % contact surface area of power piston [m2]
global jp % ratio of length AR to AB in the piston connection
global jD % ratio of length AR to AB in the displacer connection
global g % gravitational acceleration [m/s2]
global hp % ratio of length OC to OA in the piston connection
global hD % ratio of length OC to OA in the displacer connection
global mus % friction coefficient on the piston surface
global muf % friction coefficient on the displacer surface
global H % height of sealing ring [m]
global Pspr % additional pressure due to the sealing ring [Pa]
global Ddi % convenience gap of the displacer
global Dpi % convenience gap of the power piston
global Dsh % bearing diameter [m]
```

Appendix A

define_y_parameter_LTD

```
% define_y_parameter_LTD

P = 1; %pressure (Pa)
me = 2; %mass of expansion space (kg)
mk = 3; %mass of compression space (kg)
mr = 4; %mass of regenerator space (kg)
Tm = 5; %temperature of matrix (K)
QC = 6; %heat flow to cold plate (W)
QH = 7; %heat flow from hot plate (W)
Qr = 8; %heat flow of regenerator space (W)
Wk = 9; %work generated in the compression space (W)
We = 10; %work generated in the expansion space (W)
W = 11; %total work (W)
Qdiss = 12; %heat loss due to flow friction (W)
Tk = 13; %gas temperature of compression space (K)
Tr = 14; %gas temperature of regenerator space(K)
Te = 15; %gas temperature of expansion space (K)
Pk = 16; %pressure of compression space (Pa)
Pr = 17; %pressure of regenerator space (Pa)
Pe = 18; %pressure of expansion space (Pa)
Vk = 19; %volume of compression space (m3)
Ve = 20; %volume of expansion space (m3)
Vt = 21; %total volume (m3)
deltaP = 22; %pressure drop (Pa)
deltaPr = 23; %pressure drop generated in the regenerator (Pa)
epsilon = 24; %effectiveness
Tre = 25; %gas temperature of mass flow from regenerator to expansion
space (K)
Tkr = 26; %gas temperature of mass flow from compression space to
regenerator (K)
hC = 27; %heat transfer coefficient of cold plate (W/m2K)
hH = 28; %heat transfer coefficient of hot plate (W/m2K)
hM = 29; %heat transfer coefficient of matrix (W/m2K)
Reh = 30; %Reynolds number of gas in the expansion space
Rec = 31; %Reynolds number of gas in the compression space
Rem = 32; %Reynolds number of gas in the regenerator
mre = 33; %mass flow from regenerator to expansion space (kg/s)
mkr = 34; %mass flow from compression space to regenerator (kg/s)
x = 35; %displacement of piston (m)
yp = 36; %displacement of displacer (m)
Frp = 37; %friction force in the ring package of power piston (N)
FrD = 38; %friction force in the ring package of displacer rod(N)
sP = 39; %side force in acting on the power piston (N)
sD = 40; %side force in acting on the displacer rod(N)
Fox = 41; %force acting on the crankshaft in x-direction (N)
Foy = 42; %force acting on the crankshaft in y-direction (N)
Fo = 43; %total force acting on the crankshaft (N)
Pbr = 44; %gas pressure between the first and the second seals (Pa)
Pes1= 45; %pressure on the external side surface of the first ring
(Pa)
Pes2= 46; %pressure on the external side surface of the second ring
(Pa)
Frp1= 47; %friction force in the first sealing ring of the power
piston(N)
Frp2= 48; %friction force in the second sealing ring of the power
piston (N)
Frp3= 49; %friction force in the second sealing ring of the displacer
rod (N)
Frp4= 50; %friction force in the second sealing ring of the displacer
rod (N)
Mzb = 51; %torque of the rolling bearing loss (Nm)
```

Appendix A

```
Tp = 52;    %torque of the power piston (Nm)
TD = 53;    %torque of the displacer (Nm)
PTp = 54;   %power of the power piston (Nm)
PTD = 55;   %power of the displacer (Nm)
PTb = 56;   %brake power(Nm)
Tw = 62;    %wall temperature on the hot plate
```

Appendix A

GA_optimisation_LTD_Stirling_engine

```
function []=GA_optimisation_LTD_Stirling_engine

tic
% Continuous Genetic Algorithm
% Single objective function
% Edited by Kwanchai Kraitong 2009 and modified from Haupt & Haupt 2003

%Public parameter
global_file_LTD
%Setup the GA
inputdata_GA_LTD
ff='objective_function_LTD'; % objective function
% variable limits
varhi=zeros(popsiz, npar);
varlo=zeros(popsiz, npar);
for i = 1:1:popsiz
    varhi(i, :)=var_hi;
    varlo(i, :)=var_lo;
end
maxvalue=9999999; % minimum cost
Nt=npar; % continuous parameter GA Nt=#variables
% objective function
keep=floor(selection*popsiz); % #population members that survive
nmute=ceil((popsiz-1)*Nt*mutrate); % total number of mutations
M=ceil((popsiz-keep)/2); % number of matings
%Create the initial population
iga=0; % generation counter initialized
par=(varhi-varlo).*rand(popsiz, npar)+varlo; % random
result=fval(ff, par); % calculates population value using f
value1=result(:,1); % result 1 from the objective function
value2=result(:,2); % result 2 from the objective function
%*****
% single objective function
max_value1 = max(value1);
value = 1./(1+max_value1-value1); % evaluate fitness value for the maximum
problem
%*****
[value, inx]=sort(value, 'descend'); % max value in element 1
par=par(inx, :); % sort continuous
value1= value1(inx, :); value2= value2(inx, :);
Dpar1(1)=par(1,1); Dpar2(1)=par(1,2); Dpar3(1)=par(1,3); Dpar4(1)=par(1,4);
Dvalue1(1)=value1(1); Dvalue2(1)=value2(1);
maxvalue(1)=max(value1); % maxvalue contains max of population
meanvalue(1)=mean(value1); % meanvalue contains mean of population
disp(['#generations=' num2str(iga) ' best value=' num2str(value(1)) ' mean
value=' num2str(mean(value))])
disp([' brake power =' num2str(value1(1))])
disp([' thermal efficiency ='
num2str(value2(1))])
%Iterate through generations
while iga<maxit
    iga=iga+1; % increments generation counter
%Pair and mate
M=ceil((popsiz-keep)/2); % number of matings
prob=flipud([1:keep]'/sum([1:keep])); % weights chromosomes
odds=[0 cumsum(prob(1:keep))']; % probability distribution function
pick1=rand(1,M); % mate #1
pick2=rand(1,M); % mate #2
% ma and pa contain the indices of the chromosomes that will mate
ic=1;
while ic<=M
```

Appendix A

```

    for id=2:keep+1
        if pick1(ic)<=odds(id) && pick1(ic)>odds(id-1)
            ma(ic)=id-1;
        end
        if pick2(ic)<=odds(id) && pick2(ic)>odds(id-1)
            pa(ic)=id-1;
        end
    end
    ic=ic+1;
end
%Performs mating using single point crossover
ix=1:2:keep; % index of mate #1
xp=ceil(rand(1,M)*Nt); % crossover point
r=rand(1,M); % mixing parameter
for ic=1:M
    xy=par(ma(ic),xp(ic))-par(pa(ic),xp(ic)); % ma and pa mate
    par(keep+ix(ic),:)=par(ma(ic),:); % 1st offspring
    par(keep+ix(ic)+1,:)=par(pa(ic),:); % 2nd offspring
    par(keep+ix(ic),xp(ic))=par(ma(ic),xp(ic))-r(ic).*xy; % 1st
    par(keep+ix(ic)+1,xp(ic))=par(pa(ic),xp(ic))+r(ic).*xy; % 2nd
    if xp(ic)<npar % crossover when last variable not selected
        par(keep+ix(ic),:)=par(keep+ix(ic),1:xp(ic))
    par(keep+ix(ic)+1,xp(ic)+1:npar)];
    par(keep+ix(ic)+1,:)=par(keep+ix(ic)+1,1:xp(ic))
    par(keep+ix(ic),xp(ic)+1:npar)];
end
end
%Mutate the population
mrow=sort(ceil(rand(1,nmut)*(popsize-1))+1);
mcol=ceil(rand(1,nmut)*Nt);
for ii=1:nmut
    par(mrow(ii),mcol(ii))=(varhi(mrow(ii),mcol(ii))-
varlo(mrow(ii),mcol(ii)))*rand+varlo(mrow(ii),mcol(ii)); % mutation
end % ii
% The new offspring and mutated chromosomes are evaluated
result=feval(ff,par); % calculates population value using f
value1=result(:,1); % result from the objective function 1
value2=result(:,2); % result from the objective function 2
%*****
% single objective function
%value=value1;
maxvalue1 = max(value1);
if maxvalue1>max_value1
    max_value1=maxvalue1;
end
value = 1./(1+max_value1-value1); % evaluates fitness value for the
maximum problem
[value,inx]=sort(value,'descend') ; % max value in element 1
par=par(inx,:); % sort continuous
value1= value1(inx,:);
value2= value2(inx,:);
%collect data
Dpar1(iga+1)=par(1,1);
Dpar2(iga+1)=par(1,2);
Dpar3(iga+1)=par(1,3);
Dpar4(iga+1)=par(1,4);
Dvalue1(iga+1)=value1(1);
Dvalue2(iga+1)=value2(1);
maxvalue(iga+1)=max(value1);
meanvalue(iga+1)=mean(value1);
disp(['#generations=' num2str(iga) ' best value=' num2str(value(1)) ' mean
value=' num2str(mean(value))])
disp([' break power =' num2str(value1(1))])
disp([' thermal efficiency ='
num2str(value2(1))])

```

Appendix A

```
%Stopping criteria
    if iga>20 && iga<=maxit
        if maxvalue<=maxvalue(iga-20)
            break
        end
    elseif iga>maxit
        break
    end
end
%*****
%Displays the output
day=clock;
disp(datestr(datenum(day(1),day(2),day(3),day(4),day(5),day(6)),0))
disp(['optimized function is ' ff])
format short g
disp(['popsize = ' num2str(popsize) ' mutrate = ' num2str(mutrate) ' # par
= ' num2str(npar)])
disp(['#generations=' num2str(iga)])
fprintf('Brake power= %12.9f W\n',maxvalue(iga));
disp(['best solution'])
fprintf('stroke of displacer= %12.9f m \n',par(1,1));
fprintf('diameter of power piston= %12.9f m \n',par(1,2));
fprintf('stroke of power piston= %12.9f m \n',par(1,3));
fprintf('thickness of displacer or regenerator= %12.9f m \n',par(1,4));
disp('continuous genetic algorithm')
%save data
iters=0:length(maxvalue)-1;
save power-G.xls iters Dvalue1 -ascii;
save eff-G.xls iters Dvalue2 -ascii;
save Z-G.xls iters Dpar1 -ascii;
save Dp-G.xls iters Dpar2 -ascii;
save Zp-G.xls iters Dpar3 -ascii;
save HD-G.xls iters Dpar4 -ascii;

figure(1)
plot(iters,maxvalue);
xlabel('generation');ylabel('value');
title('value is function of generation ')
figure(2)
plot(iters,Dvalue1,'k');
xlabel('generation');ylabel('brake power(W)');
title('brake power is function of generation ')
figure(3)
plot(iters,Dvalue2,'k');
xlabel('generation');ylabel('Brake power efficiency');
title('Brake power efficiency is function of generation ')
figure(4)
plot(iters,Dpar1,'k');
xlabel('generation');ylabel('displacer stroke(m) ');
title('displacer stroke is function of generation ')
figure(5)
plot(iters,Dpar2,'k');
xlabel('generation');ylabel('diameter of power piston(m)');
title('diameter of power piston is function of generation ')
figure(6)
plot(iters,Dpar3,'k');
xlabel('generation');ylabel('power piston stroke(m)');
title('power piston stroke is function of generation ')
figure(7)
plot(iters,Dpar4,'k');
xlabel('generation');ylabel('thickness of regenerator (m)');
title('thickness of regenerator is function of generation ')
toc
end
```

Appendix A

objective_function

```
function ff=objective_function_LTD(x)

global_file_LTD
for i=1:1:popsiz
    inputdata_GA_LTD
    Z=x(i,1);
    Dp=x(i,2);
    Zp=x(i,3);
    HD=x(i,4);
    [eff,Power,a,RComp]= LTD_modelling;
    if isreal(Power)==0 || Power<0
        Power= 0;
    else
        Power=Power;
    end
    if isreal(eff)==0 || eff<0 || Power==0
        eff= 0;
    else
        eff=eff;
    end
    fprintf('N= %9.5f Dp= %9.5f lp= %9.5f a= %9.5f RComp= %9.5f lD=
%9.5f HD= %9.5f DD= %9.5f Z= %9.5f Zp= %9.5f Power=%9.5f eff=%9.5f
\n\n',N,Dp,lp,a,RComp,lD,HD,DD,Z,Zp,Power,eff);
    DPower(i)=Power;
    Deff(i)=eff;
end
ff = [DPower;Deff];
ff = ff';%transvere f
end
```

Appendix A

LTD_modelling

```
function [eff,Power,a,b,RComp]= LTD_modelling

% Second-order model of the LTD Stirling engine based on
% Quasi-steady flow model by Urieli [1984]and Timoumi et.al [2008]
% main file for analysis of working process and prediction of power output
% Engine space is divided into three main spaces-one compression space,
% one regenerator space,and one expansion space
% edited by Kwanchai Kraitong
% last modified 2012

%*****
%Public parameter
global_file_LTD
%*****
%define y-parameter
define_y_parameter_LTD
%*****

b=DD/Z;
VP=2*pi*Dp^2/4*Zp;
VD=pi*DD^2/4*Z;
RComp=VD/VP;
a=Dp/Zp;
Gap =0.00;
Dcylp=Dp; Dcyl=DD+2*Gap;
VswD=pi*(Dcyl^2)/4*Z;
% Twin power piston *****
VswP=pi*(Dcylp^2*0.5)^2/4*Zp;
%*****
Vcle =pi*(Dcyl)^2/4*0.0065+0.5*pi*(Dcyl^2-DD^2)/4*HD;
Vclk =pi*(Dcyl)^2/4*0.0065+2*pi*(Dcylp)^2/4*0.0265+0.5*pi*(Dcyl^2-
DD^2)/4*HD;
mm=n*pi*Dr^2/4*HD*(1-poros)*6000;
f=N/60; tT=1/f; timestep =tT/num; dt=timestep;
%*****
%calculate wall temperature on hot plate
Tex=TA; hHx=0;
y(Tw)= calTw(Tex,hHx);
%*****
% Initial conditions:
Vr=n*pi*(Dr^2)/4*HD;
Vcr=Vr*poros;
y(Te)= y(Tw); y(Tk) = TC; y(Tm) = (y(Tw)+TC)/2; y(Tr) = (y(Tw)+TC)/2;
y(hM)=20;y(hH)=10;y(hC)=10;
y(epsilon)=0.5;
t = 0;
theta=2*pi*f*t;
%*****
%gamma configuration
y(Ve)=Vcle+0.5*VswD*(1+cos(theta));
y(Vk)=Vclk+0.5*VswP*(1+cos(theta-pi/2))+0.5*(VswD)*(1-cos(theta));
y(me)=pA*y(Ve)/(R*y(Tr));
y(mk)=pA*y(Vk)/(R*y(Tr));
y(mr)=pA*(Vcr)/(R*y(Tr));
M=y(mk)+y(mr)+y(me);
y(mre)=0.001;y(mkr)=0.001;
y(P)=pO; y(Pk)=pO; y(Pe)=pO; y(Pr)=pO;
y(Qdiss)=0;y(deltaP)=0;
it= 1;check=0;
errorT=1;
while errorT>=0.001 && it <=30
    Te0=y(Te);
```


Appendix A

cal_function

```
function [y,dy]=cal_function_LTD(t,y)

%Public parameter
global_file_LTD
%define parameter y
define_y_parameter_LTD
%*****
mD= mm;
mrp=pi*0.01^2/4*lp*6000;
mrD=pi*0.01^2/4*1D*6000;
mcp=pi*0.293^2/4*0.02*6000;
mcd=pi*0.0^2/4*0.02*6000;
Irp= 0.5*pi*0.01^2/4*lp*6000*(lp/2)^2;
Ird= 0.5*pi*0.01^2/4*1D*6000*(1D/2)^2;
rD= Z/2; rp= Zp/2;
lr=HD;

%calculate angle
theta=2*pi*f*t;
thetad= theta;
thetap= thetad-pi/2;
dtheta=2*pi*f;
betap=pi+thetap;
betaD=pi+thetad;
alfaD=pi-asin(sin(betaD)*rD/1D);
alfap=pi-asin(rp/lp*sin(betap));
degree=thetad/pi*180;
% calculate displacement and volume-gamma type
x0=Zp;
yp0=Z;
y(x)=x0/2*(1+cos(theta-pi/2));
y(yp)=yp0/2*(1+cos(theta));
dy(x)=-x0/2*sin(theta-pi/2);
dy(yp)=-yp0/2*sin(theta);
y(Ve)=Vcle+0.5*VswD*(1+cos(theta));
y(Vk)=Vclk+0.5*VswP*(1+cos(theta-pi/2))+0.5*(VswD)*(1-cos(theta));
dy(Ve)=-0.5*VswD*(2*pi*f)*sin(theta);
dy(Vk)=-0.5*VswP*(2*pi*f)*sin(theta-pi/2)+0.5*(VswD)*(2*pi*f)*sin(theta);
zp=rp*cos(pi/2-theta)-lp*cos(alfap);
zD=0.2;

Ap=pi*Dp^2/4;
ADe=pi*DD^2/4;
ADk=pi*(DD^2-DrodD^2)/4;
Ae=pi*Dcyl^2/4;
Ak2=2*pi*Dcylp*(0.0265+y(x));
Ak=pi*(Dcyl^2-DrodD^2)/4-2*pi*(Dcylp^2)/4;
Ar=n*pi*(Dr^2/4);
%*****for sponge given by Tanaka*****
Acr=Ar*poros;
dr=4*poros*dM/(fshp*(1-poros));
Vcr=poros*Vr;
Awgr=4*Vcr/dr;
%*****
y(Vt)=y(Ve)+Vcr+y(Vk);
% mass flow condition
y(Tkr)=y(Tk);
if y(mkr)<0
    y(Tkr)=y(Tr);
end
y(Tre)=y(Tr);
```

Appendix A

```

if y(mre)<0
    y(Tre)=y(Te);
end
% calculate pressure by differential eq.
dy(P)=1/(Cav*y(Vt))* (R*(y(hH)*Ae*(y(Tw)-
y(Te))+y(epsilon)*y(hM)*Awgr*(y(Tm)-y(Tr))-y(Qdiss)+y(hC)*Ak*(TC-y(Tk)))-
Cap*((y(P)+y(deltaP))*dy(Ve)+y(P)*dy(Vk)));
% Conservation of energy for calculation of mass flow rate
y(mkr) = -1/(R*y(Tkr))* (-R/Cap*(y(hC)*Ak*(TC-
y(Tk)))+Cav/Cap*y(Vk)*dy(P)+y(Pk)*dy(Vk));
y(mre) = 1/(R*y(Tre))* (-R/Cap*(y(hH)*Ae*(y(Tw)-
y(Te)))+Cav/Cap*y(Ve)*dy(P)+y(Pe)*dy(Ve));
%Conservation of mass
dy(me)=y(mre);
dy(mk)=-y(mkr);
dy(mr)=y(mkr)-y(mre);
dy(Tm)=- (y(epsilon)*y(hM)*Awgr*(y(Tm)-y(Tr)))/(Cap*mm);
%calcualte heat transfer coefficient on hot plate
de = Dcyl;
ge = y(mre)/Ae;
[y(Reh),kg,mu]=Reynolds_number(ge,de,y(Te));
[y(hH)] = heatcoff_Heat(y(Te),y(Pe));
%calcualte heat transfer coefficient on cold plate
dk = (Ak*4/pi)^0.5;
gk = y(mkr)/Ak;
[y(Rec),kg,mu]=Reynolds_number(gk,dk,y(Tk));
[y(hC)] = heatcoff_Cool(y(Tk),y(Pk));
%calcualte heat transfer coefficient on the matrix
gr = ((y(mkr)+y(mre))/(2*Acr));
[y(Rem),kg,mu]=Reynolds_number(gr,dr,y(Tr));
[fr,y(hM),y(epsilon)] = foil(dr,mu,y(Rem),y(Pr),y(Tr));
%calcualte pressure drop generated in the regenerator
y(deltaPr) = -(2*fr*mu*Vcr*gr*lr/(y(mr)*(dr)^2));
y(deltaP)=y(deltaPr);
y(Pk)= y(P);
y(Pe)= y(P)+y(deltaP);
y(Pr)= y(P)+y(deltaP)/2;
%calculate gas temperature using Ideal gas Eq.
y(Te)=y(Pe)*y(Ve)/(R*y(me));
y(Tr)=y(Pr)*Vcr/(R*y(mr));
y(Tk)=y(Pk)*y(Vk)/(R*y(mk));
%calculate wall temperature at hot plate
Tex=y(Te);
hHx=y(hH);
[y(Tw)] = calTw (Tex,hHx);
%calculate heat loss due to flow friction
y(Qdiss) = y(deltaPr)*gr*Acr/(y(Pr)/(R*y(Tr)));
%calcualte heat rate
y(QC)= y(hC)*Ak*(TC-y(Tk));
y(QH)= y(hH)*Ae*(y(Tw)-y(Te));
y(Qr)=y(epsilon)*y(hM)*Awgr*(y(Tm)-y(Tr));
%calculate indicated work
y(Wk) = y(Pk)*dy(Vk);
y(We) = y(Pe)*dy(Ve);
%*****
% calcualte brake work
if check == 1
    if thetad>=0 && thetad<=pi/2 && dy(x)>=0
        Dpi= 1-muf*tan(alfap);
    elseif thetad>pi/2 && thetad<=pi && dy(x)<0
        Dpi= 1-muf*tan(alfap);
    elseif thetad>pi && thetad<=3/2*pi && dy(x)<0
        Dpi= 1+muf*tan(alfap);
    elseif thetad>3/2*pi && thetad<=2*pi && dy(x)>=0
        Dpi= 1+muf*tan(alfap);

```

Appendix A

```
end
if thetad>=0 && thetad<=pi/2 && dy(yp)<=0
    Ddi= 1-mus*tan(alfaD);
elseif thetad>pi/2 && thetad<=pi && dy(yp)<=0
    Ddi= 1-mus*tan(alfaD);
elseif thetad>pi && thetad<=3/2*pi && dy(yp)>0
    Ddi= 1+mus*tan(alfaD);
elseif thetad>3/2*pi && thetad<=2*pi && dy(yp)>0
    Ddi= 1+mus*tan(alfaD);
end
y(Pbr)=1/2*(pA+y(Pk));
y(Pes1)=1/2*(y(Pk)+y(Pbr));
y(Pes2)=1/2*(pA+y(Pbr));
if y(Pk)>=y(Pbr)
    y(Frp1)=0.16*pi*H*((y(Pk)+Pspr)*Dp-0.9*y(Pes1)*Dp);
elseif y(Pk)<y(Pbr)
    y(Frp1)=0.16*pi*H*((y(Pbr)+Pspr)*Dp-0.9*y(Pes1)*Dp);
end
if y(Pbr)>=101325
    y(Frp2)=0.16*pi*H*((y(Pbr)+Pspr)*Dp-0.9*y(Pes2)*Dp);
elseif y(Pbr)<101325
    y(Frp2)=0.16*pi*H*((100000+Pspr)*Dp-0.9*y(Pes2)*Dp);
end
if y(Pk)>=y(Pbr)
    y(Frp3)=0.3*pi*H*((y(Pk)+Pspr)*dirod-0.9*y(Pes1)*0.01);
elseif y(Pk)<y(Pbr)
    y(Frp3)=0.3*pi*H*((y(Pbr)+Pspr)*dirod-0.9*y(Pes1)*0.01);
end

if y(Pbr)>=101325
    y(Frp4)=0.3*pi*H*((y(Pbr)+Pspr)*dirod-0.9*y(Pes2)*0.01);
elseif y(Pbr)<101325
    y(Frp4)=0.3*pi*H*((101325+Pspr)*dirod-0.9*y(Pes2)*0.01);
end
if dy(x)>0
    y(Frp)= 0;
elseif dy(x)==0
    y(Frp)= 0;
elseif dy(x)<0
    y(Frp)= 0;
end
if dy(yp)>0
    y(FrD)= -(y(Frp3)+y(Frp4));
elseif dy(yp)==0
    y(FrD)= 0;
elseif dy(yp)<0
    y(FrD)= +(y(Frp3)+y(Frp4));
end
if dy(x)>0
    signp= -1;
elseif dy(x)==0
    signp= 0;
elseif dy(x)<0
    signp= 1;
end
if dy(yp)>0
    signD= -1;
elseif dy(yp)==0
    signD= 0;
elseif dy(yp)<0
    signD= 1;
end
y(sD)= (-
rD*dtheta^2*(IrD/(lD*cos(alfaD))^2*(rD*cos(betaD)^2*tan(alfaD)/(lD*cos(alfa
D))-sin(betaD))+mD*tan(alfaD)*(rD*cos(betaD))^2/(lD*cos(alfaD)^3)-
```

Appendix A

```

sin(betaD)*tan(alfaD)-
cos(betaD))+jD*mrD*(jD*rD*cos(betaD)^2*tan(alfaD)/(lD*cos(alfaD)^3)-
cos(betaD)*tan(alfaD)+sin(betaD)-
jD*sin(betaD)/cos(alfaD)^2))+g*tan(alfaD)*(mD+jD*mrD)-
y(FrD)*tan(alfaD)+1*y(Pk)*ADk*tan(alfaD)-1*y(Pe)*ADe*tan(alfaD))/Ddi;

y(sP)= (-
rp*dtheta^2*(Irp/(lp*cos(alfap))^2*(rp*cos(betap)^2*tan(alfap)/(lp*cos(alfa
p))-sin(betap))+mp*tan(alfap)*(rp*cos(betap)^2/(lp*cos(alfap)^3)-
sin(betap)*tan(alfap)-
cos(betap))+jp*mrp*(jp*rp*cos(betap)^2*tan(alfap)/(lp*cos(alfap)^3)-
cos(betap)*tan(alfap)+sin(betap)-
jp*sin(betap)/cos(alfap)^2))+g*tan(alfap)*(mp+jp*mrp)-y(Frp)*tan(alfap)-
(y(Pk)-101325)*Ap*tan(alfap))/Dpi;

y(Fox)=2*(rp*dtheta^2*sin(betap)*(mcp*hp-mrp*(1-
jp))+y(sP))+rD*dtheta^2*sin(betaD)*(mCD*hD-mrD*(1-jD))+y(sD));
y(Foy)=2*(rp*dtheta^2*(mp*(rp*cos(betap)^2/(lp*cos(alfap)^3)-
sin(betap)*tan(alfap)-
cos(betap))+mrp*(jp*rp*cos(betap)^2/(lp*cos(alfap)^3)-
jp*sin(betap)*tan(alfap)-cos(betap))+mcp*cos(betap))-
g*(mp+mrp+mcp)+y(Frp)+(y(Pk)-
101325)*Ap+signp*muf*abs(y(sP)))+(rD*dtheta^2*(mD*(rD*cos(pi/2-
(theta+pi/2))^2/(lp*cos(alfaD)^3)-sin(betaD)*tan(alfaD)-
cos(betaD))+mrD*(jD*rD*cos(betaD)^2/(lD*cos(alfaD)^3)-
jD*sin(betaD)*tan(alfaD)-cos(betaD))+mCD*cos(betaD))-g*(mD+mrD+mCD)+y(FrD)-
1*y(Pk)*ADk+1*y(Pe)*ADe+signD*mus*abs(y(sD)));
y(Fo)=(y(Fox)^2+y(Foy)^2)^0.5;
y(Mzb)=0.0015*y(Fo)*Dsh/2;
if sP >=0 && dy(x)<=0
    Epi=(1+muf*tan(betap))/(1+muf*tan(alfap));
elseif sP < 0 && dy(x)>0
    Epi=(1+muf*tan(betap))/(1+muf*tan(alfap));
elseif sP < 0 && dy(x)<=0
    Epi=(1-muf*tan(betap))/(1-muf*tan(alfap));
elseif sP >=0 && dy(x)>0
    Epi=(1-muf*tan(betap))/(1-muf*tan(alfap));
end
if sD >=0 && dy(yp)<=0
    Edi=(1+mus*tan(betaD))/(1+mus*tan(alfaD));
elseif sD < 0 && dy(yp)>0
    Edi=(1+mus*tan(betaD))/(1+mus*tan(alfaD));
elseif sD < 0 && dy(yp)<=0
    Edi=(1-mus*tan(betaD))/(1-mus*tan(alfaD));
elseif sD >=0 && dy(yp)>0
    Edi=(1-mus*tan(betaD))/(1-mus*tan(alfaD));
end

y(Tp)=0.5*(dtheta)^2*(2*Irp*Epi*((rp*cos(betap))/(lp*cos(alfap)))^2*((rp*co
s(betap))/(lp*cos(alfap))*tan(alfap)-
tan(betap))+2*mp*rp^2*(Epi*cos(betap)*tan(alfap)-
sin(betap))*(rp*cos(betap)^2/(lp*cos(alfap)^3)-sin(betap)*tan(alfap)-
cos(betap))-2*mrp*rp^2*(1-
jp)^2*sin(betap)*cos(betap)+2*mrp*rp^2*(Epi*jp*cos(betap)*tan(alfap)-
sin(betap))*(jp*rp*cos(betap)^2/(lp*cos(alfap)^3)-jp*sin(betap)*tan(alfap)-
cos(betap)))-g*rp*(mp*(Epi*cos(betap)*tan(alfap)-
sin(betap))+mrp*(Epi*jp*cos(betap)*tan(alfap)-
sin(betap))+mcp*hp*sin(betap))+y(Frp)+(y(Pk)-
101325)*Ap)*rp*(Epi*cos(betap)*tan(alfap)-sin(betap));
y(TD)=0.5*(dtheta)^2*(2*IrD*Edi*((rD*cos(betaD))/(lD*cos(alfaD)))^2*((rD*co
s(betaD))/(lD*cos(alfaD))*tan(alfaD)-
tan(betaD))+2*mD*rD^2*(Edi*cos(betaD)*tan(alfaD)-
sin(betaD))*(rD*cos(betaD)^2/(lD*cos(alfaD)^3)-sin(betaD)*tan(alfaD)-
cos(betaD))-2*mrD*rD^2*(1-
jD)^2*sin(betaD)*cos(betaD)+2*mrD*rD^2*(Edi*jD*cos(betaD)*tan(alfaD)-

```

Appendix A

```
sin(betaD))* (jD*rD*cos(betaD)^2/(lD*cos(alfap)^3)-jD*sin(betaD)*tan(alfaD)-
cos(betaD))-g*rD*(mD*(Edi*cos(betaD)*tan(alfaD)-
sin(betaD))+mrD*(Edi*jD*cos(betaD)*tan(alfaD)-
sin(betaD))+mCD*hD*sin(betaD))+ (y(FrD)-
1*y(Pk)*ADk+1*y(Pe)*Ade)*rD*(Edi*cos(betaD)*tan(alfaD)-sin(betaD));
    y(PTp)=dtheta*y(Tp);
    y(PTD)=dtheta*y(TD);
    y(PTb)=dtheta*y(Mzb);
end
end
```

Appendix A

Reynolds_number

```
function [Re,kg,mu]=Reynolds_number(g,d,y)

global Cap
global Plr
mu0 = 17.08e-6;
T0 = 273;
Tsuth = 112;
mu = mu0*(T0+Tsuth)/(y+Tsuth)*(y/T0)^1.5;
kg = Cap*mu/Plr;
Re = abs(g)*d/mu;
    if(Re < 1)
        Re = 1;
    end
end
```

heatcoff_Heat

```
function [hH] = heatcoff_Heat(Te,Pe)

global_file_LTD
%*****Eichelberg*****
hH=2.43*(2*Z*N/60)^(1/3)*(Pe/101325*Te)^0.5;
end
```

heatcoff_Cool

```
function [hC] = heatcoff_Cool(Tk,Pk)

global_file_LTD
%*****Eichelberg*****
hC=2.43*(2*Z*N/60)^(1/3)*(Pk/101325*Tk)^0.5;
end
```

foil

```
function [fr,hM,epsilon] = foil(dr,mu,Rem,Pr,Tr)

global Cap;global Plr;global Awgr;global Acr
global Nu;global poros;global VswD;global N;global R;global lr
Remmax=(1.042*pi*VswD*N*1/(60*Acr*poros))*0.98*dr/mu;
Remmean=(VswD*N*1/(30*Acr*poros))*Pr/(R*Tr)*dr/mu;
fr=(175/Remmax+1.6)*Rem;
Nu = 0.33*Remmean^0.67;
NTU=4*Nu*lr/(Plr*Remmean*dr);
hM=NTU/Awgr*Cap*(VswD*N*1/(30*Acr*poros))*Pr/(R*Tr)*Acr;
epsilon = NTU/(NTU+2);
end
```

Appendix A

calTw

```
function [Tw] = calTw(Tex,hHx)
x0=1000;
n=500;
Tw=newton_method(x0,n,TeX,hHx);
end
```

newton_method

```
function Tw = newton_method(x0,n,TeX,hHx)

% in the form f(x) = 0
global qs
global hA
global TA
global sigma
global emit
x = x0;
for i = 1:n
    k = emit*sigma*x^4+(hA+hHx)*x+(-hHx*TeX-hA*TA-emit*sigma*TA^4-qs*0.96);
    dk = 4*emit*sigma*x^3+(hA+hHx);
    xn = x - (k/dk);
    if x == xn
        i = i-1;
        break
    end
    x=xn;
end
Tw =x;
end
```

rk4

```
function [x, y, dy] = rk4(deriv,n,x,dx,y)

%Classical fourth order Runge-Kutta method
%Integrates n first order differential equations
%dy(x,y) over interval x to x+dx
%Israel Urieli - Jan 21, 2002
x0 = x;
y0 = y;
[y,dy1] = feval(deriv,x0,y);
for i = 1:n
    y(i) = y0(i) + 0.5*dx*dy1(i);
end
xm = x0 + 0.5*dx;
[y,dy2] = feval(deriv,xm,y);
for i = 1:n
    y(i) = y0(i) + 0.5*dx*dy2(i);
end
[y,dy3] = feval(deriv,xm,y);
for i = 1:n
    y(i) = y0(i) + dx*dy3(i);
end
x = x0 + dx;
[y,dy] = feval(deriv,x,y);
for i = 1:n
    dy(i) = (dy1(i) + 2*(dy2(i) + dy3(i)) + dy(i))/6;
    y(i) = y0(i) + dx*dy(i);
end
```

Appendix B

Publications

Publication 1 Title of ‘Thermodynamic and CFD Modelling of Low Temperature Difference Stirling Engines’

Kwanchai, K. and Mahkamov, K. *Thermodynamic and CFD Modelling of Low Temperature Difference Stirling Engines*. in *Proceeding of 14th International Stirling Engine Conference*. 2009. Groningen, The Netherlands.

Publication 2 Title of ‘Optimisation of Low Temperature Difference Solar Stirling Engines using Genetic Algorithm’

Kwanchai, K. and Mahkamov, K. *Optimisation of Low Temperature Difference Solar Stirling Engines using Genetic Algorithm*. in *Proceeding of World Renewable Energy Congress 2011*. 2011. Linköping, Sweden.

Appendix B

**Publication 1 Title of ‘Thermodynamic and CFD Modelling of Low
Temperature Difference Stirling Engines’**

Kwanchai, K. and Mahkamov, K. *Thermodynamic and CFD Modelling of Low Temperature Difference Stirling Engines*. in *Proceeding of 14th International Stirling Engine Conference*. 2009. Groningen, The Netherlands.

Thermodynamic and CFD modelling of Low-Temperature Difference Stirling Engines

^{*1}Kwanchai KRAITONG, ^{*2}Khamid MAHKAMOV

^{*1}Durham University, School of Engineering, Durham DH1 3LE, UK, kwanchai.kraitong@durham.ac.uk

^{*2}Durham University, School of Engineering, Durham DH1 3LE, UK, khamid.mahkamov@durham.ac.uk

Keywords: LTD Solar Stirling engine, the second-order mathematical model, 3D CFD model

Abstract

The second-order mathematical model of a kinematical gamma-type low temperature difference (LTD) Solar Stirling engine with taking into account hydraulic and mechanical losses was implemented in MATLAB software. Some results of the analysis of the working process of the LTD Stirling engine are presented in this paper in terms of volume, pressure and temperature variations as functions of the crank angle. The comparison demonstrates that there has been a good agreement between theoretical results obtained and experimental data published in open literature. Additionally, 3D CFD numerical simulations of the engine have been performed and analysis of results show that CFD modeling provides noticeable improvement in the estimation of the indicated power of the LTD engine, compared with the second-order mathematical modeling technique.

Nomenclature

C_p = specific heat at constant pressure (J/ kgK)	T_c = temperature of the cold plate (K)
C_v = specific heat at constant volume (J/ kgK)	T_e = temperature of the expansion space (K)
d_b = rolling bearing diameter (m)	T_H = temperature of the heating plate (K)
F_p = external force acting on the piston (N)	T_p = piston crank torque (Nm)
F_{fp} = frictional force between rings of the power piston and the cylinder (N)	T_m = temperature of the regenerator matrix (K)
F_{oa} = axial force acting on the crank shaft in the displacer piston connection joint (N)	T_r = temperature of regenerator space (K)
F_{op} = axial force acting on the crank shaft in the power piston connection joint (N)	t = time (sec)
f = frequency (Hz)	V_c = volume of the compression space (m ³)
g = gravitational term	V_{c1} = volume of the compression space in the displacer chamber (m ³)
m = mass of the gas in the control volume (kg)	V_{c2} = volume of the compression space in the piston cylinder (m ³)
\dot{m}_i = inlet mass flow rate (kg/s)	V_e = volume of the expansion space (m ³)
\dot{m}_o = outlet mass flow rate (kg/s)	V_r = volume of the regenerator space (m ³)
P_c = pressure in the compression space (Pa)	V_T = total volume of the engine (m ³)
P_{c1} = pressure in the compression space in the displacer chamber (Pa)	W = cyclic work (J)
P_{c2} = pressure in compression space in the piston cylinder (Pa)	W_b = cyclic brake work (J)
P_e = pressure in the expansion space (Pa)	W_i = cyclic indicated work (J)
P_b = brake power (W)	x = current displacement of the piston (m)
P_i = indicated power (W)	x_o = stroke of the piston (m)
P_r = pressure in the regenerator space (Pa)	y = current displacement of the displacer (m)
Q = heat transfer rate (W)	y_o = stroke of the displacer (m)
$Q_p(t, \beta_p)$ = piston load along the cylinder axis (N)	
S_p = piston side force (N)	
T = total crank torque (Nm)	
T_b = frictional torque of the rolling bearing (Nm)	
T_c = temperature in the compression space (K)	

Greek symbols

β_p = crank angle
μ_b = coefficient of the friction at the rolling bearing
μ_k = coefficient of friction at the piston side
θ = piston crank angle
τ = time period (sec)
k, ε = turbulent kinetic energy and dissipation turbulent kinetic energy (m ² /s ²)

Table 1

The geometric data of a twin power piston LTD Stirling engine	
working piston stroke (m)	0.0826
working piston diameter(m)	0.083
working piston swept volume (m ³)	893.8x10 ⁻⁴
displacer piston stroke (m)	0.0795
displacer piston diameter (m)	0.32
displacer piston swept volume (m ³)	6393.8 x10 ⁻⁴
swept volume ratio	7.15
Displacement phase angle of the pistons (°)	90

Dimensions of the LTD Stirling engine manufactured by Kongtragool and Wongwiset [17]

3. The second-order mathematical model

The governing equations of the mathematical model are the mass and energy conservation equations written for each control volume of the gas circuit and the ideal gas state equation. The gas circuit of the LTD Stirling engine is divided into the following three control volumes: the expansion space, the regenerator's space and the compression space. In this work, the energy loss due to the pressure drop in the regenerator is taken into account [10, 19-20]. Heat transfer to the gas from the heating plate and cold plate can be calculated by using Eichelberg's heat transfer correlation developed for reciprocating machines [21]. Furthermore, the mechanical losses due to the friction forces in the mechanical couplings are considered taking into account dynamics of the motion of the power pistons and the displacer. The displacements of the piston and of the displacer can be calculated using the harmonic functions.

The energy conservation equation and the mass conservation equation are expressed as follows:

$$C_v \frac{d(mT)}{dt} = dQ - \frac{dW}{dt} - \dot{m}_o C_p T_o + \dot{m}_i C_p T_i \quad (1)$$

$$\frac{dm}{dt} = \dot{m}_o - \dot{m}_i \quad (2)$$

The indicated cyclic work and the indicated power are calculated as

$$W_i = \oint \left(\frac{dW_i}{dt} \right) dt = \int_0^{\tau} \left(\frac{dW_c}{dt} + \frac{dW_e}{dt} \right) dt = \int_0^{\tau} \left(P_c \frac{dV_c}{dt} + P_e \frac{dV_e}{dt} \right) dt \quad (3)$$

and

$$P_i = W_i f \quad (4)$$

In order to determine the brake cyclic power, the kinetic motion equations of the mechanical transmission system of the reciprocating engine including the effect of the frictional forces in the cylinders as proposed by Hesterman et al. [22] and Guzzomi et al.[23-24] are used. The torque induced by the piston (T_p) can be obtained from the following equation:

$$T_p = \frac{1}{2} \dot{\beta}_p^2 I'(\beta_p) + g(\beta_p) + Q_p(t, \beta_p) \quad (5)$$

Here $I'(\beta_p)$ is the rate of the change in the inertia and $Q_p(t, \beta_p)$ is the force acting on the piston

$$Q_p(t, \beta_p) = (F_{rp} + \mu_b |S_p| + F_p) \quad (6)$$

The determination of the frictional forces due to the sealing rings in the displacer rod is carried out using methodology described in [11]. Furthermore, the mechanical losses due to the friction in rolling bearings can be determined as

$$T_b = \mu_b \bar{F}_O \frac{d_b}{2} \quad (7)$$

where $\mu_b = 0.0015$ and $\bar{F}_O = \bar{F}_{Op} + \bar{F}_{Od}$

The brake cyclic work and the brake cyclic power are calculated as

$$T = \sum T_p \quad (8)$$

Appendix B

$$W_b = \oint \left(\frac{dW_b}{dt} \right) dt = \int_0^{\tau} (T - T_b) \frac{d\theta}{dt} dt \quad (9)$$

$$P_b = W_b / f \quad (10)$$

For numerical calculations the above mathematical model was implemented as a computer program in MATLAB. During mathematical modeling the magnitude of the pressure drop was calculated to determine the pressure value in each space. The calculations were performed cycle by cycle until the steady state was achieved and then the predicted pressure curves in the compression and expansion spaces were used to calculate the brake cyclic work and the brake power.

4. The 3D CFD model

To achieve better understanding of the working process of the LTD Stirling engine and obtain more details on the processes taking place inside the engine, 3D CFD modeling using the standard $k-\epsilon$ turbulence model for a compressible flow was carried out to investigate the work of the engine. The geometry of the internal gas circuit in the CFD technique is split into several thousand small control volumes. The governing equations of the CFD model are the mass, momentum and energy conservation equations and the turbulent kinetic energy and the dissipation of turbulent kinetic energy equations written for each the control volume. Commercial CFD software, FLUENT was used to perform CFD simulations of the working process of the engine. During the simulations the movement of pistons was taken into account and the regenerator of the engine was treated as a homogeneous porous medium. The momentum conservation equations of the fluid flow in the regenerator's control volumes were modified with the additional terms taking into account the viscous and inertial losses terms. In addition, the special energy conservation equation which describes the heat conduction in the matrix was used [25]. The subroutines describing displacements of the pistons and the displacer were written and then connected to the main body of the programme. The cycle was divided into equal 500 time-steps and calculations were performed using a high performance computer. The average gas temperature and pressure in each engine's working space were monitored during calculations in order to determine whether the steady-state condition was reached in the simulated operation of the engine.

5. Numerical Results from the Second-Order Mathematical Modeling

Numerical simulations were performed assuming that the solar flux on the surface of the heating plate was equal to 5097 W/m^2 , the cooler surface temperature was 307 K and the engine speed was 46.5 rpm . Air at atmospheric pressure is used as the working gas in the engine. Atmospheric pressure and atmospheric temperature were taken equal to 1 bar and 305.5 K , respectively. The heat losses from the outer surface of the heating plate due to the free convection and re-radiation were calculated in accordance with [26]. The matrix material properties were assumed to be those of the SM 15 stainless steel. The diameter of the regenerator's wire was taken equal to 0.0003 m with the porosity being 0.956 [20].

Figure 3 presents results on the variation of the volumes of the expansion, compression and total volumes over the cycle. It can be seen that the variation of the total volume is relatively small because of the cross-sectional area of cylinders of the power pistons is significantly less than that of the displacer cylinder. Figure 4 shows the variation of the pressure in volumes of the engine. The pressure difference in the volumes is very low due to a small hydraulic resistance of the high porosity regenerator and the low shaft speed. The variations of the gas temperature in each control volume are shown in Figure 5. The highest temperature in the cycle is about 500 K and is achieved in the displacer cylinder. The magnitude of the temperature variation in this cylinder is about 50 K . The temperature range in the compression space is about 25 K . The calculated P-V diagrams are presented in Figure 6. The predicted indicated power and the predicted brake power were compared with the experimental results obtained by Kongtragool and Wongwises [17] at identical operating conditions. From the experimental results, the maximum brake power and the overall efficiency were 0.969 W and 0.421% , respectively. The developed second order mathematical model of the LTD engine predicts that the indicated power, the brake power and the overall efficiency are 1.327 W , 1.134 W and 0.493% , respectively.

6. Results from 3D CFD model

The simplified 3D geometry and computational mesh of the twin-power piston LTD engine is shown in Figure 7. The presence of the gap between the displacer and its cylinder is reflected in the above mesh. The value of the solar irradiance (5097 W/m^2) and the heat losses due to the free convection and re-radiation were taken account when describing boundary conditions. The P-V diagrams of the engine's cycle obtained in 3D CFD model are displayed in Figure 8. The indicated power is determined as the sum of the areas of the expansion space, of the compression spaces in the piston cylinders and of the compression space in the displacer cylinder. According to CFD modeling results, the engine generates 1.283 W of the indicated power at the 46.5 rpm speed and this value is more accurate than that

Appendix B

obtained with the use of the developed second-order mathematical model. Figure 9 shows the temperature distribution in the gas inside the engine for the instance of the cycle when the crank angle is equal to 90° and it can be seen that in the displacer cylinder the temperature difference is quite significant and this is determined by a gas flow pattern. Figure 10 shows an example of the pressure distribution inside the engine for the same instance of the cycle and results indicate a very small pressure difference due to negligible hydraulic losses.

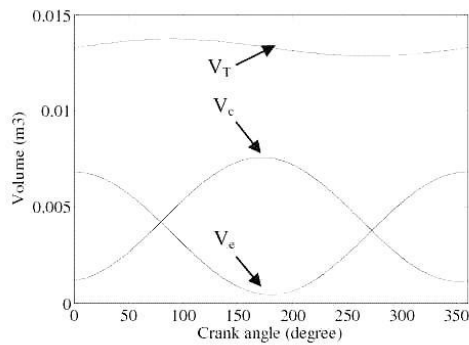


Fig. 3 The variation of the engine volumes

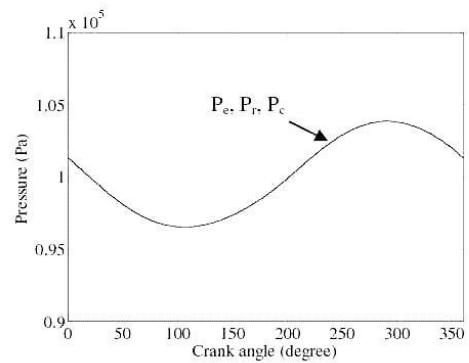


Fig. 4 The variation of the pressure in engine volumes

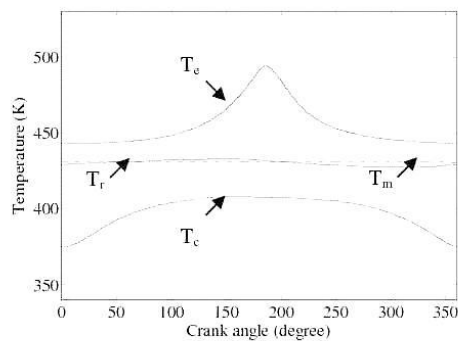


Fig. 5 The variation of the gas temperature in the engine

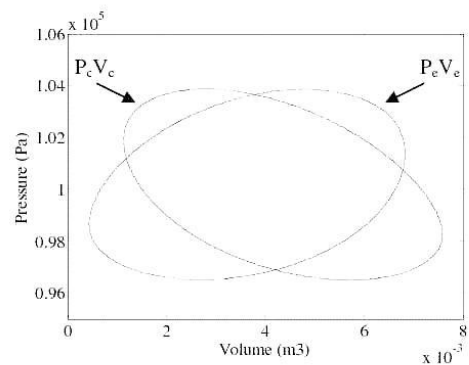


Fig. 6 P-V diagrams

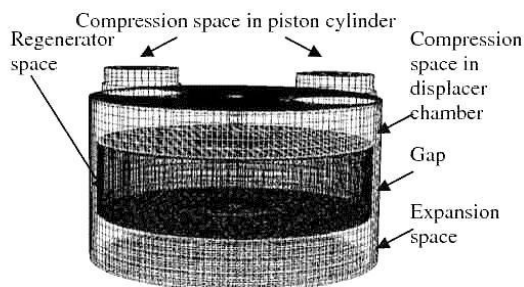


Fig. 7 The simplified geometry mesh of a LTD Stirling engine

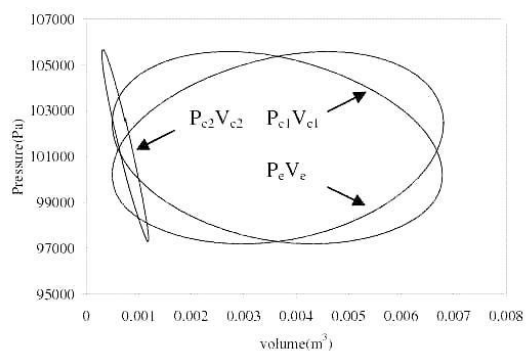


Fig. 8 P-V diagram from the 3D CFD modeling

Appendix B

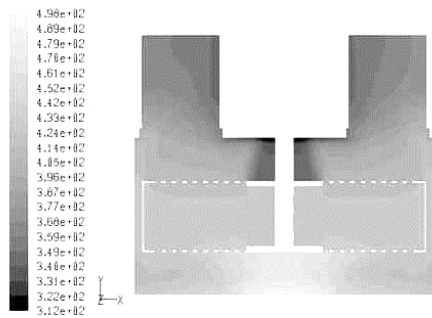


Fig. 9 The temperature distribution inside the engine

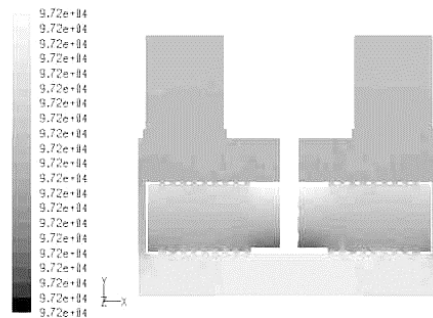


Fig. 10 The pressure distribution inside the engine

Conclusion

In this paper, the second order mathematical model and 3D CFD models of the twin-power piston gamma LTD Solar Stirling engine are described. The second order mathematical model takes into account heat losses and hydraulic resistances in the internal gas circuit and mechanical losses in the engine. From the numerical analysis of the working process it is found that the 3D CFD modeling provides better accuracy in predicting performance of the engine.

Currently the optimization subroutine is being developed based on the Genetic Algorithms technique and this will be coupled with the second-order mathematical model of the LTD Stirling engine to obtain an optimal set of design parameters to maximize the power output and efficiency of the machine.

Acknowledgements

This work is a part of a PhD study which is supported by the Ministry of Science and Technology of Royal Thai Government. Authors also would like to thank Professor Somchai Wongwises and Assistant Professor Bancha Kongtragool for providing data on their twin power piston LTD Stirling engine.

References

- [1] Kongtragool, B and Wongwises, S 2003, 'A review of solar-powered Stirling engines and low temperature differential Stirling engines' *Renewable and Sustainable Energy Reviews*, **7**, pp. 131-154.
- [2] Iwamoto, I, Toda, F, Hirata, K, Takeuchi, M and Yamamoto, T, 'Comparison of low- and high-temperature differential Stirling engines', *Proceeding of eighth international Stirling engine conference*, 1997, pp. 29-38.
- [3] Abdullah, S, Yousif, B and Sopian, K 2005, 'Design consideration of low temperature differential double-acting Stirling engine for solar application', *Renewable Energy*, **30**, pp. 1923-1941.
- [4] Kongtragool, B and Wongwises, S 2005, 'Investigation on power output of the gamma-configuration low temperature differential Stirling engines', *Renewable Energy*, **30**, pp. 465-476..
- [5] Prieto, J and Garcia, D 2005, 'Comparison between Kolin's cube law for power and other criteria for preliminary design of kinematic Stirling engines', *Proceeding of 12th international Stirling engine conference*, 2005, pp.389-397.
- [6] Rochelle, P 2005, 'LTD Stirling engine simulation and optimization using " Finite dimension thermodynamics"', *Proceeding of 12th international Stirling engine conference*, 2005, pp.358-366.
- [7] Martaj, N, Grosu, L and Rochelle, P 2007, 'Thermodynamic study of a low temperature difference Stirling engine at steady state operation', *Int. J. of Thermodynamics*, **10**, No.4, pp. 165-176.
- [8] Robson, A, Grassie, T and Kubie, J 2007, 'Modelling of a low-temperature differential Stirling engine', *J. Mechanical Engineering Science*, Proc. ImechE, **221** Part C, pp. 927-943.
- [9] Timoumi, Y, Tlili, I and Nasrallah, S 2008, 'Performance optimization of Stirling engines', *Renew Energy*, doi:10.1016/j.renene.2007.12.012.
- [10] Timoumi, Y, Tlili, I and Nasrallah, S 2008, 'Design and performance optimization of GPU-3 Stirling engines', *Energy*, doi:10.1016/j.energy.2008.02.005.
- [11] Mahkamov, K and Imgham, D, 1999, 'Analysis of the Working Process and Mechanical Losses in a Stirling Engine for a Solar Power Unit', *J. of Solar Energy Engineering*, **121**, pp. 121-127.

Appendix B

- [12] Prieto, J and Stefanovskiy, A 2003, 'Dimensional analysis of leakage and mechanical power losses of kinematic Stirling engines', *J. Mechanical Engineering Science*, Proc. Instn Mech Engrs, **217** Part C, pp. 917-934.
- [13] Toda, F, Iwamoto, S and Nagajima, K 2007, 'Development of Low-Temperature Difference Stirling engine- Behaviour of the mechanism effectiveness for the performance prediction method', *Proceeding of thirteen international Stirling engine conference*, pp.49-51.
- [14] Tan, R, Mahkamov, K and Djumanov, D 2005, 'Experimental and numerical investigations on a small physical Model of a solar Stirling engine', *Proceeding of 12th international Stirling engine conference*, 2005, pp.74-85.
- [15] Mahkamov, K, 2006, 'An Axisymmetric Computational Fluid Dynamics Approach to the Analysis of the Working Process of a Solar Stirling Engine', *J. of Solar Energy Engineering*, **128**, pp. 45-53.
- [16] Mahkamov, K, 2006, 'Design Improvements to a Biomass Stirling Engine Using Mathematical Analysis and 3D CFD Modeling', *J. of Energy Resources Technology*, **128**, pp. 203-215.
- [17] Kongtragool, B and Wongwises, S 2007, 'Performance of a twin power piston low temperature differential Stirling engine powered by a solar simulator', *Solar Energy*, **81**, pp. 884-895.
- [18] Tavakolpour, A, Zomorodian, A and Golneshan, A 2008, 'Simulation, construction and testing of a two-cylinder solar Stirling engine powered by a flat-plate solar collector without regenerator', *Renewable Energy*, **33**, pp. 77-87.
- [19] Urieli, I, Stirling Cycle Machine Analysis. Retrieved from <http://www.ent.ohiou.edu/~urieli/stirling/me422.html>
- [20] Tanaka, M and Yamashita, I 1990 'Flow and heat transfer characteristic of the Stirling engine regenerator in an oscillating flow', *JSME International Journal*, **33**, pp. 283-289.
- [21] Finol, C A and Robinson, K 2006, 'Thermal modeling of modern engines: a review of empirical correlations to estimate the in-cylinder heat transfer coefficient', *Proc. IMechE Part D: J. Automobile Engineering*, **220**, pp. 1765-1781.
- [22] Hesterman, D C and Stone, B J 1994, 'A systems approach to the torsional vibration of multi-cylinder reciprocating engines and pumps', *Proc. IMechE*, **208**, pp. 395-408.
- [23] Guzzomi, A L, Hesterman, D C and Stone, B J 2007, 'The effect of piston friction on engine block dynamics', *Proc. IMechE*, **221**, pp. 227-289.
- [24] Guzzomi, A L, Hesterman, D C and Stone, B J 2008, 'Variable inertia effects of an engine including piston friction and a crank or gudgeon pin offset', *Proc. IMechE*, **222**, pp. 387-414
- [25] Donald, A N and Bejan, A 1998, *Convective Heat Transfer in Porous Media*, Springer, New York.
- [26] Kongtragool, B and Wongwises, S 2005, 'Optimum absorber temperature of a once-reflecting full conical concentrator of a low temperature differential Stirling engine', *Renewable Energy*, **30**, pp. 1671-1687.

Appendix B

Publication 2 Title of ‘Optimisation of Low Temperature Difference Solar Stirling Engines using Genetic Algorithm’

Kwanchai, K. and Mahkamov, K. *Optimisation of Low Temperature Difference Solar Stirling Engines using Genetic Algorithm*. in *Proceeding of World Renewable Energy Congress 2011*. 2011. Linköping, Sweden.

Optimisation of Low Temperature Difference Solar Stirling Engines using Genetic Algorithm

Kwanchai Kraitong, Khamid Mahkamov*

School of Computing, Engineering and Information Sciences, Northumbria University,
Newcastle upon Tyne, NE1 8ST, UK*

*Corresponding author. Tel: +44 191 2274739, Fax: +44 191 2437630,
Email: khamid.mahkamov@northumbria.ac.uk

Abstract: This paper presents results of theoretical investigations on the determination of optimal design parameters of a Low Temperature Difference (LTD) Solar Stirling Engine using optimisation method based on Genetic algorithms. The developed thermodynamic mathematical model of the engine takes into account hydraulic and mechanical losses in the engine's working process and this model was coupled to the optimisation algorithm. A set of such design parameters as the stroke of the displacer and diameter and stroke of the power piston and the thickness of the regenerator placed in the displacer have been considered as variables. The engine's performance parameter such as the brake power is used as the objective function of the optimisation algorithm. The GA code is implemented in MATLAB. The accuracy of the optimal design engine's performance is examined using 3D CFD modelling of the working process of the engine. The set of design parameters obtained from the optimisation procedure provides the noticeable improvement of the engine's performance compared with the performance of the original LTD Solar Stirling engine with the same operating condition.

Keywords: LTD Stirling engine, Second-order mathematical model, Mechanical losses, CFD, Genetic algorithm.

Nomenclature

C_p	specific heat at constant pressure... $J \cdot kg^{-1} K^{-1}$	Value.....	fitness value
C_v	specific heat at constant volume ... $J \cdot kg^{-1} K^{-1}$	V_c	volume of the compression space..... m^3
D_p	diameter of piston..... m	V_{c1}	volume of the compression space in the displacer chamber..... m^3
D_D	diameter of displacer..... m	V_{c2}	volume of the compression space in the piston cylinder..... m^3
f	frequency..... Hz	V_{dc}	dead volume of the compression space... m^3
H_d	thickness of regenerator..... m	V_{de}	dead volume of the expansion space..... m^3
m	mass of the gas in the control volume..... kg	V_e	volume of the expansion space..... m^3
maxvalue	maximum fitness value in the value map	V_{SP}	swept volume of the piston m^3
\dot{m}_i	inlet mass flow rate..... $kg \cdot s^{-1}$	V_{SD}	swept volume of the displacer..... m^3
\dot{m}_o	outlet mass flow rate..... $kg \cdot s^{-1}$	W	work..... J
P_b	brake power..... W	W_b	cyclic brake work..... J
P_c	pressure in the compression space..... Pa	W_c	work of the compression space..... J
P_{c1}	pressure in the compression space in the displacer chamber..... Pa	W_e	work of the expansion space..... J
P_{c2}	pressure in compression space in the piston cylinder..... Pa	x	current displacement of the piston..... m
P_e	pressure in the expansion space..... Pa	x_0	stroke of the piston..... m
P_i	indicated power..... W	y	current displacement of the displace..... m
Q	heat transfer rate..... W	y_0	stroke of the displacer m
T	total crank torque..... $N \cdot m$	Z_D	stroke of displacer..... m
T_b	frictional torque of the rolling bearing, $N \cdot m$	Z_p	stroke of piston..... m
T_i	inlet temperature..... K	θ	piston crank angle..... rad
T_o	outlet temperature..... K	φ	displacement phase angle of the piston.. rad
T_p	piston crank torque..... $N \cdot m$	k, ε	turbulent kinetic energy and dissipation
t	time..... sec		turbulent kinetic energy..... $m^2 \cdot s^{-2}$

1. Introduction

Low Temperature Difference (LTD) Stirling engines, though provide low electricity production, can be used as solar energy and waste heat recovery system due to their simple design and low cost production [1]. There is an interest towards development of LTD Stirling engines for deployment in rural areas of developing countries for production of power on the small scale. Because of this reason, numerous studies have been conducted for determination of optimal design parameters of LTD Stirling engines. Several thermodynamic mathematical models have been used for the determination of the optimum power and efficiency of such engines [2-7]. Furthermore, a considerable work was done on the development of optimisation algorithms for conventional high temperature engines [8, 9]. The search method which uses the Genetic algorithm (GA) code coupled to the mathematical model accounting for heat and mechanical losses using the theorem of forced work was presented by Altman in [9]. This work presents the determination of optimal design parameters of a LTD Stirling engine using GA optimization method, coupled to the second-order model of the engine, which takes into account hydraulic and mechanical losses, developed by Kraitong and Mahkamov [10]. Additionally, 3D CFD simulations using CFD FLUENT software were performed to calibrate results of the optimization calculations.

2. Physical model

Figure 1a represents a schematic diagram of the kinematical gamma LTD Stirling engine. The main components of the LTD Stirling engine are the power piston and displacer with corresponding cylinders, the hot and cold plates, the regenerator placed inside the displacer and the drive mechanism with the flywheel. In this paper, a twin-power piston LTD Stirling engine, see Fig. 1b, manufactured by Kongtragool and Wongwises [11] is used in numerical investigations. This engine consists of two power pistons and one displacer with the built-in regenerator. The regenerator is made of coarse stainless steel mesh placed in the casing perforated at its top and bottom. Table 1 presents data on the physical dimensions of this Stirling engine.

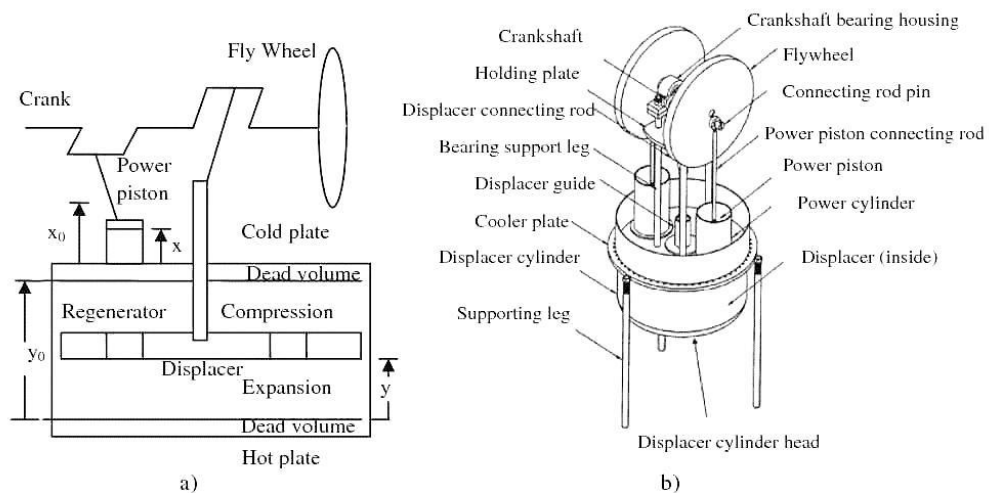


Fig. 1. a) A Schematic diagram of the kinematic gamma LTD Stirling engine and b) The physical characteristic of the twin power piston LTD Stirling from Kongtragool and Wongwises [11].

Table 1. Dimensions of the LTD Stirling engine manufactured by Kongtragool and Wongwiset [11]

The geometric data of a twin power piston LTD Stirling engine	Value
working piston stroke (m)	0.0826
working piston diameter(m)	0.083
working piston swept volume (m ³)	893.8x10 ⁻⁶
displacer piston stroke (m)	0.0795
displacer piston diameter (m)	0.32
displacer piston swept volume (m ³)	6393.8 x10 ⁻⁶
swept volume ratio	7.15
displacement phase angle of the pistons (°)	90

3. Modelling Procedure

3.1. Thermodynamic modelling

The second-order mathematical model taking into account the pressure drop and the mechanical losses developed by Kraitong and Mahkamov [10] was used for the performance prediction of the engine. This model is the modification of that developed by Timoumi et al. [7] and Urieli [12]. The equations of energy and mass conservation for each control volume are expressed as follows:

$$C_v \frac{d(mT)}{dt} = dQ - \frac{dW}{dt} - \dot{m}_o C_p T_o + \dot{m}_i C_p T_i \quad (1)$$

$$\frac{dm}{dt} = \dot{m}_o - \dot{m}_i \quad (2)$$

Work done by the working gas inside the compression space and the expansion space can be calculated as $\frac{dW_c}{dt} = P_c \frac{dV_c}{dt}$ and $\frac{dW_e}{dt} = P_e \frac{dV_e}{dt}$, respectively.

Volumes of the compression and expansion spaces are expressed as

$$V_c = V_{dc} + \frac{V_{SP}}{2} (1 + \cos(\theta - \varphi)) + \frac{V_{SD}}{2} (1 - \cos \theta) \quad (3)$$

$$V_e = V_{de} + \frac{V_{SD}}{2} (1 + \cos \theta) \quad (4)$$

$$\text{where } V_{SP} = \pi \frac{D_p^2}{4} Z_p \text{ and } V_{SD} = \pi \frac{D_D^2}{4} Z_D.$$

In order to determine the brake cyclic power, the kinetic motion equations of the mechanical transmission system of the reciprocating engine proposed by Guzzomi et al. [13,14] were used. The determination of the frictional forces in the sealing rings of the displacer rod is carried out using methodology described in [15]. These results were used to calculate the torque induced by the pistons (T_p). The brake cyclic work and the brake cyclic power, therefore, are calculated as

$$T = \Sigma T_p \quad (5)$$

$$W_b = \int \left(\frac{dW_b}{dt} \right) dt = \int_0^{\tau} \left(T - T_b \right) \frac{d\theta}{dt} dt \quad (6)$$

$$P_b = W_b f \quad (7)$$

For numerical calculations, the cycle was split into 1000 time-steps and calculations were performed until the pressure and temperature curves converged and the overall heat balance in the system was reached.

3.2. CFD modelling

To achieve better understanding of the working process of the LTD Stirling engine and obtain more accuracy in the performance prediction, 3D CFD modeling using the standard $k-\varepsilon$ turbulence model for a compressible flow was carried out to investigate the work of the engine. Commercial CFD software, FLUENT was used to perform CFD simulations of the working process of the engine. During the simulations the movement of pistons was taken into account and the regenerator of the engine was treated as a homogeneous porous medium. The subroutines describing displacements of the pistons and the displacer were written and then connected to the main body of the programme. The cycle was divided into equal 500 time-steps and calculations were performed using a high performance computer. The average gas temperature and pressure in each engine's working space were monitored during calculations in order to determine whether the steady-state condition was reached in the simulated operation of the engine.

3.3. Optimisation modelling

Genetics algorithm is a stochastic optimisation method based on the mechanism of natural selection for survival as the procedure in order to obtain optimal results [16]. The real-valued GA or the continuous GA is applied in this work for the quantitative limitation and the reduction of the computing time [17]. The structure of the continuous GA of the LTD Stirling engine is represented in Fig. 2.

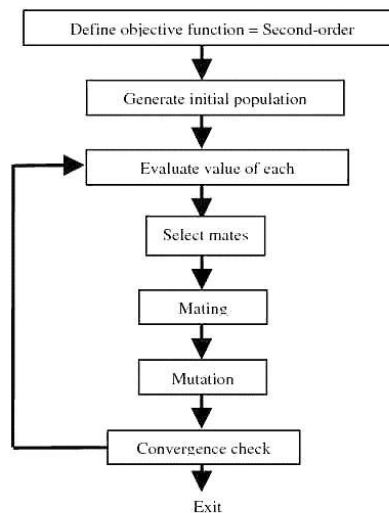


Fig. 2. The structure of the continuous GA of the LTD Stirling engine.

Appendix B

Several original engine design and operational parameters, namely the diameter of the displacer of 0.32 m, the engine speed of 46.5 rpm, the solar irradiation of 5097 W/m² created using a solar simulator and the cooler surface temperature of 307 K, are accepted to be fixed as constant values in this work. There are only four engine design parameters are defined as variables. These are the diameter and the stroke of the power piston, the stroke the displacer and the thickness of the regenerator:

$$\text{Chromosome} = (D_p; Z_p; Z_D; H_d) \quad (6)$$

The upper and the lower bound of each variable are as follows;

$$\begin{aligned} 0.02 < D_p < 0.13 & ; D_p \text{ is diameter of piston (m)} \\ 0.04 < Z_p < 0.3 & ; Z_p \text{ is stroke of piston (m)} \\ 0.04 < Z_D < 0.3 & ; Z_D \text{ is stroke of displacer (m)} \\ 0.01 < H_d < 0.2 & ; H_d \text{ is thickness of regenerator (m)} \end{aligned}$$

The above boundaries are defined based on the practical manufacturing and design considerations. The maximum diameter of the piston is limited by the diameter of the cold plate which is equal to the fixed displacer diameter. The range of the displacer stroke to be investigated is typical for displacers of LTD Stirling engines [18]. Only one of the engine's performances, namely the brake power, is defined to be the chromosome value because the heat source is solar energy which is assumed to be cost-free. The the brake power of the engine obtained using the developed second-order mathematical model is used as the objective function:

$$\text{Brakepower} = f(\text{chromosome}) = f(D_p; Z_p; Z_D; H_d) \quad (7)$$

In GA, there is no effect of the guessed initial chromosomes on the convergence of the solution, thus the initial population is created by using the absolutely random procedure. A generated initial population is in the matrix formation of various chromosomes. The size of the population effects the convergence in the optimization procedure. The number of chromosomes between 30 and 100 is the typical size to operate GA [19]. In this study, the number of chromosomes in a generation of 30 is used. The chromosome value which is the brake power is evaluated by the fitness function for locating in the value map of each generation [20]:

$$\text{Fitnessvalue} = \frac{1}{1 + \text{maxvalue} - \text{value}} \quad (8)$$

The fitness value of each chromosome is descending order to determine survival chromosomes for the next generation. The number of survival chromosomes is defined by the selection rate of 0.5 from the weighted random pairing selection and the rank weighting technique [17]. The single point crossover is used for the mating process that the parents are operated by the reproduction operator to produce some offsprings for the next generation. Fittest chromosomes of the ranking are randomly selected to be the parents for the reproduction operation. The second operator of the reproduction called the mutation is used as a tool to avoid finding only the local solution. The mutation rate of 0.2, though probably is high, results in the gradual convergence and ensures that the global maximum is not missed out in during simulations [17].

Finally, the new generation is produced and the population of new design parameters in this generation is then evaluated by the developed thermodynamic model and the fitness function is checked for the ranking until the solution found satisfying the termination condition. The maximum number of generation in the computing process of 80 is defined to obtain the convergence of this algorithm. The optimisation code was modified from [19] and implemented in MATLAB. In this case, the continuous GA was used to obtain the optimal design parameters for the performance's improvement of an original LTD Stirling engine. Simulations were, thus, conducted for the same operating condition. A set of optimal design parameters from the numerical simulations was then used to create the engine mesh for the 3D CFD simulation to more accurately predict the engine power.

4. Results from optimisation cacluations

The modelling of the engine with the SM15-matrix regenerator was performed for the constant solar flux of 5097 W/m^2 , the cooler surface temperature of 307 K, the engine speed of 46.5 rpm with air at 1 bar pressure used as a working fluid. Figure 3 represents the best brake power for each generation. The best brake power first sharply increases and then gradually reaches the convergence with its value of 1.515 W. The design parameters of this generation are presented in Table 2. The corresponding indicated power is 1.668 W.

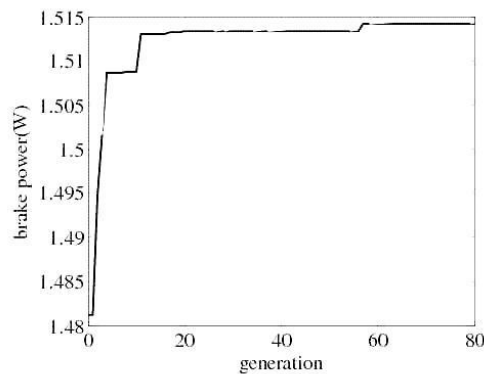


Fig. 3. The best brake power of each generation as the function of generations.

Table 2. The first set of optimal engine design parameters obtained from optimisation simulation.

Optimal engine design parameters	Value
working piston stroke (m)	0.228
working piston diameter(m)	0.065
displacer piston stroke (m)	0.074
displacer thickness (m)	0.056

However, it could be seen that the stroke of the power piston of 0.228 m which is much longer than the stroke of the displacer of 0.074 m. This may be unsuitable for the practical engine. Thus, the power piston and displacer strokes were fixed at 0.1 m and a new set the optimisation simulations with two variables were run. Optimal engine parameters from the second run are presented in Table 3 and the maximum brake and indicated power is 1.346 W and 1.47 W, respectively. There is only 11% reduction in power when compared with the results of the first optimization run.

Appendix B

Table 3. The second set of optimal engine design parameters is obtained from optimisation simulation.

Optimal engine design parameters	Value
working piston stroke (m)	0.1
working piston diameter(m)	0.1
displacer piston stroke (m)	0.095
displacer thickness (m)	0.058

Finally, two engines with optimal engine parameters shown in Tables 2 and 3 were modelled using 3D CFD simulation. The indicated power of the first and the second engine calculated from P-V diagrams which are shown in Fig. 4a and Fig. 4b are 1.427 W and 1.352 W, respectively. 3D CFD modelling results demonstrate that the second-order thermodynamic model used in optimisation procedure has an adequate accuracy in the prediction of the engine performance.

5. Conclusion

The developed second-order mathematical model of the LTD Stirling engine was developed which accounts for hydraulic and heat losses in the working process and mechanical losses in the engine. This model was used with GA optimisation code. As a result of optimization simulations a set of design parameters for the engine was obtained which provides a considerable improvement in the performance. Results obtained using the developed second-order thermodynamic model were calibrated using 3D CFD modeling technique. The optimisation procedure developed in his work can be applied to improve the design of a wide range of Stirling engines, including high temperature ones.

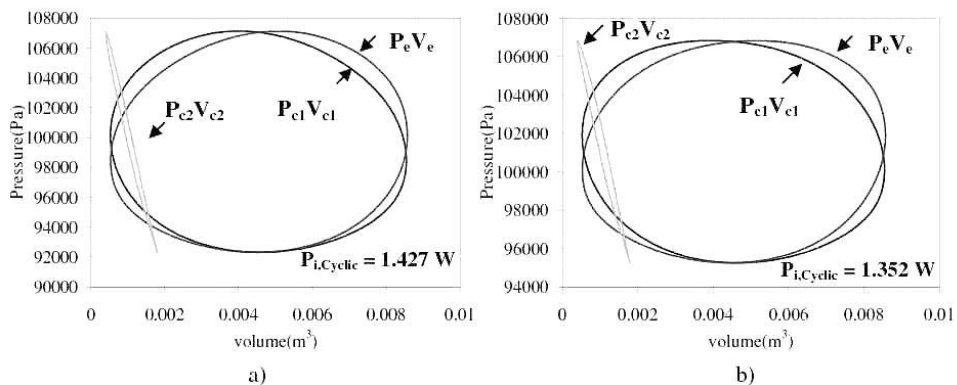


Fig. 4. 3D CFD modeling results: a) P-V diagrams for the first optimal parameters set obtained using and b) P-V diagrams for the second optimal parameters set

6. Acknowledgements

This work is a part of a PhD study which is supported by the Ministry of Science and Technology of the Royal Thai Government. Authors also would like to thank Professor Somchai Wongwises and Assistant Professor Bancha Kongtragool for providing data on their twin power piston LTD Stirling engine.

References

- [1] B. Kongtragool, S. Wongwises, A review of solar-powered Stirling engines and low temperature differential Stirling engines, *Renewable and Sustainable Energy Reviews*, 2003, pp. 131–154.
- [2] L. Erbay, H. Yavuz, Analysis of the Stirling heat engine at maximum power conditions, *Energy* 22, 1996, pp. 645–650.
- [3] S. Hsu, F. Lin, J. Chiou, Heat-transfer aspects of Stirling power generation using incinerator waste energy, *Renewable Energy* 28, 2003, pp. 59–69.
- [4] A. Tavakolpour, A. Zomorodian, A. Golneshan, Simulation, construction and testing of a two-cylinder solar Stirling engine powered by a flat-plate solar collector without regenerator, *Renewable Energy* 33, 2008, pp. 77–87.
- [5] N. Martaj, L. Grosu, P. Rochelle, Exergetical analysis and design optimisation of the Stirling engine, *Int. J. of Exergy* 3, 2006, pp. 45–46.
- [6] B. Orunov, V. T. Krykov, A. P. Korobkov, K. Mahkamov, D. Djumanov, The first stage of the development of a small Stirling tri-generation power unit, *Proceeding of 12th international Stirling engine conference*, 2005, pp. 416–423.
- [7] Y. Timoumi, I. Tlili, S. Nasrallah, Design and performance optimization of GPU 3 Stirling engines, *Energy* URL doi:10.1016/j.energy.2008.02.005.
- [8] Y. C. Hsieh, T. C. Hsu, J. S. Chiou, Integration of a free-piston Stirling engine and a moving grate incinerator, *Renewable Energy* 33, 2008, pp. 48–54.
- [9] A. Altman, SNAPpro: Stirling numerical analysis program, URL <http://home.comcast.net/snapburner/SNAPpro ISEC 2004.pdf>, 2004.
- [10] K. Kraitong, K. Mahkamov, Thermodynamic and CFD Modelling of Low Temperature Difference Stirling engines, *Proceeding of 14th international Stirling engine conference*, 2009.
- [11] B. Kongtragool, S. Wongwises, Performance of a twin power piston low temperature differential Stirling engine powered by a solar simulator, *Solar Energy* 81, 2007, pp. 884–895.
- [12] I. Urieli, Stirling Cycle Machine Analysis, URL <http://www.ent.ohiou.edu/urieli/stirling/me422.html>, 2008.
- [13] D. C. Hesterman, B. J. Stone, A systems approach to the torsional vibration of multi-cylinder reciprocating engines and pumps, *Proc. IMechE* 208, 1994, pp. 395–408.
- [14] A. L. Guzzomi, D. C. Hesterman, B. J. Stone, The effect of piston friction on engine block dynamics, *Proc. IMechE* 221, 2007, pp. 227–289.
- [15] K. Mahkamov, D. Ingham, Analysis of the Working Process and Mechanical Losses in a Stirling Engine for a Solar Power Unit, *J. of Solar Energy Engineering* 121, 1999, pp. 121–127.
- [16] D. E. Goldberg, *Genetic Algorithms in Search, Optimization & Machine Learning*, Addison-Wesley Publishing Company, USA, 1989, ISBN 0- 201-15767-5.
- [17] R. L. Haupt, S. E. Haupt, *Practical Genetic Algorithm*, John Wiley & Sons, USA, Edition 2nd, 2004, ISBN 0-471-45565-2.
- [18] J. R. Senft, *An Introduction to Low Temperature Differential Stirling Engines*, Moriya Press, USA, 2007, ISBN-13: 978-0965245517.
- [19] A. M. S. Zalzal, P. J. Fleming, *Genetic Algorithms in Engineering Systems*, The Institution of Electrical Engineers, UK, 1997, ISBN 0-85296- 902-3.
- [20] S. Elisaveta, B. Natasha, BASIC-A genetic algorithm for engineering problems solution, *Computers and Chemical Engineering* 30, 2006, pp. 1293–1309.